The cell adhesion molecule coxsackie virus and adenovirus receptor (CAR) modulates intracellular Ca^{2+} concentration and Cl^- conductance in cultivated mouse cortical neurons.

Inaugural-Dissertation
to obtain the academic degree
Doctor rerum naturalium (Dr. rer. nat)
submitted to the Department of Biology, Chemistry and Pharmacy
of the Freie Universität Berlin

by

Jadwiga Schreiber
from Krakow

2009

The present thesis was prepared between August 2006 and October 2009 at Max Delbrück Centrum for Molecular Medicine at the Department of Developmental Neurobiology under the supervision of Prof. Dr. Fritz G. Rathjen.

1. Reviewer: Prof. Dr. Fritz G. Rathjen

2. Reviewer: Prof. Dr. Rosemarie Grantyn

Date of defence: 27.11.2009

1. Introduction

1.1 The cell adhesion molecule coxsackie virus and adenovirus receptor (CAR) and its function in cells

1.1.1 The development of neuronal networks and cell adhesion molecules

The mammalian brain contains about 10^{12} nerve cells, each of which maintain an average of 1000 contacts (e.g. synapses) with other nerve cells. This results in a highly complex but specific network, connecting 10^{12} nerve cells with up to 10^{15} synapses that regulate brain functions, ranging from simple motor movement to complex emotional and cognitive behavior (Brose, 1999). The immense complexity of the central nervous system and the stunning specificity of neuronal networks, results from genetic determinants and multiple epigenetic processes, which define temporal expression patterns of specific genes regulating brain development. Epigenetic factors such as neurotrophins (e.g. brain-derived neurotrophic factor, BDNF, (Eide et al., 1993; Huang and Reichardt, 2001; Korsching, 1993) and cell surface molecules (e.g. cell adhesion molecules) mediate signals stimulating and modulating cell differentiation, migration and synaptogenesis (Gopinath et al., 1996; Kolkova et al., 2000; Nikonenko et al., 2003; Schmid and Maness, 2008). In addition, spontaneous and sensory-driven activity is equally important and essential for the development of the central nervous system. Proliferation, migration, differentiation, activity-dependent synapse formation and neuronal survival all depend to various extents on forms of electrical activity, both in embryonic and adult stages (Goda and Davis, 2003; Khazipov and Luhmann, 2006; Mennerick and Zorumski, 2000; Spitzer, 2006). Thus, a complex cooperation of different factors regulates the specific differentiation of any given neuron up to the point of the formation of a functioning neuronal network.

For efficient synaptic function, different types of cell adhesion molecules (CAMs) are required: to mediate and regulate various levels of synaptic specificity; to determine target region; pre- and postsynaptic compartments; transmitter specificity of synapses; and synapse strength, size, plasticity and stability (Brose, 1999; Fields and Itoh, 1996; Suzuki et al., 1997; Yuasa, 1995). CAMs are enriched at synaptic junctions and include several members such as neuroligins, synaptic cell adhesion molecule (SynCAM), neural cell

adhesion molecule (NCAM), L1-CAM, cadherins, protocadherins, and integrins (Craig et al., 2006; Dean and Dresbach, 2006; Gerrow and El Husseini, 2006).

Another cell adhesion molecule, which may also be involved in neuronal-network formation in the developing nervous system, is the coxsackie virus and adenovirus receptor (CAR) mediating homo- and heterophilic interaction between cells (Cohen et al., 2001; Honda et al., 2000; Hotta et al., 2003; Mirza et al., 2006; Patzke et al., 2009, sumbitted; Zen et al., 2005).

1.1.2 Coxsackie virus and adenovirus receptor (CAR)

The CAR has been identified as a cell surface protein enabling the group B coxsackie viruses and adenoviruses 2 and 5 to attach to the surface of cells (Bergelson et al., 1997; Carson and Chapman, 2001; Tomko et al., 1997). Coxsackie B viruses are non-enveloped RNA viruses and belong to human picornaviruses of the enterovirus group (Melnick, 1996). They cause non-specific febrile illnesses as well as myocarditis (Bergelson et al., 1998; Grist et al., 1975), meningoencephalitis (Melnick, 1996) and pancreatic inflammation (Imrie et al., 1977; Yoon et al., 1984). Adenoviruses are non-enveloped DNA viruses of about 90 nm in diameter, associated with a significant number of human respiratory and gastrointestinal diseases (Brandt et al., 1969; Wadell and Norrby, 1969). They are classified into six subgroups (A-F), which are further divided into more than 50 different serotypes based on their immunological properties (Bailey and Mautner, 1994; Law and Davidson, 2005; Rux and Burnett, 2004). All groups of adenoviruses are able to attach to CAR (Bergelson et al., 1997; Roelvink et al., 1998; Tomko et al., 1997). Serotype 2 and 5 of subgroup C are the most extensively studied of the human adenoviruses and have a global distribution (Rux and Burnett, 2004). All adenoviruses, regardless of which host they infect, share a common morphology. Adenoviruses form icosahedral particles with 240 copies of the trimeric hexon protein arranged on the planes and a penton complex at each of the 12 vertices (Boudin and Boulanger, 1982; Devaux et al., 1987; Devaux et al., 1990; Stewart et al., 1991). The hexon protein has mainly a structural role in capsid formation. The penton complex consists of a pentameric penton base, which interacts with five hexons, and an externally protruding trimeric fiber (Devaux et al., 1987; Stewart et al., 1991).

The fiber protein (582 amino acid residues, 61,960 Da) arises from the 12 vertices of the virion (Fig. 1). It consists of three domains: an N-terminal tail that attaches to the penton base, a central shaft with repeating motifs of 15 residues, and a C-terminal globular

"knob" (fiber knob) domain that functions as the cellular attachment site (Henry et al., 1994; Louis et al., 1994; Philipson et al., 1968). The fiber knob possesses a natural ability to form trimers. An application of synthesized fiber knob can compete with intact virus for binding to the cellular receptor (Henry et al., 1994; Rux and Burnett, 2004). Subsequent to attachment via the fiber knob protein, internalization of adenoviruses requires binding of the viral penton base protein to integrins $\alpha_V\beta_3$ or $\alpha_V\beta_5$ on the host cell (Wickham et al., 1993). Receptor-mediated endocytosis then takes place, representing the infectious pathway of entry (Chardonnet and Dales, 1970; FitzGerald et al., 1983; Varga et al., 1991). However, integrin-independent pathways of adenovirus internalization also exist (Bai et al., 1993).

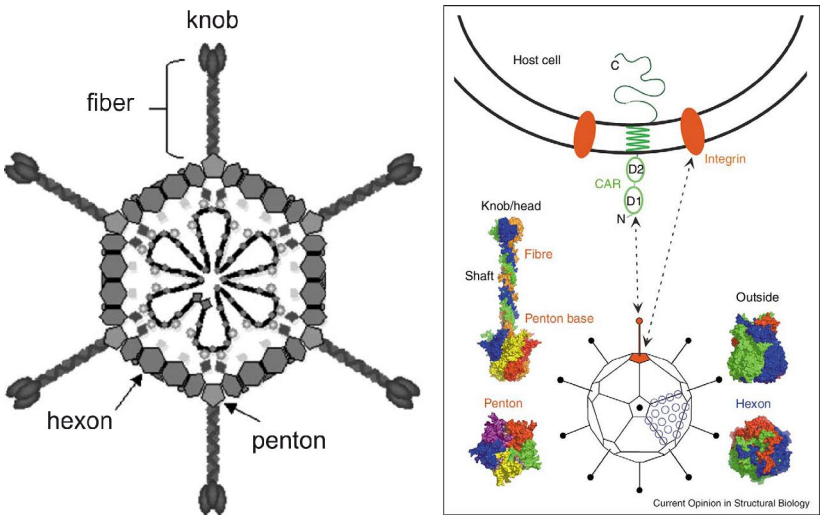

Fig. 1: A schematic adenovirus structure (left) and its interaction with CAR (right). The hexon, penton base, fiber and fiber knob structures are shown. Adenovirus capsids contain up to a 36-kilobase double-stranded DNA genome, shown as the dark line inside the capsid (Glasgow et al., 2006). Most adenovirus serotypes attach to cells through binding of the fiber knob to the extracellular domain of CAR, but internalization requires further interaction of the penton base with cellular integrins (Cusack, 2005).

CAR is a type I transmembrane protein, a cell adhesion protein (Cohen et al., 2001; Excoffon et al., 2004; Excoffon et al., 2007; Honda et al., 2000; Philipson and Pettersson, 2004), that belongs to the CTX (cortical thymocyte marker in Xenopus)-subfamily of the immunoglobulin superfamily (IgSF; Coyne and Bergelson, 2005; Philipson and Pettersson, 2004). The hallmark of the CTX protein family is the presence of V-type and C-type immunoglobulin domains, where the C-domain, in most members, contains an extra pair of cysteines. CTX proteins span the membrane once and harbor an intracellular tail of varying length (Philipson and Pettersson, 2004). Members of the CTX superfamily consist of: CTX, CAR, A33, JAMs (junctional adhesion molecules), ESAM (endothelial

cell-selective adhesion molecule), BT-IgSF (brain-testis IgSF) and CLMP (CAR-like membrane protein, Bazzoni, 2003; Chretien et al., 1998; Raschperger et al., 2004; Raschperger et al., 2006; Suzu et al., 2002).

Structurally, CAR is a 46 kDa protein, 355-365 amino acids (aa), composed of an N-terminal signal peptide (19 aa), an extracellular domain (216 aa) containing a V (D1) and C2 (D2) Ig domain, a single transmembrane domain (23 aa) and an intracellular tail (107 aa or 94 aa; Coyne and Bergelson, 2005; Freimuth et al., 2008; Fig. 2). CAR is highly conserved throughout evolution. Mouse CAR is highly homologous to human CAR, with 90% -aa identity in the extracellular domain and 95% identity in the intracellular segment (Asher et al., 2005). CAR appears in two dominant isoforms, originating from differential splicing of its pre-mRNA. These isoforms show an identical amino acid composition until the extreme C-terminal part of the intracellular segment, where two alternative PDZ-domain binding motifs are found: TVV (Thr-Thr-Val; CAR-1) and SIV (Ser-Ile-Val; CAR-2). The SIV form has an intracellular domain consisting of 107 residues, whereas the intracellular domain of the TVV form has 94 residues (Bergelson et al., 1998; Coyne and Bergelson, 2005; Philipson and Pettersson, 2004; Tomko et al., 1997; Fig. 2). CAR is a glycoprotein with two putative glycosylation sites, one on each of its two extracellular Ig-domains, D1 and D2. CAR detected by Western blot reveals two bands, one at about 40 kDa and one at about 46 kDa, representing non-glycosylated and glycosylated forms respectively (Honda et al. 2000). Incubation with peptide N-glycosidase F (PNGase F) thus reduces the 46 kDa band to 40 kD (Excoffon et al., 2007; Honda et al., 2000).

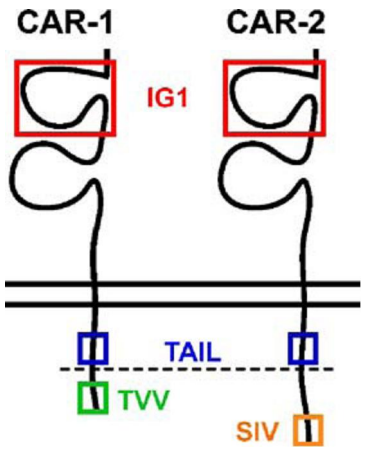

Fig. 2: Schematic presentation of CAR. CAR consists of an extracellular part with two Ig-like domains, a single transmembrane region and an intracellular tail. The C-terminal parts of the two splice isoforms, CAR-1 and CAR-2, differ in amino acid composition (TVV, SIV; Raschperger et al., 2006).

1.1.3 The expression of CAR in different tissues

Expression of CAR has been analyzed in different cell lines as well as in the tissues of many species including: zebrafish, dog, pig, mouse, rat and human by analysis of mRNA levels by Northern blotting, in situ hybridization, reverse transcription polymerase chain reaction (RT-PCR) and Western blotting (Bergelson et al., 1998; Fechner et al., 1999; Petrella et al., 2002). Results suggest that CAR is widely and variably expressed in many tissues as well as in different primary tumors and tumor cell lines (Coyne and Bergelson, 2005; Philipson et al., 1968; Philipson and Pettersson, 2004). Furthermore, CAR expression is developmentally regulated. During embryogenesis CAR is highly expressed in numerous tissues including the central and peripheral nervous system (Honda et al., 2000; Hotta et al., 2003; Tomko et al., 2000), the heart (Ito et al., 2000), skeletal muscle (Nalbantoglu et al., 1999) and various epithelia (Raschperger et al., 2006; Tomko et al., 2000). In the brain of newborn mice, strong expression was observed in the cerebral cortex, midbrain, hippocampus, various thalamic nuclei and the meninges, whereas relatively low expression was detected in cerebellum and olfactory bulb (Honda et al., 2000). No expression was found in the corpus callosum, anterior commissure or cerebellar white matter (Honda et al., 2000). In contrast, CAR expression is downregulated in the brain of adult mice. Additionally, studies on the subcellular localization of CAR in cultured hippocampal cells, by means of immunocytochemisty with antibodies against CAR, revealed that CAR was distributed throughout cell bodies, neurites and growth cones (Honda et al., 2000; Patzke et al., 2009, submitted).

CAR is also very strongly expressed in the cardiomyocytes of both embryonic and newborn rodent hearts (Kashimura et al., 2004) as well as human hearts (Fechner et al., 2003). Similarly to in the brain, CAR expression drastically decreases in the adult heart. Widespread expression of CAR in adults is predominantly found in epithelial cells, from several organs such as the testes, gastrointestinal tract, liver, lung, pancreas and kidney (Mirza et al., 2006; Raschperger et al., 2006). CAR found in epithelial cells lining the body cavities is often co-expressed with tight junction components zonula occludens (ZO-1) and occludin (Raschperger et al., 2006). For example, in tracheal epithelial cells, co-localization of CAR and ZO-1 has been shown by means of immunogold staining (Cohen et al., 2001). CAR expression correlated positively with the maturity of tight junctions (TJs) and inversely with their permeability. It has been shown that both CAR isoforms

(CAR1 and CAR2) were equally co-expressed in most epithelial cell-cell contacts (Raschperger et al., 2006).

1.1.4 The cellular function of CAR

CAR has been identified as the primary cellular receptor for the entrance of several adenoviruses and coxsackie B viruses (CBV) into the cell (Bergelson et al., 1997; Tomko et al., 1997). Besides its role as a viral receptor, CAR's precise cellular function is largely unknown. However, CAR appears to be involved in many biological processes, such as homotypic adhesion (Carson and Chapman, 2001; Cohen et al., 2001; Honda et al., 2000), neutrophil transmigration (Bruning and Runnebaum, 2003; Zen et al., 2005), protein trafficking and modulation of cellular growth and motility (Excoffon et al., 2004; van Raaij et al., 2000; Walters et al., 2002). The very strong expression of CAR during embryonic development and its rapid decrease after birth has been hypothesized to suggest a function in tissue formation and repair (Honda et al., 2000; Ito et al., 2000; Kashimura et al., 2004; Nalbantoglu et al., 1999).

CAR is expressed in the mouse heart from embryonic day E7 at a relatively high level and thus would be expected to play an essential role in cardiac development. Indeed, it has been shown that CAR knock-out mice die between day E9.5-E11.5 due to abnormal development of the heart (Asher et al., 2005; Dorner et al., 2005). CAR-deficient mice displayed ventricular myocardial abnormalities and aberrant cardiomyocyte differentiation (Asher et al., 2005; Chen et al., 2006; Dorner et al., 2005). Cellular contacts between cells were also disturbed, a finding consistent with the role of CAR in cell-cell contact formation. Although CAR expression is downregulated in the adult rat heart, its expression can be induced by experimental autoimmune myocarditis (Ito et al., 2000). Moreover, myocardial infarction in the rat results in strong upregulation of CAR in cardiomyocytes in the infarct zone (Fechner et al., 2003). Also in human hearts, expression of CAR in cardiomyocytes was shown to be increased in different cases of dilated cardiomyopathy, but CAR was not found in healthy hearts (Noutsias et al., 2001). The strong and abundant CAR expression in developing cardiomyocytes and in diseased hearts, compared to the weak or no expression in adult, healthy hearts, suggests a role for CAR in the formation and repair of functional myocardium.

In adult skeletal muscles, in both humans and rodents, CAR expression is barely detectable. Nevertheless, skeletal muscle is susceptible to coxsackie virus B1-induced myositis (Nalbantoglu et al., 1999; Ytterberg et al., 1987; Zoll et al., 1993). Human

patients suffering from inflammatory muscle diseases have been tested positive for coxsackie B virus (CBV) RNA (Bowles et al., 1999; Bowles et al., 1987). Reports showed that CAR expression at the neuromuscular junction is isoform specific and restricted to the CAR2 (SIV) isoform. Furthermore, the CAR TVV isoform is present in the skeletal muscle vasculature (Shaw et al., 2004).

In primary tumors and tumor cell lines, CAR expression seems to inversely correlate with the rate of cell proliferation, suggesting that CAR may act as a tumor suppressor (Fuxe et al., 2003; Okegawa et al., 2000). Induced expression of CAR has been shown to inhibit tumor cell growth in human prostate cancer (Okegawa et al., 2000; Rauen et al., 2002), bladder cancer (Li et al., 1999; Okegawa et al., 2001) and glioma cell lines (Kim et al., 2003), indicating CAR tumor inhibitory properties. Other reports also showed that absent or reduced expression of CAR is associated with a higher tumor grade in human prostate and bladder cancer patients, while healthy tissues express easily detectable CAR (Okegawa et al., 2001; Rauen et al., 2002).

CAR is a cell adhesion molecule and is involved in the formation of cell-cell contacts. In epithelial cells in culture, CAR molecules form homotypic interactions with neighboring cells (Cohen et al., 2001). CAR is localized at the most apical region at the lateral surface of polarized epithelial cells and is concentrated in TJs. CAR expressed at TJs is associated with ZO-1, the first identified TJ scaffolding protein important for TJ structure and assembly (Anderson et al., 1988; Stevenson et al., 1986). Whereas overexpression of CAR in cultured epithelial cells results in increased transepithelial electrical resistance (TER; Excoffon et al., 2004), application of soluble CAR or anti-CAR antibodies disturbs TJs. This suggests that CAR is involved in the barrier function of TJs (Walters et al., 2002). Furthermore, increased CAR expression in transfected MDCK (Madin-Darby canine kidney) cells resulted in higher trans-epithelial resistance, suggesting that CAR may modulate paracellular ion flow and therefore paracellular permeability (Cohen et al., 2001).

1.1.5 Known interaction partners of CAR

Several scaffolding proteins containing PDZ-domains that interact with PDZ-binding motifs present at the C-terminus of the two CAR isoforms have been identified. These proteins include: ZO-1 (Anderson et al., 1988; Cohen et al., 2001; Stevenson et al., 1986), MAGI-1b, PICK1 and PSD-95 (Excoffon et al., 2004), MUPP-1 (Coyne et al., 2004) and

LNX and LNX-2 (Sollerbrant et al., 2003). However, the functional role of these interactions is currently unknown.
Association of CAR with ZO-1 was shown by co-precipitation from polarized epithelia and by relocalization of ZO-1 that occurs in CAR-transfected Chinese hamster ovary (CHO) cells (Cohen et al., 2001). As a result of a yeast two-hybrid screen, MUPP1 was identified to interact directly with the cytoplasmic segment of CAR, suggesting that CAR is involved in MUPP1 recruitment to TJs.
CAR has also been shown to interact with components of adherens junctions such as β-catenin in A549 cells (Walters et al., 2002). Yeast-two-hybrid studies also revealed that CAR interacts with the ligand of Numb-X (LNX; Sollerbrant et al., 2003), a PDZ protein regulating Notch signaling in the central nervous system.
Furthermore, CAR interacts via its membrane distal Ig domain (D1) with junctional adhesion molecule-like protein (JAM-L; Luissint et al., 2008; Zen et al., 2005) and JAM-C (Ebnet et al., 2003; Mirza et al., 2006).
Recently, interaction of extracellular CAR domains with extracellular matrix (ECM) proteins such as fibronectin, fibulin-1, laminin-1 and agrin as well as interaction via the cytoplasimc CAR segment with α-actinin and profilin-1 has been demonstrated (Patzke et al., 2009, submitted).

1.1.6 What is interesting about CAR?

Many cell adhesion molecules have been reported to be essential for the formation and development of functional neuronal networks. CAR is a cell adhesion molecule and a viral receptor that shows complex and developmentally regulated expression patterns in different tissues. It is involved in different cellular processes, and its cellular function is strongly dependent on its localization and interaction partners. Furthermore, abundant expression of CAR in different parts of the developing mouse brain has been reported (Honda et al., 2000; Hotta et al., 2003; Tomko et al., 2000), suggesting a possible role in neuronal development. Yet, the physiological function of CAR in the central nervous system remains largely unknown. CAR's implied role in neuronal network development and the unsettled question about its physiological function, therefore makes it an interesting target for investigation.

A most common approach in neuroscience to investigate the function of a single protein and its involvement in cellular processes is the characterization of

electrophysiological properties of neurons lacking this protein or neurons in which the function of the protein can be modulated (e.g. by blocking with antibodies). The following chapters will therefore describe the basic principles of electrical properties of neurons.

1.2 Neuronal cell membrane properties

The cell capacitance (C_m) and the membrane resistance (R_m) are usually referred to as passive electrical properties of the neuronal cell membrane. They determine the time course and the amplitude of the postsynaptic potentials as well as determining whether a synaptic potential generated in a dendrite will reach a threshold depolarization at the trigger zone on the axon hillock. The R_m depends on the density (number) and conductance properties of ion channels in the membrane as well as on the size and the morphology of the cell. The activity of ion channels, and thus the value of the R_m, can be additionally modulated by different mechanisms e.g. changes in the membrane potential, changes in the basal Ca^{2+} concentration or binding of a ligand.
In the following chapters (1.2.1-1.2.5) different aspects of the neuronal membrane properties will be described, including the distribution of ions across the membrane, the generation of the resting membrane potential, the electrical properties of neuronal membrane components and different types of transmembrane proteins (e.g. ion channels and gap junctions). This information was introduced for better understanding: 1) how the passive and active membrane properties of the neuronal membrane are established. 2) how they can be modulated and 3) how they might influence neuronal development.
In addition, an overview of Ca^{2+} homeostasis, its function in neurons and a possible correlation between cell adhesion molecules and intracellular Ca^{2+} will be described.

1.2.1 Unequal ion distribution across the membrane and the resting membrane potential

The neuronal plasma membrane, a phospholipid bilayer, separates the intracellular cytoplasm from the extracellular environment. Both media consist of watery salt solutions with different types of charged conductive ions. However, there is an unequal distribution (concentration) of ions in intra- and extracellular solutions and thus across the neuronal cell membrane (Table 1). The cytoplasm is rich in K^+ (about 140 mM), while it is relatively poor in Na^+ (7 mM), Cl^- (7-45 mM) and Ca^{2+} (0.1 µM; Table 1). Although the membrane itself is an effective barrier against movement of charged molecules, these small ions can move across the membrane through different ion channels and transport

proteins incorporated in the membrane. In addition to small ions, the inside of the neuronal cell is rich in anions such as proteins and phosphates, which have a large molecular mass and do not cross the membrane through channels. In contrast, the extracellular concentration of large anions is very low.

Unequal ion concentration across the neuronal cell membrane			
Ion	Intracellular concentration (mM)	Extracellular concentration (mM)	Nernst reversal potential (mV)
K^+	140	3	-97
Na^+	7	140	+75
Cl^-	7-45	140	-80 - -30
Ca^{2+}	0.0001	1.5	+129

Table 1: Examples of ionic concentrations in the extracellular and intracellular media and the resulting Nernst potential for each ion at 25 °C (Hammond, 2001).

Unequal distribution of ions across the neuronal cell membrane, their charge and their different permeability properties through ion channels result in the generation of the membrane potential (V_m). The V_m represents the difference between the potential of the intracellular and the extracellular side of the membrane ($V_m=V_i-V_e$). The intracellular side is negatively charged compared to the extracellular side (due to large, negatively charged anions in the cytoplasm). In neurons at rest, when no synaptic input is carried, the V_m is called resting membrane potential (RMP) and shows values of about -40 to -90 mV depending on neuron type (Lu et al., 2007; Purves et al., 2008).
Ions move through the membrane because of two physical causes: 1) down their concentration gradient and 2) according to the membrane potential (V_m). Both forces together form the electrochemical gradient, which determines the direction of movement for a particular ion across the membrane.

1.2.2 Electrical circuit as a model of the neuronal cell membrane

As mentioned above, the neuronal cell membrane is an effective barrier against movement of conductive and charged ions present in the intra- and extracellular solutions. Thus, the neuronal cell membrane forms an insulator between two conductors. However, ion channels and different transporters existing in the cell membrane allow ions to move across the membrane and decrease the resistance of the membrane insulator. Movement of ions through the membrane is expressed as a current (I). The amount of current produced

depends on the electrochemical gradient and the membrane resistance (resistance of ion channels). The membrane resistance (R_m; Fig. 3 A) is determined by the number of functional ion channels are in the membrane. It may also be expressed as a conductance (*g)* through the membrane due to ion channels (g=1/R_m, Fig. 3 B). Conductance depends on particular channel properties and represents how easily ions can pass through this channel.

The total ionic current is represented by the sum of all ionic currents (I_{ionic}, Fig. 3 A) passively flowing through the membrane. At the RMP this current consists predominantly of leak currents of Na^+, K^+ and Cl^- ions. An electrical circuit model was conceived to represent ion flow through the membrane (Fig. 3 A, B, Kandel et al, 2000). This circuit consists of resistors (ion channels; R_m Fig. 3 A or as g Fig. 3 B), batteries (electrochemical gradient across the membrane) and capacitors (charge storage; C_m Fig. 3 A, B). Cell membrane capacitance (C_m, Fig. 3 A, B) is defined as the ability of the membrane to store charge (ions).

Ohm's law appropriately describes the electrical behavior of neurons, representing the relationship between voltage (V; across the membrane) and current (I) flowing through resistors (R; ion channels in the membrane).

Ohm's law: $I = V/R$

Where:

R – cell membrane resistance (R_m; MOhm)

V – cell membrane potential (V_m; mV)

I – current (I_{ionic}; pA)

As mentioned above, cell resistance (R_m) may also be presented in the form of conductance (g) where $g = 1/R$. In this case Ohm's law has the following equation:

$$I = g*V$$

The relationship between current and voltage can be presented as a simple plot (I-V relation, Fig. 3 C, left side), measurement of conductance (g, ion channels permeability, or by single channel recording the permeability of a single channel). If this relation is linear, it is said to show an Ohmic behavior (Fig. 3 C, left side), meaning that the current flowing through the channels of the membrane changes linearly with varying potential. It behaves as a simple resistor following Ohm's law (Ohmic behavior of channel/channels). The conductance (g) of Ohmic channels (or channel) is constant at all voltages. If an I-V relationship is not linear (Fig. 3 C right side) and the current flowing is not linear in relation to the changing potential, it can be described as rectifying (e.g. rectifying

channels), meaning that the conductance is not linear, but variable and depending on membrane potentials. Such channels tend to conduct ions more easily in one direction than in the other and are therefore described as either inwardly or outwardly rectifying. Often, leak (resting) channels show Ohmic behavior, meaning that ions are conduced through the membrane at the RMP. In contrast, ligand-gated channels often behave in a rectifying manner, changing their conductance depending on e.g. voltage (Hammond, 2001; Kandel et al., 2000).

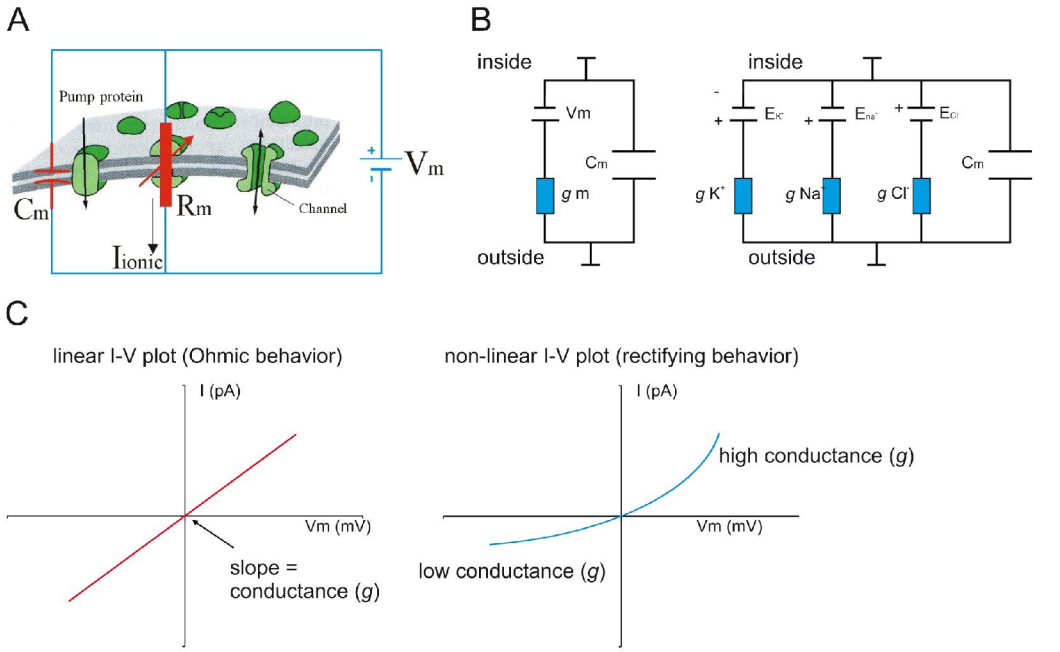

Fig. 3: Electrical model of the neuronal cell membrane. (A, B) Schematic overview of the membrane indicates an existing voltage across the membrane (V_m), ionic current through ion channels in the membrane (I_{ionic} in A, or as conductance *g* for particular ions in B), and its capacitive properties (C_m). Activity of (leak) ion channels influences R_m directly, whereas transport proteins (e.g. pump protein) are involved in determining of the RMP. (C) A linear I-V plot represents Ohmic behavior of ion channels with constant conductance (left side), whereas the non-linear I-V plot describes variable conductance and rectifying behavior (modified form Kandel et al., 2000).

1.2.3 Nernst equation and Goldman equation

Under RMP conditions, the neuronal membrane is only slightly permeable for Na^+, Cl^-, and Ca^{2+}, while it is highly permeable for K^+. Due to the concentration gradient, K^+ will move out of the cell, inducing a relatively negative internal potential. This negativity will oppose further outward movement of K^+ until an equilibrium is reached and the K^+ concentration gradient cancels the electrical force. Such equilibrium is called equilibrium potential (reversal potential; E*rev*). Thus, at the membrane potential corresponding to

E*rev*, K^+ ions move in and out of the cell, but there is no net change in its concentration across the membrane. E*rev* can be calculated using the Nernst equation.

$$E = RT/zF * \ln([Ion]_{in}/[Ion]_{out})$$

Where:

R – universal gas constant: $R = 8.314472\ JK^{-1}mol^{-1}$
T – absolute temperature in Kelvin, 298 K (25°C)
z – ion valence
F – the Faraday constant, $F = 9.64853399 \times 10^4\ Cmol^{-1}$
ln – natural logarithm
$[Ion]_{in}$ - concentration of ions in the cell
$[Ion]_{out}$ - concentration of ions outside the cell

Assuming intracellular K^+ is 140 mM and extracellular is 3 mM, the reversal potential (E*rev* $_{(K+)}$) would be -97 mV (Table 1). At this membrane potential there is no net K^+ transport across the membrane. Table 1 also lists calculated E*rev* for Na^+, Cl^- and Ca^{2+}. However, the gradients for all ions is complexly regulated e.g. by transporter activity (e.g. Na^+/K^+ ATPase pump; Fig. 4) and intracellular sequestration and thus the precise E*rev* value prediction is limited.

The V_m, consisting of physical properties of several ion types (K^+, Na^+ , Cl^- ions), is determined not only by their concentration but also by their permeability (P) across the membrane. The dependence of the V_m on ionic permeability and concentration is quantitatively presented by the Goldman equation:

$$E = RT / F * \ln((P_K[K^+]_{out} + P_{Na}[Na^+]_{out} + P_{Cl}[Cl^-]_{in}) / (P_K[K^+]_{in} + P_{Na}[Na^+]_{in} + P_{Cl}[Cl^-]_{out}))$$

Where:

R – universal gas constant: $R = 8.314472\ JK^{-1}mol^{-1}$
T – absolute temperature in Kelvin, 298 K (25°C)
F – Faraday constant, $F = 9.64853399 \times 10^4\ Cmol^{-1}$
ln – natural logarithm
P_K– permeability of K^+
$[Ion]_{in}$ - concentration of ions in the cell
$[Ion]_{out}$ - concentration of ions outside the cell

The greater concentration and permeability of a particular ion type, the greater is its role in determining the V_m. Studies from Alan Hodgkin and Bernard Katz (1949, using giant

squid axon) on the Goldman equation revealed the following permeability ratio at the RMP:

$$P_K:P_{Na}:P_{Cl} = 1.0: 0.04: 0.45$$

In contrast, at the peak of an action potential the permeability ratio would be quite different:

$$P_K:P_{Na}:P_{Cl} = 1.0: 20: 0.45$$

and the Goldman equation could be reduced to:

$$E= RT/F*\ln [Na^+]_{in}/[Na^+]_{out}$$

Contribution of Cl^- ions to the V_m depends on Cl^- transport across the membrane and its electrochemical gradient. In neurons, which do not have active transport of Cl^- against the electrochemical gradient, the movement of Cl^- is regulated only by passive forces (electrochemical gradient) through Cl^- leak channels that are open at RMP. In this case contribution of Cl^- to the resting potential is relatively low. However, in many cells, the Cl^- gradient is regulated by Cl^- transporters, which can move Cl^- against its electrochemical gradient. For example, the Cl^-/K^+ transporter moves one ion of Cl^- and one ion of K^+ out of the cell (the energetically favorable outward K^+ flux is able to drive the energetically unfavorable outward Cl^- flux). As a result, the net in-out movement of Cl^- is greater than when it would only be driven by the electrochemical gradient. This increasing Cl^- gradient then contributes to the determination of V_m (Hammond, 2001; Kandel et al., 2000; Purves et al., 2008).

1.2.4 Current flow across the membrane

The current flow through the membrane depends on ion channels in the cell membrane. There are two main groups of ion channels: leak channels (or resting channels, non-gated channels) and gated channels, both having distinctive roles in the establishment of neuronal properties and in neuronal signaling (Fig. 4). Leak ion channels are important for maintaining the RMP. They are generally open at the RMP and are directly involved in the determination of the R_m. Gated channels, in contrast to the leak channels, are closed at the RMP and their probability of opening depends on different factors e.g. membrane potential and extracellular or intracellular legends binding to them (Hammond, 2001; Kandel et al., 2000). Voltage-gated ion channels represent active properties of neuronal membrane and do not participate in the determination of the R_m. They are activated at membrane potentials, which are not in the range of the RMP.

1.2.4.1 Leak channels and background conductance at RMP

Leak conductance (through leak channels) and pump current (generated by pump and transporter activity) are the major determinants of the RMP and the membrane resistance (R_m), which are two key components of neuronal excitability (Edman et al., 1986; Lesage, 2003; Salkoff et al., 2001). The existence of background conductance in neurons had been originally postulated by Hodgkin and Huxley (Hodgkin and Huxley, 1990).

In general, the transmembrane exchange of Na^+, K^+, and Cl^- at the RMP is accomplished by active and passive transport, which add up to zero in a steady state for each ion involved (Edman et al., 1986).

Active transport requires selective transporter molecules (pumps and/or co-transporters) and energy expenditure e.g. energy coming from ATP hydrolysis. Active transport enables ions to move against their electrochemical gradient and two ion types are frequently coupled to a single transport molecule (co-transporter; exchanger) e.g. Na^+/K^+-ATPase pump. The Na^+/K^+-ATPase pump is an electrogenic transporter, which carries 3 ions of Na^+ out of the cell and 2 ions K^+ into the cell and thus produces the net charge transfer of one ion (Fig. 4). The Na^+/K^+-ATPase pump plays a fundamental role in exchanging intracellularly accumulated Na^+ for extracellular K^+ in order to maintain the correct ionic gradient across the membrane (maintaining the RMP; Brodie et al., 1987; Brodie and Sampson, 1985; Glitsch, 2001). However, there can be no net charge transfer called electroneutral transport, when, for example, one positive ion is moved out of and a similar positively charged ion into the cell (Goldshleger et al., 1990). In addition to the Na^+/K^+ pump, several other transporters participate in maintaining the RMP and ion concentrations across the neuronal membrane: the Cl^--ATPase pump (Gerencser and Zhang, 2003;I nagaki et al., 1996), the Ca^{2+}-ATPase pump (Guerini et al., 1999), the Ca^{2+}/H^+ pump (Khodorov et al., 1995; Khodorov, 2000), the Na^+/Ca^{2+} exchanger (DiPolo and Beauge, 2006; Török TL, 2007), different types of K^+/Cl^- cotransporters (Kanaka et al., 2001; Pearson et al., 2001; Ueno et al., 2002), and the $Na^+/K^+/2Cl^-$ cotransporter (NKCC; Alvarez-Leefmans et al., 1988; Luo et al., 2008; Schomberg et al., 2001).

Passive transport describes the movement of ions, along their electrochemical gradients through leak channels incorporated in the membrane (Edman et al., 1986). As mentioned above, leak channels are involved in the establishment of the RMP, and most of them are open at the RMP, generating leak conductance (Lesage, 2003; McCormick and Huguenard, 1992; Theander et al., 1996). Many different leak channels have been

identified. In the past few years, an entire family of genes encoding leak K^+ channels has been described (two-pore-domain (KCNC) K^+ channels family). The main representatives of this family in the nervous system are the TASK (T WIK-related a cid-sensitive K^+; TWIK, for tandem P domains in a weak inwardly rectifying K^+) channels and TREK channels. They are open at the RMP, insensitive to a broad spectrum of known K^+ channels blockers and show only little voltage- and time-dependence (Goldstein et al., 2001; Lesage, 2003; Talley et al., 2001; Talley et al., 2003). Compared to K^+ leak conductance, little is known about leak Na^+ conductance (IL-Na). Although IL-Na is believed to play an important role in the regulation of neuronal excitability, the *in vivo* function of IL-Na has not yet been tested because of the lack of specific blockers for IL-Na channels. Hyperpolarization-activated cyclic-nucleotide gated (HCN) channels show high permeability for both K^+ and Na^+ at the RMP and thus are likely to contribute to the overall leak current but they are also regulated by voltage and/or by binding of intracellular cyclic nucleotides (Aponte et al., 2006; Bolivar et al., 2008; Lyashchenko and Tibbs, 2008). Furthermore, the voltage-independent, non-selective, non-inactivating cation channel NALCN (Na^+ leak channel nonselective), permeable to Na^+, K^+, and Ca^{2+} may also produce a leak current (Lu et al., 2007; McCormick and Huguenard, 1992). Additionally to NALCN, the existence of other Ca^{2+} leak channels has been reported (Montano and Bazan-Perkins, 2005; Pinilla et al., 2005; Tu et al., 2006). Although Cl^- leak conductance has often been observed in neurons, no specific channels have yet been identified (Edman et al., 1986; Gestrelius et al., 1981; McClintock and Ache, 1989; Simpson et al., 2005).

1.2.4.2 Gated channels and active current flow through the cell membrane

Ion channels, which are not constantly open at the RMP, but require a stimulus to open, form a complex group of gated channels. Channel opening (activation), switching from the closed to the open state, may be controlled by different gating mechanisms such as: 1) change in the membrane potential (voltage-gated ion channels; Fig. 4), 2) binding of an extracellular ligand e.g. neurotransmitter (extracellular ligand-gated ion channels; Fig. 4), 3) binding of an intracellular ligand e.g. a cyclic nucleotide or Ca^{2+} (intracellular ligand-gated ion channels), and 4) mechanical stimulus e.g. stretching (mechanoreceptors (Hammond, 2001; Kandel et al., 2000; Purves et al., 2008).

Voltage-gated ion channels have a three-dimensional structure containing an aqueous pore and a voltage-sensitive region. At the RMP they are in a closed state and ions cannot flow through them. Change in the V_m causes conformational change and opening of the channel. Most often these channels open transiently, due to depolarization, but there are also channels activated by hyperpolarization. The aqueous pore of voltage-gated ion channels is in general permeable to only one type of ion. Thus, voltage-gated ion channels are named after their most permeable ions. In neuronal cells, at least three different types of voltage-gated ion channels have been identified and well characterized: voltage-gated potassium channels, voltage-gated sodium channels and voltage-gated calcium channels. Opening of such channels due to a change in voltage, results in active current flow across the membrane and a fast change of cellular V_m. Voltage-gated Na^+ channels are responsible for initial Na^+ inward current during the depolarization phase of action potentials. Thus, they are very important for initiation and propagation of action potentials. Diverse types of voltage-gated Ca^{2+} channels determine Ca^{2+} entry into the cell, participate in the generation of Ca^{2+} action potentials and enable triggering of Ca^{2+}-dependent intracellular processes (e.g. neurotransmitter release).

Extracellular-ligand gated ion channels open as a result of binding of an extracellular ligand e.g. neurotransmitter (acetylcholine, GABA, glutamate, glycin). These channels contain an extracellular ligand binding site and an ionic channel with an aqueous pore, to pass the ions. In general, when the neurotransmitter binds to the receptor site, the receptor protein changes its conformation and transiently switches to an open state, allowing ions to flow through the aqueous pore. When activated these channels cause a rapid change in membrane permeability and thereby enable fast synaptic transmission. The best investigated members of this group include: the nicotinic acetylcholine receptor, the $GABA_A$ receptor and the NMDA glutamate receptor.

Intracellular-ligand gated ion channels are gated by intracellular second messengers such as Ca^{2+}, inositol 1,4,5-trisphosphate (IP3), cyclic nucleotides, or by GTP-dependent proteins (G proteins). This group shows high diversity because of a large number of possible intracellular ligands depending on cell type. For example in the central and peripheral nervous system, the G-protein-gated inwardly rectifying K^+ (GIRK) channel is directly modulated by binding of G protein.

Such channels are coupled via G proteins to many different neurotransmitter receptors and are involved in decreasing the firing rate. Another group belonging to these channels is the group of Ca^{2+}-activated ion channels e.g. Cl^- or K^+ channels. An intracellular increase in

Ca^{2+} concentration enhances the opening probability of these channels. Also cyclic nucleotide-gated (CNG) channels belong to this group. Although they are activated by binding of cAMP or cGMP and not by voltage, their structure is very similar to that of voltage-gated ion channels.

Mechanically gated channels open by mechanical stimulus. To this group belong all sensory receptors activated by pressure, stretching or auditory or vestibular stimulus, which underlay senses as propioception, hearing, touch and balance (Hammond, 2001; Kandel et al., 2000; Purves et al., 2008).

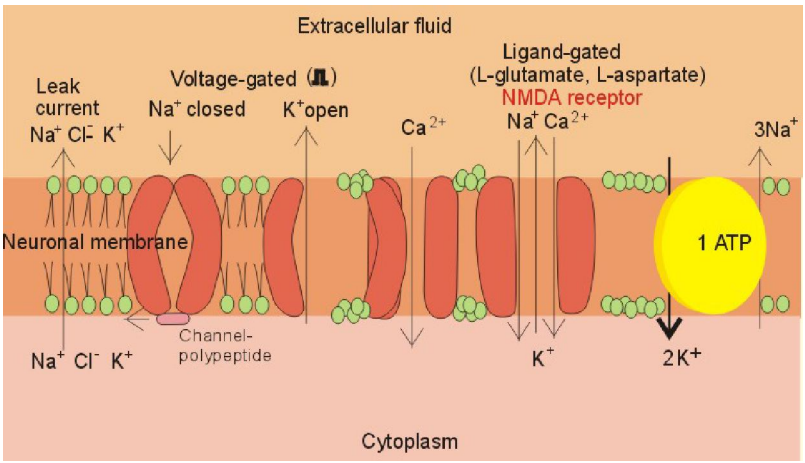

Fig.4: Schematic view of different ion channels and Na^+/K^+ ATPase pump incorporated in the neuronal cell membrane (Paulev, 2000).

1.2.5 Gap junctions

Another group of transmembrane proteins, which play important role in neuronal development and might also be important for passive membrane properties (in particular for the R_m) are gap junctions.

Gap junctions are formed by connexins, a complex protein family, which have a conducting function between two neighbor cells (Bennett et al., 1981; Caveney, 1985; Rozental et al., 2000; Sosinsky and Nicholson, 2005). In contrast to the channels mentioned above, these proteins exchange ions or molecules between two cells and not between intra- and extracellular media. Such an exchange of signal molecules has been implicated in various cellular mechanisms, including ionic homeostasis, electrical synchronization, proliferation and cell migration (Bittman et al., 1997; Bruzzone et al., 1996; Miragall et al., 1997; Nadarajah et al., 1998; Sosinsky and Nicholson, 2005; Wei et al., 2004). Two cells connected by a gap junction are said to be coupled. Gap junctions are non-ion selective and can pass molecules up to 1000 Da (Loewenstein, 1987; Wolpert,

1969). They have a hexametric structure and each hexameter belongs to the membrane of one of the coupled cells. This hexameter is built of six connexin proteins (connexin, named also hemichannel; Fig. 5; Bennett et al., 2003; Ebihara, 2003; Goodenough and Paul, 2003). There are many different subtypes of gap junctions named after their molecular mass, e.g. Connexin 32, 36, 43, 45. Particular subtypes of connexins are activated by different mechanisms. Some of them are open at the RMP and/or for some of them the opening is enhanced at 0 mV membrane potential (voltage-dependent properties; Dermietzel et al., 1991; Banach and Weingart, 2000; Giaume et al., 1991) or their opening is regulated by the transjunctional potential (the potential difference between two coupled cells). Their opening can also be modulated by intracellular and extracellular ligands, second messengers, pH, intracellular Ca^{2+} concentration, cyclic nucleotides and temperature (Braet et al., 2003; Bruzzone et al., 2001; Bukauskas and Weingart, 1993; Contreras et al., 2002; Kamermans et al., 2001; Pottek et al., 2003; Romanello and D'Andrea, 2001; Spray et al., 1981;Stout et al., 2002; Weissman et al., 2004; Ye et al., 2003). Thus, the opening mechanisms as well as the modulation of gap junction coupling is very complex and involves interaction of many different factors at the same time. Gap junctions play an essential role in the early development of the nervous system. In the central nervous system they are expressed in neurons, oligodendrocytes and astrocytes (Dermietzel et al., 1989; Dermietzel and Spray, 1993; Hormuzdi et al., 2001; Hormuzdi et al., 2004; Theis et al., 2005). Gap junctions are prevalent during the early stages of neurogenesis, they form electrical synapses and thus, are crucial for electrical and metabolic signal transduction in developing neurons. For example, rapid propagation of action potentials by connexins allows synchronic neuron activity to occur (Bennett and Zukin, 2004; Hormuzdi et al., 2004).

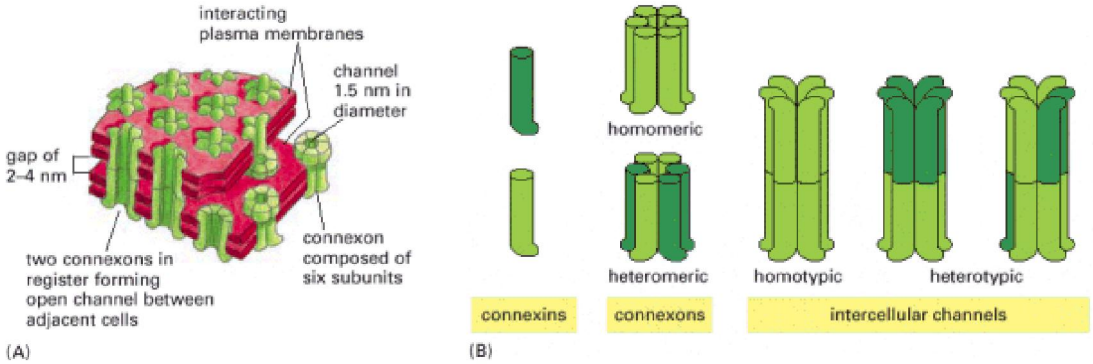

Fig. 5: Schematic structure of gap junctions. (A) A three-dimensional drawing showing interacting plasma membranes of two adjacent cells connected by gap junctions. The lipid bilayers (red) are penetrated by protein assemblies called connexons (green), each of which is formed by six connexin subunits. Two connexons join across the intercellular gap to form a continuous aqueous channel connecting the two cells. (B) The organization of connexins into connexons and connexons into intercellular channels. The connexons can be homomeric or heteromeric, and the intercellular channels can be homotypic or heterotypic (Alberts et al., 2002).

1.2.6 Calcium homeostasis in neurons

Calcium ions act as a second messenger inside neurons to mediate and regulate a wide spectrum of neuronal functions including gene transcription (Bading et al., 1993; Gallin and Greenberg, 1995; Greer and Greenberg, 2008), synaptic transmission (Aguado et al., 2002; Catterall and Few, 2008; Dunlap et al., 1995; Snutch and Reiner, 1992), neurite outgrowth (Ciccolini et al., 2003; Gomez and Spitzer, 1999; Gu and Spitzer, 1995; Kocsis et al., 1994) neuronal development, survival and death (Koike et al., 1989; Porter et al., 1997; Trump and Berezesky, 1996). At their resting state, neurons maintain a baseline intracellular Ca^{2+} concentration ($[Ca^{2+}]_i$) of approximately 100 nM through Ca^{2+} homeostatic mechanisms. This basal concentration is crucial for neurons to respond effectively to various Ca^{2+} signals elicited by extracellular stimuli or membrane depolarizations that often produce a concentration between several hundreds of nanomolar and a few micromolar (Berridge et al., 2003; Clapham, 1995; Clapham et al., 2001). The resting level of $[Ca^{2+}]_i$ is maintained by Ca^{2+}-ATPase-dependent uptake into internal stores via sarcoendoplasmatic reticular Ca^{2+}-ATPAses (SERCA pumps) and extrusion out of the cell via plasma membrane Ca^{2+}-ATPases (PMCA pumps, Clapham, 1995; Garcia and Strehler, 1999) as well as by the Na^+/Ca^{2+} and Na^+/Ca^{2+}-K^+ exchangers (Blaustein et al., 1991; Clapham, 1995).

The diversity of events controlled by Ca^{2+} must partly be a consequence of the distinct types of Ca^{2+} signal that differ spatially, temporally and in magnitude (Berridge et al.,

2000). At the synapse, for example, Ca^{2+} triggers exocytosis within microseconds whereas regulation of gene transcription or cell proliferation occurs within minutes or hours (Berridge et al., 2000; Berridge et al., 2003). The differing outcomes will also be a consequence of the actions of a range of Ca^{2+} sensor proteins that transduce the Ca^{2+} signals into specific intracellular pathways. The specificity of the outcome depends on the affinity of the different sensors for Ca^{2+}, their localization in relation to the Ca^{2+} signal and their interactions with other proteins. A number of Ca^{2+}-binding proteins expressed in neurons have been described including calmodulin (Chin and Means, 2000), synaptotagmin (Fernandez-Chacon et al., 2001) and members of neuronal calcium sensor (NCS) protein family (Burgoyne et al., 2004; Burgoyne and Weiss, 2001). The physiological roles of these proteins include modulation of neurotransmitter release, synaptic plasticity, neuronal growth, control of cyclic nucleotide metabolism, biosynthesis of polyphosphoinositides, regulation of gene expression and in the direct regulation of ion channels (Burgoyne and Weiss, 2001).

Ca^{2+}-signaling systems function often by generating brief pulses of cytosolic Ca^{2+} increase. This Ca^{2+} is derived from either internal stores or from the extracellular medium. In the case of the latter, Ca^{2+} enters cells using different channel families: 1) voltage-gated Ca^{2+} channels (VGCCs) of which several subtypes have been described based on voltage-dependence and pharmacology (L, P/Q, N, R types; Waterman, 2000;Weiss and Burgoyne, 2002; Yamakage and Namiki, 2002); 2) neurotransmitter-gated receptors e.g. muscarinic receptors, metabotropic glutamate receptors, NMDA receptors (Garashchuk and ., 1998; Marshall et al., 2003); 3) second-messenger operated channels e.g. CNG channels (Leinders-Zufall et al., 1997); and 4) capacitive Ca^{2+} channels, which are controlled by the filling state of the cellular Ca^{2+} stores (Berridge et al., 2000; Berridge et al., 2003; Herms et al., 2003; Niu et al., 2009). Several types of intracellular organelle are currently believed to serve as intracellular Ca^{2+} storage compartments including the endoplasmic reticulum (ER), the mitochondria and the nuclear envelope (Blaustein and Golovina, 2001; Gerasimenko et al., 2003; Verkhratsky and Petersen, 1998). There are two major classes of intracellular Ca^{2+} release channels in neurons, ryanodine receptor channels (RyR; Hoesch et al., 2002; Kato and Rubel, 1999; Poulsen et al., 1995; Sandler and Barbara, 1999) and IP3-receptors (IP3Rs; Hoesch et al., 2002; Kato and Rubel, 1999; Nakamura et al., 2000; Poulsen et al., 1995; Yamamoto et al., 2000). RyRs are sensitive to cytosolic Ca^{2+} whereas the IP3Rs are sensitive to both IP3 and Ca^{2+}. The sensitivity of

IP3Rs to both IP_3 and Ca^{2+} enable these receptors to respond differentially to a broad range of stimulus combination and intensities (Berridge et al., 2000; Kaftan et al., 1997).

1.2.6.1 Ca^{2+}-activated currents in neurons

In neurons, an increase in the intracellular Ca^{2+} concentration often causes a change in the membrane permeability for different ions. Ca^{2+}-dependent channels may be classified in two broad categories, which are selective for potassium ions or chloride ions (Hartzell et al., 2005; Marty, 1989; Weiger et al., 2002). Ca^{2+}-dependent K^+ channels are activated by rises in cytosolic calcium, often in response to Ca^{2+} influx via voltage-gated calcium channels that open during action potentials. Activation results in outwardly flowing K^+ current. Activation of Ca^{2+}-activated K^+ channels is involved in the control of a number of physiological processes, ranging from the firing properties of neurons to the control of neurotransmitter release (Vergara et al., 1998; Latorre et al., 1989). Three families of Ca^{2+}-activated K^+ channels have been identified, which can be separated on both biophysical and pharmacological grounds (Shah and Haylett, 2000; Vergara et al., 1998): large conductance maxi-K channels (or BK channels; Marty, 1981), small conductance channels (SK channels; Blatz and Magleby, 1986; Lang and Ritchie, 1987), and intermediate conductance channels (IK channels; Ishii et al., 1997; Joiner et al., 1998). Ca^{2+}-activated Cl^- channels (CaCCs) have been identified in various populations of neurons (Hartzell et al., 2005; Lalonde et al., 2008). They open in response to an increase in intracellular Ca^{2+} due to Ca^{2+} influx through voltage-gated or ligand-gated channels as well as Ca^{2+} release from intracellular stores. Enhanced Cl^- conductance influences V_m and regulates electrical excitability, such as the response to synaptic input or spike rate (Frings et al., 2000). The family of CaCCs consists of at least two functionally distinct groups of channels: 1) CaCCs, which open when Ca^{2+} ions bind to specific Ca^{2+}-binding site on the cytosolic side of the channel protein, and 2) Ca^{2+}/calmodulin-dependent protein kinase II (CaMK II)-activated Cl^- channels, whose activation is mediated by CaMK II. These channels may not posses a Ca^{2+}-binding site and are probably activated upon phosporylation (Frings et al., 2000). The hallmarks of the CaCCs are Ca^{2+} and voltage dependency, outward rectification, permeability for halides and sensitivity to specific pharmacological blockers (Eggermont, 2004; Frings et al., 2000; Matchkov et al., 2004). Three factors dictate the direction of Cl^- movement through the CaCCs: the membrane potential, the Cl^- conductance and the intracellular Ca^{2+} concentration. In most neurons the RMP is more negative than the reversal potential of Cl^- ($E_{rev(Cl-)}$). As a consequence,

when $[Ca^{2+}]_i$ increases, Cl^- exits the cell, which results in the depolarization of the cell membrane (Hartzell et al., 2005).

1.2.6.2 Cell adhesion molecules and Ca^{2+}-signaling

The ability of different cell adhesion molecules (CAMs) to transduce cell surface signals into intracellular responses has been reported (Crossin and Krushel, 2000; Doherty et al., 1991; Doherty and Walsh, 1989; Doherty and Walsh, 1992). The expression of CAMs on the cell surface and the formation of cell-cell contacts has been shown to contribute to neurite outgrowth (Williams et al., 1995) by the activation of G protein-dependent mechanisms (Doherty and Walsh, 1992; Saffell et al., 1997; Schuch et al., 1989). Intracellular Ca^{2+} can be elevated by mobilization of intracellular Ca^{2+} stores through G-protein-linked activation of phospholipase C (Berridge, 1993). L1 and N-CAM (neural cell adhesion molecule) have been reported to activate G_i-like proteins, which inhibit phospholipase C (PLC) leading to reduced level of IP2 and IP3, and thus an increase in $[Ca^{2+}]_i$ via activation of L- and N-type of voltage-gated Ca^{2+} channels (Doherty et al., 1991; Schuch et al., 1989). However, N-CAM has also been shown to activate PLC leading to an increase in production of diacylglicerol (DAG), which is subsequently hydrolyzed to arachidonic acid (AA). AA stimulates an increase in intracellular Ca^{2+} via activation of VGCCs (Doherty et al., 2000; Kiryushko et al., 2006). N-CAM-mediated $[Ca^{2+}]_i$ increase and neurite outgrowth has also been shown to be dependent upon activation of Src-family kinases (Kiryushko et al., 2006), protein kinase C (PKC), or the Ras–mitogen-activated protein (MAP) kinases (Kolkova et al., 2000). Also, another cell adhesion molecule, the limbic system-associated membrane protein (LAMP) promotes neurite outgrowth in different types of neurons via activation of L-type voltage-gated Ca^{2+} channels (Zhukareva et al., 1997). These findings suggest that multiple signaling pathways and mechanisms to change the intracellular Ca^{2+} concentration contribute to cell adhesion molecules-mediated neurite outgrowth and neuronal differentiation.

1.3 Aim of the study

The aim of this study was to investigate the physiological role of CAR in developing cultivated neurons. The following questions were addressed: 1) Does CAR posses a further function in neurons, besides its role as a cell adhesion molecule and a viral receptor? 2) What is the cellular function of CAR? Is CAR involved in neuronal development by influencing intracellular processes such as signaling pathways, neuronal

membrane properties or neuronal morphology and neurite outgrowth? Which intracellular pathways are affected and how are they affected by CAR-mediated processes?
I have chosen an electrophysiological approach and a Ca^{2+} imaging method to search for CAR-mediated cellular mechanisms. Passive and active properties of the neuronal membrane of cultivated CAR KO and WT neurons prepared from E10.5 embryos were investigated. In addition, properties of cultivated cortical neurons prepared from E15 embryos and treated with Ad2, a fiber knob of adenovirus, which binds directly to CAR, were compared to untreated cells. Observed changes in membrane resistance (R_m) suggested altered membrane conductance in CAR KO neurons (E10.5) and Ad2 treated neurons (E15). Therefore, further investigation focused on different ion channels and transport proteins, which directly and indirectly determine passive membrane properties and in particular the R_m. Voltage-gated ion channels, leak channels, ionic pumps and gap junctions were considered to be potential candidates for the observed differences. Furthermore, ionic conductance of particular ions such as K^+, Na^+ or Cl^- across the membrane was studied. The obtained results suggested a role of CAR in the regulation of membrane conductance and a possible implication of CAR in intracellular signaling pathways. Therefore further experiments focused on Ca^{2+}-dependent cascades by means of Ca^{2+} imaging.
In addition, consequences of CAR-mediated processes on the formation and the functionality of neuronal network activity as well as on neuronal outgrowth were studied to test whether CAR might be implicated in these complex mechanisms.

2. Materials and methods

2.1 Materials

2.1.1 Animals

Fertilized chick eggs (*Gallus gallus domesticus)* were delivered by Lohmann Tierzucht GmbH (Germany). Pregnant wild type mice **(***Mus musculus)* C57BL/6N were delivered by Charles River Laboratories (Germany).
Heterozygote CAR mice were obtained from the research group's breeding stock at the MDC animal facility. Generation of CAR-deficient mice by gene targeting has been described by Dorner et al. (2005). Embryos from CAR heterozygous pregnant mice were prepared at embryonic day 10.5. The genotype of each embryo was then verified by PCR as described by Dorner et al. (2005). Only wild type and CAR knock-out (KO) animals were used for experiments.

2.1.2 Cell lines

Parental HeLa cells were obtained from the laboratory's own stock. HeLaCx36 (stable cell line expressing Connexin 36) and HeLaCx43 (stable cell line expressing Connexin 43) were kindly provided by Prof. K. Willecke (Molecular genetics and cell biology of intercellular gap junction channels, Bonn, Germany). Parental HeLa cells were kept in DMEM/10%FCS and transfected HeLa cells were kept in DMEM/10%FCS complemented with 1 µg/ml puromycin (Sigma; P9620). The medium was changed twice a week and cells were split after reaching confluence. Cells were plated on glass coverslips, which were kept in 12-well (or 24-well) plates at a density of 800-1000 cells/mm^2 and maintained at 37°C in a humidified atmosphere of 95% air and 5% CO_2.

2.1.3 Antibodies

Antibodies used in experiments are listed in Table 2.

Antibody	Concentration	Company	Order number
Polyclonal anti-CAR-Fc Rb80	3 µg/ml	AG Rathjen	
Monoclonal anti-CAR RmcB	3 µg/ml	AG Rathjen	
Rabbit anti-Connexin 36	1-2 µg/ml	Zymed Laboratoires	36-4600 (WB)
Rabbit anti-Connexin 36	1-2 µg/ml	Zymed Laboratoires	51-6300 (IF)
Mouse anti-Connexin 43	1-2 µg/ml	Transduction Laboratories	C13729
Rabbit anti-Connexin 43	1-2 µg/ml	Zymed Laboratories	71-0700
Mouse anti-Connexin 26	1-2 µg/ml	Zymed Laboratoires	13-8100
Monoclonal anti-Connexin 32	1-2 µg/ml	Sigma	C6344
Monoclonal anti γ-Tubulin	1 µg/ml	Sigma	T 6557
Mouse monoclonal anti-Na^+/K^+-ATPase alpha 3	1 -5 µg/ml	Novus Biologicals	NB300-540
Goat anti-mouse Cy3	1:400	Dianova	115-165-146
Goat anti-rabbit Cy3	1:400	Dianova	112-165-003
Goat anti-mouse IgG Alexa Fluor 488	1:400	Molecular Probes	A11001
Goat anti-mouse IgG HRP	1:20000	Dianova	115-035-003
Goat anti-mouse IgG AP	1:400	Dianova	115-055-003

Table 2: Antibodies used in immunocytochemical staining and Western blot analysis. Abbreviations: WB – Westen blot, IF – immunofluorescence

2.1.4 Proteins

Fiber knob of Adenovirus

The recombinant fiber knob from adenovirus Ad2 C428N was expressed in *Escherichia coli* (*E. Coli*) bacterial strain BL21-DE3 (Novagen Inc., Madison, WI) and prepared by AG Rathjen following a modified protocol used for Ad12 fiber knob (Freimuth et al., 1999; Howitt et al., 2003). The proteins were purified via ion exchange and nickel-nitriloacetic acid affinity chromatography (Qiagen Inc., Valencia, CA). Fiber knob formed a stable trimer, as assessed by SDS-polyacrylamide gel electrophoresis of unheated protein samples.

In the present work the abbreviation Ad2 is used for the fiber knob.

CAR extracellular Ig-domains: D1, D2 and CAR-D1D2

Both extracellular CAR Ig domains: D1 (D1 122 and D1 213) and D2 as well as CAR-D1D2 were produced by Christopher Patzke (AG Rathjen). CAR fragments were expressed in *E. coli* bacteria as GST-fusion proteins and isolated with glutathione-sepharose beads. GST was removed by proteolytic cleavage and proteins were purified by size-exclusion chromatography.

Proteins used in experiments are listed in Table 3.

Protein	Company (Order Number)	Applied concentration
Ad2 (fiber knob)	AG Rathjen	500 µg/ml
CAR D1 122	Christopher Patzke (AG Rathjen)	100- 500 µg/ml
CAR D1 213	Christopher Patzke (AG Rathjen)	100- 500 µg/ml
CAR D2	Christopher Patzke (AG Rathjen)	100-500 µg/ml
CAR-D1D2	Christopher Patzke (AG Rathjen)	100- 250 µg/ml
Fibronectin	Sigma (F2006)	500 µg/ml
Rb80 CAR AB	AG Rathjen	500 µg/ml

Table 3: Proteins applied in experiments.

2.2 Methods

2.2.1 Cell Culture

Three different embryonic primary cell cultures were maintained: 1) primary cell culture from chick (*Gallus gallus*) embryos prepared between E6-E8 (depending on the tissue) 2) cortical primary cell culture from wild type mice prepared at E15 (*Mus musculus*, C57BL/6N, delivered from Charles River, Germany). 3) telencephalic primary cell culture from wild type and CAR knock-out mice embryos prepared at E10.5 (from AG Rathjen's own CAR breeding in the MDC animal facility).

2.2.1.1 Primary chick cell culture

Solutions:

PBS (phosphate buffered saline, Biochrom)

HBSS (Hank's buffered salt solution, Invitrogen)

Trypsin solution: 1 mg/ml trypsin (Sigma) in HBSS

DMEM/10%FCS: 10% FCS (100%, Invitrogen), 0.05% penicillin/treptomycin (Sigma), DMEM (Dulbecco's modified eagle medium, Invitrogen)

DMEM/N2: 2% N2 supplement (Invitrogen), 0.05% penicillin/streptomycin (Sigma), DMEM (Invitrogen)

Lumox dishes and chamber slide preparation

Permanox chamber slides (Nunc) were mounted on sterile lumox membrane dishes (6 chambers per dish, Greiner Bio One). Each chamber was coated with laminin (10-12 µg/ml, Invitrogen), poly-D-lysine (PDL, 0.1 mg/ml, Sigma) or fibronectin (5 µg/ml, Sigma) over night at 37°C. Before the cells were plated, the chambers were washed twice with HBSS and once with DMEM/10% FCS.

Cell culture

Primary retinal cultures were prepared from chick eye on embryonic day 8 (E8) in HBSS. Dissected retinal cells were suspended in 1 mg/ml trypsin solution for 20 min at 37°C, washed twice with DMEM/10%FCS followed by washing in serum free DMEM containing the N2 supplement. Cells were then triturated with a glass pipette to dissociate the cells. The cells were plated on laminin (or PDL and fibronectin) treated permanox chamber slides (Nunc) in a total volume of 150 µl per chamber and a cell density of 500-650 cells/mm^2. Cell cultures were maintained at 37°C in a humidified atmosphere of 95% air and 5% CO_2.

The same protocol was used for telencephalic and tectal cultures prepared from chick brain on embryonic day 6 (E6).

2.2.1.2 Primary mouse cell culture E15

Solutions

HBSS: 10 mM HEPES (4-(2-hydroxyethyl)-1-piperazineethanesulfonic acid; Roth), 6 mM Glucose in HBSS (Hank's buffered salt solution; Invitrogen)

S1: papain 35U (Sigma), L-cysteine 0.02%, $CaCl_2$, 0.2 mM, EDTA (ethylenediaminetetraacetic acid; Merck), 0.1 mM in HBSS

S2: 0.35 mM BSA (bovine serum albumin, Biomol), 1.25 mM trypsin inhibitor (Roche), 0.06% DNase (Sigma) in Neurobasal (NB) medium

NB/10%FCS: 10% FCS (100%, Invitrogen), 25 µM β-mercaptoethanol (Merck), 0.25 mM L-glutamine (Sigma), 0.05% penicillin/streptomycin (Sigma), 2% BEM amino acid (50x; Sigma) in Neurobasal (NB) medium (Invitrogen)

NB/B27: 2% B27 supplement (100%, Invitrogen), 25 µM β-mercaptoethanol (Merck), 0.25 mM L-glutamine (Sigma), 0.05% penicillin/streptomycin (Sigma), 2% BEM amino acid (50x; Sigma) in Neurobasal (NB) medium (Invitrogen)

Coverslip preparation

Glass coverslips (12 or 15 mm diameter; Assistant) were treated for 5 hours with alkaline (NaOH/Ethanol (100%)), then washed 5 times with distilled water and treated with 3.2 % HCl for 5 hours, again washed 5 times with distilled water and then treated with 100 % ethanol. Coverslips were dried over flame, placed in 12-well or 24-well plates and coated with PDL (0.1 mg/ml, Sigma) over night at 37°C. Before the cells were plated, PDL was

removed and the coverslips were washed twice with HBSS containing HEPES and glucose and once with NB/10%FCS.

Cell culture

Primary cortical cultures were prepared from mouse brains on embryonic day 15 (E15, WT, C57/B6N strain, Charles River, Germany) in PBS. Dissected cortical hemispheres were suspended in papain solution (S1) for 10 min at 37°C, washed once in protease inhibitor solution (S2), twice in NB/10%FCS and then triturated with a glass pipette to dissociate the cells. Cells were plated in 12-well (or in 24-well) plates with washed and PDL treated glass coverslips (Assistant) at a cell density of 600-700 cells/mm^2. After the neurons had attached to the substrate (after 24 hours), NB/10%FCS was partly removed and the neurons were maintained in NB/B27 medium. Cell cultures were maintained at 37°C in a humidified atmosphere of 95% air and 5% CO_2.

2.2.1.3 Primary mouse cell culture E10.5

Solutions

PBS (phosphate buffered saline, Biochrom)

HBSS (Invitrogen)

Trypsin solution: 1 mg/ml trypsin (Sigma) in HBSS

DMEM/10%FCS: 10 % FCS (100%, Invitrogen), 0.05 % penicillin/streptomycin (Sigma), DMEM (Dulbecco's modified eagle medium, Invitrogen)

DMEM/B27: 2% B27 supplement (Invitrogen), 0.0 5% penicillin/streptomycin (Sigma), 10 ng/ml BDNF (Brain-derived neurotrophic factor; Pepro Tech), DMEM medium (Invitrogen)

Coverslip preparation

Termanox plastic cover slips (Nunc) were coated with 10 µg/ml laminin (Invitrogen) over night at 37ºC. Before the cells were plated, coverslips were washed twice with HBSS and once with DMEM/10%FCS.

Cell culture

Telencephalic parts of mouse brain were prepared on embryonic day 10.5 (E10.5). Tail samples of each embryo were harvested for genotyping by PCR analysis. Each telencephalon tissue was collected separately in a falcon tube with HBSS. Dissected tissue was suspended in trypsin (1 mg/ml) solution for 10 min at 37°C, washed twice with

DMEM/10% FCS and then triturated with a glass pipette to dissociate the cells. Cells were plated on termanox cover slips at a cell density of 400-750 cells/mm^2. After the neurons attached to the substrate (after 24 hours), DMEM/10%FCS was partly removed and the neurons were maintained in DMEM/B27/BDNF medium. Cell cultures were maintained at 37°C in a humidified atmosphere of 95% air and 5% CO_2.

2.2.2 Genotyping of CAR mice by PCR and DNA electrophoresis

Tail samples from embryos at embryonic day 10.5 (E10.5) were digested in 200 µl tail lysis buffer (Viagen DirectPCR-Tail, PeqLab) and 100 µg/ml proteinase K (Roche) over night at 55ºC. Proteinase K was inactivated by heating the samples to 85ºC for 45 min. Samples were centrifuged for 10 sec at 14000 rpm. Supernatants containing DNA were used for PCR.

Genotyping was carried out with 2 µl tail lysate and 0.2 µl LA Taq polymerase (TaKaRa BIO INC) in a mix buffer containing: 11.38 µl digest water, 2 µl buffer La 10x, (TaKaRa BIO INC), 2 µl 25 mM $MgCl_2$ (TaKaRa BIO INC), 3.2 µl dNTP Mix (2.5 mM; TaKaRa BIO INC) and primers: G53, Dor25, Neo2L (Table 4) in a total volume of 20 µl. The following PCR program was used: 96°C/2 min, 94°C/4 min, (95°C/44 sec, 68,7°C/45 sec, 72°C/2 sec+1 sec per cycle) x39 cycles, 72°C/10 min. PCR products were analyzed on 1 % agarose gels containing ethidium bromide and visualized by exposure to ultraviolet (UV) light.

G53 (WT)	5’ ATC CCG CAC AAG AGC ACG AAG 3’
Dor 25	5’ CAC TTC TAA ATA ACT TGC CCA CCA AGA 3’
Neo2L (K.O.)	5’ GGC ATC AGA GCA GCC GAT TG 3’

Table.4: Primer sequences for CAR genotyping.

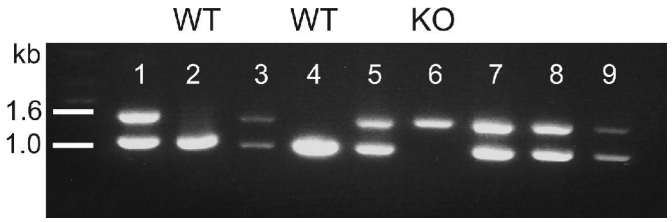

Fig. 6: PCR products for genotyping were separated on 1 % agarose gel. 1.0 kb band represents WT (nr. 2, 4), 1.6 kb band represents CAR-/- (nr.6), both bands (1.0 and 1.6 kb) represent heterozygote (1, 3, 5, 7, 8, 9).

2.2.3 SDS-PAGE and Western blot

Tissue preparation

Brain tissue of wild type mice from different postnatal developmental stages (P1- P30 (adult)) and telencephalic tissue of wild type and CAR knock-out embryos at 10.5 were homogenized in detergent solution containing 1 % octylglucoside (Sigma) and protease inhibitors: 20 µl Aprotinin (Sigma), 20 µl Pepstatin A (Sigma), 20 µl Leupeptin (Sigma), 10 µl PMSF (phenylmethyl sulfonyl fluoride; Sigma) in 10 ml PBS. Homogenates were centrifuged for 15 min at 4°C at 14000 rpm. Supernatants were used for further experiments. Protein concentration was determined by measurement of UV absorbance at 280 nm using a photometer (Biophotomether 6131, Eppendorf, Hamburg). Sample-buffer (100 mM Tris, pH 6.8, 2% SDS (sodium dodecyl sulphate), 15 % glycerol, bromophenol blue) and βME (β-mercaptoehanol, Merck) were added and the samples were boiled for 3 min at 95°C. 10-25 µg of total protein was loaded per lane and analyzed by SDS-PAGE and Western blot.

SDS-PAGE

Solutions

1M Tris-HCl (tris(hydroxymethyl)aminomethane-HCl; Merck), pH 8.8
1M Tris-HCl, pH 6.8
30% acrylamide/0.8 % piperazine diacrylamide (PDA)
10% SDS (sodium dodecyl sulphate) buffer in distilled water
10% ammonium persulfate (AP, 0.1mg/ml; PlusOne) in distilled water
N,N,N',N'-tetramethylethylene diamine (TEMED; PlusOne)
10x running buffer
0.1 % SDS running buffer

10x running buffer

30.3 g Tris base
144 g glycine, all diluted in
1 l distilled water
pH = 8.3

10% separating gel (total volume: 10 ml)

2.8 ml distilled water
3.75 ml 1M Tris pH 6.8
100 µl 10% SDS
3.3 ml 30% acrylamide/0.8% piperazine diacrylamide (PDA)
50 µl 10% AP
5 µl TEMED

Stacking gel (total volume:10 ml)
3.7 ml H_20
625 µl 1 M Tris pH 6.8
50 µl 10% SDS
650 µl 30% acrylamide/0.8% piperazine diacrylamide (PDA)
50 µl 10 % AP
5 µl TEMED

Transfer buffer
10% 10x running buffer
20% Methanol (Merck)
70% distilled water

Samples were electrophoresed on 10-12% SDS-PAGE gels at 90-150 V for 1 hour followed by electrotransfer of the separated polypeptides onto blotting paper (nitrocellulose membrane) in cold transfer buffer. The gel, nitrocellulose membrane, and blotting papers were arranged in a transfer cassette and put in a transfer tank filled with cold transfer buffer. Transfer was run for 1 hour at 340 mA. After transfer, the blots were washed in PBS and loaded protein was verified using Ponceau red staining followed by washing in H_2O and PBS/0.5% Tween 20. Blots were incubated in 4% milk blocking solution for 1 hour at room temperature (RT), washed 3 times with PBS/0.5% Tween 20 (Sigma) and primary antibodies were applied in 4% milk solution over night at 4°C. Blots were washed in PBS/0.5% Tween 20 and the appropriate secondary antibodies (alkaline phosphatase-conjugated antibody, in dilution: 1:400 or horseradish peroxidase enzyme (HRP)-conjugated antibody, in dilution 1:20000; Dianova) in 4 % milk solution were applied for 2 hours at RT. Finally, blots were analyzed using the enhanced chemiluminescence (ECL) detection system or alkaline phosphatase (AP) system. For the

AP detection system, blots were incubated in substrate solution consisting of AP-buffer with 1% BCIP (5-bromo-4-chloro-3-indolyl phosphate, Roth), and 1.5% NBT (nitro-blue tetrazolium Chloride; Sigma), until protein bands appeared. The reaction was stopped by washing with distilled water.

AP-buffer

100 mM Tris pH 9.7

5 mM $MgCl_2$

0.01 mM $ZnCl_2$

Distilled water

Substrate solution

1% BCIP (5-bromo-4-chloro-3-indolyl phosphate) in 100% DMF (dimethylformamide)

1.5% NBT (Nitro Blue Tetrazolium) in 70% DMF

AP-buffer

For the enhanced chemiluminescence detection system, blots were incubated for 1 min in substrate solution consisting of equal parts of peroxide solution (detection reagent 1) and Luminol enhancer solution (detection reagent 2; Pierce ECL Western Blotting Substrates, Thermo Scientific). After 1 min blots were removed from the working solution and placed in a clear plastic wrap. Excess liquid was removed with absorbent tissue and air bubbles between the blot and the plastic wrap were pressed out. The blot was then placed in a film cassette with the protein side facing up. In the dark, the Lumi-film (Lumi-Film Chemiluminescent Detection Film, Roche) was placed on top of the membrane and different exposure times were applied, between 10 sec and 1 h, to achieve optimal results. The film was developed using the Curix 60 processing machine (Agfa).

2.2.4 Immunocytochemistry

For immunocytochemistry, cells on cover slips were fixed with 3.7 % formaldehyde (FA) in phosphate-buffered saline (PBS, pH 7.4) for 10 min at RT, and then washed three times with PBS containing 0.1% BSA followed by washing with NH_2Cl for 15 min at RT. Cells were then permeabilized with PBS/0.1%BSA containing 0.1% Triton X-100 (PBS/BSA/T-X) and incubated with primary antibodies (Table 2) for 60 min at RT and then washed three times with PBS/0.1% BSA. The secondary antibody (anti-rabbit or anti-mouse, coupled to Cy3 or Alexa 488, Table 2) at a dilution of 1:400 was applied for 45 min at RT

and cells were then washed three times with PBS/0.1% BSA and mounted using 10% moviol (Sigma) on glass slides.

For cell surface staining, cells on cover slips were incubated with primary antibody (Table 2) for 10 min at 37ºC, washed, then fixed in 3.7% formaldehyde in PBS for 10 min and the washed three times in PBS for 10 min. After washing, cells were incubated with secondary antibody (anti-rabbit or anti-mouse, coupled to Cy3 or Alexa 488, Table 2) for 45 min at RT and cells were then washed and mounted in 10% moviol on glass slides.

Fluorescent images of the neurons were obtained using the Axiovert 135 Fluorescent Microscope (Zeiss, Germany) linked to the AxioCam MRc Camera (Zeiss, Germany) and AxioVision software.

2.2.5 Electrophysiology

2.2.5.1 Basic principle

Electrophysiological techniques are used to study the function of ion channels by recording either the currents that flow through open ion channels or by observing changes in voltage across the membrane. From such recordings, active and passive membrane properties (e.g. membrane potential, calculation of the membrane resistance) as well as information about synaptic activity may be obtained.

The patch clamp technique was invented by Neher and Sakmann in 1976 in order to study currents through single acetylcholine-activated channels in cell-attached patches of cell membrane of the frog skeletal muscle (Neher et al., 1978; Neher and Sakmann, 1976). Subsequent improvements (Hamill et al., 1981) have led to high resolution recordings of currents in cell-attached, whole-cell and in isolated membrane patches. The patch (or voltage) clamp technique is one of the most powerful methods available for studying functional aspects of ion channels.

Single ion channel recordings were carried out by clamping the voltage across a small patch of membrane on a surface of a cell by a glass microelectrode with a tip of about 1 µm in diameter (patch electrode, cell-attached mode, Fig. 7 B; Hamill et al., 1981). Such recordings provide information about unitary conductance and kinetic properties of ionic channels. Disadvantages arise from the fact that the cell is still intact. Thus, the composition of the intracellular solution and the patch potential are unknown, in contrast to recording in the whole-cell patch-clamp mode.

One of the most important requirements for the patch-clamp technique is the ability to form a tight seal between the patch electrode (filled with suitable electrolyte solution) and the plasma membrane of the targeted cell. This seal should have an electrical resistance in the range of gigaohms (10^9 Ohm) and is called “gigaseal”. Under these conditions the glass pipette and the cell membrane will be less than 1 nm apart. The gigaseal is important for two reasons: 1) the higher the seal resistance, the better the electrical isolation between the membrane patch and the pipette; 2) high seal resistance reduces the noise of recordings, allowing high resolution of single channel currents. Because of the high mechanical stability of the seal, beside the cell-attachted mode, three other voltage clamp recording configurations can be used: inside-out, whole-cell and outside-out (Fig. 7 B).
In the whole-cell voltage-clamp configuration (Fig. 8) a patch of membrane is electrically isolated from the surrounding solution by pressing an electrolyte-filled glass patch pipette against the surface of the cell and subsequently applying suction. A silver/silver chloride electrode couples the electrolyte in the patch pipette to a special electrical circuit shown schematically in Fig. 7 A. While maintaining a gigaseal the cell membrane under the patch pipette is removed using suction so that the cell, whose intracellular solution comes in contact with the solution in the pipette, may be voltage clamped (or current clamped) across the entire cell (and not only across the tiny patch, Fig. 7 B). The cell contents equilibrate over the recording time with the pipette solution and this is how the intracellular solution can be experimentally determined. During the whole-cell voltage-clamp, two basic electrical functions are performed: 1) control of voltage and 2) measurement of flowing current. Thus, this method can be useful in providing measurements of both passive (cell capacitance (C_m), membrane resistance (R_m), Fig. 8) and active membrane properties of voltage-gated channels e.g. sodium channels as well as synaptic currents (e.g. miniature postsynaptic currents). Current clamp mode in the whole-cell configuration provides information about the RMP and allows action potentials to be recorded.
Figure 7 A represents the equivalent electrical circuit for the patch clamp recording set up.

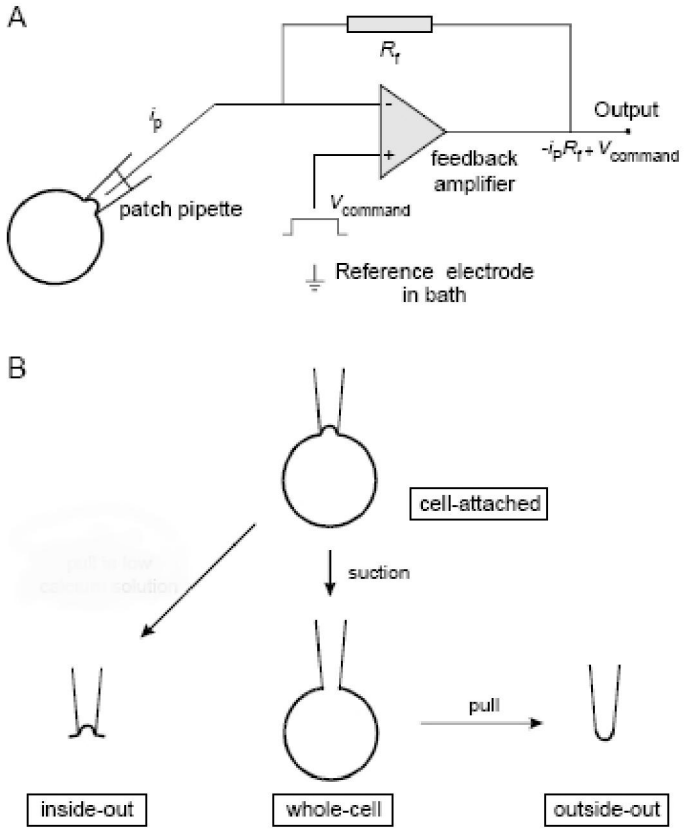

Fig. 7: Schematic patch-clamp circuit with the main features of the headstage amplifier used in patch-clamp experiments. (A) The patch pipette is connected to the negative (-) input of a feedback amplifier. The positive (+) input of the feedback amplifier is connected to a variable voltage source and can be set at a desired value (holding potential, V_h, $V_{command}$). In the case of voltage differences between these two inputs of the feedback amplifier, current is delivered from its output so that the patch pipette is clamped at the holding potential. The current through the patch (i_p) is measured as the voltage drop across the feedback resistor (R_f). (B) Three different patch-clamp configurations: inside-out, whole-cell and outside-out.

2.2.5.2 Circuit in the whole-cell patch-clamp configuration

After formation of the gigaseal the cell membrane was ruptured and a test pulse of 10 mV was applied (Fig. 11 A left side). A successful opening of the cell is indicated by the current response to the test pulse in the form of large capacitive transients (Fig. 9 A, C) at the beginning and end of the voltage pulse. The transient response is formed by the cell capacitance (C_m) in series with the pipette (R_p) and access resistance (R_a, Fig. 8). Pipette resistance and access resistance are connected in series and form a circuit called series resistance (R_s, $R_s=R_a+R_p$, Fig. 8). A large, quick capacitive transient indicates optimal combination of good cell capacitance and low series resistance. After capacitance transients, a steady-state component determined by the membrane resistance appears (R_m,

Fig. 8). R_m and R_s are also connected in series (series circuit, Fig. 8). The R_m is the largest resistor and R_s (R_a+R_p) should be kept as low as possible so that it causes only a very small voltage drop in the series circuit. The measured current represents mostly current flowing through the cell membrane.

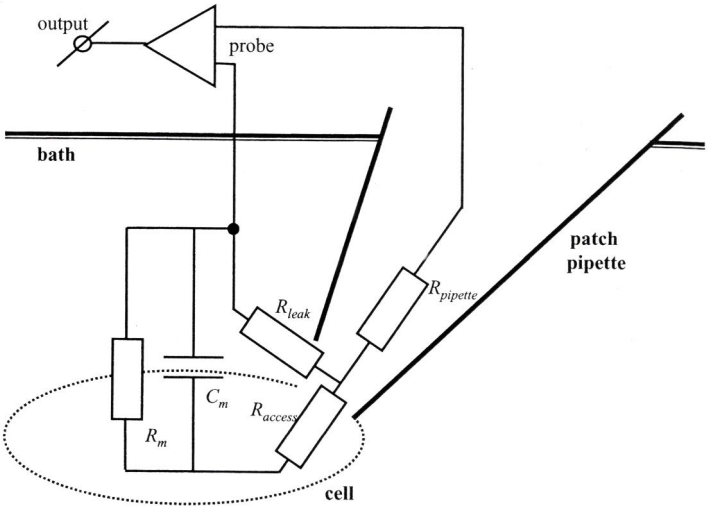

Fig. 8: Equivalent circuit for the whole-cell patch clamp configuration (modified from Molleman, 2002).

2.2.5.3 Electrophysiology in cell culture

Whole-cell patch-clamp recordings using the conventional whole-cell configuration were performed on 1- to 20-day-old cultured neurons prepared at embryonic day 15 (WT) and 10.5 (CAR WT and CAR-/-). For electrophysiological recordings, cells were placed in a recording chamber (chamber volume < 1 ml) containing bathing solution (Table 5, 6). All experiments were performed at room temperature (20 - 25°C). Whole-cell recordings were performed using an EPC-10 amplifier and Tida 5.2 software (HEKA, Lambrecht, Germany). Patch pipettes were made from borosilicate glass (Borosilicate Glass Capillaries, Kwik-Fil, World Precision Instrument, USA) and, when filled with the intracellular solutions (Table 7, 8), had a resistances of 2–5 MOhm.

The liquid junction potential (LJP) was defined as the potential of the bath solution with respect to the pipette solution (Barry and Lynch, 1991). For solutions used in experiments the LJP was calculated using JPCalc computer program, provided by Prof. Barry (Barry, 1994). Before pipette contact to the cell, an online correction of the calculated LPJ and pipette offset was conducted using the V0Auto function in the Tida software. In general, small junction potentials (-3 – - 8 mV) were introduced by using a silver:silver chloride electrode during recordings. A high salt (3 M KCl) agar (3% agarose) bridge was

employed only in experiments with altered chloride concentration (Shao and Feldman, 2007).

After a gigaohm seal was formed, breakthrough to whole-cell mode was achieved by applying gentle suction. For standard whole-cell recording, cells were clamped at a holding potential (V_h) of -70 mV (voltage-clamp, VC). Different voltage step-protocols were applied in order to characterize passive and active cell membrane parameters as well as synaptic activity.

2.2.5.4 Equations and voltage protocols used in experiments

Access resistance (R_a), membrane resistance (R_m) and membrane capacitance (C_m) as well as specific membrane resistance (R_m *specific*) are described as passive membrane properties under RMP conditions. R_a, R_m, C_m and R_m *specific* values were obtained from currents induced by 10 mV steps, at V_h of -70 mV to -60 mV (ΔU=10 mV) for 200 ms (Fig. 9 A, B; Fig. 11 A) and calculated by the following equations:

$R_a = \Delta U / I_{max}$ (MOhm); ΔU=10 mV

$R_m = \Delta U / I_{offset}$ (MOhm)

$C_m = 1/\Delta U * \text{Int Idt}$ (pF)

R_m *specific* = $R_m * C_m$ (kOhm*cm^2) where C_m (pF) is converted to a specific membrane capacitance presented as 1µF/cm^2 (Cole, 1968).

Only cells with R_a lower than 30 MOhm were selected for further analysis.

Application of a 10 mV voltage step (U) to cells clamped at V_h= -70 mV resulted in current (I) flow through the cell membrane (resistance, R). This current was measured and membrane resistance was calculated using Ohm's low: R = U/I (Fig. 9 A, B). Additionally to the 10 mV steps, the membrane resistance was estimated by application of 3 hyperpolarizing (-5, -10, -15 mV) steps and 3 depolarizing steps (5, 10, 15 mV) from V_h= -70 mV, each step for 200 ms. The R_m was calculated relating applied voltage (V) and measured current (I; I-V relation, Fig. 11 A). Both calculation methods revealed the same results, thus the one step protocol was primarily used. Calculation of R_m was obtained in the range of the RMP, when the cell is clamped at -70 mV and the 10 mV or 5, 10, 15 mV voltage steps did not activate voltage gated sodium (Na^+), potassium (K^+) or calcium (Ca^{2+}) channels (linear slope see Fig. 3 C, 18 C, Fig. 19 C). Thus, the measured current used to calculate the R_m was a mixture of different ions, cations and anions passively moving across the cell membrane, out of or into the cell, due to their electrochemical

gradients, through different specific and non-specific ion channels (leak current channels), transporters, co-transporters and/or ion pumps.

For activation and opening of voltage-gated ion channels, a specific voltage threshold has to be reached. Usually this voltage threshold is about 30 - 40 mV less negative than the RMP e.g. around -40 mV for voltage-gated Na^+ channels. Activation threshold, maximal amplitudes and current density (current/cell capacitance) for voltage-gated K^+, Na^+ and Ca^{2+} channels were obtained from the current-voltage (I-V) relation.

For I-V relation of voltage-gated K^+ and Na^+ channels,10 mV depolarizing voltage steps were applied from V_h= -70 mV to +30 mV (10 steps, each for 200 ms), then 10 hyperpolarizating correcting steps from -70 to -90 mV were applied to correct the passive ion (leak) conductance from voltage activated currents (Fig. 11 B left side). For these recordings KCl-based IC (Table 7, 8) and NaCl-based EC solutions (Table 5, 6) were used.

For voltage-gated Ca^{2+} channels (VGCCs) 12 depolarizing steps from V_h = -90 mV to +30 mV (200 ms) and then 12 correcting steps (from -90 to -110 mV) were applied (similar as in Fig. 11 B left side, V_h = -90 mV instead of -70 mV). For these recordings VGCCs-IC solution (Table 7, 8) and VGCCs-EC solution (Table 5, 6) containing different blockers for K^+ (CsCl, TEA-Cl, Apamin, 4-AP) and Na^+ (TTX) currents were used. In VGCCs-EC solution, 2 mM $CaCl_2$ was replaced by 10 mM $BaCl_2$. The substitution of Ca^{2+} by Ba^{2+} increases current magnitudes, because Ba^{2+} has higher permeability through high voltage-activated (HVA) calcium channels, allowing for a more accurate characterization of VGCC properties.

In addition to the depolarizing steps used for channels opening by depolarization, hyperpolarizing steps (10 mV steps, each for 200 ms) from V_h= -70 mV to -160 mV were applied in order to look for ion conductance under hyperpolarized conditions (Fig. 11 C). Some ion channels, such as HCN channels, are non-specific cation channels, which open due to hyperpolarization. Thus, at first 3 depolarizing control steps, 5, 10 and 15 mV from V_h= -70 mV, were applied and then 9 10 mV hyperpolarizing voltage steps from V_h= -70 mV to -160 mV (200 ms).

In some experiments (junctional conductance of HeLa cells or measurements of chloride current) another I-V protocol was applied. 10 depolarizing and then 10 hyperpolarizing 10 mV steps, each for 200 ms (for Cl^- current) or for 10 s (for junctional conductance), from V_h = -70 mV or V_h = 0 mV were applied (Fig. 11 D).

Depending on which ion conductance/current was the experimental goal, suitable IC and EC solutions, blockers and modulators (Table 9) as well as appropriate I-V protocols were applied.

On I-V plots the negative currents correspond to an inward current and thus to cation influx or anion efflux across the plasma membrane, whereas positive currents - the outward currents, represent either cation efflux or anion influx (Halm and Frizzell, 1992; Hammond, 2001; Herness and Sun, 1999).

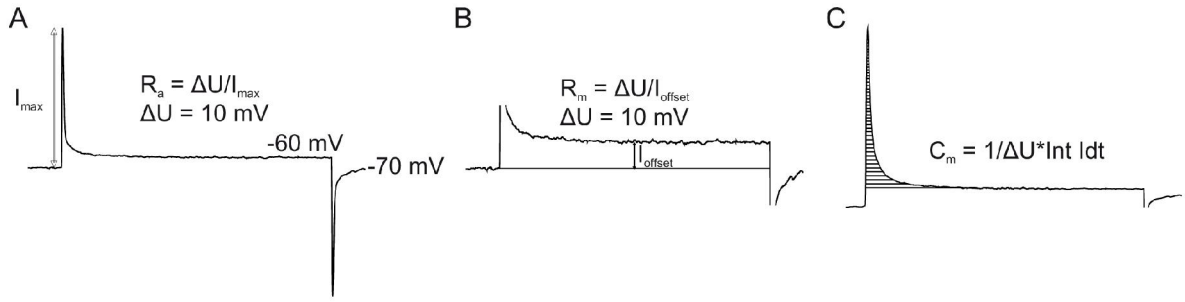

Fig. 9: Estimation of passive membrane properties. (A, B) Access resistance (R_a; A) and: membrane resistance (R_m; B) is calculated by Ohm's law. (C) Cell capacitance (C_m) is calculated using an integral equation.

Besides passive and active parameters, synaptic activity of neurons was recorded. Application of specific blockers (Table 9) made is possible to distinguish between spontaneous or miniature currents as well as between inhibitory and excitatory currents. Synaptic activity was recorded from each cell 10 times for 10 s in voltage clamp (V_h = -70 mV). Recordings were made for up to 10 min from each cell, depending on changes in series resistance. Current amplitudes, frequency and kinetic parameters of synaptic events (decay time constant (tau; τ), rise time, Fig. 10) were analyzed with customized software (Tida (Heka), PeakCount, Origin 7 (Microcal Software, Northampton, Ma)). The rise time was estimated as the time needed for a 10–90% increase of the peak current response (Fig. 10). Decay time constants (tau, τ) were calculated by fitting single exponential functions to each measured postsynaptic current using the following algorithm:

$f(x)= a + b*e^{(time/\tau)}$

Where:

a – baseline offset

b – current amplitude

e^x – mathematical constant, exponential function, e ≈ 2.72

τ – decay time constant

The decay time constant (τ) is the time it takes for the synaptic current to decay by 1/e (1/2.72 = 0.367 ≈ 37%), meaning a decay of about 37% of its peak amplitude (Fig. 10).

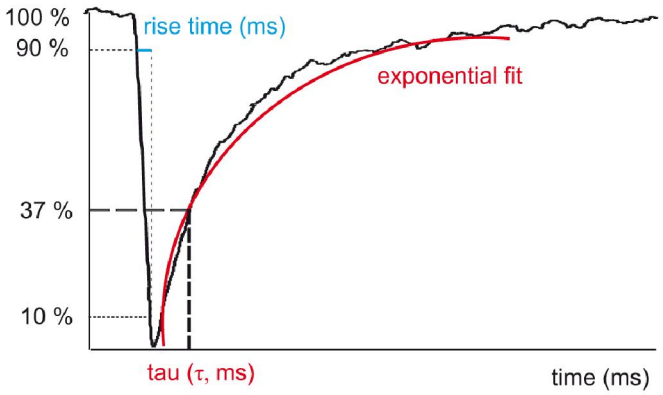

Fig. 10: Kinetic parameters of synaptic current: decay time constant (tau, τ in blue) and exponential fit curve to calculate the rise time (10-90%, in red)

Measurement of the RMP and recording of action potentials (APs) was achieved in whole-cell current-clamp (CC) mode. Data were collected from cells with membrane potentials more negative than -35 mV for cells prepared at E10.5 and -40 mV for cells prepared at E15. It has been observed that RMP becomes more negative in cultured neurons during development. RMPs were recorded using either KCl-based IC or CsCl-based IC and NaCl-based EC, with low or high osmolality, according to the cell culture.
Besides the RMP, spontaneous APs, occurring at the real RMP of the cell (-40 - -70 mV) were recorded to analyze their frequency. In addition to the spontaneous APs recorded, generation of APs was induced by application of current steps. 20 steps of 20 pA (each for 200 ms) were applied to the cell (Fig. 12) and the frequency of recorded APs was analyzed.

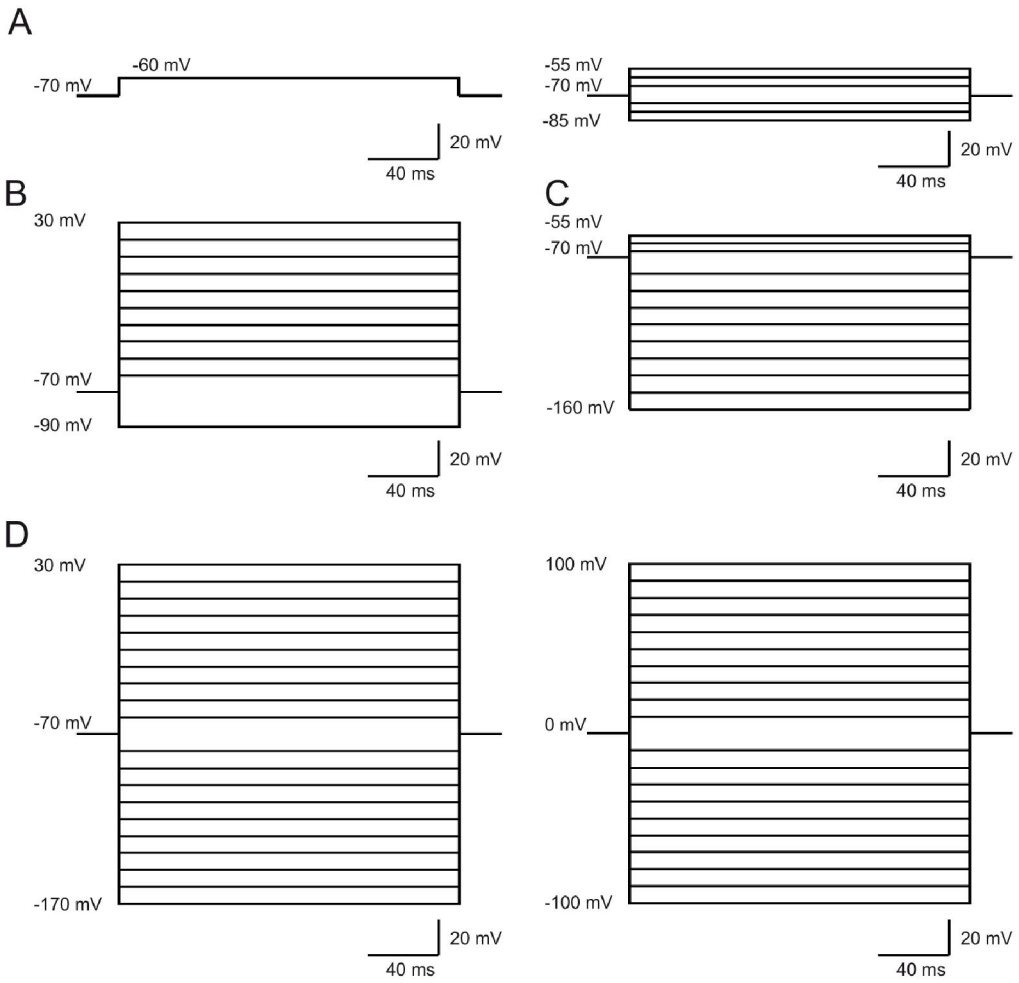

Fig. 11: Voltage protocols used during patch-clamp recordings. (A) Voltage steps to estimate the passive membrane properties (e.g. R_m, C_m). (B, C) Depolarizing (B) and hyperpolarizing (C) voltage steps for activation of voltage-gated channels, with correcting steps. (D) Depolarizing and hyperpolarizing voltage steps without correcting steps.

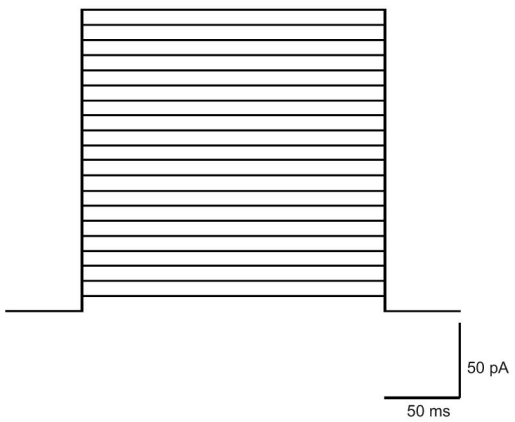

Fig. 12: Current injection protocol for AP recording in current-clamp mode, 20 steps each 20 pA for 200 ms.

2.2.5.5 Double patch-clamp

Double whole-cell patch-clamp method was used to characterize junctional membrane conductances in HeLa cell-pairs transfected with connexin 36 (Cx36). Recordings were performed similarly to the approach described by Spray (1981). For these recordings the double EPC-9 amplifier and Tida software (HEKA, Lambrecht, Germany) were used. In general, the same procedure was applied as in single whole-cell patch-clamp. Two tight neighbor cells were selected and each of them was approached by a recording pipette (Fig. 13). A gigaseal was formed for cell 1 and then for the second cell (cell 2). After that both of them were opened and clamped at the holding potential: V_h= -70 mV or at 0 mV, and different voltage protocols were applied (Fig. 11 C) in order to characterize and quantify coupling of cells. 10 mV steps were applied for 10 s in order to test the voltage-dependency of electrical coupling.

Junctional voltage (V_J), junctional current (I_J) and junctional conductance (G_J) were calculated using the following equations:

$V_J=V_2-V_1$

$I_J=I_2$

$G_J=I_2/V_J$

Where:

V_J – junctional voltage

V_1 – membrane potential of cell 1

V_2 – membrane potential of cell 2

I_J – junctional current

I_1 – current flowing through the membrane of cell 1

I_2 –current flowing through the membrane of cell 2

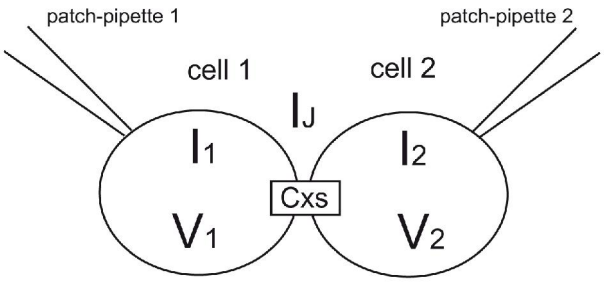

Fig. 13: Scheme of double patch-clamp recording. Two adjacent cells (cell 1 and cell 2) are connected by connexins (Cxs). Application of voltage to the first cell (V_1) generates current flow in the cell (I_1), which flows through Cxs, generating a junctional current (I_J) that can be recorded in the second cell (I_2).

2.2.5.6 Reversal potential (E*rev*) and Nernst equation

The reversal potential (E*rev*) of a particular ion is the membrane potential (V_m) at which there is no net flow of these ions from one side of the membrane to the other. The direction of ion flow through the membrane depends on its concentration, its charge and the V_m. The neuronal membrane shows a negative membrane potential, about -70 mV, caused by unequal distribution (concentrations) of differently charged ions across the membrane e.g. low K^+ concentration in the cell ($[K^+]_{in}$= 3 mM), but high concentration outside the cell, ($[K^+]_{out}$= 120 mM). This difference forces ions to move across the membrane in order to balance unequal concentration (chemical gradient). On the other hand each ion possesses an electric charge (e.g. K^+ has a positive charge: +1, Cl^- has a negative charge: -1), which forces the ion to move along its electrical gradient. Together these two forces (chemical and electrical gradients) produce an electrochemical gradient for a particular ion to move across the cell membrane. At the V_m when both of these forces counterbalance and there is no net flow of this ion, the reversal potential (E*rev*) for a particular ion has been reached.

E*rev* can be calculated from the Nernst equation:

$$E= RT/zF*\ln([Ion]_{in}/[Ion]_{out})$$

Where:

R – universal gas constant: R = 8.314472 $JK^{-1}mol^{-1}$
T – absolute temperature in Kelvin; 298.15 K (25°C)
z – ion valence
F – Faraday constant, $F = 9.64853399\times10^4\ Cmol^{-1}$
$[Ion]_{in}$ - concentration of ions in the cell
$[Ion]_{out}$ – concentration of ions outside the cell

The concentration of a particular ion is known because the composition of the pipette solution and extracellular solution is established by experimentator (Table 5-8). Thus, for each ion present in the solution, the E*rev* could be calculated (Table 13). Changing ion concentration or replacing a particular ion by another, also changes the value of E*rev* (E*rev* shift, Table 13; Hammond, 2001; Kandel et al., 2000).

2.2.5.7 Solutions, modulators and blockers

Solutions

Thelencephalic cells prepared at E10.5 were cultivated in high osmolality DMEM medium (ca. 340 mOsmol/kg), whereas the cortical cells prepared at E15 were maintained in low osmolality neurobasal medium (ca. 230 mOsmol/kg). Thus, two different osmolality range solutions were used. Low osmolality solutions were used for cortical neurons prepared at embryonic day 15 (E15), with the extracellular (EC) solution adjusted to 230-240 mOsmol/kg and the intracellular (IC, pipette solution) to 190-210 mOsmol/kg. High osmolality solutions were used for neurons prepared at E10.5, with EC adjusted to 330-340 mOsmol/kg and IC adjusted to 290-310 mOsmol/kg. A solution's osmolality was verified before each experiment, using a Vapor Pressure Osmometer 5520 (Wescor), calibrated with 290 mOsmol/kg osmolality standard (Opti-Mole). All solutions were adjusted to pH 7.3 with NaOH for EC and KOH for IC.

Different EC and IC solutions were used depending on the aim of the recording (Table 5-8). NaCl based EC and KCl-based IC solutions were used for control recordings of passive and active cell parameters as well as all for recordings of synaptic activity. Other solutions were used depending on the aim of the experiment e.g. in order to look on ion conductance across the membrane for a particular ion type, its concentration was changed or the ion was replaced by another in the EC, the IC or both solutions (see results).

All pharmacological modulators and proteins used in electrophysiological experiments are listed in Table 9 and 10.

EC solution (in mM)	NaCl-based	Cl^-- current	NaBr-based	NaI-based	lowCl^-/Na^+	VGCCs
NaCl	105	82			30	70
KCl	3					3
HEPES	10	10	10	10	10	10
Glucose	5	5	5	5	5	10
$CaCl_2$	2	2	2	2	2	
$MgCl_2$	1	1	1	1	1	2
$BaCl_2$						10
CsCl		3			3	
TEA-Cl		20			20	20
TEA-Br			15			
TEA-I				15		
NaBr			90			
CsBr			3			
NaI				90		
CsI				3		
L-mannitol					100	

Table 5: Low osmolality EC solutions (all concentrations in mM).

EC solution (in mM)	NaCl-based	Cl^-- current	NaBr-based	NaI-based	lowCl^-/Na+	VGCCs
NaCl	145	112			30	110
KCl	3					3
HEPES	20	20	20	20	20	20
Glucose	20	20	20	20	20	20
$CaCl_2$	2	2	2	2	2	
$MgCl_2$	1	1	1	1	1	2
$BaCl_2$						10
CsCl		3			3	
TEA-Cl		20			20	20
TEA-Br			20			
TEA-I				20		
NaBr			110			
CsBr			3			
NaI				110		
CsI				3		
L-mannitol					120	

Table 6: High osmolality EC solutions (all concentrations in mM).

IC solution (in mM)	KCl-based	CsCl-based	KGluc-based	Ca^{2+} free	Ca^{2+} high	NMDG-Cl -based	CsBr-based	CsI-based	CsCl-TEA-Cl-based	VGCCs
KCl	90									
NaCl	3	3	3	3	3				3	
EGTA	5	5	5	5	5	5	5	5	5	10
HEPES	5	5	5	5	5	5	5	5	5	5
Glucose	5	5	5	5	5	5	5	5	5	5
CaCl2	0.5	0.1	0.1		2	0.1	1	1	1	0.5
MgCl2	4	4	4	4	4	4	4	4	4	4
CsCl		90		90	90				90	90
KGlu			90							
NMDG-Cl						90				
TEA-Cl									10	
TEA-Br							10			
TEA-I								10		
CsBr							90			
NaBr							3			
CsI								90		
NaI								3		

Table 7: Low osmolality IC solutions (all concentrations in mM).

IC solution (in mM)	KCl-based	CsCl-based	KGluc-based	Ca^{2+} free	Ca^{2+} high	NMDG-Cl -based	CsBr-based	CsI-based	CsCl-TEA-based (Cl^- current)	VGCCs
KCl	120									
NaCl	4	4	4	4	4				4	
EGTA	5	5	5	5	5	5	5	5	5	10
HEPES	5	5	5	5	5	5	5	5	5	10
Glucose	5	5	5	5	5	5	5	5	5	10
CaCl2	0.5	0.1	0.1		2	0.1	1	1	1	0.5
MgCl2	4	4	4	4	4	4	4	4	4	4
CsCl		120		120	120				120	100
KGlu			120							
NMDG-Cl						120				
TEA-Cl									10	
TEA-Br							10			
TEA-I								10		
CsBr							120			
NaBr							4			
CaI								120		
NaI								4		

Table 8: High osmolality IC solutions (all concentrations in mM).

Blocker/ modulator	Full name	Company (Order Number)	Applied concentration
4-AP	4-Aminopyridine	Alexis	2 mM
2-APB	2-aminoethoxydiphenyl borate	Tocris	100 µM
Agatoxin 4a		Sigma	250 nM
Apamin		Sigma	1 mM
Biccuculine	Biccuculine methobromide	Alexis	20 µM
Calyculin		Alexis	50 nM
CBX	Carbenoxolone	Sigma	250 µM
Conotoxin GVIa		Sigma	1 µM
Conotoxin MVIIa		Almone Labs	300 nM
Conotoxin MVIIc		Almone Labs	500 nM
Cytochalasin B		Alexis (ALX-350-053-M001)	10 µM
Dandrolene			30 µM
DIDS	4, 4'-diisothiocyanatostilbene-2, 2'-disulfonic acid	Calbiochem	100 µM
DL-APV	2*R*-amino-5-phosphonovaleric acid	Tocris	10 µM
DNQX	6,7-Dinitroquinoxaline-2,3-dione	Tocris	10 µM
GABA	γ-Aminobutyric acid		
Gabapentin		Sigma	100 µM
Heptanol		Roth	1m M
Hexanol		Roth	1m M
Latrunculin A		Alexis (ALX-350-130)	2 µM
Nifedipine		Sigma	
Nimodipine		Sigma	
Nocodazol		Sigma	5 µM
NPPB	5-nitro-2-(3-phenylpropylamino) benzoic acid	Biomol (CM-100)	15-100 µM
Octanol		Roth	1 mM
Okadaic acid	Okadaic acid sodium salt	Alexis	100 nM
Ouabain	Ouabain octahydrate	Sigma	10 µM
PhospStop		Roche (04906845001)	1:10 diluted
Picrotoxin		Calbiochem	100 µM
PP1		Calbiochem	5 µM
PP2		Calbiochem	5 µM
Ryanodine		Calbiochem	25 µM
SNX 482		Sigma	300 nM
Strychnine		Sigma	0.5 µM
Thapsigargin		Alexis	1 µM
TMA	Trimethylamine hydrochloride	Sigma	10 µM
TTX	Tetrodotoxin	Almone Labs	1 µM
Verapamil		Sigma	20 µM
ZD-7288		Alexis	100 µM
U73122		Calbiochem	20 µM

Table 9: Blockers and modulators used in patch-clamp experiments.

Protein	Company	Applied concentration
Ad2 C284N	AG Rathjen	500 µg/ml
CAR D1 122	Christopher Patzke (AG Rathjen)	100- 500 µg/ml
CAR D1 213	Christopher Patzke (AG Rathjen)	100- 500 µg/ml
CAR D2	Christopher Patzke (AG Rathjen)	100- 500 µg/ml
CAR extra	Christopher Patzke (AG Rathjen)	100-500 µg/ml
Fibronectin	Sigma (F2006)	500 µg/ml
Rb80 CAR AB	AG Rathjen	500 µg/ml

Table 10: Proteins applied in patch-clamp experiments.

2.2.6 Calcium imaging

2.2.6.1 Fluorometric $[Ca^{2+}]_i$ measurements

Fluorescent ion indicator dyes selectively bind particular ions and upon binding exhibit altered fluorescent properties e.g. fura-2 binds Ca^{2+}. Fluorescent ion indicator dye loaded into living cells e.g. in cell culture, can be used to observe and record dynamic changes in the intracellular concentration of the respective ion.

Calcium is one of the most important ions in cellular signaling pathways, which is reflected by the fact that more studies have been done with fluorescent indicator dyes for Ca^{2+} than for any other ion. In 1985 Roger Tsien and collaborators developed a calcium imaging technique using fura-2, which became the most widely used fluorescent dye for measuring $[Ca^{2+}]_i$ changes in single cells (Grynkiewicz et al., 1985). One characteristic of fura-2 is its high affinity to Ca^{2+} (*in vitro* K_d= 224 nM, Grynkiewicz et al., 1985), which makes it most suitable for measurements of $[Ca^{2+}]_i$ changes between 20 nM - 2 µM (Takahashi et al., 1999). Fura-2 binds Ca^{2+} in a 1:1 ratio. In its free form, fura-2 has a high excitation efficiency at 380 nm and a low excitation efficiency at 340 nm (Fig. 14). When fura-2 binds to Ca^{2+}, the excitation spectrum of the dye shifts to shorter wavelengths and the peak excitation of fura-2, when bound to Ca^{2+}, is 340 nm (Fig. 14). With increasing concentration of calcium, the excitation efficiency at 380 nm decreases, whereas simultaneously, that of 340 nm increases (Fig 12.). The ratio of fluorescence intensities obtained at these two excitation wavelengths (340 and 380 nm) provides a proper measurement of $[Ca^{2+}]_i$. The fluorescent emission of the dye is monitored at 510 nm.

At 358 nm, fura-2 fluorescence excitation is independent of $[Ca^{2+}]_i$ (isosbestic wavelength). The ratio F_{340}/F_{380} obtained by dividing the fluorescence emitted during excitation at 340 nm by that emitted during excitation at 380 nm changes in the same direction as $[Ca^{2+}]_i$. Thus, ratiometric estimation of $[Ca^{2+}]_i$ is independent of dye concentration, cell thickness, dye

leakage, excitation light intensity, photobleaching, or camera sensitivity (Grynkiewicz et al., 1985), since these should affect the measurements at both excitation wavelengths to the same extent (Grynkiewicz et al., 1985; Henke et al., 1996; Neher, 1995).

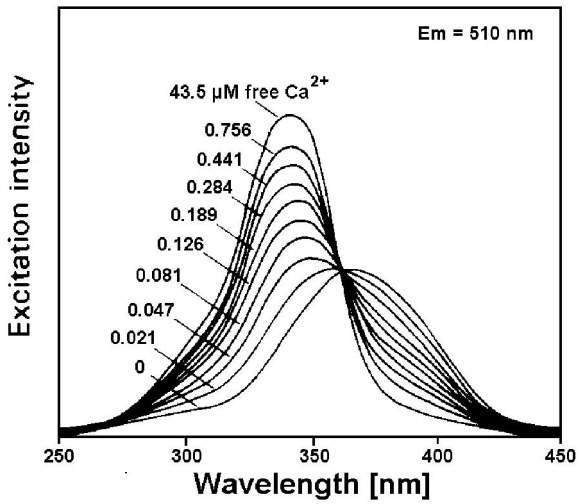

Fig. 14: Intensity of fluorescence plotted versus excitation wavelength for different calcium concentrations (Molecular Probes, Inc.: Handbook 1992-1994).

2.2.6.2 Ca^{2+} imaging in cell culture and data analysis

Cells were loaded with 1-2 µM of fura-2-AM and 0.01 % Pluronic acid F-127 for 60 min at 37°C in medium solution, washed twice with appropriate extracellular solution, and used within 3-4 h. During experiments, cells were placed on a glass coverslip that was attached to an open perfusion chamber. They were continuously perfused with bathing solution.
Images were captured using a TILL Photonics Imago camera (Photonics GmbH, Germany) attached to an inverted microscope Axsioskop (Zeiss, Germany), and recorded with an imaging system TILLVisION 4.0 (Photonics GmbH, Germany).The fluorescence signals were recorded, at video-frame rate with a 63x magnification objective. Cycle time, intervals between two ratio images at 340/380 nm, varied between 250-1000 ms and the number of recorded cycles was between 1500 and 2500. Both parameters (cycle time and cycle number) were adjusted depending on the aim of the measurement.
In each field of view, enclosing several cells, cells were analyzed by calculating the mean increase in $[Ca^{2+}]_i$ (ΔF, Fig. 15) compared to the starting control point (F_0, Fig. 15) within areas defined with a light-sensitive pen on a view field image showing the morphology of cells (regions of images, ROIs).
To quantify changes of $[Ca^{2+}]_i$ due to applied modulators during calcium imaging, the following parameters and calculation were made (Fig. 15):
F_0 – baseline values of imaged cells
F_{max} – maximal values at peak due to stimulation

$\Delta F = F_{max} - F_0$

By dividing ΔF by $F_{0\,r}$ ratio ($\Delta F/F_0$) was calculated.

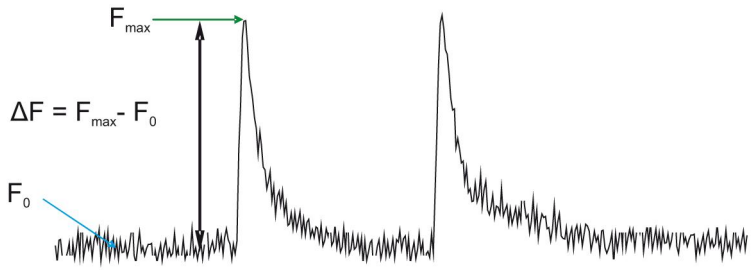

Fig. 15: Example trace of spontaneous Ca^{2+} transients in cortical neurons (E15, WT) with indication of the baseline (F_0), maximal observed $[Ca^{2+}]_i$ concentration change (F_{max}) and calculated increase in $[Ca^{2+}]_i$ ($\Delta F = F_{max} - F_0$).

2.2.7 Dye spreading

Analysis of dye spreading was performed in confluent parental and stably transfected HeLa cells similar to other published reports (Cao et al., 1998; Charpantier et al., 2007; Valiunas et al., 2004). Individual HeLa, HeLaCx36 and HeLaCx43 cells were microinjected for 1-20 min, using sharp glass pipettes pulled to a resistance of 50–60 MOhm. The pipette contained the tracer: 4% Lucifer Yellow (LY; Sigma L0259) diluted in 3 M/l LiCl. The dye was iontophoretically injected for maximal 20 min, by applying pulses of 0.1 nA amplitude. The number of cells filled with dye was registered after the first min of injection and then every 5 min. Fluorescent images of LY-filled HeLa cells were obtained using the Axiovert 135 fluorescent microscope (Zeiss, Germany) linked to the AxioCam MRc camera (Zeiss, Germany) and AxioVision software.

2.2.8 Quantification of cell aggregates and neurite outgrowth

Effects of the fiber knob (Ad2) on cultivated chick and mouse neurons were visualized and the images were acquired using 10x and/or 20x objectives of the phase contrast Axiovert 135 microscope (Zeiss, Jena) equipped with a AxioCam HRc camera (Zeiss, Jena). To determine cell number and cells forming aggregates, cell nuclei were visualized by Hoechst staining (bis-benzimide H 33258). The total number of cells and the number of cells forming aggregates were counted and the total sum of neurite length was measured per image (field of view) using AxioVision 3.1 (Carl Zeiss) software. Measurements of these chosen parameters were carried out manually for each image. 16 images of each culture dish (16 images for each control dish and 16 images for each Ad2 treated culture dish) were selected randomly from 10 independent experiments in chick and 8 independent experiments in mouse cell culture. The

data were then analyzed by applying statistical Student's *t* test (Deumens et al., 2006; Lankford et al., 1987; Pearson et al., 2003).

2.2.9 Statistics

All data were averaged, if not mentioned otherwise, and the standard error of the mean was calculated (SEM). The statistical significance of differences between mean values was assessed using Student's *t* test.

The significance for the success rate in chapter 3.9.2 was calculated using chi^2 test online calculator (http://www.people.ku.edu/~preacher/chisq/chisq.htm).

Differences were regarded as statistically significant when $p < 0.05$.

In figures, p values are indicated by *,** and *** for $p < 0.05$, $p < 0.005$ and $p < 0.0005$ respectively.

The correlation between time of Ad2 application and the reduction of R_m was calculated using Michealis-Menten kinetic principles. Time of the half maximal effect (50%) of Ad2 on the R_m was established. Data presented in Fig. 19 E were converted into a Lineweaver-Burk linear plot (using Origin software). The time when Ad2 had reduced the R_m by 50% of the maximal reduction level was calculated using the following equation:

$y = A + B*x$

where:

y = 1/value (%)

A and B - coefficients of linear regression (values calculated by Origin software)

x = 1/time (min)

3. Results

3.1 Expression of CAR on neurons and HeLa cells

CAR was identified and purified from HeLa cell lysates by immunoaffinity chromatography using mAb RmcB (Bergelson et al., 1997). In agreement with this report, immunocytochemical staining of HeLa cells with antibodies against CAR (RmcB, Table 2) revealed an abundant expression of CAR at the cell membrane with a strong localization at cell-cell contact sides (Fig. 16 A, B, cell-cell contacts indicated by arrows).
Furthermore, strong expression of CAR was shown by means of immunocytochemical staining using antibodies against CAR (Rb80, Table 2) in cultivated neurons prepared at embryonic day 10.5 (E10.5, Fig. 16 C) or 15 (E15, Fig. 16 E). CAR is abundantly expressed throughout the whole cell membrane of the soma of a neuron, as well as along neurites. No differences in the intensity or subcellular localization of CAR expression were observed between neurons cultivated for 6 or 13 days *in vitro* (DIV, Fig. 16 C, E).
To test the specificity of the anti-CAR antibodies, telencephalic CAR-deficient neurons (KO; E10.5) were immunostained. No labeling was observed (Fig. 16 D; DIV 6).
Expression of CAR was also analyzed in mouse brain tissues by means of Western blot analysis using antibodies against CAR (Rb80, Table 2). Different mouse brain regions were prepared from different postnatal (P) days starting at P1 to adulthood (P30). Two molecular mass forms were detected by antibodies against CAR: one migrating at 40 kDa and one at 46 kDa. As shown in Fig. 17 CAR is strongly expressed in mouse cortex (Fig. 17 A), bulbus olfactorius (BO; Fig. 17 B), cerebellum (Fig. 17 C) and retina (Fig. 17 D) at early postnatal stages (P1-P15). Its expression then decreases drastically in the adult animal. These results are in accordance with earlier published reports (Hotta et al., 2003;Tomko et al., 2000).

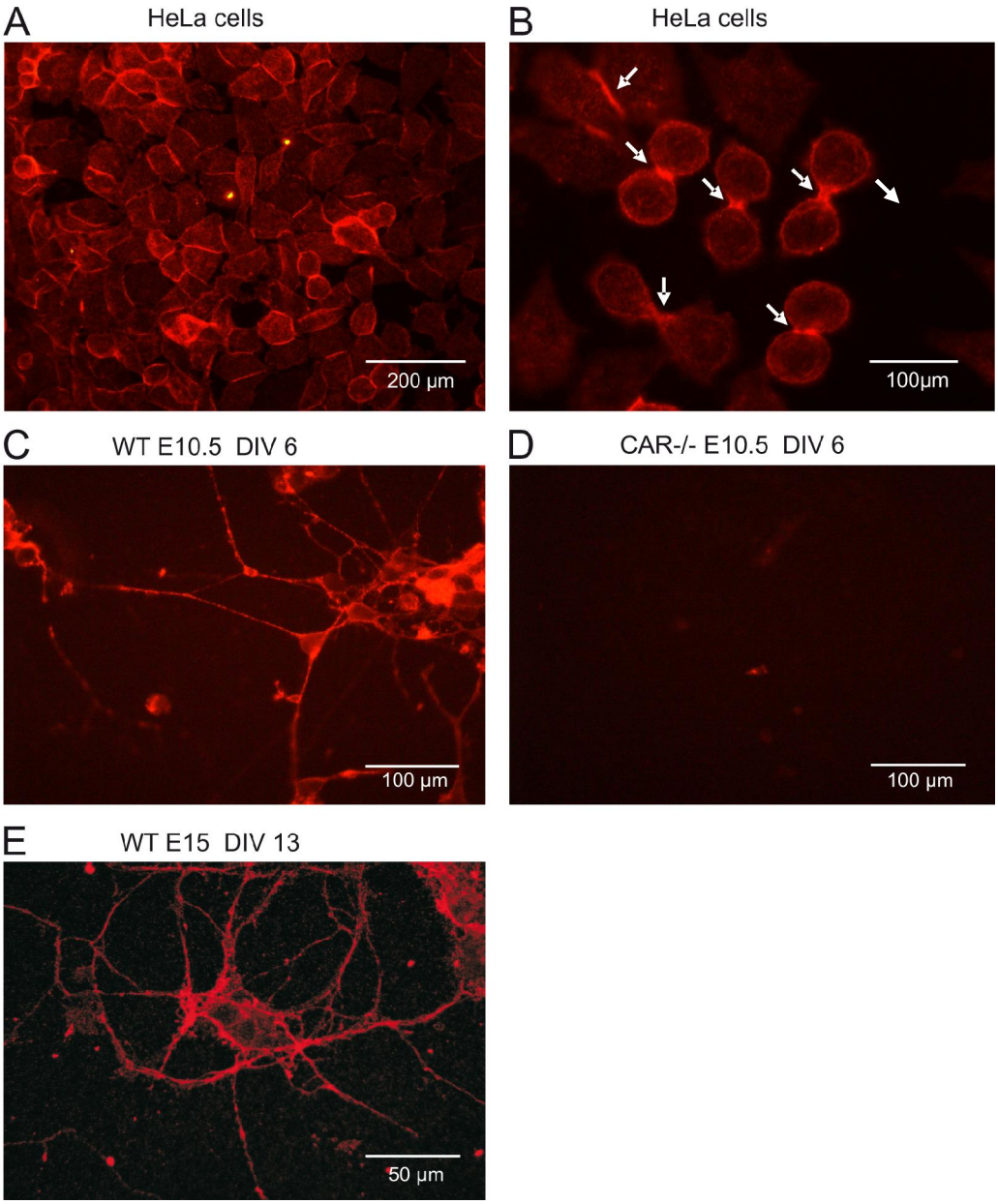

Fig. 16: CAR is strongly expressed in HeLa cells and cultivated cortical neuronal cells. (A, B) Immunostaining using antibodies against CAR (RmcB, 3µg/ml) in parental HeLa cells revealed strong CAR expression, in particular at cell-cell contacts (arrows). (C) Abundant expression was also found in telencephalic WT neurons prepared at E10.5 and cultivated for 6 DIV. (D). Specificity of antibodies against CAR was tested in CAR-deficient neurons (prepared at E10.5). No staining was observed. (E) Immunostaining using anti-CAR antibody (Rb80 CAR, 3 µg/ml) in cortical neurons prepared at E15 (DIV 13) yielded strong expression in the cell soma and in neurites.

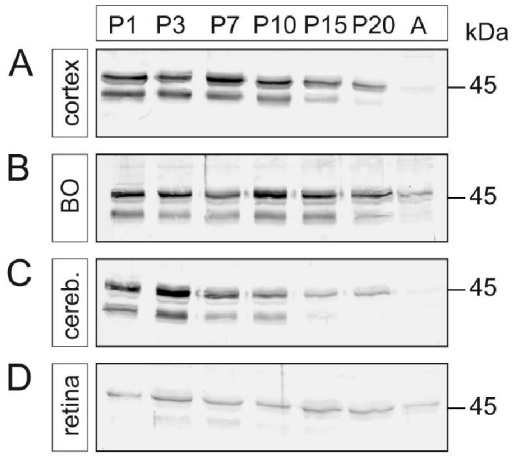

Fig. 17: CAR expression was investigated by Western blot analysis. Two molecular mass forms were detected, one migrating at 40 kDa and one at 46 kDa. CAR is strongly expressed at early postnatal stages in different mouse brain tissues: cortex (A), bulbus olfactorius (BO; B), cerebellum (C), retina (D), while its expression is drastically decreased in these tissues in adult animals.

3.2 Analysis of the function of CAR by patch-clamp recordings

To study the function of CAR, neurons from E15 cortex or from E10.5 telencephalon were cultivated for up to three weeks in the presence or absence of anti-CAR antibodies or the fiber knob (Ad2) followed by electrophysiological measurements. These reagents may evoke opposite effects. Binding of antibodies to an antigen on the surface of cells often blocks its function, whereas application of Ad2 might mimic the binding of the adenovirus and may result in the activation of intracellular signaling pathways which are affected by the presence of infectious adenovirus.

Another approach used to investigate the function of CAR, was to compare CAR-deficient neurons to wild type neurons by different electrophysiological recordings. Since CAR-deficient embryos die at E11 (Doerner et al., 2005) neurons were prepared from the telencephalon of embryos at E10.5.

3.3 Membrane resistance

3.3.1 The R_m in CAR-deficient neurons is increased

Passive properties of neuronal cell membranes were measured using high osmolality NaCl-based extracellular (EC) solution (Table 6) and high osmolality KCl-based intracellular (IC) solution (Table 8). Cells were clamped at V_h = -70 mV. The membrane resistance (R_m) was calculated using Ohm's law (R=ΔU/I, Fig. 9 A, B). Application of a 10 mV pulse (ΔU) resulted in a significantly smaller current (I) flow through cell membranes of CAR-deficient

neurons compared to the WT cells (Fig. 18 A). Thus, the calculated R_m was significantly higher in CAR knock-out cells compared to WT cells (Fig. 18 D, $p < 0.0005$). This difference remained significant during the cultivation period studied, although the R_m concomitantly decreased during prolonged cultivation in both types of cells (DIV 7-8 n = 50-55, DIV 10-14 n = 88-95, DIV 16-20 n = 75-80, Fig. 18 D). The overall decrease in R_m in wild type and CAR-deficient neurons during the cultivation period is most probably a result of an increasing number of different ion channels and transport proteins incorporated into the plasma membrane.

In addition to the single test pulse (10 mV), a series of 3 depolarizing (5, 10 and 15 mV) and 3 hyperpolarizing (-5,-10 and -15 mV, Fig 18 B) voltage steps starting from V_h = - 70 mV were applied. This was done to determine whether the measured current used for estimating the R_m (in the range of V_h = -70 mV) consists only of passive current flow and/or of an active current from voltage-gated ion channels. A linear plot of the applied voltage and measured current (I-V relation, Fig. 18 C) indicates that the measured current consists only of passive currents (leak currents) through the membrane at the RMP without activation of voltage-gated ion channels (voltage-gated ion channels are closed under applied experimental conditions). Consistent with results presented above, current responses to applied voltage steps in CAR KO cells were also smaller in amplitude compared to WT cells (Fig. 18 C).

Another important passive cell membrane parameter is whole-cell capacitance (C_m), a measure of the membrane area. The whole-cell C_m of CAR KO and WT cells was calculated using the equation shown in Fig. 18 E. No significant differences were observed between CAR-deficient and WT neurons (Fig. 18 E). In both cell types, C_m increased during cultivation presumably because cells grow and the total cell surface is getting larger.

By multiplying R_m by C_m, the specific membrane resistance (R_m *specific*, kOhm*cm^2, Chapter 2.2.5.4) can be calculated (Antic, 2003; Barrett and Crill, 1974) and tested whether the difference in R_m was due to a change in the cell size. The observation that R_m *specific* is also higher in CAR-deficient neurons in comparison to WT neurons, suggests that the measured difference is not the result of the size of neurons in the absence of CAR (Fig. 18 F, $p < 0.0005$).

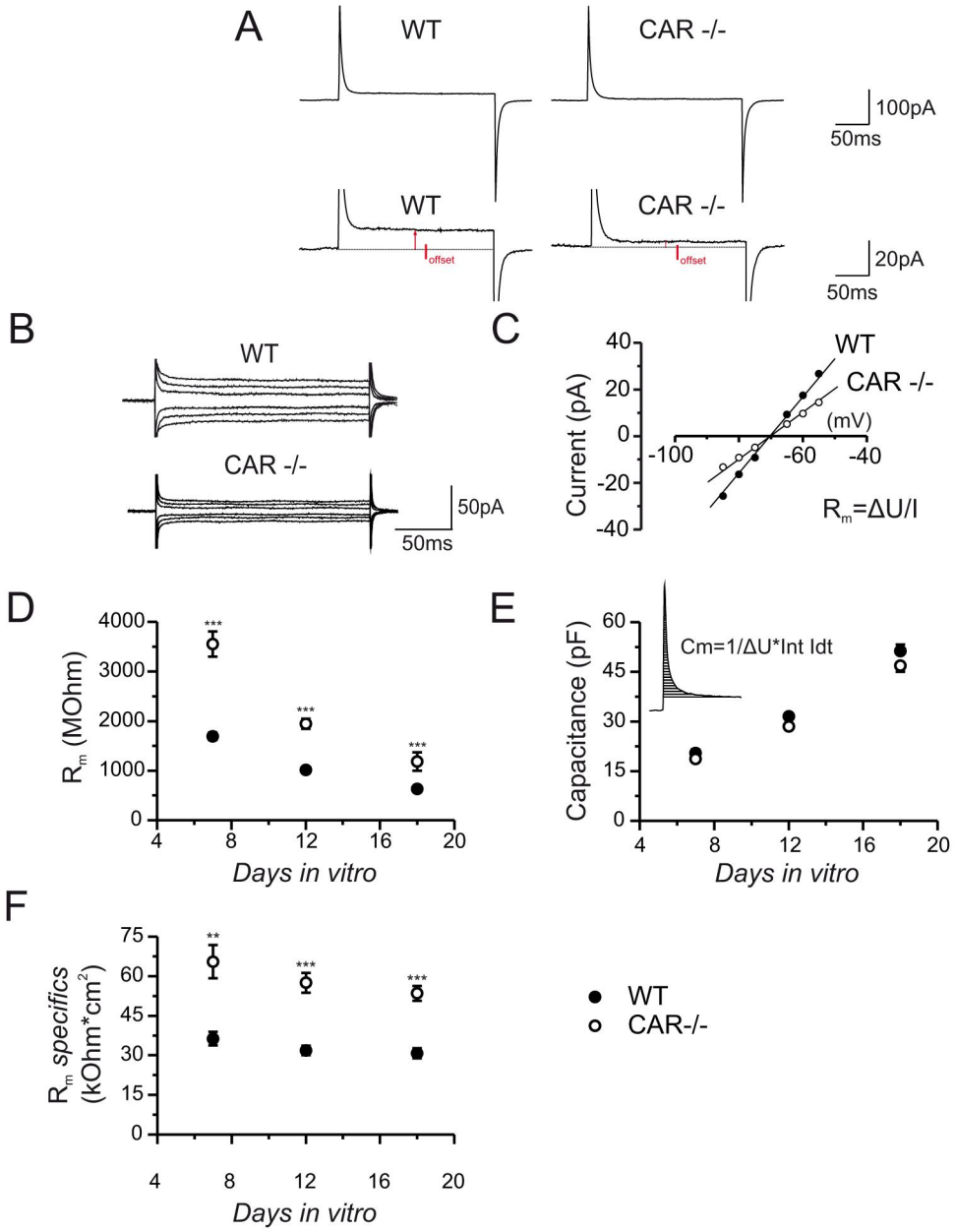

Fig. 18: The membrane resistance (R_m) is higher in CAR-deficient neurons in comparison to WT neurons (prepared at E10.5). (A, B) Example traces of current responses to 10 mV (A) test pulses and 5, 10 and 15 mV (B) test pulses. Current flowing through the membrane (arrows in A) was significantly smaller in CAR-deficient neurons. (C) Current-voltage (I-V) relationship. Application of 3 test pulses (shown in B) resulted in smaller current amplitudes in CAR-deficient neurons compared to WT neurons. (D) R_m change during development. Although in both WT and CAR-deficient neurons R_m decreases during development, R_m difference between WT and KO remains significant. (E) Whole-cell capacitance (C_m) correlates to some degree with the cell size and increases during cultivation period. No significant differences were observed between WT and CAR-deficient neurons. (F) Specific membrane resistance (R_m *specific*) is calculated by multiplying the R_m by the specific C_m. CAR-deficient neurons showed significantly higher R_m *specific* compared to WT cells (D, F: ** - $p < 0.005$, *** - $p < 0.0005$).

3.3.2 The R_m in fiber knob (Ad2) treated neurons is reduced

Using the whole-cell voltage-clamp technique, passive membrane properties of cultivated neurons prepared from E15 embryos and treated with the fiber knob (Ad2) of the adenovirus were analyzed. For measurements low osmolality NaCl-based EC solution (Table 5) and low osmolality KCl-based IC solution (Table 7) were used. Cells were clamped at V_h= -70 mV. Using the same voltage protocols and calculations as described above for CAR-deficient neurons, the R_m, C_m and R_m *specific* of fiber knob (Ad2; 500 µg/ml, added for 5,7 or 14 days) treated neurons and control neurons were calculated.

Application of different voltage steps (10 mV or 5, 10 and 15 mV) from V_h = -70 mV resulted in higher current amplitude in Ad2 treated cells (Fig. 19 A, B). A linear current-voltage (I-V) relationship (Fig. 19 C) indicated that no voltage-gated ion channels were activated and that the measured current was passive. The calculated R_m was significantly lower in Ad2 treated cells than in control cells (Fig. 19 D, $p < 0.0005$). Although R_m decreased during the cultivation period, the differences between Ad2 treated and control cells remained significant (DIV 5 n = 20-25, DIV 7-8 n = 84-90, DIV 12-14 n = 79-80). In order to test the time it takes for Ad2 to reduce R_m, the incubation period was gradually shortened. Ad2 was able to reduce the R_m to 40.89 % from the starting level. 50% of the maximal reduction occurred 17.48 min after Ad2 application (Fig. 19 E).

The calculated C_m of Ad2 treated cells and control cells revealed no significant differences (Fig. 19 F). C_m increased during development because of cell maturation.

The calculated R_m *specific* was significantly lower in Ad2 treated neurons than in control cells, suggesting that the R_m difference is independent of neuron size (Fig. 19 G, $p < 0.0005$). Similar to R_m values, the difference in R_m *specific* remained significant throughout the development of cultivated neurons.

To study the specificity of the Ad2, CAR-deficient neurons from E10.5 embryos were treated with Ad2 followed by patch-clamp recordings. No effect on the R_m was observed. In contrast, treatment of WT neurons (E10.5) with Ad2 resulted in a significantly lower R_m (Fig. 20).

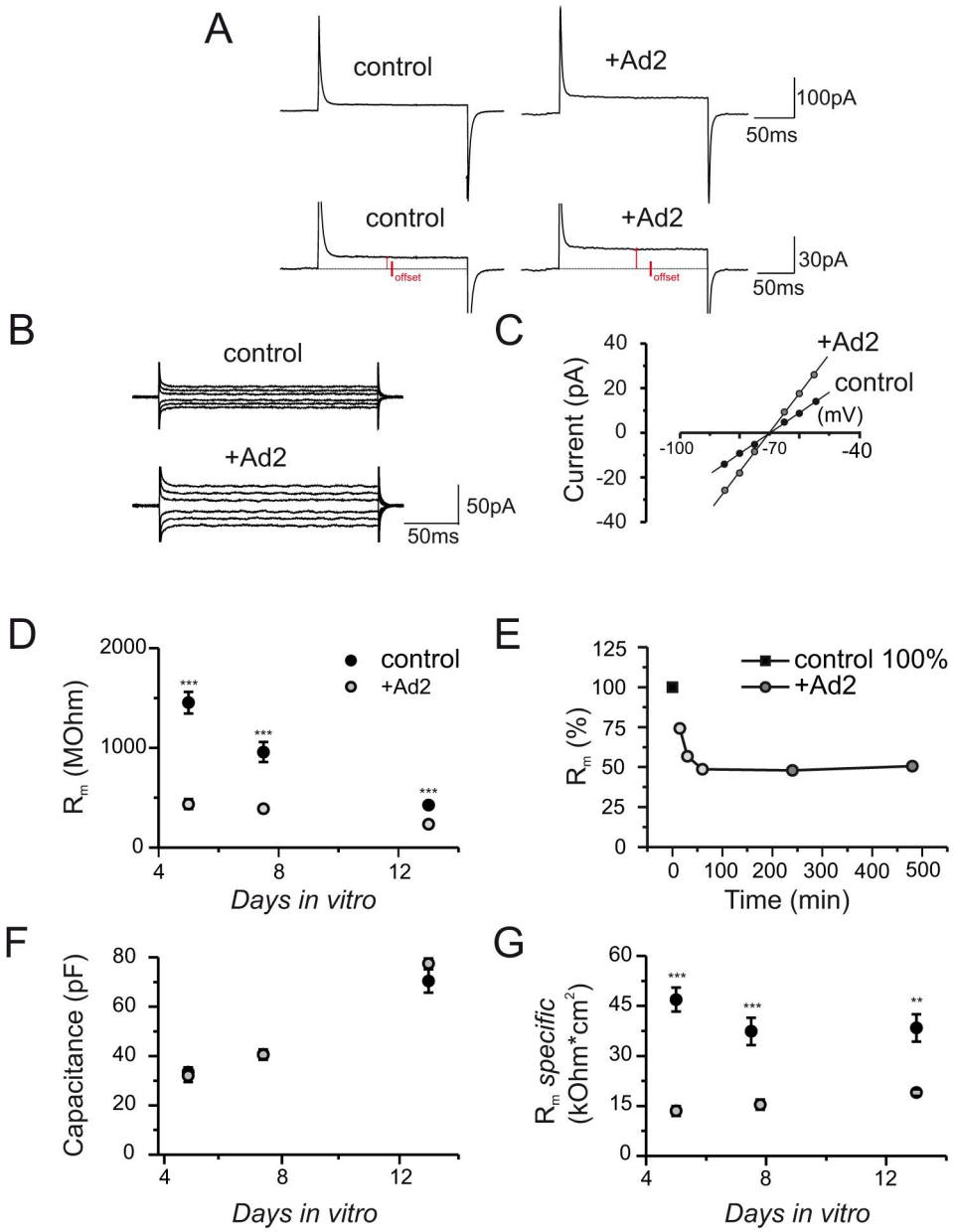

Fig. 19: The membrane resistance (R_m) is significantly reduced in fiber knob (Ad2) treated neurons prepared from E15 embryos. (A, B) Example traces of current responses to 10 mV (A) test pulses and 5, 10 and 15 mV (B) test pulses. The current flowing through the membrane (arrows in A) was significantly larger in Ad2 treated neurons. (C) Current-voltage (I-V) relationship. Application of 3 test pulses (shown in B) resulted in a much larger current flow in Ad2 treated cells. (D) R_m change during development. Although in both, control and Ad2 treated neurons, the R_m decreases during development, the lower R_m in Ad2 treated cells remains significant. (E) Ad2 was able to reduce the R_m to 40.89 % of the initial level. Then the change remained stable over time. 17.48 min after Ad2 application the R_m was decreased to 50% of the maximal reduction. (F) C_m is an indicator of cell size and increases during cultivation period. No significant differences were observed between control and Ad2 treated neurons.(G) Specific membrane resistance (R_m *specific*) was significantly lower in Ad2 treated neurons compared to control cells (D, G; ** - $p < 0.005$, *** - $p < 0.00005$).

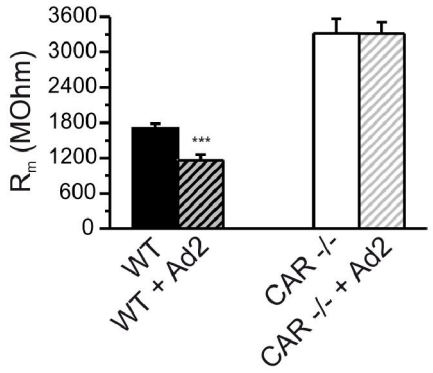

Fig. 20: Ad2 reduces R_m in WT but not in CAR KO cells, indicating that the effect observed in presence of Ad2 is mediated by CAR ($p < 0.0005$). Neurons were prepared from wild type and CAR-deficient E10.5 embryos and cultivated for 8 DIV followed by a treatment with Ad2 (500 µg/ml) for 8 hours.

3.3.3 The R_m in anti-CAR ABs (Rb80) treated neurons is increased

Using the whole-cell voltage-clamp technique, passive neuronal membrane properties of neurons prepared form embryos at E15 and treated with anti-CAR antibodies (Rb80) were analyzed. Anti-CAR ABs (500 µg/ml) were added for 7 or 14 days to the medium of cultivated cortical neurons and incubated at 37°C.

Surprisingly, application of anti-CAR ABs resulted in a detachment of many cells from the substrate (poly-D-lysine) as revealed by cell nuclei staining using Hoechst 33258 (Fig. 21 A-D; DIV 7; $p < 0.0005$). This result is consistent with previous observations made on chicken neurons (Patzke et al., 2009, submitted).

Based on whole-cell patch-clamp recordings, neurons that stayed attached to the matrix remained viable. No significant differences in R_m (Fig. 22 A), C_m (Fig. 22 B) and R_m *specific* (Fig. 22 C) between control and anti-CAR AB treated cells were observed (DIV 7 n = 26-33; DIV 14 n = 16-19). The slightly decreased R_m and R_m *specific* in anti-CAR AB treated cells may have been due to cell membrane damage.

To test whether anti-CAR ABs may have a short-term effect on passive membrane properties, cells were incubated with 500 µg/ml of anti-CAR ABs 1h before recordings started. 1h preincubation with ABs resulted in a significantly higher R_m (Fig. 22 D, $p < 0.005$) and higher (not significantly) R_m *specific* (Fig. 22 F). No changes in C_m were observed (Fig. 22 E; DIV 7 n = 22). After 1 hour of incubation with anti-CAR ABs neurons remained attached to the substrate in contrast to the above described antibodies treatment.

Presented data indicate that anti-CAR ABs exert short-term effects on passive membrane properties (increase in the R_m and R_m *specific*) and are able to disturb CAR-mediated cell interactions (long-term effect).

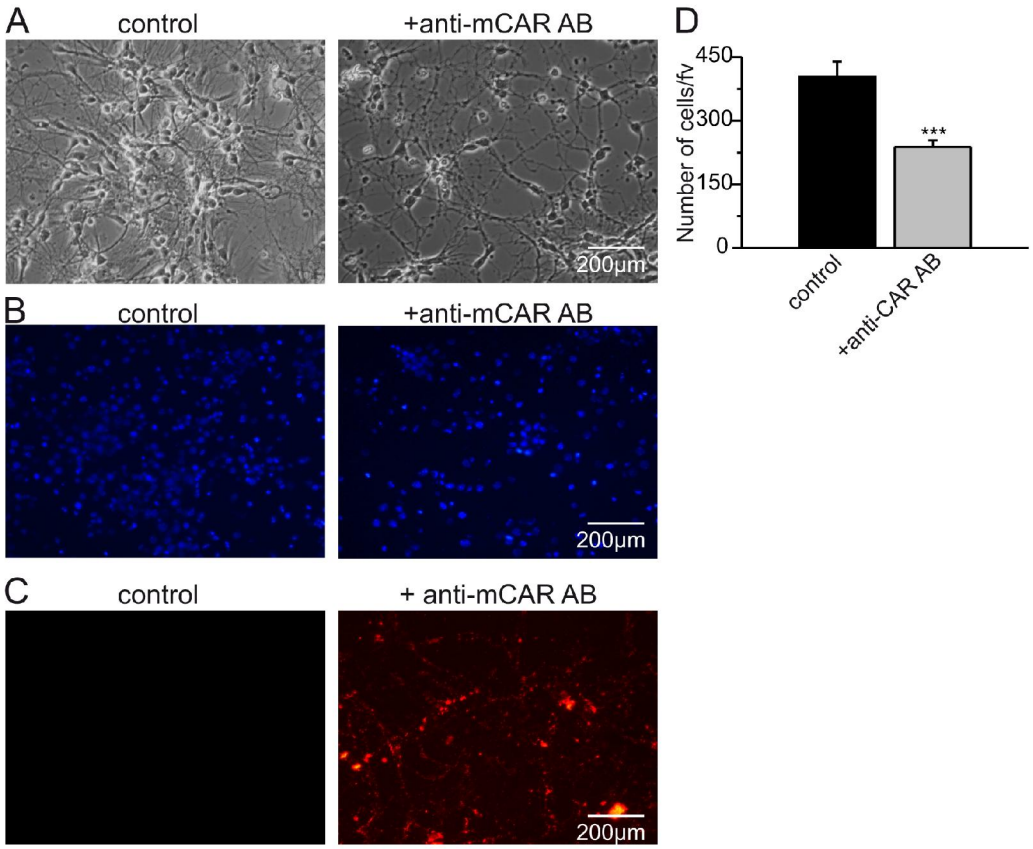

Fig. 21: Detachment of cortical neurons (E15) in culture after incubation with antibodies against CAR (Rb80 anti-CAR ABs). (A) Cells treated with Rb80 anti-CAR ABs, for 7 days, detached from the substrate. (B) Hoechst 33258 staining (cell nuclei staining). Number of cells that stayed attached to the substrate was significantly lower in cells treated with Rb80 anti-CAR ABs than in control cells (see also D; $p < 0.0005$). (C) Added Rb80 anti-CAR ABs bound to cortical cells (revealed by secondary anti rabbit antibody coupled to Cy3). No staining was observed in control cells. (D) Quantification of reduced cell number in Rb80 anti-CAR AB treated cells. Abbreviation: fv – field of view.

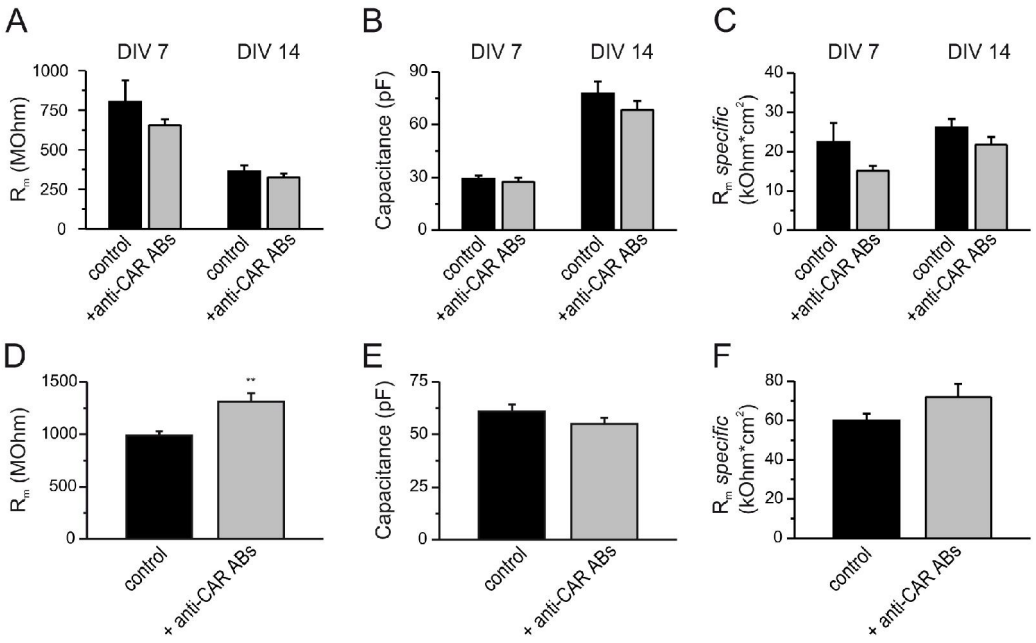

Fig. 22: Effects of anti-CAR ABs on cortical neurons in culture prepared from E15 embryos. (A-C) No significant changes in passive membrane properties were observed after treatment of neurons with anti-CAR ABs for 7 or 14 days. Slightly decreased R_m (A) and R_m *specific* (C) may have resulted from cell membrane damage. (D-F) 1 h incubation (at 37°C) of cortical neurons with anti-CAR ABs resulted in a significantly higher R_m (D, $p < 0.005$) and a higher, not significantly, R_m *specific* (F). No significant changes in C_m were observed (E; DIV 7 n = 22).

3.3.4 The R_m in D1 and D2 treated neurons is not changed

In addition to experiments with Ad2 or anti-CAR ABs, passive membrane properties of neurons treated with CAR domains were analyzed. CAR is composed of two immunoglobulin-like (Ig) domains termed D1 and D2, in its extracellular part. Both were generated in bacteria and kindly provided by Christopher Patzke (AG Rathjen). Two different forms of D1 (D1 122, amino acid residues: 22-140 and D1 213, amino acid residues: 22-144) and one form of D2 (amino acid residues: 141-237) were used. D1 122, D1 213 or D2 (500 µg/ml) were added to the medium of cultivated cortical neurons 1 hour before electrophysiological recordings started (DIV 7). Additionally, to test whether CAR domains cause immediate changes in membrane properties, CAR domains were added followed by recordings without further delay (500 µg/ml).

For cells treated with both forms of D1 or D2 no significant differences in R_m (Fig 23 A, D), C_m (Fig. 23 B, E) and R_m *specific* (Fig. 23 C, F) were observed (D 122 n = 20-21, D1 213 n = 20-30, D2 n = 19-20).

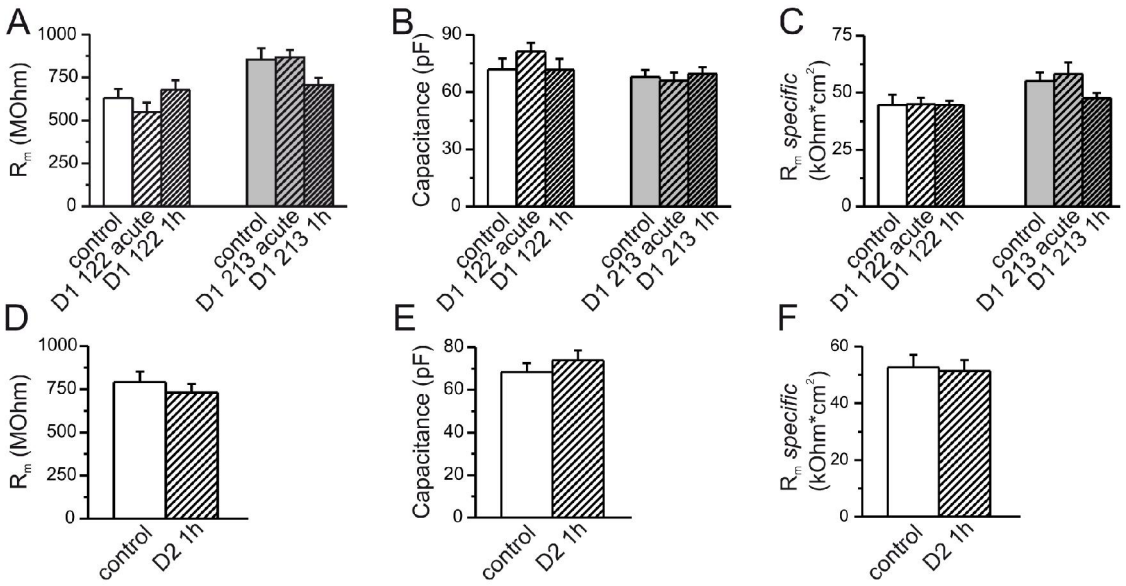

Fig. 23: The passive membrane properties of neurons prepared from E15 embryos and cultivated for 7 days did not change after treatment with extracellular CAR domains: D1 and D2. (A, B, C) In cells treated with D1 122 or D1 213 no significant differences were observed in R_m (A), C_m (B) and R_m *specific* (C). (D, E, F) Similar observations were made after treatment with D2. No changes in R_m (D), C_m (F) and R_m *specific* (F) in comparison to control cells could be detected (D1 122 n = 20-21, D1 213 n = 20-30, D2 n = 19-20).

3.3.5 Investigations on the R_m in CAR-deficient and Ad2 treated neurons

The observed differences in R_m, between WT and CAR-deficient neurons as well as between control and Ad2 treated neurons, result from altered current flow through the membrane. In general, there may be a change in the number of ion channels or in their properties. As described above (chapter 3.3.1 and 3.3.2), R_m was calculated from the current of passive ion conductance at the range of the RMP. Thus, resting (leak) channels (generating leak conductance at the RMP) and transport proteins maintaining the RMP would be appropriate candidates for further investigation. Since the characterization of gated-channels for instance voltage-gated channels may result in critical information about the maturity of the cultivated neurons, their properties were also investigated.

3.4 Characterization of voltage-gated ion channels in CAR-deficient neurons and Ad2 treated cells

3.4.1 Na^+ and K^+ voltage-gated channels in CAR-deficient neurons

Voltage-gated Na^+ and K^+ ion channels play an essential role for action potential generation in neurons. There is an early transient inward Na^+ current depolarizing the membrane above its RMP, followed by a delayed outward K^+ current, predominantly responsible for membrane repolarization. A common method to investigate properties of voltage-gated ion channels is

the application of several depolarizing voltage steps from V_h. Depolarization of the cell membrane results in an activation of particular voltage-gated ion channels and an active current flow through the membrane. By plotting the membrane potential (V) versus the measured current (I), the current-voltage (I-V) relationship is obtained. The relation between membrane voltage and current provides many basic and important characteristics of voltage-gated ion conductance such as activation, voltage range or reversal potential (Hammond, 2001; Kandel et al., 2000).

Voltage-gated Na^+ and K^+ currents were investigated in cultured telencephalic neurons of WT and CAR-deficient cells. For these recordings high osmolality NaCl-based EC solution (Table 6) and high osmolality KCl-based IC solution (Table 8) were used. Recordings of K^+ and Na^+ currents were performed at different cultivation periods (DIV 7-8 n = 45-50, DIV 12-14 n = 45-46, DIV 16-20 n = 48-50). Cells were clamped at V_h = -70 mV and 10 voltage steps (10 mV each, 200 ms; Fig. 11 B left side) starting at V_h= -70 to +30 mV were applied. At the RMP, no active currents could be observed (Fig. 24 E), but a rapid activation of voltage-gated Na^+ and subsequently K^+ channels occurred after depolarization of the membrane (Fig. 24 E, Fig. 25 A, B). Activation of the Na^+ current was observed between -50 and -40 mV for both WT and CAR-deficient neurons (Fig. 24 E, Fig. 25 B), whereas activation of the K^+ current occurred between -40 and -30 mV in both genotypes (Fig. 24 E). Thus, in both genotypes identical voltage thresholds for these two types of voltage-gated ion channels were observed. At each applied voltage step, peak amplitudes of Na^+ and K^+ currents were measured. No significant differences in the maximal currents, measured at +30 mV for K^+ (Fig. 24 A) and at about -20 mV for Na^+ (Fig. 24 C) between CAR-deficient and WT neurons were observed. In neurons of both genotypes the amplitudes of K^+ and Na^+ currents increased during the cultivation period.

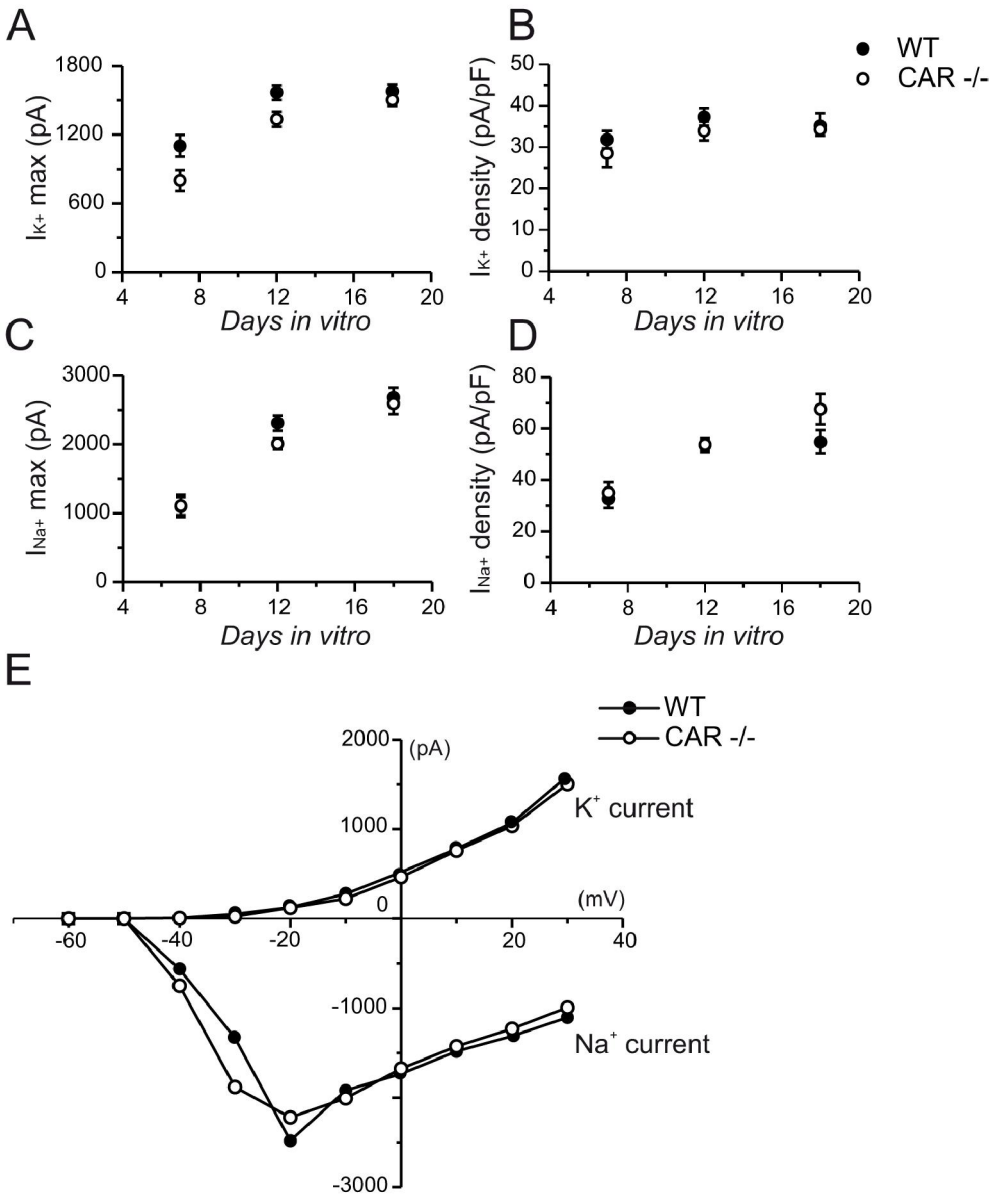

Fig. 24: Similar properties of voltage-gated Na^+ and K^+ ion channels in CAR-deficient and WT neurons prepared from E10.5 embryos. (A-D) Similar amplitudes of maximal K^+ (A) and Na^+ (C) currents of CAR-deficient and WT neurons during development. K^+ (B) and Na^+ (D) current densities in CAR knock-out and WT cells showed no significant differences during development. The amplitude and current density in cells of both genotypes increased during the cultivation period due to cell maturation. (E) I-V relationship of inward Na^+ current and outward K^+ current in CAR KO and WT cells. (DIV 7-8 n = 45-50, DIV 12-14 n = 45-46, DIV 16-20 n = 48-50).

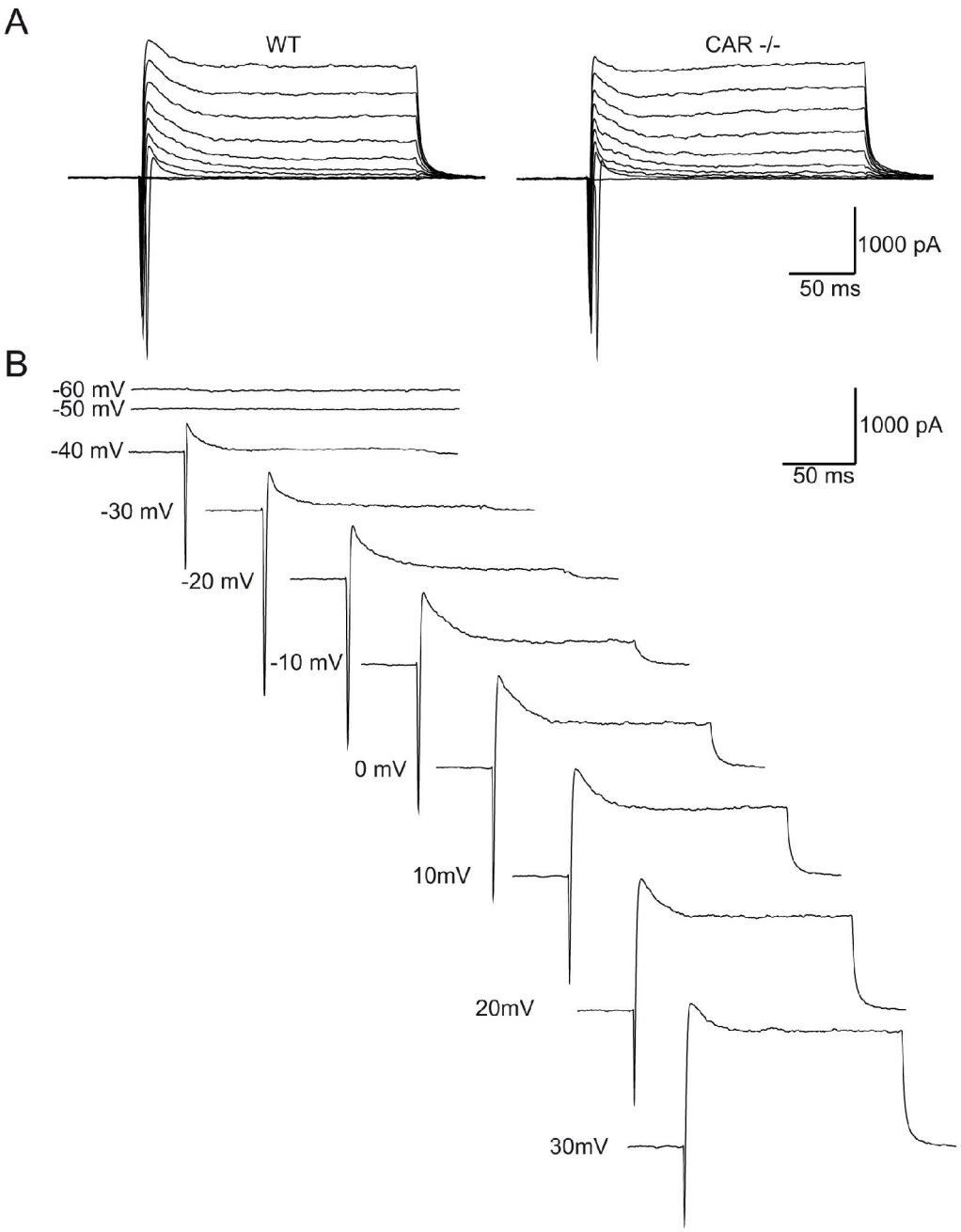

Fig. 25: Examples of Na^+ and K^+ currents in CAR-deficient and WT neurons prepared from E10.5 embryos and cultivated for 14 DIV. (A) Example traces of Na^+ and K^+ currents after application of 10 depolarizing voltage steps from V_h= -70 mV to + 30 mV. No differences in recorded currents between genotypes were observed. (B) Examples of single traces at each depolarizing voltage step recorded from WT cells. Activation of Na^+ voltage-gated ion channels was observed between -50 and -40 mV, whereas activation for K^+ voltage-gated ion channels occurred between -40 and -30 mV.

Additionally, the density of each current type was estimated. This parameter describes how K^+ or Na^+ current flows per area of the cell membrane (expressed as cell capacitance (C_m)). Thus, the current density was calculated by dividing the maximal Na^+ or K^+ current by the value of C_m of the cell, where the current was measured (for Na^+: $I_{Na^+ density^+}=I_{Max\ Na^+}/C_m$; Fig.

24 B, D). Similar current density values for K^+ (Fig. 24 B) and Na^+ (Fig. 24 D) currents in CAR-deficient and WT neurons were obtained. These results suggest that there are no significant differences in the properties of voltage-gated Na^+ and K^+ channels in WT and CAR-deficient neurons.

Furthermore, blockage of Na^+ and K^+ currents through voltage-gated ion channels by application of TTX or by substitution of K^+ by Cs^+ or by both, did not influence the R_m differences between WT and CAR KO cells (Fig. 28 A, C, D and see chapter 3.6.1, Fig. 45) suggesting that these ion channels are not implicated in the observed changes in R_m.

3.4.2 Na^+ and K^+ voltage-gated channels in Ad2 treated neurons

Voltage-gated Na^+ and K^+ ion channels were also investigated in cultivated neurons after treatment with Ad2 (500 µg/ml, 7 or 14 days incubation).

For recordings low osmolality NaCl-based EC solution (Table 5) and low osmolality KCl-based IC solution (Table 7) were used. Recordings of K^+ and Na^+ currents were performed at different cultivation periods (DIV 7-8 n = 65-70, DIV 12-14 n = 38-40). Cells were clamped at V_h= -70 mV and 10 voltage steps (10 mV each, 200 ms; Fig. 11 B left side) from V_h= -70 to +30 mV were applied.

The activation threshold for the Na^+ current was observed between -50 and -40 mV for both Ad2 treated and control neurons (Fig. 26 E, Fig. 27 B), whereas the activation threshold for the K^+ current occurred between -40 and -30 mV (Fig. 26 E, Fig. 27 B). Thus, in both Ad2 treated and untreated cells, very similar activation thresholds for these two types of voltage-gated ion channels were observed.

Similar to procedures used for CAR-deficient neurons, amplitudes of Na^+ and K^+ currents were measured at each step of applied voltage. No significant differences in the maximal currents, measured at +30 mV for K^+ and at -30 mV for Na^+ (Fig. 26 E) were observed between Ad2 treated and control neurons (Fig. 26 A, C). In both, Ad2 treated and control neurons, the amplitudes of K^+ and Na^+ currents increased during development.

Current density was calculated by dividing the maximal Na^+ or K^+ current by the value of C_m of the cell (Fig. 26 B, D). Similar current density values for K^+ (Fig. 26 B) and Na^+ (Fig. 26 D) currents in Ad2 treated and control neurons were obtained.

Thus, no significant differences in properties of voltage-gated Na^+ and K^+ channels between Ad2 treated and control cells were observed. Furthermore, no differences could be observed, when Ad2 was added acutely or only for 1 hour before recordings were performed (data not shown).

Moreover, after blockage of Na^+ and K^+ currents through voltage-gated ions channels, the differences in R_m between Ad2 treated and control cells remained significant, suggesting that, similar to the finding for CAR-deficient neurons, these channels are not involved in changes in R_m (Fig. 28 B, and see chapter 3.6.1, Fig. 45).

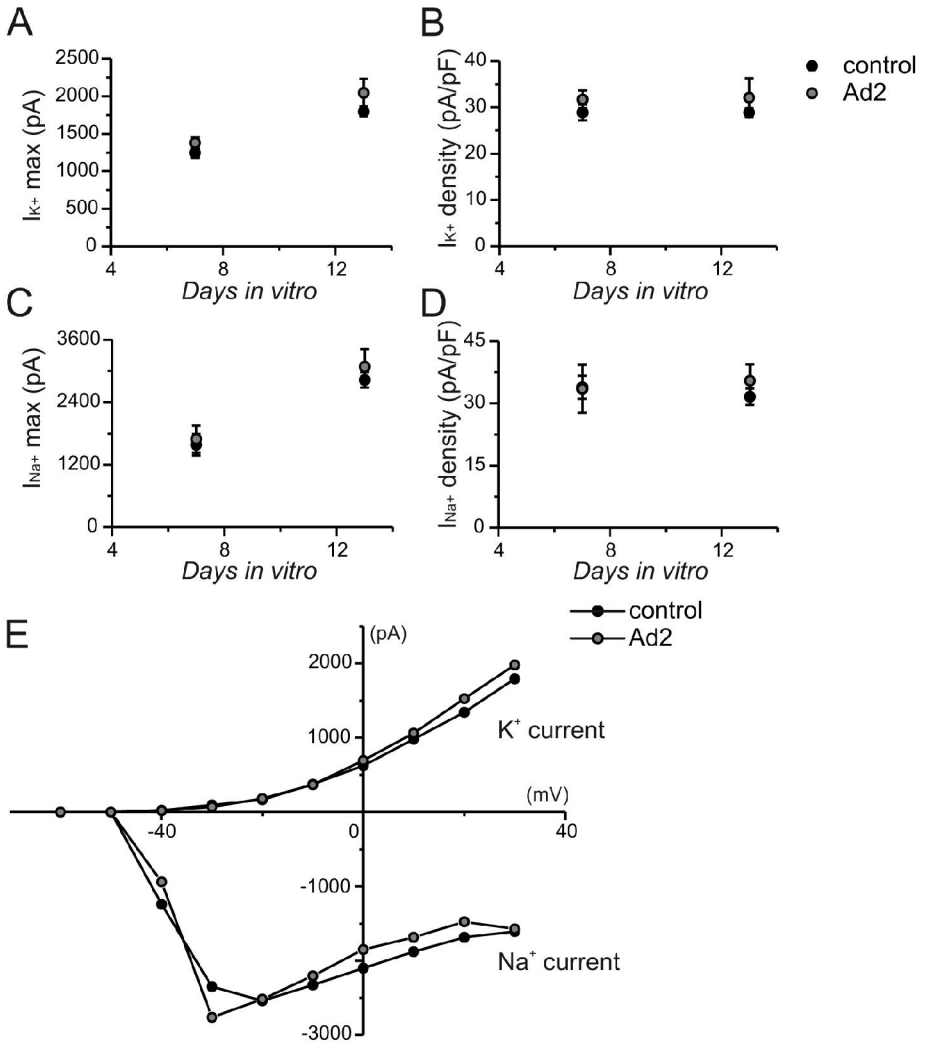

Fig. 26: Similar properties of voltage-gated Na^+ and K^+ ion channels in Ad2 treated neurons and control cells prepared from E15 embryos. (A-D) Similar amplitudes of maximal K^+ (A) and Na^+ (C) currents of Ad2 treated and control cells at different DIV were observed. Also K^+ (B) and Na^+ (D) current densities showed no significant differences. The amplitude and current density increased during cultivation period due to cell maturation. (E) I-V relationship of inward Na^+ current and outward K^+ current in Ad2 treated and control cells. (DIV 7-8 n = 65-70, DIV 12-14 n = 38-40).

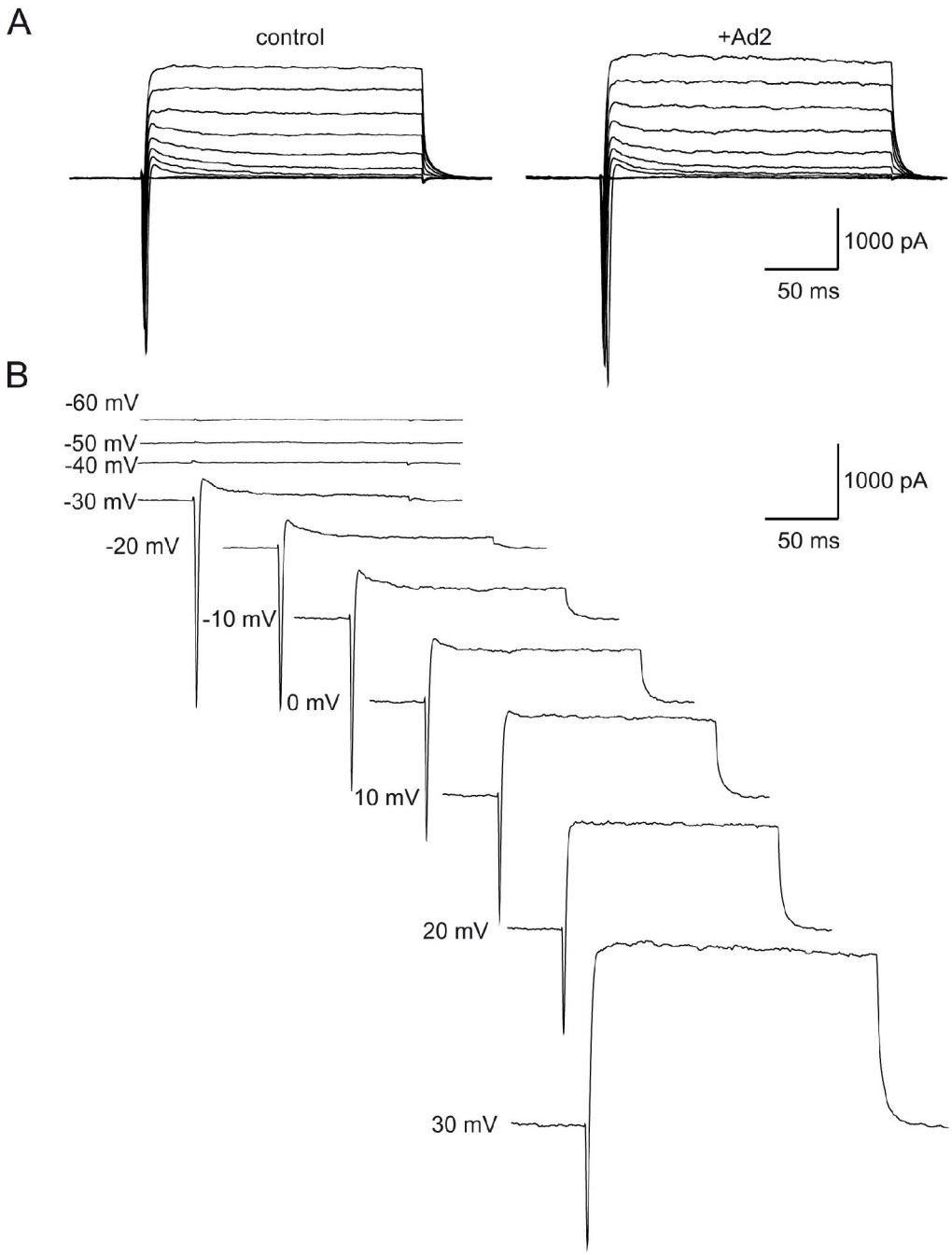

Fig. 27: Examples of Na^+ and K^+ currents in Ad2 treated and control cells prepared from E15 embryos and cultivated for 8 DIV. (A) Example traces of Na^+ and K^+ during application of 10 depolarizing voltage steps from V_h= -70 mV to + 30 mV. (B) Examples of single traces at each depolarizing voltage step recorded from a control cell. Activation of Na^+ voltage-gated ion channels was observed between -50 and -40 mV, whereas activation of K^+ voltage-gated ion channels occurred between -40 and -30 mV.

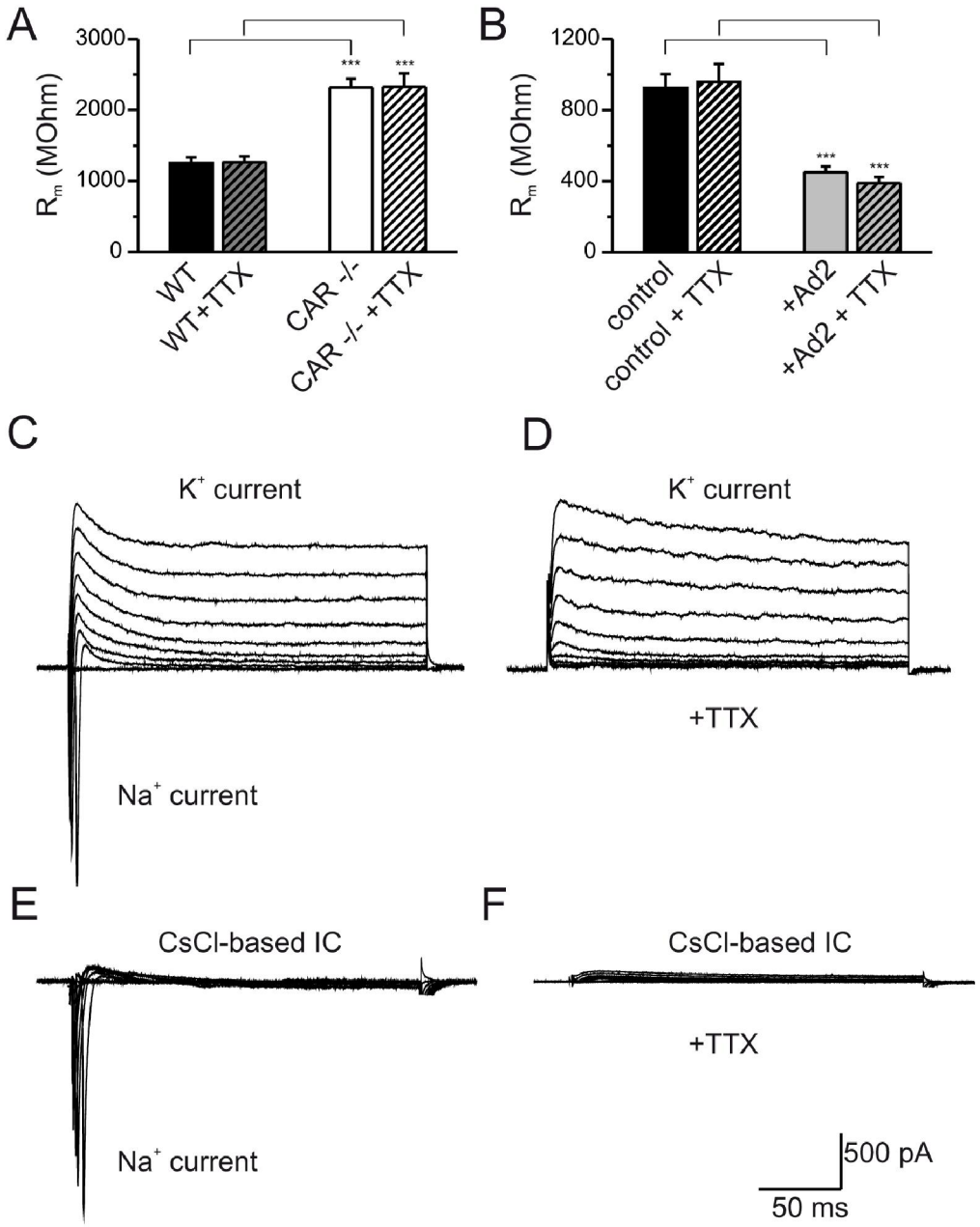

Fig. 28: After blockage of Na^+ currents, R_m in CAR KO and Ad2 treated cells was still significantly changed. (A, B) Application of TTX did not influence the R_m difference between CAR KO and WT cells (E10.5, DIV 14) as well as between Ad2 treated and control cells (E15, DIV 8). (C) Example traces of Na^+ and K^+ currents during application of 10 depolarizing steps (I-V relationship). (D) Blockage of voltage-gated Na^+ channels by TTX suppressed Na^+ inward current; (E) Substitution of K^+ ions by Cs^+ inhibited K^+ outward current; (F) Application of TTX as well as replacement of K^+ by Cs^+ blocked both inward and outward currents ($p < 0.0005$).

3.4.3 Voltage-gated Ca^{2+} channels in CAR-deficient neurons

The properties of voltage-gated calcium channels (VGCCs) were investigated in cultivated CAR-deficient and WT neurons (E10.5). For these recordings high osmolality VGCCs-EC

solution (Table 6) and high osmolality VGCCs-IC solution (Table 8) containing different blockers for K^+ (CsCl, TEA-Cl, Apamin, 4-AP) and Na^+ (TTX) currents were used. Additionally, in the EC solution 2 mM $CaCl_2$ was replaced by 10 mM $BaCl_2$, which has a higher permeability through high voltage-activated (HVA) calcium channels compared to Ca^{2+}. Under these experimental conditions Ca^{2+} currents could be easily identified. For these recordings cells were clamped at V_h= -90 mV and 12 voltage steps (10 mV each, 200 ms) starting at V_h = -90 to +30 mV were applied. Changes in the V_m caused by increasing voltage steps resulted in a rapid transient inward Ca^{2+} current (Fig. 29 C, Fig. 30 A, B). An activation threshold for Ca^{2+}current was observed between -60 and -50 mV for both CAR-deficient and WT neurons (Fig. 29 C, Fig. 30 B).

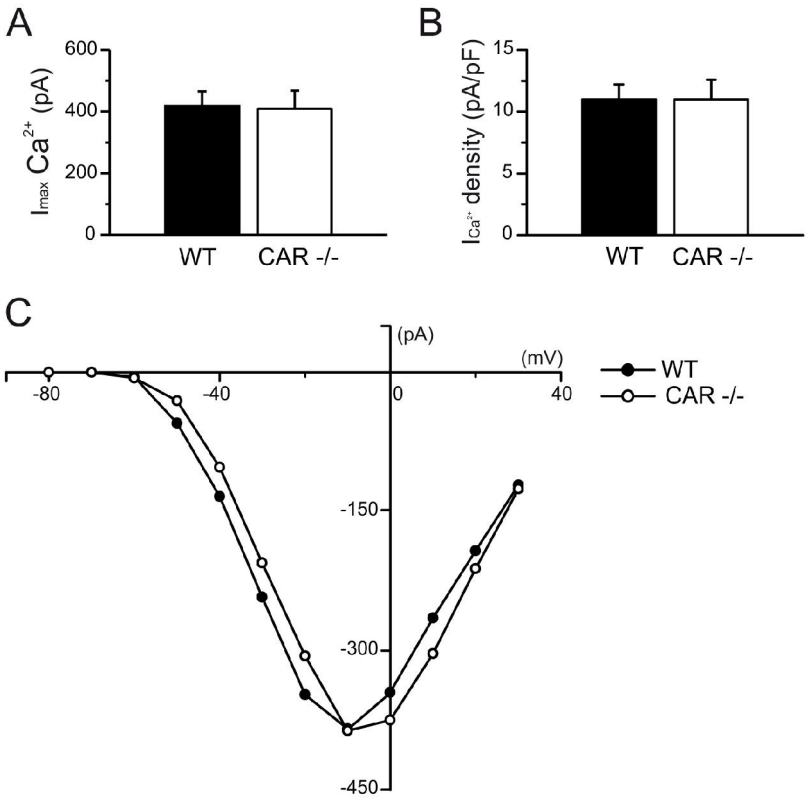

Fig. 29: Similar properties of voltage-gated Ca^{2+} channels in CAR-deficient neurons and WT cells prepared from E10.5 embryos and cultivated for 12 DIV. (A, B) The maximal Ca^{2+} amplitude (A) as well as the Ca^{2+} current density (B) were very similar in both genotypes (n = 31-35). (C) I-V relationship of the recorded Ca^{2+} current in CAR KO and WT cells.

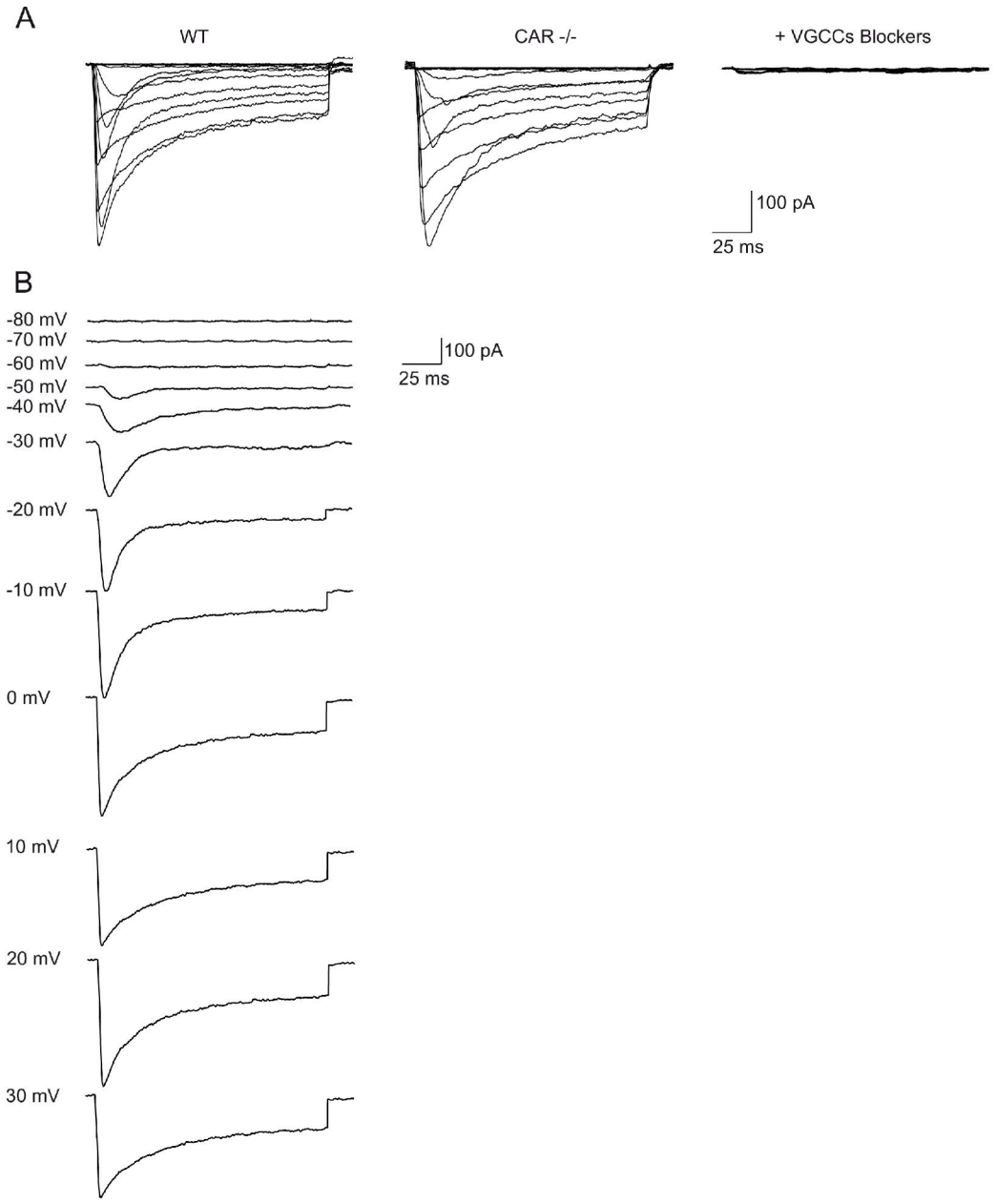

Fig. 30: Example traces of inwardly directed Ca^{2+} currents in CAR KO and WT cells prepared from E10.5 embryos and cultivated for 12 DIV. (A) Ca^{2+} currents in WT (left traces) and CAR-deficient neurons (middle traces) during application of 12 voltage steps. Application of different blockers for VGCCs (Table 11) blocked almost completely all Ca^{2+} currents (right traces). (B) Examples of single traces at each applied voltage step recorded in a WT cell.

At each applied voltage step, the peak amplitude of the Ca^{2+} current was measured. The maximal Ca^{2+} current measured at about -10 mV (Fig. 29 C), was indistinguishable between CAR-deficient and WT neurons (Fig. 29 A, n = 31-35).

Furthermore, the current density was calculated by dividing the maximal Ca^{2+} current by C_m for each cell resulting in similar current densities for CAR knock-out and WT cells (Fig. 29 B). Thus, taken together these data do not reveal differences in the properties of voltage-gated Ca^{2+} channels between CAR-deficient and WT neurons.

To further confirm, that the currents recorded were indeed due to calcium influx, different blockers for VGCCs were applied (Table 11). The reagents almost completely blocked all recorded currents (Fig. 30 A right side, Table 11).

Ion channel type	***N*-type**	***L*-type**	***P/Q* type**	***R*-type**
Voltage dependence	HVA	HVA	HVA	LVA/HVA
Ion selectivity	Ba^{2+}>Ca^{2}	Ba^{2+}>Ca^{2}	Ba^{2+}>Ca^{2}	Ba^{2+}>Ca^{2}
Antagonist and their final concentration	ω-contoxin MVIIa 300 nM ω-conotoxin MVIIc 500 nM	Verapamil 20 µM Nimodipine 5 µM	ω-Agatoxin IVa 250 nM ω-conotoxin MVIIc 500 nM	SNX 482 300 nM

Table 11: Blockers of different types of VGCCs applied in experiments. Ba^{2+} has a higher permeability through VGCCs compared to Ca^{2+}. Abbreviations: LVA - Low voltage activated; HVA - High voltage activated.

3.4.4 Voltage-gated Ca^{2+} channels in Ad2 treated neurons

Properties of VGCCs were also investigated in cultivated cortical neurons (E15) after treatment with Ad2 (500 µg/ml, 1 hour pre-incubation). For recordings low osmolality VGCCs-EC solution (Table 5) and low osmolality VGCCs-IC solution (Table 7) containing different blockers for K^+ (CsCl, TEA-Cl, Apamin, 4-AP) and Na^+ (TTX) currents were used. Additionally, as mentioned above, 2 mM $CaCl_2$ was replaced in the EC by 10 mM $BaCl_2$. Cells were clamped at V_h = -90 mV (voltage-clamp mode) and 12 voltage steps (10 mV each, 200 ms) starting at V_h = -90 to +30 mV were applied. Changes in V_m caused by voltage steps resulted in rapid transient inward Ca^{2+} currents (Fig. 31 A, Fig. 32 A, B). An activation of the Ca^{2+} current was observed between -60 and -50 mV in Ad2 treated neurons and control neurons (Fig. 31 C, Fig. 32 B). At each applied voltage step, the amplitude of the Ca^{2+} current was measured. No significant differences in the maximal Ca^{2+} current, measured at about -10 mV (Fig. 31 C) between Ad2 treated and control neurons were observed (Fig. 31 A, n = 22-23). Furthermore, current densities of the Ca^{2+} current for both Ad2 treated and control cells were indistinguishable (Fig. 31 B). Thus, in general, the application of Ad2 did not result in differences of the properties of VGCCs.

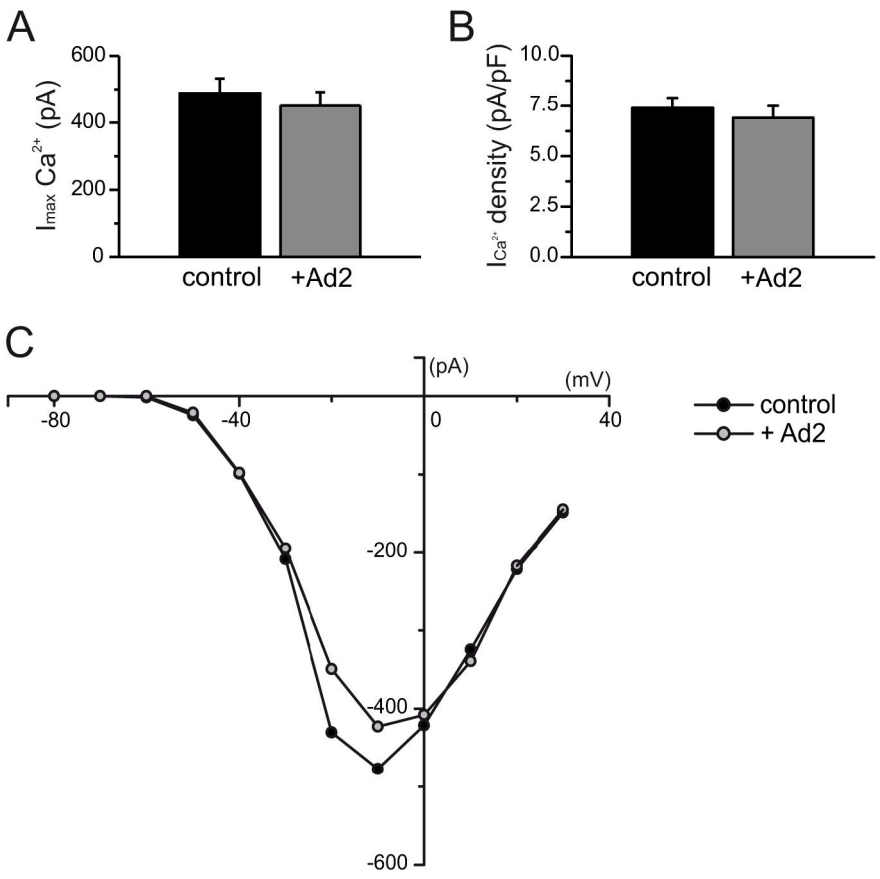

Fig. 31: Similar properties of voltage-gated Ca^{2+} channels in Ad2 treated and control neurons. Cortical neurons were prepared from E15 embryos and cultivated for 8 DIV. The maximal Ca^{2+} amplitude (A) as well as Ca^{2+} current density (B) were very similar in both cell types. (E) I-V relationship of recorded Ca^{2+} currents in Ad2 treated and control cells. Activation of the Ca^{2+} current, observed between -60 and -50 mV, was not changed in Ad2 treated neurons (n = 22-23).

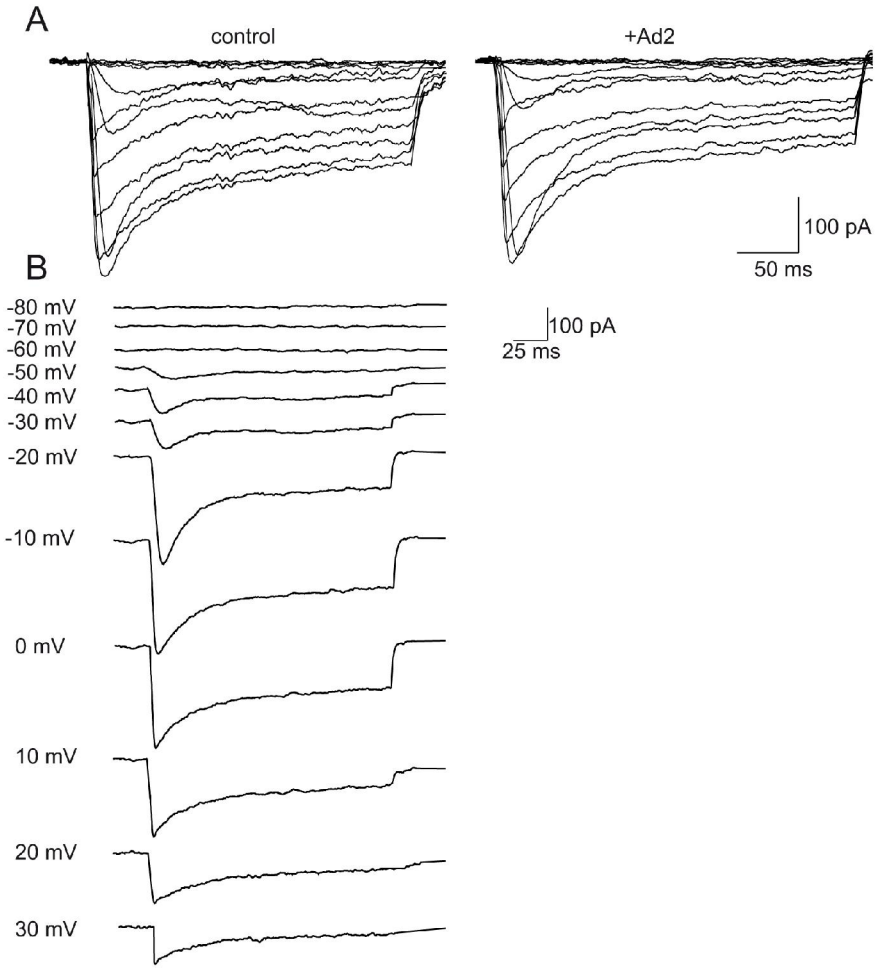

Fig. 32: Example traces of inward calcium currents in Ad2 treated and control cells. Cortical neurons were prepared from E15 embryos and cultivated for 8 DIV. (A) Ca^{2+} currents in control (left traces) and Ad2 treated neurons (middle traces) during application of 12 voltage steps. (B) Examples of single traces at each applied voltage step recorded from a control cell.

3.5 Non-voltage gated ion channels and other transport proteins in CAR-deficient neurons and Ad2 treated cells

As described above, voltage-gated ion channels are not constantly open at the RMP and thus, most probably, are not implicated in passive ion conductance occurring at the RMP. In addition to voltage-gated ion channels, there are many other channels and transport proteins which need to be considered in the context of the modulation of R_m. These could be ligand-gated channels (e.g. neurotransmitter-gated channels, cyclic-nucleotide-gated (CNG) channels), transport proteins (e.g. Na^+/K^+-ATPase pump), gap junctions or numerous leak ion channels. A strict classification of non-voltage-gated ion channels and transport proteins is often difficult due to their enormous diversity and their cell type-specificity.
In the following chapters several membrane proteins (channels) will be considered as potential candidates to explain changes in R_m in CAR KO and Ad2 treated cells.

3.5.1 Role of gap junctions in CAR mediated differences in R_m

Gap junctions (connexins) were considered in this study for the following reasons: 1) CAR is a cell surface protein mediating cell-cell contacts (Carson and Chapman, 2001; Cohen et al., 2001; Honda et al., 2000). In the absence of CAR the formation of cell-cell contacts (Dorner et al., 2005) and consequently the establishment of gap junctions might be affected. Furthermore, it has been reported that dye transfer through gap junctions was increased in cardiomyocytes of a heart-specific inducible CAR KO mice, suggesting that CAR might influence gap junction communication (Lisewski et al., 2008). 2) Connexins form large channels (pores) in the cell membrane and thus, their opening or closure can influence the R_m. (Russo et al., 2008; Sakai et al., 1992; Shelley et al., 2006; Sutor et al., 2000). 3) Different types of connexins are open at the RMP (their voltage dependency is beyond the RMP range). 4) Diverse connexins are abundantly expressed in neurons and glial cells and are very important in early stages of nervous system development. 5). On the one hand it has been shown that CAR interacts with the scaffolding protein ZO-1 in TJ of epithelial cells (Raschperger et al., 2006), on the other hand ZO-1 is associated with connexin 36 in retinal neurons (Cx36; Ciolofan et al., 2006). Thus, an indirect interaction between CAR and connexins is possible.

To investigate whether gap junctions are implicated in CAR-mediated changes, pharmacological blockers of gap junction were applied followed by the analysis of dye and electrical coupling. Furthermore, the expression pattern of different connexins was studied by Western blot and immunocytochemistry. Different gap junction blockers (Table 12) were acutely added to cultivated telencephalic CAR-deficient and WT neurons (DIV 7-12) during electrophysiological measurements. Application of carbenoxolone (CBX), a common gap junction blocker, to neurons resulted in a significant increase of R_m in WT cells, whereas no changes were observed in CAR-deficient neurons (Fig. 33 A; n = 22-25). This change in R_m occurred between 30 seconds and 1 min after application. Application of other blockers such as octanol, heptanol or NPPB showed similar results: R_m significantly increased in WT cells, whereas no effect could be observed in CAR KO neurons (Fig. 33 B, Table 12; n = 15-20 for each blocker). Hexanol, another alcohol related to heptanol or octanol, has been reported not to close gap junctions at concentrations below 5 mM (Rozental et al., 2001). Therefore, hexanol was applied to WT and CAR-deficient neurons. In both cultures no influence on R_m was observed (Fig. 33 B; n = 15). The lack of changes in the R_m in CAR KO neurons in the presence of gap junction blockers might indicate that gap junctions are not present or are inactive in knock-out cells. To further test the function of gap junctions, trimethylamine

(TMA) was applied, which has been reported to enhance gap junction opening probability (Hormuzdi et al., 2001; Pais et al., 2003). TMA slightly decreased R_m in WT neurons (not significant) which was not detectable in CAR-deficient neurons (Fig. 33 B; n = 15). These data suggest an abnormality in connexin function in CAR KO neurons. To test whether connexins are expressed in KO cells, protein levels and cellular distribution of different connexins were investigated by Western blot analysis and immunocytochemistry (Table 2). As shown in Fig. 33 D in both WT and CAR KO brain tissue (E10.5) the expression of Cx32, Cx36, Cx43 and Cx50 was indistinguishable. Cx26 was not detected in brain tissue but observed in liver tissue of adult WT or CAR heterozygote mice (Fig. 33 D lowest panel). Strong expression of Cx32, Cx36 and Cx43 was also detected in WT cortex tissue at different postnatal stages (Fig. 33 E). Interestingly, the expression pattern of Cx36 showed a similar expression profile as CAR during postnatal development (Fig. 33 E second and fouth panel). Immunocytochemical stainings revealed also no differences in subcellular distribution of Cx32 and Cx36 in CAR-deficient and WT neurons (Fig. 34).

In addition to pharmacological experiments in CAR-deficient and WT neurons (E10.5), an interesting observation was made after application of CBX to cortical neurons (E15) treated previously with Ad2 (500 µg/ml, 1 hour pre-incubation). CBX could partly abolish the Ad2-mediated effect on R_m (Fig. 33 C, n = 30-34).

To clarify whether the results obtained using gap junctional blockers are specific, dye and electrical coupling experiments in the presence of Ad2 were performed. In this set of experiments HeLa cell line was used for the following reasons: 1) HeLa cells express CAR endogenously. 2) HeLa cells were constantly available in contrast to CAR KO and WT cells (E10.5 and E15). 3) They are easy to handle. 4) HeLa cell lines are commonly used for investigations in dye or electrical coupling experiments (Bukauskas et al., 1995; Dobrowolski et al., 2007; Eckert et al., 1993; Lurtz and Louis, 2007). Initially, parental HeLa cells were characterized by patch-clamp recordings after 1 hour preincubation with Ad2. As shown in Fig. 35 A, Ad2 reduced R_m in HeLa cells, however the date did not reach statistical significance (n = 22). The C_m was not affected (Fig. 35 B). Therefore R_m *specific* was also reduced (not significant, Fig. 35 C).

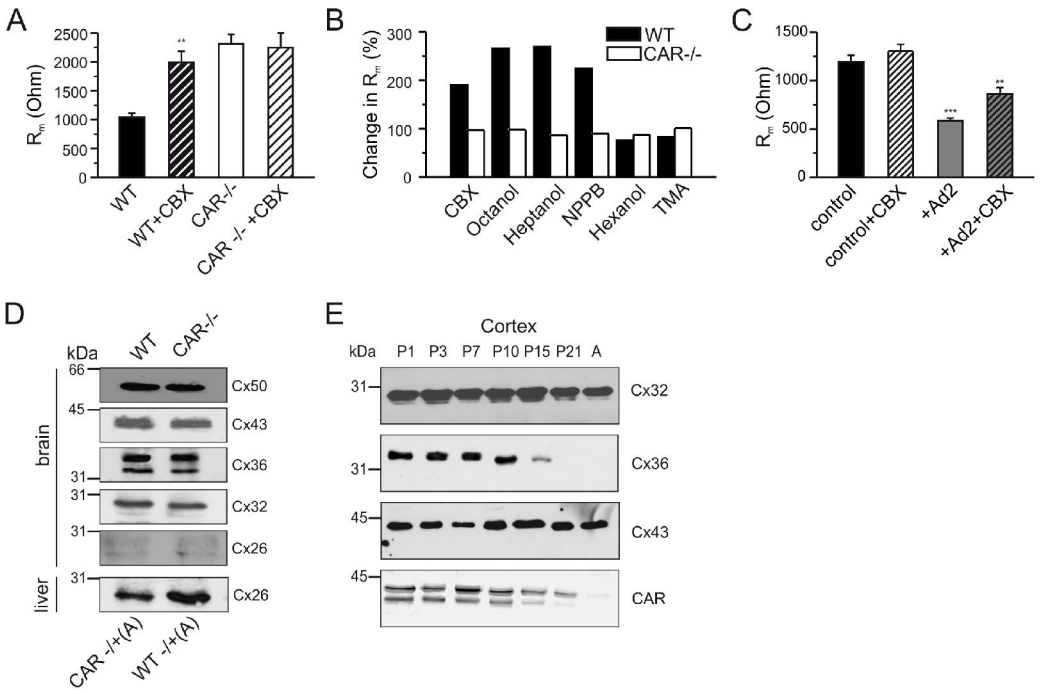

Fig. 33: Effect of different connexin blockers on R_m in cultivated neurons (E10.5) and expression of Cxs in neuronal tissue. (A) Application of CBX, a gap junction blocker, increased R_m in WT but not in KO cells. (B) Increase in R_m in WT cells, but not in KO cells after application of other gap junction blockers, presented in percent (%). R_m values for WT and KO cells were set to 100% before blockers were added. (C) Application of CBX to Ad2 treated cortical neurons (E15) partly abolished the effect of Ad2 on the R_m. (D) Protein expression levels of different Cxs in WT and KO brain tissue. (E) Expression pattern of different Cxs in WT cortex tissue during postnatal development (** - $p < 0.005$, *** - $p < 0.0005$).

Full name	**Abbr.**	**Final concentration**	**Selected references**	**Effect on connexins**
Carbenoxolone	CBX	250 µM	(Ye et al., 2003) (Weissman et al., 2004) (Kamermans et al., 2001) (Pottek et al., 2003) (Juszczak and Swiergiel, 2009)	blocker
5-nitro-2-(3-phenylpropylamino) benzoic acid	NPPB	15 µM	(Braet et al., 2003) (Srinivas and Spray, 2003) (Fioretti et al., 2004)	blocker
Octanol		1 mM	(Ye et al., 2003) (Bruzzone et al., 2001) (Contreras et al., 2002)	blocker
Heptanol		1 mM	(Ye et al., 2003) (Bruzzone et al., 2001) (Kondo et al., 2000)	blocker
Hexanol		1 mM	(Rozental et al., 2001)	neutral
Trimethylamine hydrochloride	TMA	10 µM	(Nassiri-Asl et al., 2008) (Pais et al., 2003)	opener

Table 12: Blockers used to study gap junctions in WT and CAR-deficient neurons.

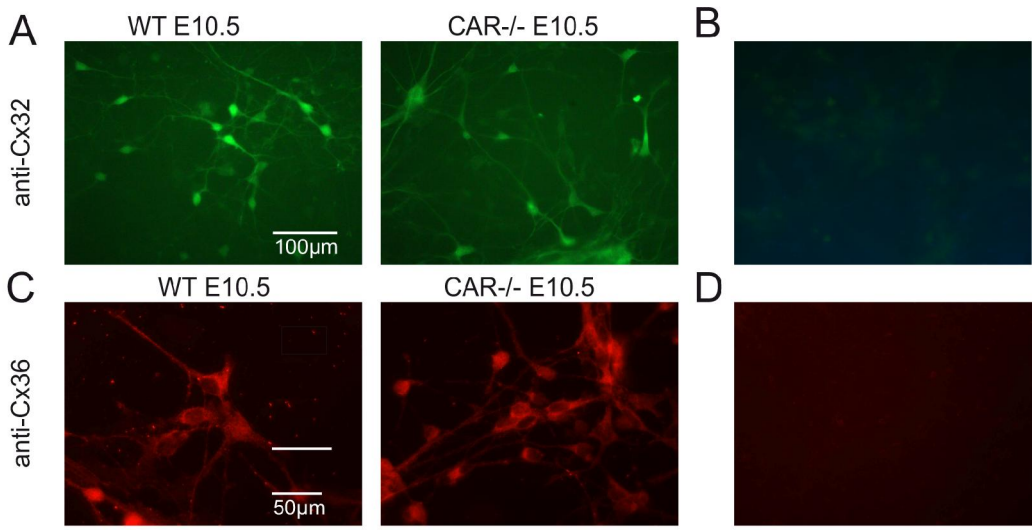

Fig. 34: Immunocytochemical staining revealed a similar distribution of Cx32 (A) or Cx36 (C) in CAR KO and WT neurons (E10.5). Stanings with only secondary antibodies (coupled to Alexa488 in B and coupled to Cy3 in D right image) were both negative.

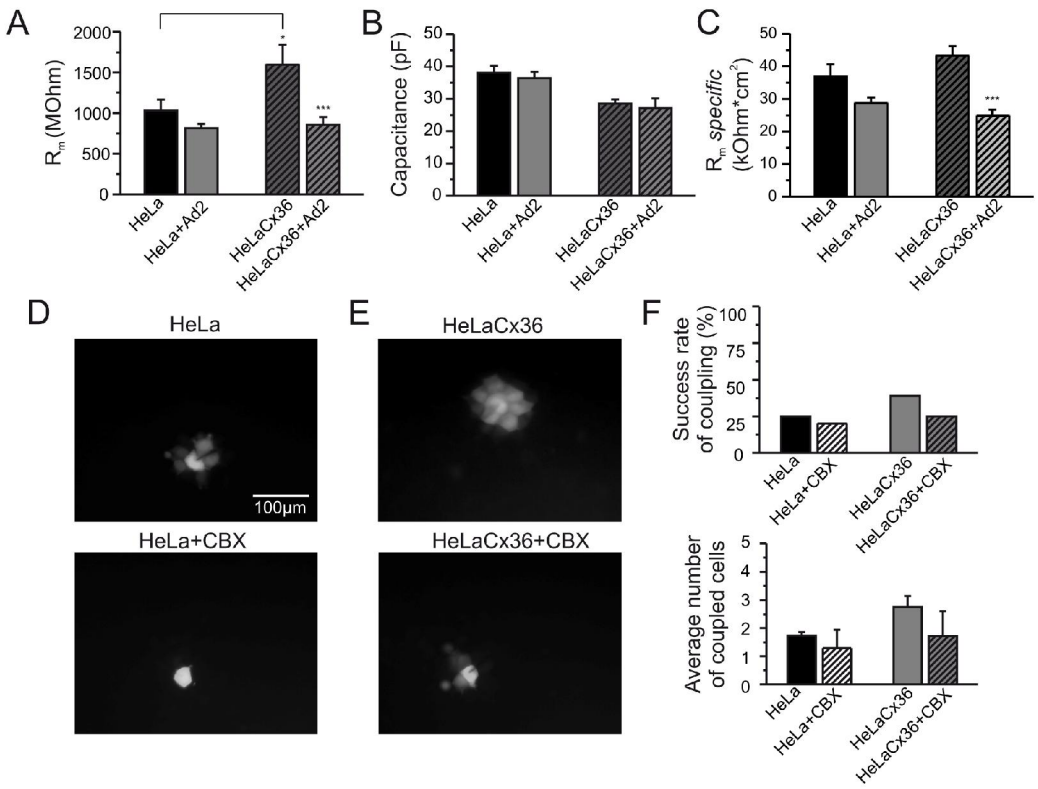

Fig. 35: Effect of Ad2 on R_m and LY spreading in parental HeLa cells and HeLa cells stably transfected with connexin 36 (HeLaCx36). (A-C) Ad2 was able to reduce R_m (A) in both types of cells (n = 22-29). The C_m (B) remained unchanged and therefore the R_m *specific* (C) was also reduced. (D, E, F) Injection of LY revealed a very low spreading rate (F) in parental HeLa cells with a maximal number of 6 cells filled with dye (D) and an average of 1.73±0.14 cells (F) compared to transfected HeLaCx36 cells with maximally 10 cells filled with dye (E) and an average of 2.75±0.4 (F) after 10 min of injection (* - $p < 0.05$, *** - $p < 0.0005$).

Next, dye coupling experiments with Lucifer yellow (LY) were performed, a dye commonly used to investigate dye spreading via gap junctions in confluent cells (Bossinger and Schierenberg, 1996; Lavado et al., 1997; Chanson et al., 2001;Chaytor et al., 1999). 4% LY diluted in LiCl was injected with a sharp electrode into a selected HeLa cell. The dye immediately filled the cell and spread over time (1-20 min) to neighboring cells. However, in parental HeLa cells a very low rate of dye spreading was observed, as shown in Fig. 35 D and F. Application of the commonly used gap junction blocker CBX resulted in a slight decrease in dye spreading (Fig. 35 D, F). Thus, parental HeLa cells seemed to express connexins at a very low level and therefore were not suitable for investigation of gap junction coupling properties. Therefore, HeLa cells stably transfected with connexins 36 (HeLaCx36, kindly provided by Prof. K. Willecke) were used in further experiments. Connexin 36 (Cx36) was chosen because it shows a similar expression pattern as CAR (Fig. 33 E) and is found in neurons (Condorelli et al., 2000; Martin et al., 2003).

As shown in Fig. 35 A, Ad2 application for 1 hour significantly reduced R_m in HeLaCx36 cells (n = 25-29; $p < 0.0005$). Since C_m was not affected (Fig. 35 B), R_m *specific* was also significantly reduced (Fig. 35 C; $p < 0.0005$). An interesting finding was that the R_m of control HeLaCx36 cells was significantly higher than in parental control cells (Fig. 35 A; $p < 0.05$).

Next, dye coupling was investigated using HeLaCx36 cells. As shown in Fig. 35 E and F HeLaCx36 cells were coupled more to each other than parental cells (E). About 40% of tested cells showed dye transfer with an average of about 3 coupled cells (F). Treatment of HeLaCx36 with CBX reduced dye transfer between cells (Fig. 35 E lower image and 35 F). In addition to dye injection experiments, Cx36 protein level was tested by means of Western blot and immunocytochemical staining. Western blot analysis revealed very strong expression of Cx36 in transfected HeLaCx36 cells (Fig. 36 A), whereas Cx36 was almost not detectable in parental HeLa cells (Fig. 36 A). Specificity of the antibodies was tested in liver tissue, where no expression was detected (Fig. 36 A) as previously reported (Srinivas et al., 1999). Immunocytochemical stainings revealed strong expression of Cx36 in HeLaCx36 cells (Fig. 36 C), especially concentrated at cell-cell contacts (Fig. 36 C, see arrows), similar to the expression of CAR in these cells (Fig. 36 D, see arrows). Cx36 was not detectable in parental HeLa cells (Fig. 36 B). These results suggested that transfected HeLaCx36 cells were more suitable for further investigation of junctional coupling.

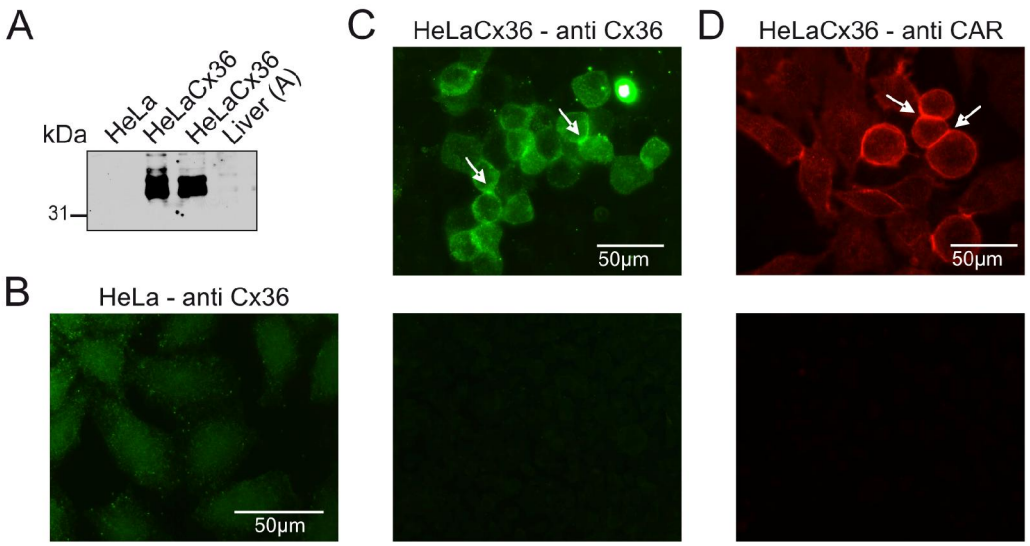

Fig. 36: Western blot analysis and immunofluorescence analysis of Cx36 and CAR. (A) Western blot analysis revealed strong expression of Cx36 in transfected HeLa cells, whereas no signal was detected in parental HeLa cells. (B-D) Cx36 was detected primarily at cell-cell contacts in transfected HeLaCx36 cells (C, see arrows), whereas almost no expression was found in parental HeLa cells (B). Staining with only secondary antibodies was negative (C lower image). (D) Expression of CAR in transfected HeLaCx36 cells was concentrated at the cell membrane and at cell-cell contacts (arrows). Staining with only secondary antibodies was negative (D, lower image).

To investigate electrical coupling, a dual whole-cell patch-clamp recording technique was applied. That is two neighboring cells were recorded simultaneously to measure the junctional current (I_J; Fig. 13). Both cells were clamped at V_h = 0 mV. In one cell (cell 1, red in Fig. 37 A, B) one 10 mV step (Fig. 37 A) or 10 10 mV steps (Fig. 11 C right side, from V_h = 0 mV to +100 mV and to -100 mV, each step for 10 s; Fig. 37 B) were applied. In the case of coupling by gap junctions, a current (I_J) could be recorded from the neighboring cell (cell 2, black in Fig. 37 A, B). Since gap junctional coupling is bidirectional (see arrows in Fig. 37 A), the same voltage protocols were applied in cell 2 to measure I_J in cell 1. Cells showed different current responses to applied voltages, depending on their passive membrane properties (e.g. R_m; Fig. 37 A - example traces of two different recorded pairs: pair 1 and pair 2). From the recorded I_J and calculated junctional voltage (V_J; V_J = V2 – V1; where V2 is not changing V_h = 0 mV and V1 is changing between -100 to 100 mV), the junctional conductance (G_J; $G_J = I_J/V_J$) could be calculated.

To investigate if CAR may be implicated in the modulation of junctional coupling, Ad2 treated (1 hour per-incubation) HeLaCx36 cells and control HeLaCx36 cells were measured. As shown in Fig. 37 B similar current responses to the applied voltage steps were recorded in Ad2 treated and control cells. From the measured I_J and calculated junctional voltage (V_J) values, the junctional conductance (G_J; $G_J = I_J/V_J$) in both types of cells was deduced (Fig. 37

C). Calculated G_J were normalized by normalizing G_J at +10 and -10 mV to 1. No significant differences were observed in I_J or in G_J between Ad2 treated and control HeLaCx36 cells. In both cases the junctional coupling showed voltage dependency (Fig. 37 B, C) with a higher and linear conductance at membrane potentials around 0 mV and lower conductance at higher positive and more negative potentials (e.g. +80 to +100 or -80 to -100 mV, Fig. 37 C). These data suggest that Ad2 had no influence on electrical coupling of HeLaCx36 cells.

Since Cx36 is not the only gap junction protein, HeLa cells expressing Cx43 were analyzed in the presence of Ad2 (HeLaCx43; kindly provided by Prof. K. Willecke). These HeLaCx43 cells show an efficient coupling rate (Elfgang et al., 1995;Haubrich et al., 1996). LY injection resulted in very fast and efficient dye spreading to over 100 neighboring cells in up to 10 min (Fig. 38 A, B). This dye diffusion could be efficiently blocked by application of the gap junction blocker CBX (Fig. 38 A, right image). However, no significant differences in the number of cells and the spread dye area were observed between control HeLaCx43 cells (number of cells: 152.9±16.2, area: 69.3±7.1 mm^2; n = 14 injections, Fig. 38 A, B) and Ad2 treated cells (number of cells: 143.3±2.7, area: 60.3±7.9 mm^2; n = 14 injections; Fig. 38 A, B). Thus, Ad2 did not influence gap junctional coupling in HeLaCx43 cells.

Taken together, the following conclusions can be drawn: 1) Treatment with gap junction blockers resulted in an increase of R_m in WT neurons (E10.5 and E15), whereas application of a gap junction opener TMA slightly reduced R_m (E10.5). 2) Gap junction blockers had no effect on R_m in CAR KO cells (E10.5). 3) Western blot analysis and immunocytochemical stainings revealed similar levels of expressions of different connexin proteins in CAR KO and WT brain tissue and cultivated neurons, suggesting that connexins are present in CAR-deficient neurons. 4) The gap junction blocker CBX could partly abolish the effect of Ad2 on R_m in cultivated cortical neurons (E15). 5) Application of Ad2 to parental HeLa cells and HeLa cells transfected with Cx36 decreased R_m. 6) Ad2 did not affect dye spreading and electrical coupling in HeLaCx36 or HeLaCx43 cells.

Although pharmacological experiments suggest that Cxs might be implicated in the observed changes in R_m in CAR KO neurons and Ad2 treated cells, no further evidence for their involvement could be found. Furthermore, applied Cxs blockers have been reported to have side effects e.g. influencing Ca^{2+} channels and synaptic activity (Leshchenko et al., 2006; Ross et al., 2000; Rouach et al., 2003; Vapaatalo et al., 1978; Vessey et al., 2004; Yang and Ling, 2007) and thus the results with gap junctional blockers should be considered with caution.

Results from dye spreading and electrical coupling experiments using cell lines and Ad2 treatment, may exclude that gap junctions are affected by Ad2.

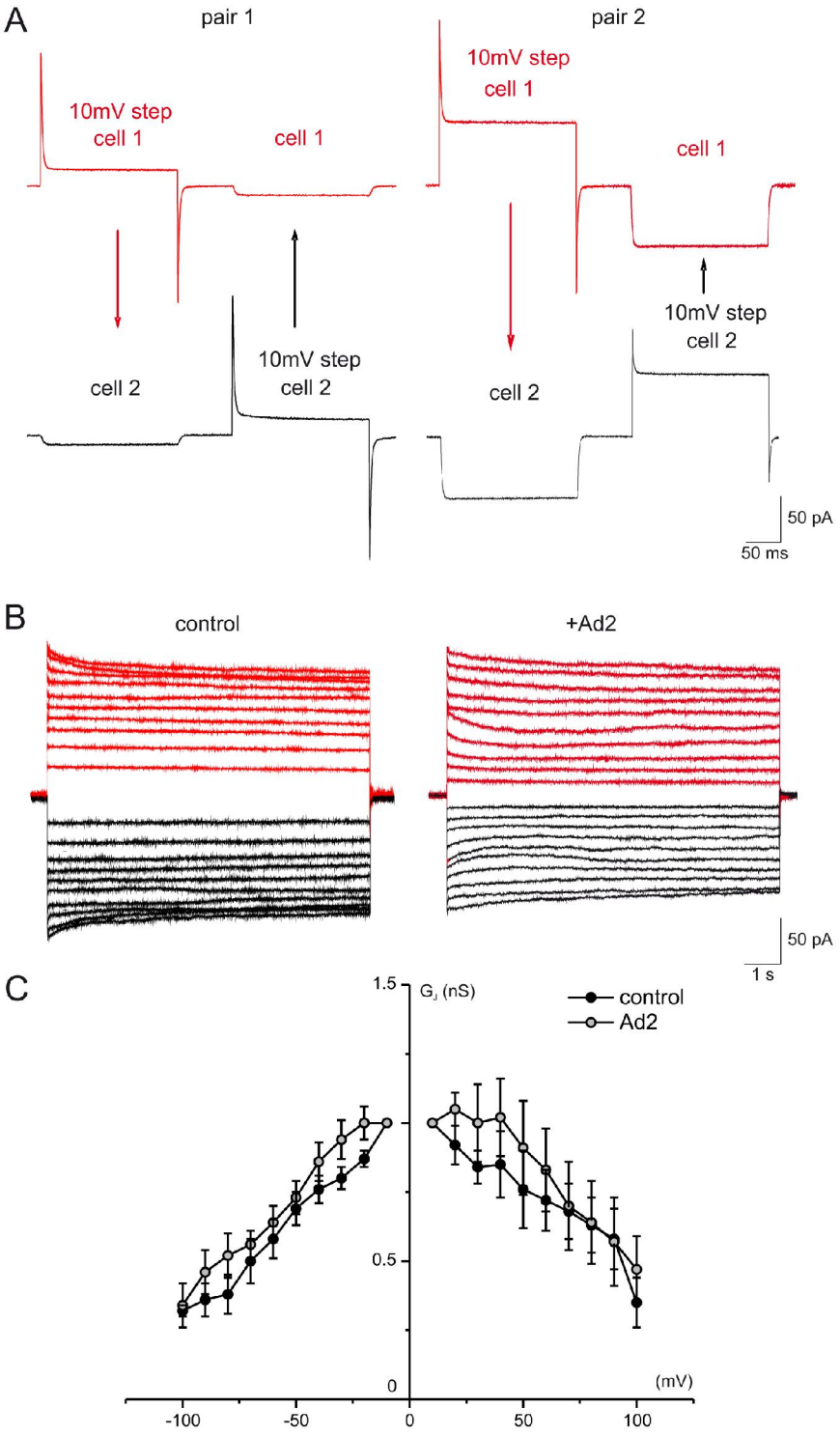

Fig. 37: Electrical coupling in transfected HeLaCx36 cells was not affected by treatment with Ad2 (1 hour pre-incubation). (A) Example traces of two different pairs of coupled cells. Application of a 10 mV voltage step in cell 1 (red) resulted in current flow in cell 2 (black). Voltage could also be applied in cell 2 and recorded in cell 1 (see arrows) because junctional coupling is bidirectional.(B) Example traces of recorded I_J from Ad2 treated cells and control cells. No significant differences were observed. (C) Calculated G_J was also not changed after treatment with Ad2. G_J showed typical voltage-dependency.

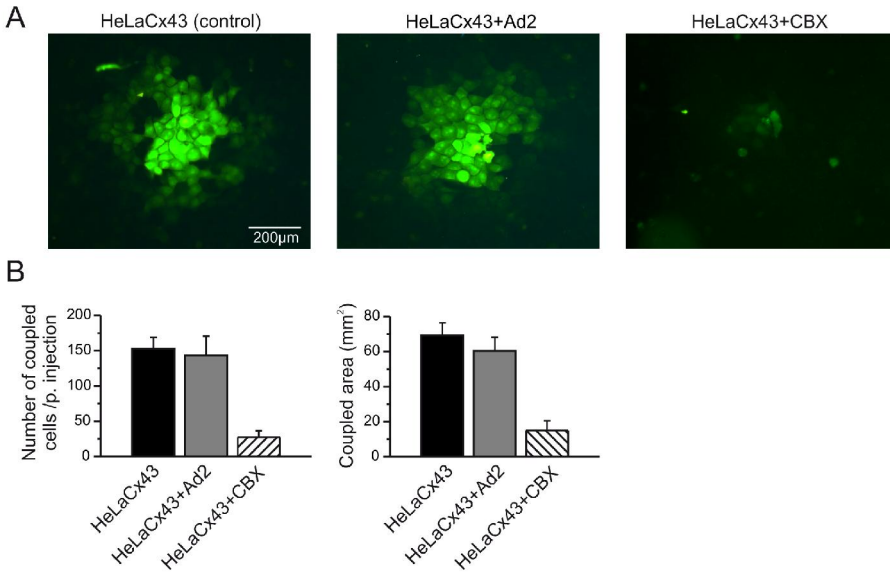

Fig. 38: Ad2 did not influence dye spreading in transfected HeLaCx43 cells. (A) 4% LY was injected by a sharp electrode to one cell and diffused to over 100 neighboring cells over a short time (1-20 min; n = 14 injections). (A) No differences in dye diffusion between control and Ad2 treated cells could be observed. Application of CBX blocked dye transfer. (B) Quantification of dye spreading in control and Ad2 as well as CBX treated cells. A similar number of cells filled with dye and a similar area of coupled cells were measured in Ad2 treated and control cells. CBX reduced the number and the area of coupled cells significantly.

3.5.2 Neurotransmitter-gated receptors

3.5.2.1 Neurotransmitter-gated ionotropic receptors

Neurotransmitter-gated receptors can be classed as ionotropic or metabotropic receptors. Both groups are activated by binding of a neurotransmitter. Metabotropic receptors are often coupled to G proteins and their activation leads to a series of intracellular events among which activation of some ion channels may occur as a secondary effect (indirect activation). Binding of a neurotransmitter to an ionotropic receptor leads directly to the opening of that ion channel. Such receptors are located mainly at synapses to convert the chemical signal of presynaptically released neurotransmitters directly and very quickly into a postsynaptic electrical signal. To this group belong e.g. $GABA_A$ receptors, nicotinic acetylcholine receptors (nAChRs) or glutamatergic receptors (e.g. AMPA, kainate and NMDA receptors). As an example of a neurotransmitter-gated ionotropic receptor, the $GABA_A$ receptor, was considered in the context of CAR and Ad2. Upon activation, by GABA (γ-aminobutyric acid), the $GABA_A$ receptor selectively conducts Cl^- through its pore, resulting in depolarization or hyperpolarization of the neuron depending on Cl^- concentration in the cell. Due to synaptic activity, GABA release and receptor activation occurred in cultivated WT and CAR KO neurons (E10.5). Under these conditions, a significantly higher R_m in CAR KO cells

compared to the WT cells was observed as already described (see Fig. 18 A-C, Fig. 39, n = 36-40). When the $GABA_A$ receptor was selectively blocked by application of biccuculine, the difference in R_m still remained (Fig. 39), suggesting that the $GABA_A$ receptor is not implicated in the increased R_m in CAR KO cells.

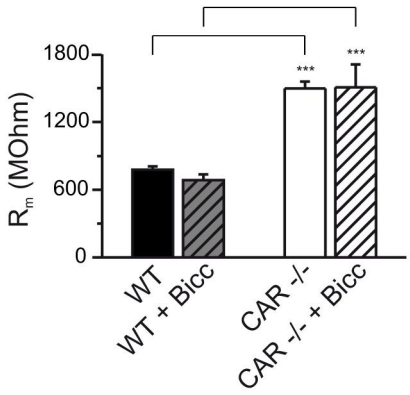

Fig. 39: The R_m difference between CAR KO and WT neurons remained significant after blocking of $GABA_A$ receptors ($p < 0.0005$, n = 36-40). Neurons were prepared from wild type and CAR-deficient embryos at E10.5 and cultivated for 14 DIV followed by acutely treatment with biccuculine (20 µM) and patch-clamp recordings. Abbreviation: Bicc - biccuculine

For the following reasons other neurotransmitter-gated ion channels are most likely not a cause for the R_m differences observed between CAR -/- and WT neurons or between Ad2 treated and untreated neurons: 1) Neurotransmitter-gated channels are in general closed at the RMP and open only when a neurotransmitter binds. In none of the experiments neurotransmitters were applied. In cultivated neurons a spontaneous release of neurotransmitters occurs due to synaptic input in both WT and CAR-deficient neurons (see chapter 3.9.2). Additionally, the spontaneous activity at DIV 7 is very rare, but observed differences in R_m are highly significant at this stage, suggesting that synaptic activity is not implicated in this effect. 2) Neurotransmitter-gated ion channels open only for a very short period (ms). This time scale is most likely too short to permanently influence R_m.

3.5.3 Na^+/K^+-ATPase pump

The Na^+/K^+-ATPase pump has been considered in this study because of numerous reasons: 1) CAR binds to agrin (Patzke et al., 2009, submitted), and agrin has been shown to inhibit the Na^+/K^+-ATPase through binding to its α3 subunit (Hilgenberg et al., 2006; Hilgenberg and Smith, 2004). Furthermore, CAR and agrin co-localize at the neuromuscular junction (Shaw et al., 2004) and in the inner plexiform layer of the developing retina (Kroger et al., 1996). It is therefore conceivable that CAR modulates the Na^+/K^+-ATPase indirectly via agrin. 2) The pump is electrogenic and thus responsible for ionic current through the membrane under RMP

(Brodie et al., 1987; Deleze, 1960; Glitsch, 2001; Sjodin, 1982; Thomas, 1972). When it is activated, it causes a significant hyperpolarization (Bray et al., 1976; Locke and Solomon, 1967). 3) Blockage of the Na^+/K^+-ATPase pump with ouabain has been reported to increase the R_m (Matsumoto et al., 2008; Planelles and Anagnostopoulos, 1987). 4) The Na^+/K^+-ATPase pump plays an important role in the determination of the RMP (Brodie et al., 1987; Brodie and Sampson, 1985; Glitsch, 2001; Thomas, 1972; Volkov et al., 2000). Thus it is active at the RMP. 5) The Na^+/K^+-ATPase pump appears to be an ubiquitous characteristic of all cells and it is the main representative of membrane transporters for ions in the cell membrane (other pumps will to a lesser degree participate in the establishment of the RMP compared to the Na^+/K^+ pump). Thus, if the Na^+/K^+-ATPase would be impaired in CAR KO cells, the current amplitude flowing through the membrane would be affected and so in turn would the R_m. This should also have consequences for synaptic transmission because modulation of the Na^+/K^+-ATPase pump activity influences de- or hyperpolarization of the cell, depending upon its inhibited or activated state respectively.

To test whether this protein is expressed in CAR-deficient neurons, immunocytochemical staining using antibodies against neuronal alpha-3 subunit of the Na^+/K^+-ATPase (Table 2) was performed. A similar expression level as well as distribution throughout the neuron was observed in CAR KO and WT cells, suggesting that this protein is normally expressed in CAR-deficient neurons (E10.5; Fig. 40 A).

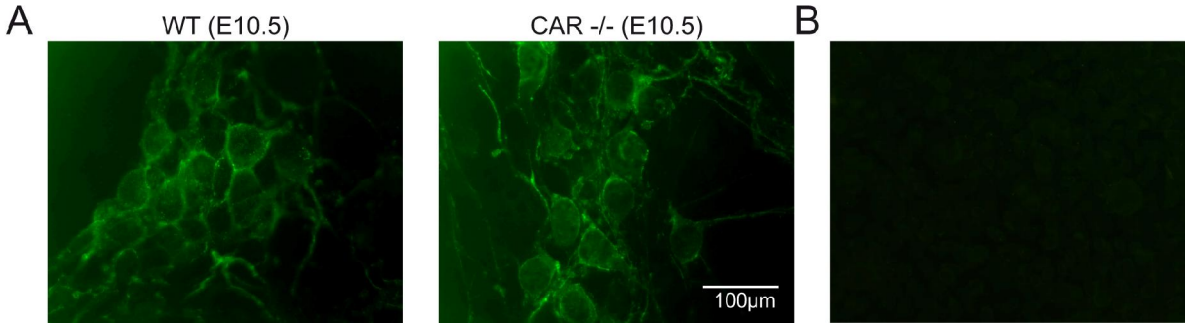

Fig. 40: Expression of the alpha 3 subunit of the Na^+/K^+-ATPase was similar in CAR KO and WT cells prepared from embryos at E10.5 and cultivated for 12 DIV (A). (B) Staining with only secondary antibodies (coupled to Alexa 488) was negative.

To evaluate the function of the Na^+/K^+-ATPase in CAR-deficient neurons, ouabain (10 µM) was acutely applied to CAR KO and WT neurons (E10.5, DIV 10, n = 20-22). Ouabain immediately increased R_m significantly in WT cells (and respectively the R_m *specific*, Fig. 41 A, C, D; $p < 0.05$), but had no effect on CAR KO cells (Fig. 41 A, C, D). In addition to a change in R_m, a change in spontaneous synaptic activity was observed. Blocking of the Na^+/K^+-ATPase resulted in a significant increase in the frequency of spontaneous

postsynaptic currents in both WT and CAR KO cells (Fig. 41 E). The effect of ouabain on spontaneous synaptic activity lasted only a very short time before the frequency drastically decreased until none of the recorded cells showed any synaptic currents (Fig. 41 E). This was due to the depolarization of neurons caused by the Na^+/K^+-ATPase blocker. Depolarization resulted in a less negative RMP (Fig. 41 F), which could not be restored because of the blocked pump and consequently all neurons remained depolarized resulting in an absence of synaptic currents (Brodie and Sampson, 1985).

Although ouabain caused an increase in R_m only in WT cells and not in CAR KO cells, an increase in the frequency of spontaneous activity indicates that the pump was active and can be blocked in both genotypes. I therefore conclude that the Na^+/K^+-ATPase is functional in CAR KO neurons and suggest that Na^+/K^+-ATPase is most probably not involved in R_m differences between CAR KO and WT cells.

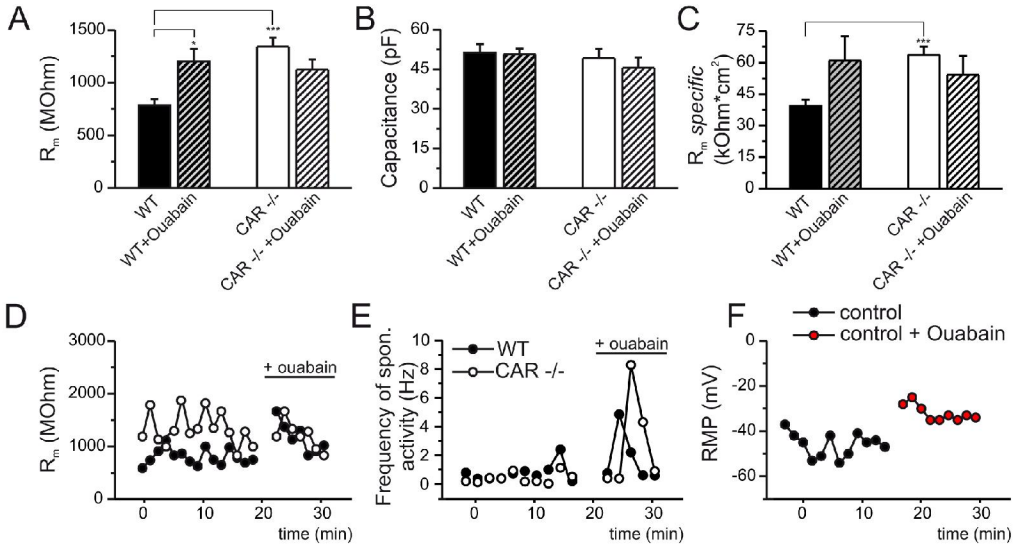

Fig. 41: Effect of ouabain (10 µM) on R_m and synaptic activity in CAR KO and WT cells (E10.5). (A) Application of ouabain (10 µM) increased R_m significantly in WT ($p < 0.05$, n = 20-22), but not in CAR KO cells. (B) C_m in both cell types was not changed. (C) R_m *specific* in WT cells was increased (not significantly). (D) R_m values of single cells before and after ouabain application. (E) Acute ouabain treatment caused an increase in frequency of spontaneous postsynaptic currents in both WT and CAR KO cells. This occurred only for a short time because blockage of the Na^+/K^+-ATPase pump caused depolarization of neurons. (F) Application of ouabain to control cells (WT, E15) resulted in a less negative RMP. Abbreviation: spon. – spontaneous.

3.5.4 Hyperpolarization-activated cyclic nucleotide-gated cation channels

HCN channels were considered in this study because of their important role in the determination of the neuronal RMP (Luthi and McCormick, 1998; Pape, 1996; Poolos, 2004; Tan et al., 2007). These channels show a high permeability for K^+ and Na^+ at the RMP and their permeability is enhanced by hyperpolarization and/or by binding of intracellular cyclic

nucleotides e.g. cyclic adenosine monophosphate (cAMP; Aponte et al., 2006; Bolivar et al., 2008; Lyashchenko and Tibbs, 2008). This channel is open and allows ionic flow at the RMP. It may therefore play a role in passive membrane properties including R_m. Although it appears to be demanding to identify HCN mediated currents due to complex properties of HCN channels (voltage-gating, ligand-gating and passive conductance at RMP for both K^+ and Na^+), recordings were performed to investigate whether HCN channels are functional in CAR KO and WT neurons.

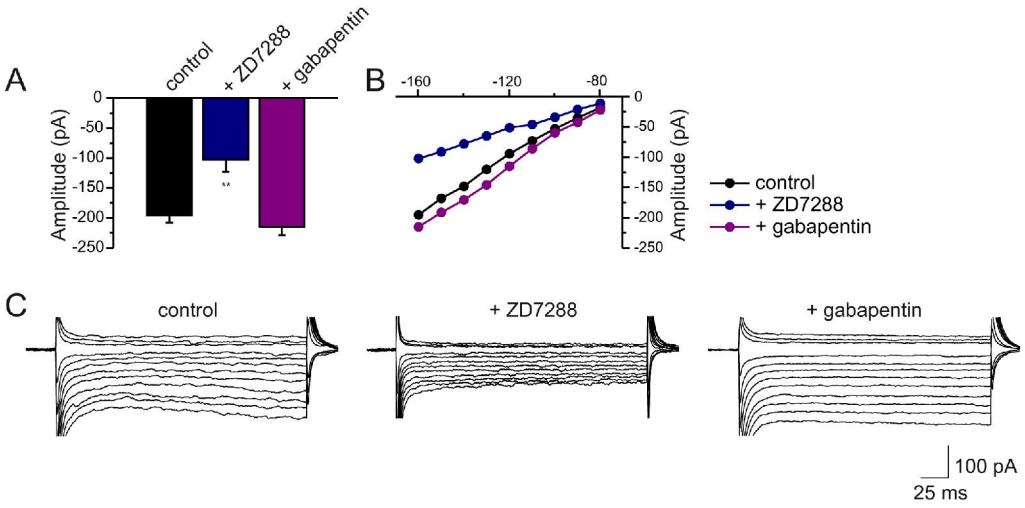

Fig. 42: Characterization of the HCN current in cortical neurons (E15, DIV 12). (A) Maximal current amplitude measured at -160 mV in control cells (E15). The amplitude was significantly reduced in cells treated with blocker ZD7288 (100 µM; $p < 0.005$, n = 16) and slightly increased in cells treated with the enhancer gabapentin (100 µM, n = 8). (B) Current-voltage (I-V) relationship representing voltage-dependency of the HCN current. The amplitude could be influenced by application of a blocker or enhancer. (C) Example traces of currents evoked by application of 3 depolarizing steps (from -70 to -55 mV) followed by 9 hyperpolarizing steps (from -70 to -160 mV) in a control cell (left traces), in a cell treated with the blocker ZD7288 (100 µM, middle trace) and in a cell treated with the enhancer gabapentin (100 µM, right trace).

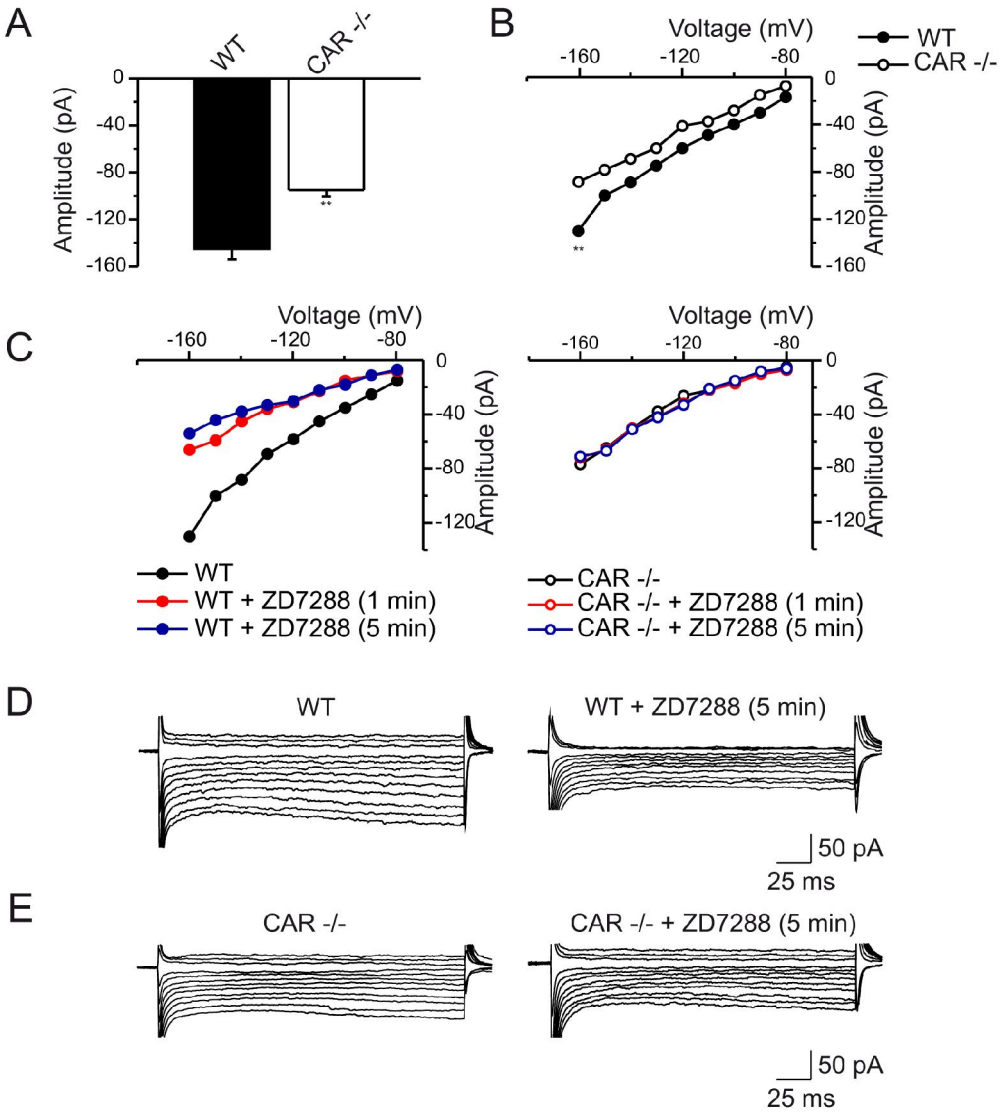

Fig. 43: Characterization of the HCN current in WT and CAR KO cells (E10.5). (A) The maximal amplitude of the HCN current measured at -160 mV was significantly lower in CAR KO cells than in WT cells ($p < 0.005$, n = 33-37) (B) Current-voltage (I-V) relationship showing voltage-dependency of the HCN current in both WT and KO cells. The current recorded in CAR KO cells was smaller than in WT cells. (C) Application of blocker ZD7288 (100 µM) reduced the current amplitude in WT cells, but not in CAR KO cells (n = 8). (D, E) Example traces of currents evoked by application of 3 depolarizing steps followed by 9 hyperpolarizing steps in WT neurons (D) and CAR KO neurons (E) before (left traces) and after application of blocker ZD7288 (100 µM, right trace).

In this study the HCN current was identified by application of known modulators and by application of hyperpolarizing voltage steps (Fig. 11 C) to control neurons (E15). From V_h = -70 mV, three control depolarizing steps were applied (5, 10 and 15 mV, from -70 to -55 mV) followed by 9 hyperpolarizing steps, each 10 mV for 200 ms (from V_h = -70 mV to -160 mV). Hyperpolarizing steps evoked inward currents (Fig. 42 C). The current-voltage (I-V) relationship revealed that with increasing voltage amplitude, the HCN-current amplitude

increases (Fig. 42 B; Fig. 43 B, C). This was in accordance with published reports describing HCN currents (Ludwig et al., 1998; Matsumoto et al., 2008; Moosmang et al., 2001; Surges et al., 2003). The maximal current was measured at the steady-state stage at the end of the pulse. Application of the commonly used blocker ZD7288 (100 µM; Bedner et al., 2006; Felix et al., 2003; Gonzalez-Iglesias et al., 2006; Prole and Yellen, 2006) significantly reduced the amplitude of the recorded current (Fig. 42 A, B, C left and middle traces, n = 16), whereas treatment with a known enhancer gabapentin (100 µM; Lin et al., 2009; Wickenden et al., 2009) slightly increased the current, which, however, did not reach statistical significance (Fig. 42 A, B, C left and right traces, n = 8). Thus, the recorded inwardly directed current showing voltage-dependency and sensitivity to ZD7288 or gabapentin was defined as the HCN current.

In the following experiments, the properties of the HCN current in CAR-deficient neurons were analyzed. Application of hyperpolarizing voltage steps (Fig. 11 C) resulted in an inward current with significantly lower maximal amplitude in CAR-deficient neurons compared to WT cells (Fig. 43 A, B, n = 33-37). Furthermore, in contrast to WT neurons, ZD7288 was unable to reduce the current amplitude in CAR KO cells (Fig. 43 C, E, n = 8).

Consistent with these results, treatment of control neurons with Ad2 (1 hour pre-incubation) resulted in a higher current amplitude than in untreated cells (E15; Fig. 44 A, B, C, n = 20-25, only the maximal HCN current amplitude was significantly higher, $p < 0.05$). In both control and Ad2 treated cells, the characteristic voltage-dependency of the HCN current was observed (Fig. 44 B, C).

From these results no clear conclusion can be drawn about the involvement of HCN channels in CAR-mediated R_m changes. These data do not exclude HCN channels as a candidate for observed changes in membrane properties in CAR KO cells and Ad2 treated cells, but do not give sufficient evidence for their implication. These data confirm that at the RMP and at high negative membrane potentials, less current flows through the membrane of CAR KO cells compared to WT cells, and more current flows through the cell membrane of Ad2 treated cells compared to control cells, suggesting altered membrane conductance in both cases.

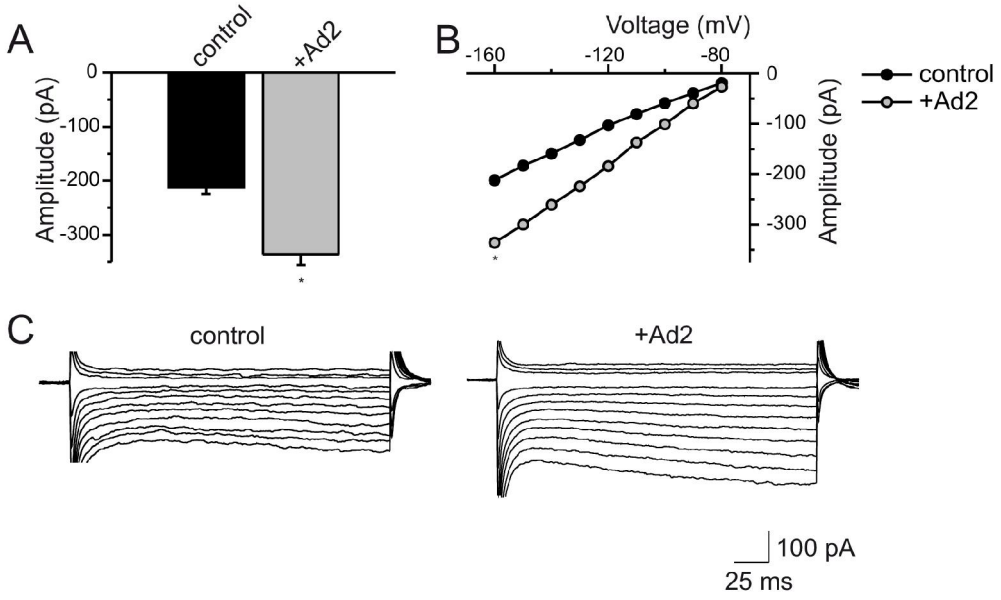

Fig. 44: Treatment of cells with Ad2 resulted in higher HCN current amplitudes compared to untreated neurons (E15, DIV 8). (A) Maximal amplitude of the HCN current measured at -160 mV was significantly higher in Ad2 treated cells compared to control cells ($p < 0.05$, n = 20-25). (B) Current-voltage (I-V) relationship showing voltage-dependency of the HCN current in both control and Ad2 treated cells. (C) Example traces of currents evoked by application of 3 depolarizing steps followed by 9 hyperpolarizing steps in control cells (left traces) and Ad2 treated neurons (right trace).

3.6 Changes in passive conductance through the neuronal membrane in CAR KO cells and Ad2 treated neurons

To identify the reason for the increased or decreased R_m in CAR-deficient neurons and Ad2 treated neurons, respectively, the passive membrane conductance for particular ions was investigated. The advantage of this method is that although a specific ion (e.g. K^+, Na^+, Cl^-) may cross the membrane through different ion channels/transport proteins under RMP, the whole passive current, produced by this ion, can be measured. Thus, this method focuses on the identification of the ion that is responsible for the changes in R_m rather than on the channels which might be involved. In order to address this question and to distinguish particular ion currents, different recording solutions (EC and IC) as well as specific blockers were used for recordings.

3.6.1 Passive potassium (K^+) conductance is not involved in R_m changes

Since the neuronal membrane is most permeable for K^+ ions, the passive conductance for K^+ through the membrane was initially investigated. The R_m of CAR WT and KO neurons was measured at standard K^+ concentration and in K^+ free conditions in order to test whether K^+ conductance might be involved in the R_m difference between CAR KO and WT cells. Under standard conditions a KCl-based IC solution was used, where the intracellular K^+ concentration was 90 mM or 120 mM (Table 7, 8) and E*rev* $_{(K+)}$ = -91 mV or -94 mV for low and high osmolality solution, respectively (E*rev* calculated using Nernst equation, see chapter 2.2.5.6). The extracellular K^+ concentration was 3 mM in both low and high osmolality EC solutions. Under these concentration conditions and V_h = -70 mV, K^+ moves out of the cell due to its electrochemical gradient. Measurements of passive membrane properties using a KCl-based IC solution revealed a significantly higher R_m in CAR KO cells compared to the WT cells (Fig. 18, Fig. 45 A, B; $p < 0.0005$). To verify if the R_m difference is due to passive K^+ conductance through the membrane, K^+ was substituted in the IC solution by Cs^+ ions (CsCl-based IC, Table 7, 8).Thus, the intracellular K^+ concentration was about 0 mM, whereas the extracellular K^+ concentration remained unchanged at about 3 mM. Under these conditions there was no passive K^+ conductance through the membrane because there were no K^+ ions to leave the cell. Exchanging K^+ by Cs^+ shifted the E*rev* $_{(K+)}$ form -91 to +29 mV. Using K^+ free IC solution (CsCl-based IC), the R_m in CAR WT and KO cells was measured. As shown in Fig. 45 A, B in the absence of intracellular K^+, the difference in R_m between CAR KO and WT cells remained significant (n = 30-40; $p < 0.0005$). The calculated R_m *specific* (R_m*C_m) was also significantly higher in CAR KO cells in the absence of K^+ (Fig. 45 B right diagram; $p < 0.0005$). Removal of K^+ from the solution slightly increased the R_m in both CAR KO and WT cells compared to the R_m obtained in KCl-based IC solution, suggesting that in both cases the K^+ conductance was successfully blocked (Fig. 45 A). An increase of R_m after the removal of K^+ from the cell indicates the importance of K^+ conductance in maintaining the R_m (Fig. 45 A). However, these results suggest that passive conductance of K^+ through the membrane is not responsible for the R_m differences between CAR KO and WT cells.

Consistent with the data from CAR KO and WT neurons, Ad2 was also able to significantly reduce R_m under K^+ free conditions (n = 22-27; Fig. 45 C, D; $p < 0.0005$) in a manner similar as observed with the standard K^+ concentration (in KCl-based solution). Furthermore, removal of K^+ also slightly increased R_m in both control and Ad2 treated cells compared to

the R_m measured in KCl-based IC solution, suggesting that K^+ conductance could be blocked efficiently (Fig. 45 C, D). Together with the observation using CAR KO neurons, these results suggest that K^+ conductance is mot probably not the cause for Ad2 induced changes in R_m.

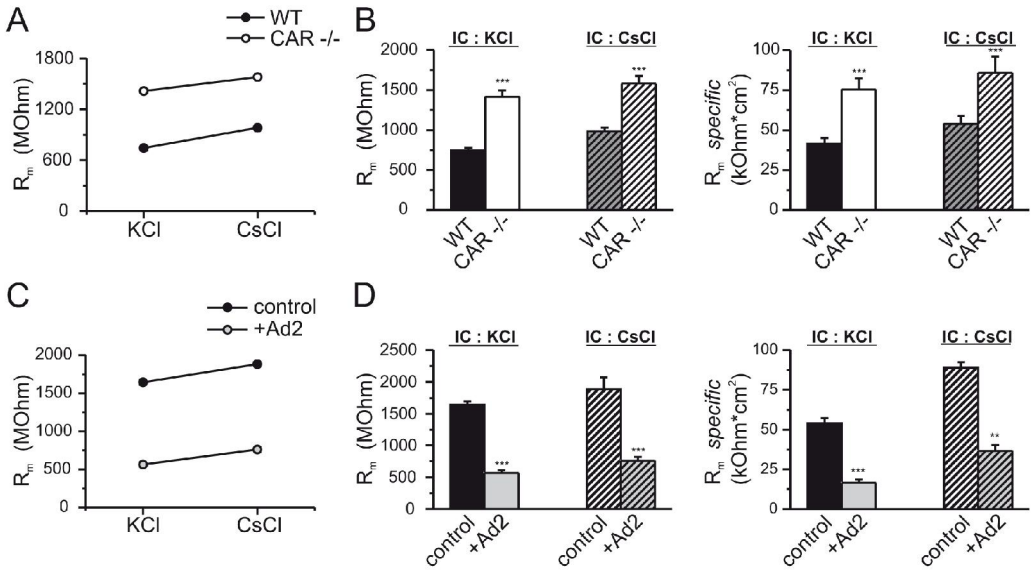

Fig.45: Passive K^+ conductance is not responsible for the R_m difference between CAR KO and WT cells as well as between Ad2 treated and control cells. (A) Substitution of K^+ by Cs^+ slightly increased R_m in both CAR KO and WT cells, suggesting effective blockage of passive K^+ conductance in both types of cells. (B) Under K^+ free conditions the difference in R_m (and also in R_m *specific*) between CAR KO and WT cells remained significant (n = 30-40).(C) Substitution of K^+ by Cs^+ slightly increased R_m in control and Ad2 treated cells, suggesting efficient blockage of passive K^+ conductance. (D) Under K^+ free conditions the difference in R_m (and also in R_m *specific*) between Ad2 treated and control cells remained significant (** - $p > 0.005$, *** - $p < 0.0005$)

3.6.2 Passive chloride (Cl^-) conductance is impaired in CAR KO cells.

To test whether chloride conductance may be implicated in R_m differences, several electrophysiological measurements including chloride ion substitution in the IC solution, measurement of chloride conductance only, as well as shifting of Cl^- reversal potential, were performed. Substitution experiments were carried out first. Under standard recording conditions (KCl-based – IC solution/ NaCl-based – EC solution; Table 5-8) the concentration of Cl^- was very similar on the inside and on the outside of the cell (97/111 mM and 128/144 mM for IC/EC solutions for low and high osmolality, respectively). These concentrations in addition to the negative V_h = -70 mV applied during the recordings, resulted in the calculated $E_{rev\ (Cl-)}$ = -3.6 mV (for low osmolality solution or -3.3 mV for high osmolality solution, Table 13) and an outflow of Cl^- ions due to its electrochemical gradient. Removal of Cl^- ions from the IC solution and replacement by gluconate ions (KGluc-based IC, Table 7, 8) caused

a shift of the E*rev* $_{(Cl-)}$ from -3.6 mV to -70 mV (for low osmolality solution and from -3.3 to -75 mV for high osmolality solution, Table 13), resulting in no net chloride movement (conductance) through the membrane at V_h (V_h = – 70 mV). Thus, under these conditions Cl^- could not influence the R_m. Measurement of R_m in CAR KO and WT cells under intracellular Cl^- free conditions did not yield differences in R_m (Fig. 46 A, B; n = 19-22). The calculated R_m *specific* also did not reveal significant differences (Fig. 46 B right diagram). This result suggests that Cl^- conductance might be implicated in the observed R_m differences between WT and CAR KO cells.

Consistent with these results, Ad2 was not able to significantly reduce R_m (and also not R_m *specific*) under Cl^- free conditions (Fig. 46 C, D, n = 33-37).

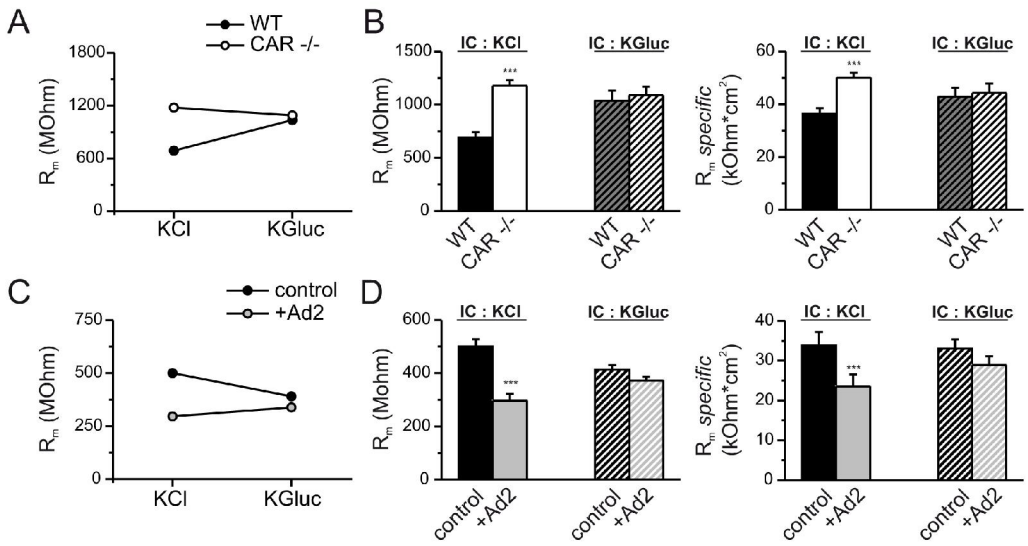

Fig. 46: Under Cl^- free conditions no differences in R_m were observed. (A, B) Significant differences in R_m (and R_m *specific*, $p < 0.0005$) between CAR KO and WT cells that were observed at normal Cl^- concentrations, disappeared under Cl^- free conditions (n = 19-22). (C, D) Ad2 did not reduce R_m and R_m *specific* under Cl^- free conditions, suggesting that Cl^- conductance might be involved in the observed changes in R_m (n = 33-37).

Another set of experiments was carried out to test whether Cl^- conductance is responsible for changes in R_m. The R_m was measured under conditions, where the membrane was mainly permeable for Cl^-, while conductances for other ions were pharmacologically blocked by using IC and EC solutions without K^+ and with inhibitors for different ion channels (TTX, TEA, 4-AP, Apamin; CsCl-TEA-based IC solution, Cl^--current EC solution, Table 5-8). Calculated E*rev* $_{(Cl-)}$ was 0 mV (or -3.3 mV, depending on type of the solution, Table 13). A voltage protocol of 10 depolarizing and 10 hyperpolarizing steps (each step 10 mV for 200 ms) from V_h = -70 mV or 0 mV was applied. Under conditions, when mainly Cl^- conductance

was measured, the R_m was significantly higher in CAR KO cells at both V_h (-70 and 0 mV) compared to the WT cells (Fig. 47 A; n = 28-33; $p < 0.0005$). Furthermore, the recorded I-V relationship revealed significantly lower current amplitudes in CAR-deficient neurons (Fig. 47 B, C). In line with these results, the R_m in cells treated with Ad2 was significantly lower at both V_h (Fig. 47 D; * - $p < 0.05$, ** - $p < 0.005$) and the I-V relationship yielded higher amplitudes in Ad2 treated cells compared to untreated cells (Fig. 47 E, F; n = 18-20). These results support the hypothesis that Cl^- conductance might be responsible for the measured changes in R_m.

Furthermore, application of Ad2 to WT cells (E10.5, Fig. 47 G left graph; n = 10) resulted in higher Cl^- current amplitudes, whereas Ad2 had no effect on CAR-deficient cells (Fig. 47 G right graph; n = 5), confirming that the observed effects of Ad2 were mediated by CAR.

To obtain further support for the above described results commonly used Cl^- channel blockers (DIDS, NPPB) were applied (Akasu et al., 1990; Baron et al., 1991; Frings et al., 2000; Greenwood et al., 1995; Greenwood et al., 1997; Hogg et al., 1994; Nilius et al., 1997a; Wladkowski et al., 1998; Wu and Hamill, 1992; Zholos et al., 2005). Acute application of DIDS (100 µM) and NPPB (100 µM) significantly reduced recorded Cl^- currents compared to cells not treated with blockers (Fig. 48 A, B; $p < 0.05$; n = 10-11). Furthermore, application of these blockers to WT cells reduced the Cl^- current (Fig. 48 C; n = 8), but evoked no changes in CAR KO cells (Fig. 48 D, n = 5). This pharmacological evidence supports the hypothesis that the measured current was caused by Cl^- conductance and that this conductance may be impaired in CAR KO cells.

Interestingly, in all recorded cells, measured currents showed an outward rectification (Fig. 47 B, C). This is in accordance with numerous published reports showing outward rectification as a characteristic of the Cl^- current (Arreola et al., 2002; Eder et al., 1998; Herness and Sun, 1999; Matchkov et al., 2004; Mignen et al., 2000; Nilius et al., 1997b; Schroeder et al., 2008; Zholos et al., 2005) and confirms that the outwardly rectifying current identified during the presented experiments is a Cl^- conductance.

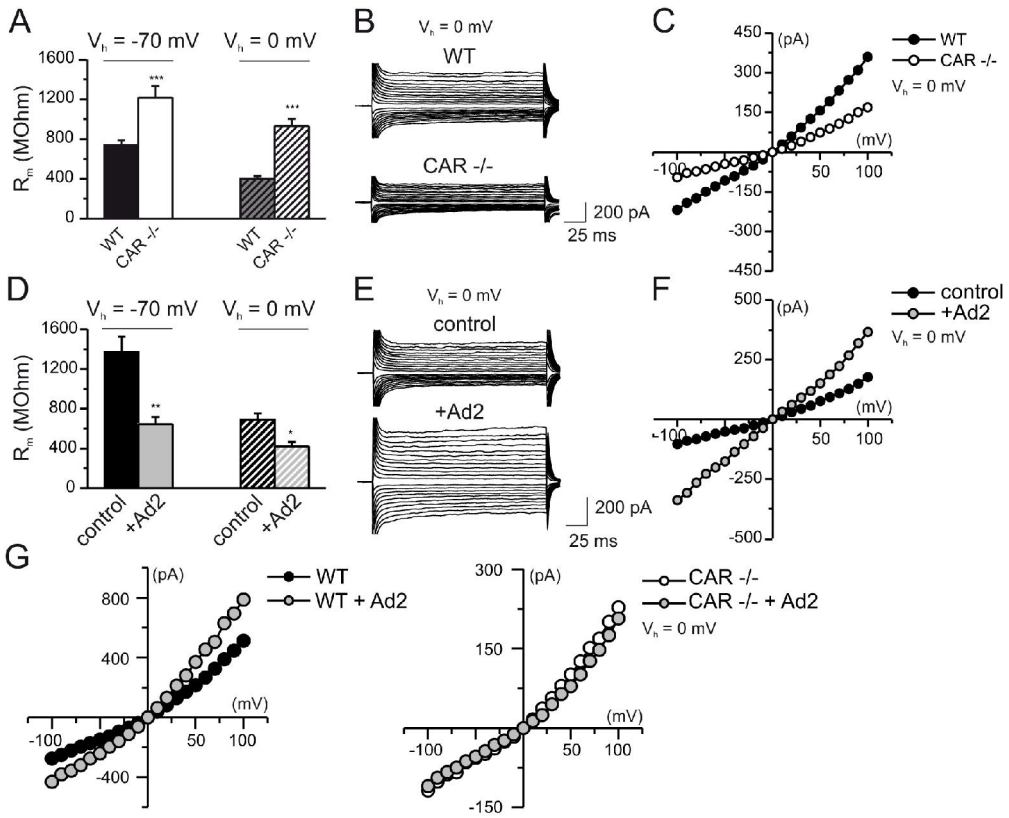

Fig. 47: Cl^- conductance is affected in CAR-deficient and Ad2 treated cells. (A) Estimated R_m under mainly Cl^- conductance conditions was significantly higher in CAR KO cells, at both V_h (0 and -70 mV; $p < 0.0005$). (B) Example traces of measured Cl^- current activated by application of voltage steps for both genotypes are shown (V_h = 0 mV). (C) The I-V relationship of Cl^- conductance in CAR KO neurons revealed significantly lower current amplitudes compared to WT cells (V_h = 0 mV, n = 28-33). (D) Estimated R_m under mainly Cl^- conductance conditions was significantly lower in Ad2 treated cells, at both V_h. (E) Example traces of measured Cl^- current in control and Ad2 treated cells are shown. (F) The I-V relationship of Cl^- conductance in Ad2 treated neurons revealed significantly higher current amplitudes compared to control cells (E15, n = 18-20). (G) Application of Ad2 to WT cells (E10.5) enhanced the measured Cl^- current, whereas Ad2 had no effect on CAR KO cells, confirming the specificity of Ad2 binding to CAR.

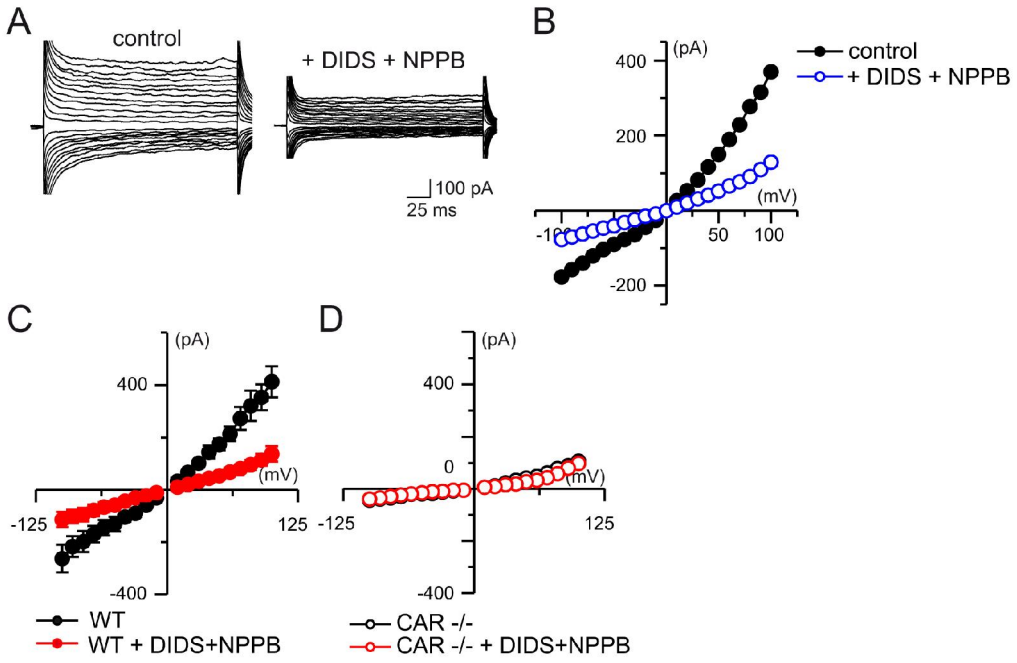

Fig. 48: Cl^- channel blockers reduced Cl^- conductance. (A) Example traces of Cl^- conductance before (left trace) and after treatment with Cl^- channel blockers (right trace) are shown. (B) The I-V relationship showed significantly lower current amplitudes after acute application of Cl^- channel blockers: DIDS (100 µM) and NPPB (100 µM, n = 10-11). (C, D) application of DIDS and NPPB reduced Cl^- current in WT (C, n = 8), but not in CAR KO cells (D, n = 5).

Further evidence for the implication of a Cl^- conductance was obtained by identification of a current that was enhanced by Ad2 and lacking in CAR KO neurons. Therefore, the I-V relationship in CAR KO and Ad2 treated cells under standard conditions (standard K^+, Na^+ and Cl^- concentrations; KCl-based IC solution and NaCl-based EC solution, Table 5-8) was investigated. Application of 10 depolarizing and then 10 hyperpolarizing steps starting at V_h = -70 mV, resulted in inward and outward currents which represented a mixture of a variety of conductances through the membrane (K^+, Cl^-, Na^+ and Ca^{2+}; Fig. 49 A, D). The current resulting from applied voltage steps was smaller in CAR KO cells than in WT cells (Fig. 49 A, B, n = 26-36). Consistently, the current measured in Ad2 treated cells was larger than in control cells (Fig. 49 D, E). Current consisting of different ionic conductances reversed at -35.0±1.4 (E*rev*) mV in WT cells and at -40.8±1.8 mV in CAR KO cells (Fig. 49 B) as well as at -36.0±2.0 mV in control cells and at -34.0±1.4 mV in Ad2 treated cells (Fig. 49 E). Subtraction of the current measured in CAR KO cells from the current recorded in WT cells resulted in the identification of a specific current lacking in CAR-deficient neurons (Fig. 49 C). The E*rev*, of this missing current in CAR KO cells was -4.8 mV (E*rev* = -4.8 mV, Fig. 49 C). On the basis of the known concentrations of ions present in the recording solutions (Table 5-8), the E*rev* for each particular ion could be calculated using the Nernst equation (Table 13).

E*rev* of the identified current (-4.8 mV) was very close to E*rev* calculated for Cl^- ($Erev_{(Cl-)}$ = -3.3 mV). This suggests that a Cl^- conductance is missing in CAR KO cells.
In agreement with these data, the subtraction of the current measured in control cells from the current recorded in Ad2 treated cells resulted in the identification of an additional current. This current reversed at E*rev* = -1.3 mV (Fig. 49 F, n = 27-34), thus, again close to $Erev_{(Cl-)}$ (Table 13) confirming that Cl^- is, most probably, the reason for the observed changes in the membrane conductance.

E*rev* (mV)	**Na^+**		**K^+**		**Cl^-**		**Ca^{2+}**	
IC/EC solution	Low osmo	High osmo	Low osmo	High osmo	Low osmo	High osmo	Low osmo	High osmo
KCl-based IC / NaCl-based EC	+91	+91	-91	-94	-3.6	-3.3	+78	+78
KCl-based IC / Low Na^+/Cl^- EC	+66	+66	-91	-94	+17	+20	+78	+78
KGluc-based IC/NaCl-based EC	+91	+91	-91	-91	-70	-75	+78	+78
CsCl-TEA-based IC/Cl^- current EC	+88	+96			0	-3.3	+78	+78

Table 13: Values of E*rev* calculated for different ions in specific recording solutions at 25°C using the Nernst equation. Abbr.: osmo - osmolality

Another approach to test the Cl^- conductance as the reason for changes in R_m, was to change the Cl^- and Na^+ concentrations and to study the shift of E*rev* of the Ad2-induced current and the current lacking in CAR KO neurons. The simultaneous change of concentrations of two ions Cl^- and Na^+, shifting E*rev* shifts in opposite directions (E*rev* of Cl^- in a more positive direction and E*rev* of Na^+ in a more negative direction), would, most probably, also change E*rev* of the additional current recorded after treatment with Ad2 and thus the current lacking in CAR KO cells (if one of these ions is involved). Therefore the extracellular Cl^- concentration was lowered from 110 mM to 46 mM, which shifted the $Erev_{(Cl-)}$ from -3.6 mV (Table 13) to a more positive value of about +17 mV (Low Na^+/Cl^- EC for high and low osmolality; Table 7, 8, 13). Simultaneously the extracellular Na^+ concentration was decreased from 105 mM to 30 mM, which shifted the $Erev_{(Na+)}$ from +91 mV in a more “negative” direction, to +66 mV (Low Na^+/Cl^- EC solution for high and low osmolality Table 7, 8, 13). The shift of E*rev* of the additional current measured after treatment with Ad2 (or of the current, which is missing in CAR KO neurons) to a more positive potential would suggest an involvement of Cl^- conductance. In contrast, shift of E*rev* in a negative direction would hint to a participation of Na^+ conductance in this current.

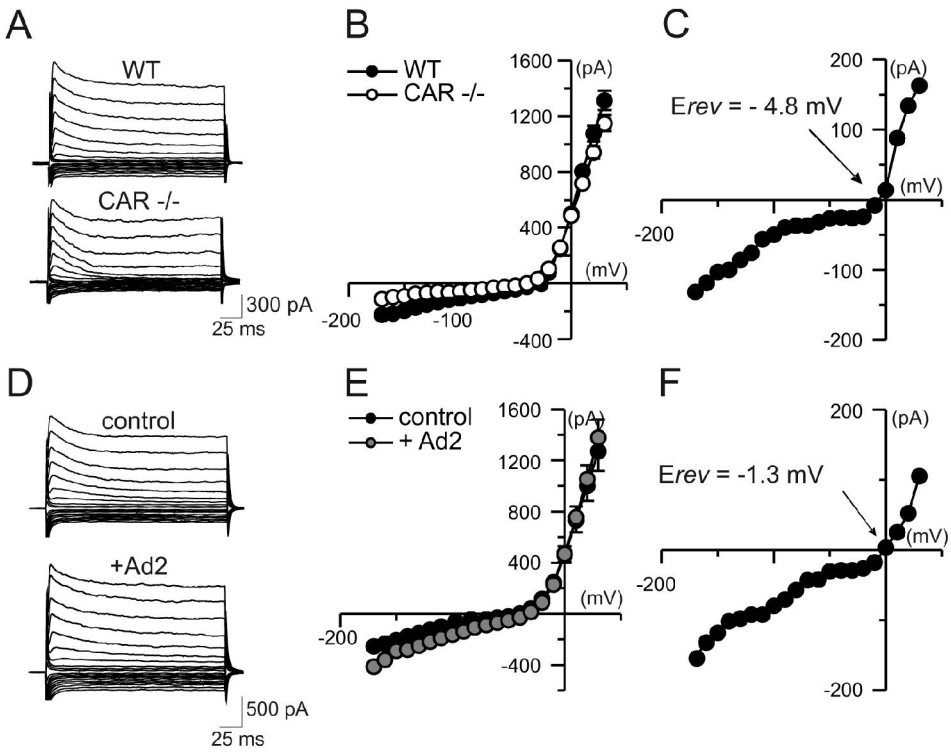

Fig. 49: Identified current missing in CAR KO cells and the additional current recorded after treatment with Ad2 showed E*rev* to be close to the calculated E*rev* of Cl^-. (A) Example traces of the I-V relationship for all ionic conductances in CAR KO and WT cells are shown. (B) The I-V relationship revealed slightly lower current amplitudes in CAR KO cells compared to WT cells (n = 26-36). (C) Subtraction of the recorded CAR KO current from the WT current resulted in the identification of a specific current missing in CAR-deficient neurons. This current reversed at a potential very close to the E*rev* of Cl^-. (D) Example traces of the I-V relationship for all ionic conductances in Ad2 treated cells and control cells are shown (E15). (B) The I-V relationship revealed higher current amplitudes in Ad2 treated cells (n = 27-34). (C) Subtraction of the current recorded in Ad2 treated cells from the current in control cells resulted in the identification of the additional current measured after treatment with Ad2. E*rev* of this current was very close to the E*rev* of Cl^-.

The I-V relationship estimated under low Na^+ and Cl^- concentration conditions shifted the E*rev* of the current lacking in CAR KO cells to +6.9 mV (Fig. 50 B, C, n = 21-25). Furthermore, under these experimental conditions, the additional current recorded in Ad2 treated neurons also showed E*rev* at about +12.2 mV (Fig. 50 E, F, n = 16-18). The shift of E*rev* to a more positive potential in both cases suggests that the Cl^- conductance was most probably affected in CAR-deficient neurons and in cells treated with Ad2.
Consequently, these results also indicate that the Na^+ conductance is, most probably, not involved in the observed changes in the membrane conductance.
Taken together, all data regarding passive Cl^- conductance, indicate that the Cl^- current through the membrane is responsible for the observed differences in R_m between CAR KO neurons and WT neurons, and between Ad2 treated and control cells. The Cl^- conductance is

therefore impaired in CAR-deficient neurons, whereas treatment with Ad2 enhances the Cl^- current.

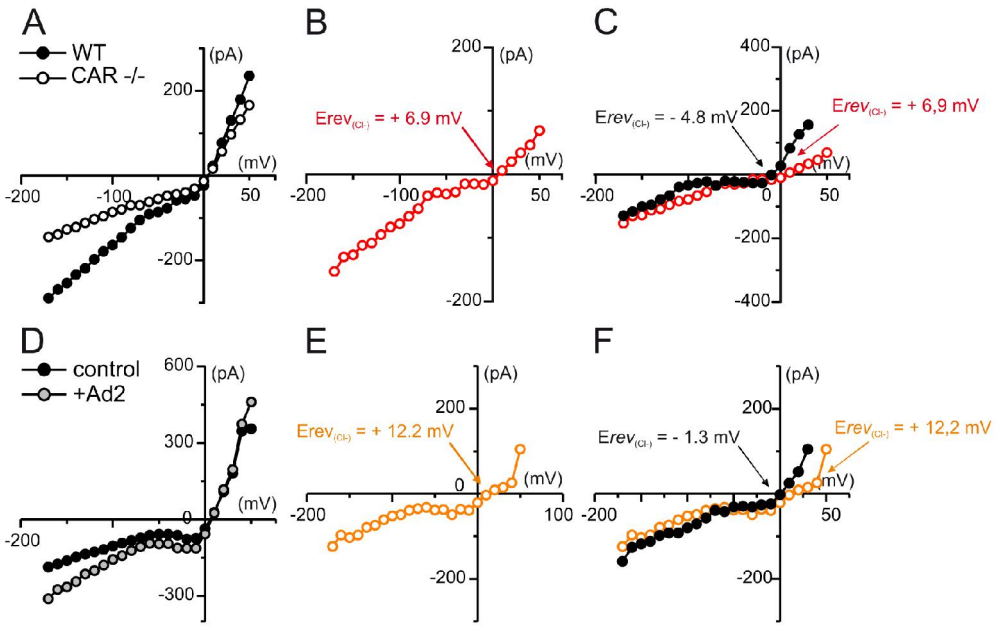

Fig. 50: The shift of E*rev* to a more positive potential suggests that the Cl^- conductance is involved in the current measured after treatment with Ad2 and in the current lacking in CAR KO cells. (A) The I-V relationship under low Cl^- and Na^+ concentration conditions in WT and CAR KO cells are presented. The recorded currents were smaller in CAR -/- neurons. (B) The difference between the current recorded in WT and the current recorded in CAR KO cells resulted in a current that reversed at + 6.9 mV (n = 21-25). (C) The shift of E*rev* of the current missing in CAR KO cells is due to changes in extracellular Cl^- and Na^+ concentrations (compare to Fig. 49 B, C). (D) The I-V relationship under low Cl^- and Na^+ is shown. The recorded current was larger in Ad2 treated neurons. (E) The difference between the current measured after treatment with Ad2 and the current in control cells resulted in a current which reversed at + 12.2 mV (n = 16-18). (F) The shift of E*rev* of the additional current recorded after treatment with Ad2 due to changes in extracellular Cl^- and Na^+ concentrations is shown (compare to Fig. 49 E, F).

3.6.3 Characterization of the current obtained after Ad2 treatment and the current that is missing in CAR KO cells.

As mentioned in chapter 3.6.2 the recorded Cl^- current showed an outward rectification. Such a characteristic has been reported for the Ca^{2+}- activated Cl^- current ($I_{Cl(Ca)}$; Ca^{2+}-activated Cl^- channels (CaCCs; Arreola et al., 2002; Eder et al., 1998; Herness and Sun, 1999; Matchkov et al., 2004;Mignen et al., 2000; Nilius et al., 1997b; Schroeder et al., 2008; Zholos et al., 2005) as well as for volume-regulated Cl^- current ($I_{(Cl-)vol}$; volume-regulated Cl^- channels (VRCCs); (Diaz et al., 1993;Kelly et al., 1994).

Due to the observations made and presented in Fig. 47 the involvement of CaCCs was investigated. Measurements were performed under conditions that allow the recording of mainly Cl^- conductance. These recordings revealed an enhanced Cl^- current in Ad2 treated

cells and a loss of outward rectification (Fig. 47 E, F). As mentioned above, outward rectification depends on the concentration of intracellular Ca^{2+}. An increase in $[Ca^{2+}]_i$ causes a loss or a decrease of outward rectification. This observation provides the first evidence that the measured Cl^- current might consists of a Ca^{2+}-activated Cl^- current and that Ad2 might be able to influence the concentration of intracellular Ca^{2+}.

To address the question whether CaCCs might be involved in the measured Cl^- conductance, the effect of intracellular Ca^{2+} on the identified Cl^- current was investigated. Cl^- conductance was measured under conditions of either free or high (2 mM) intracellular Ca^{2+} concentrations. The current-voltage (I-V) relationship under intracellular Ca^{2+}-free conditions yielded significantly lower amplitudes of the Cl^- current compared to high-Ca^{2+} intracellular concentrations (Fig. 51 A, B, n = 15-20). This result indicates that $[Ca^{2+}]_i$ is able to influence the Cl^- conductance.

In addition to the $[Ca^{2+}]_i$-dependency, the selectivity for halides of the measured Cl^- current was investigated. It has been reported that Ca^{2+}-activated chloride channels show a characteristic permeability for halides: $I^- > Br^- > Cl^- > F^-$ (Eggermont, 2004; Frings et al., 2000; Greenwood and Large, 1999; Matchkov et al., 2004; Mignen et al., 2000; Rychkov et al., 1998). Therefore, substitution experiments were carried out by replacing Cl^- ions by I^- or Br^- ions in the IC solution and EC solution (CsBr-based IC/EC solutions; CsI-based IC/EC solutions, Table 5-8). As shown in Fig. 51 C and D, substitution of Cl^- by Br^- increased current amplitudes (n = 12-15), but the pronounced outward rectification remained. Furthermore, replacement of Cl^- by I^-, enhanced the Cl^- current even more than the current increase observed with Br^- ions (Fig. 51 E compared to D). These results are in agreement with published reports (Eggermont, 2004; Frings et al., 2000; Matchkov et al., 2004). Additionally, substitution of Cl^- by Br^- in WT cells (E10.5; n = 12) increased the Cl^- conductance (Fig. 52 A, B), whereas it had no effect on CAR-deficient neurons (Fig. 52C, D, n = 10), confirming that the Cl^- conductance is, most probably, impaired in CAR-deficient neurons.

The outward rectification and the modulation of the Cl^- current by intracellular Ca^{2+} and halide ions suggests that the identified Cl^- conductance might consist of a Ca^{2+} activated Cl^- current.

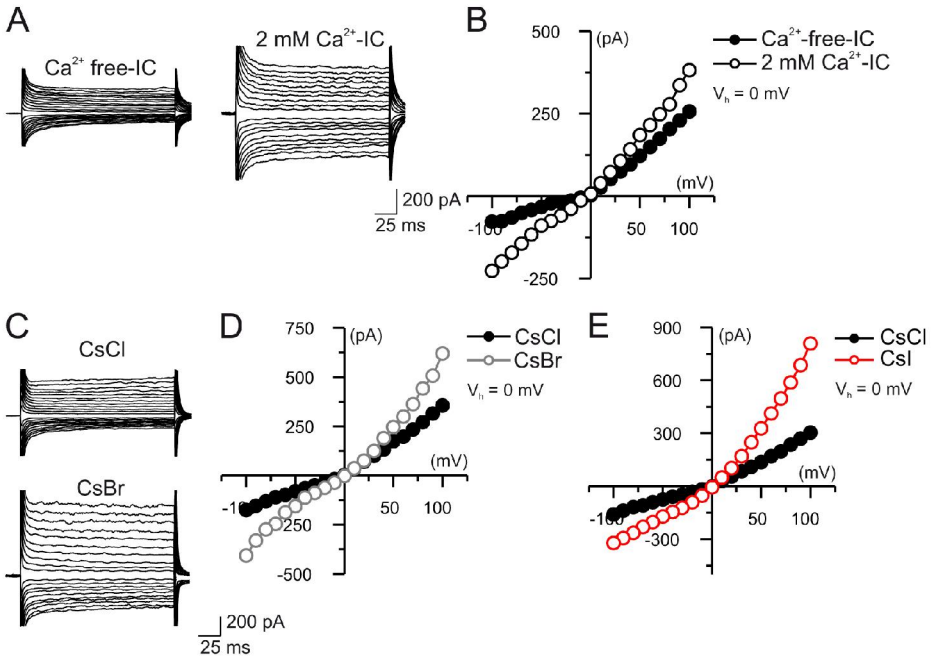

Fig. 51: Modulation of Cl^- conductance by intracellular Ca^{2+} and halide ions. (A) Under intracellular Ca^{2+}-free conditions (left trace) the Cl^- current was significantly smaller compared to the current at 2 mM Ca^{2+} concentration (right trace; V_h = 0 mV). (B) The I-V relationship of Cl current under Ca^{2+}-free and 2 mM Ca^{2+} concentration conditions (n = 15-20). (C-E) Replacement of Cl^- by either Br^- (C, D) or I^- (E) ions enhanced the Cl^- current (n = 12-15). A characteristic outward rectification remained (V_h = 0 mV).

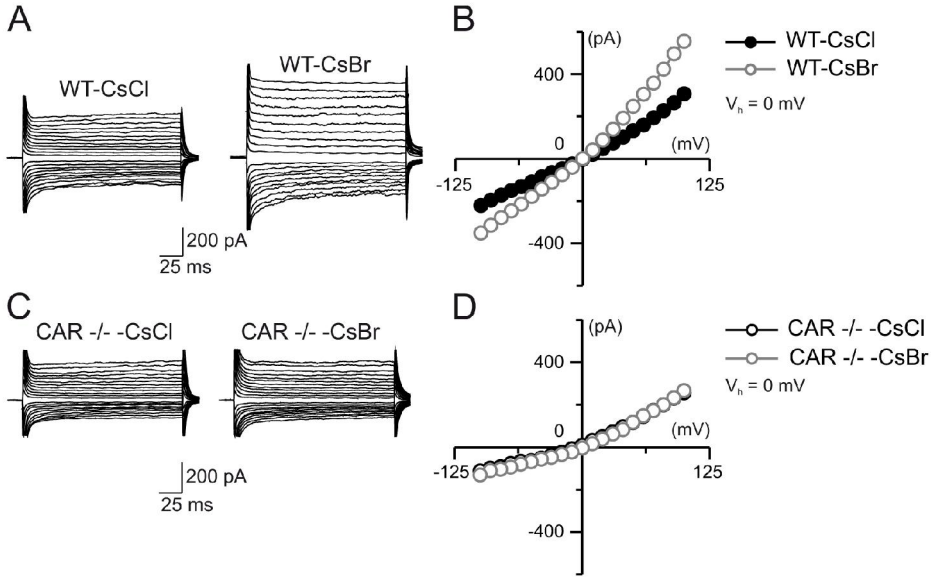

Fig. 52: The substitution of Cl^- by Br^- ions had no effect on Cl^- conductance in CAR KO neurons (E10.5). (A) Example traces of currents recorded in WT cells before Cl^- substitution (left trace) and after replacement of Cl^- by Br^- (right trace) are shown. The replacement of Cl^- by Br^- in recording solutions significantly enhanced Cl- currents in control neurons (E15). (B) Comparison of the I-V relationship of Cl^- currents in WT cells before and after Cl^- substitution is shown. (C) Example traces of currents recorded in CAR KO cells before (left trace) and after substitution with Br^- (right trace) are shown. Replacement of Cl^- ions by Br^- did not influence current in CAR KO cells. (D) The I-V relationship of recorded currents, in CAR KO cells, was not changed by Br^- ions. V_h = 0 mV.

3.7 CAR-mediated increase of intracellular Ca^{2+}

3.7.1 Application of Ad2 induces an increase of intracellular Ca^{2+}

To support the hypothesis, that a Ca^{2+} activated Cl^- current contributes to the identified Cl^- current recorded after treatment with Ad2, intracellular Ca^{2+} levels were determined by calcium imaging. Cells are loaded with the ratiometric fluorescent dye fura-2 which allows microscopic detection of intracellular Ca^{2+} concentrations. As mentioned in chapter 2.2.6.2, changes in intracellular Ca^{2+} levels are presented as ratio of $\Delta F/F_0$.

In the absence of Ad2, either a stable base Ca^{2+} concentration (baseline; F_0) or sometimes spontaneously occurring Ca^{2+} transients could be observed (Fig. 53 A, top trace). Application of Ad2 briefly enhanced the frequency of spontaneous Ca^{2+} transients and significantly increased the intracellular Ca^{2+} concentration (Fig. 53 A bottom trace, Fig. 53 B). The Ca^{2+} increase due to Ad2 occurred within seconds and lasted for over 10 min, gradually increasing (Fig. 53 B), if Ad2 was not washed out (data not shown). Consistent with this result are observations made by whole-cell patch-clamp recording. Application of Ad2 resulted in an immediate increase of spontaneous postsynaptic currents (Fig. 53 C bottom trace). This effect lasted for about one minute followed by a complete loss of synaptic activity. Most likely this was caused by a continuous increase of $[Ca^2]_i$ concentration, which enhanced the frequency of postsynaptic currents followed by an extensive depolarization that does not allow further synaptic events to arise. These patch-clamp recordings support the view that treatment with Ad2 increases intracellular Ca^{2+}.

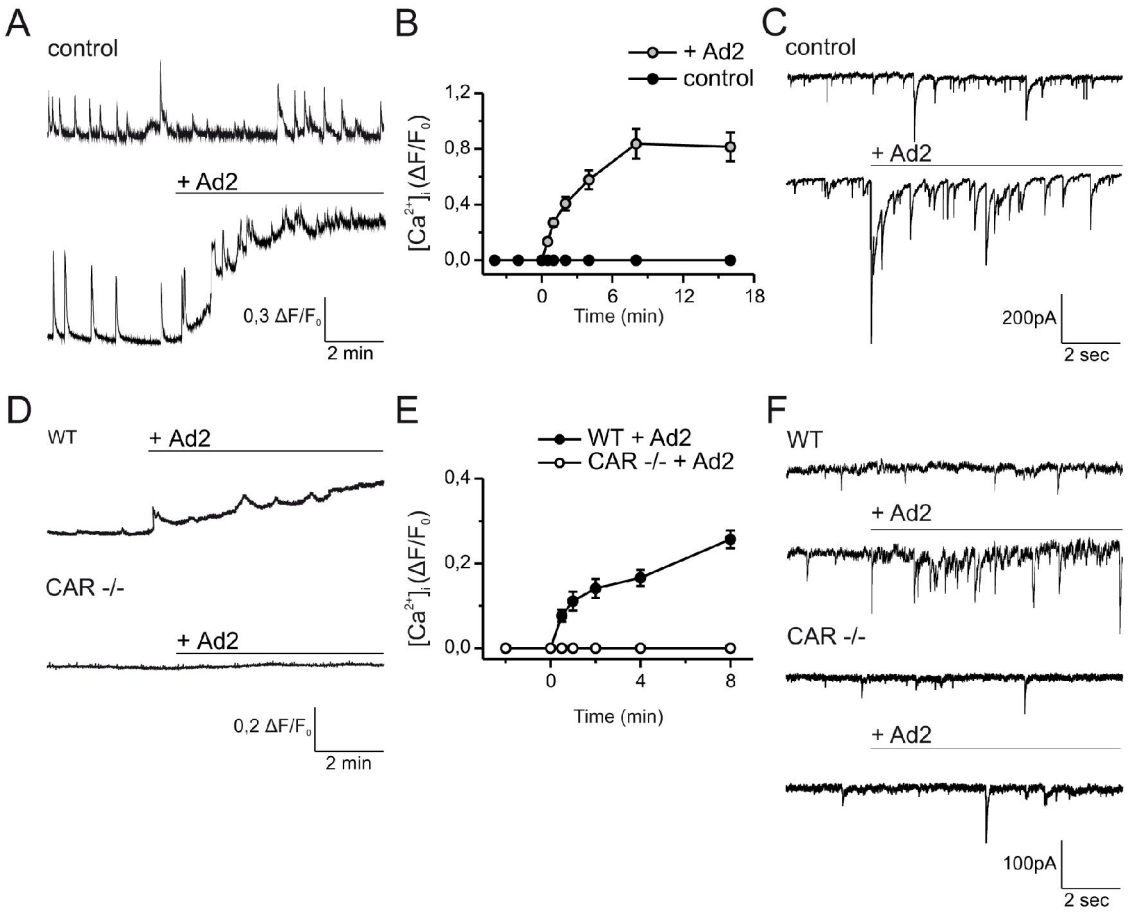

Fig. 53: Ad2 induces an increase of intracellular Ca^{2+} concentration. (A) Control cells (top trace) showed a stable base level of Ca^{2+} concentration as well as spontaneous Ca^{2+} transients. Acute application of Ad2 increased the intracellular Ca^{2+} concentration and thus, the frequency of spontaneous Ca^{2+} transients. (B) For quantification, the ratio of ΔF (difference between maximal Ca^{2+} increase and F_0) to the base Ca^{2+} level (F_0) was plotted against recording time (min). (C) Whole-cell patch-clamp recordings showed that the acute application of Ad2 enhanced the frequency of spontaneous postsynaptic currents. (D) Ad2 effect on intracellular Ca^{2+} is dependent on the presence of CAR. Acute application of Ad2 increases the intracellular Ca^{2+} concentration in WT cells (top trace, n = 6), but not in CAR -/- neurons (bottom trace; n = 5). (E) For quantification, the ratio $\Delta F/F_0$ was plotted versus the recording time (min). (F) Whole-cell patch-clamp recordings confirmed that the Ad2 effect was dependent on the presence of CAR. Acute application of Ad2 enhanced frequency of spontaneous postsynaptic currents in WT cells (two top traces) but not in CAR KO neurons (bottom traces).

In order to test whether the effect of Ad2 was dependent on the expression of CAR, Ad2 was applied to cultivated CAR KO cells. Calcium imaging experiments revealed no increase in intracellular Ca^{2+} in CAR KO cells after application of Ad2 (Fig. 53 D bottom trace, n = 5). Furthermore, after treatment of CAR KO cells with Ad2 no change in the frequency of spontaneous postsynaptic currents was observed, suggesting no increase in an intracellular Ca^{2+} concentration (whole-cell patch-clamp recordings, Fig. 53 F bottom trace, n = 4). In contrast, treatment of WT cells with Ad2 increased the intracellular Ca^{2+} level (calcium

imaging experiments, n = 6; Fig. 53 D top trace) and enhanced the frequency of spontaneous postsynaptic currents (whole-cell patch-clamp recording, Fig. 53 F top trace, n = 6). These results indicate that the effect induced by Ad2 requires the presence of CAR.
The increase of the Ca^{2+} concentration induced by Ad2 was stronger in neurons from E15 in comparison to E10.5 neurons (Fig. 53 B, E). This might reflect different stages of differentiation, since neurons from E10.5 embryos showed a lower frequency of synaptic currents.

3.7.2 Ad2 induces a release of Ca^{2+} from intracellular stores

To address the question of by which mechanism Ad2 induces an increase in the intracellular Ca^{2+} concentration, further Ca^{2+} imaging experiments in the presence of pharmacological reagents or Ca^{2+} free EC solution were performed.
An increase in intracellular Ca^{2+} concentration may be mediated by an influx of Ca^{2+} through VGCCs or by the release of Ca^{2+} from intracellular stores. As shown in Fig. 54 B, blockage of Ca^{2+} influx from the extracellular side via VGCCs did not inhibit a rise of intracellular Ca^{2+}. This suggests that extracellular Ca^{2+} is not required for the effect mediated by Ad2 (see also chapter 3.4.4).
Furthermore, no differences in Ca^{2+} influx from the extracellular side through VGCCs in CAR KO and WT neurons were observed. As shown in Fig. 55 A and B application of 40 mM KCl, which causes depolarization and influx of Ca^{2+} from the extracellular side into the cells, resulted in a similar increase in intracellular Ca^{2+} in both cell types (WT n = 44 cells; CAR KO n = 48 cells). This is in agreement with data obtained by whole-cell patch-clamp recordings (Chapter 3.4.3), which revealed similar properties of VGCCs in CAR KO and WT cells, suggesting that these channels are not responsible for observed changes in membrane conductance.
To test whether Ad2 mediates Ca^{2+} release from intracellular Ca^{2+} stores, Ca^{2+} release and refill from intracellular Ca^{2+} stores was blocked. There are two main groups of receptors which lead to the release of Ca^{2+} from stores if activated: IP3 receptors (IP3Rs; Hoesch et al., 2002; Kato and Rubel, 1999; Nakamura et al., 2000; Poulsen et al., 1995; Yamamoto et al., 2000) and ryanodine receptors (RyRs; Hoesch et al., 2002; Kato and Rubel, 1999; Poulsen et al., 1995; Sandler and Barbara, 1999). Refill of intracellular Ca^{2+} stores from the cytosol is accomplished by the Ca^{2+}-ATPase pump (Kato and Rubel, 1999; Krizaj et al., 1999; Nakamura et al., 2000; Poulsen et al., 1995; Sandler and Barbara, 1999; Shmigol et al., 1995). Application of Ad2 to cells pre-incubated with blockers for Ca^{2+} release and refill of stores (Table 14) did not result in a Ca^{2+} increase (Fig. 54 C, D). Thus, blockage of intracellular

stores abolished the effect of Ad2, suggesting that intracellular Ca^{2+} is required for this process.

This result raises the question of whether Ad2 influences an intracellular signaling pathway or whether CAR acts directly on Ca^{2+} stores.

In order to compare Ca^{2+} release from intracellular Ca^{2+} stores between CAR KO and WT cells, Ca^{2+} release has to be activated. It has been reported that metabotropic glutamate receptor (mGluR) activation or muscarinic acetylcholine receptor (AChR) stimulation can increase intracellular Ca^{2+} concentration via IP3- and ryanodine-sensitive Ca^{2+} stores in neurons (Bianchi et al., 1999; Congar et al., 1997; Fagni et al., 2000; Kato and Rubel, 1999; Ohta et al., 2002; Rose and Konnerth, 2001; Sakaki et al., 1996; Simpson et al., 1996; Yamamoto et al., 2000). Therefore, the release of Ca^{2+} from intracellular Ca^{2+} stores by application of glutamate was investigated in CAR KO and WT cells. In the presence of blockers for iontropic glutamatergic receptors (APV for NMDA receptors and DNQX for AMPA and kainate receptors) acute application of glutamate (1 mM) would stimulate only metabotropic glutamatergic receptors. Activation of mGluRs evoked a Ca^{2+} increase in both types of cells (Fig. 56 A). However, responses in CAR cells were smaller (although not significantly) than in WT cells, suggesting that Ca^{2+} stores might be affected in CAR-deficient neurons (Fig. 56 B; WT n = 18; CAR KO n = 22 cells).

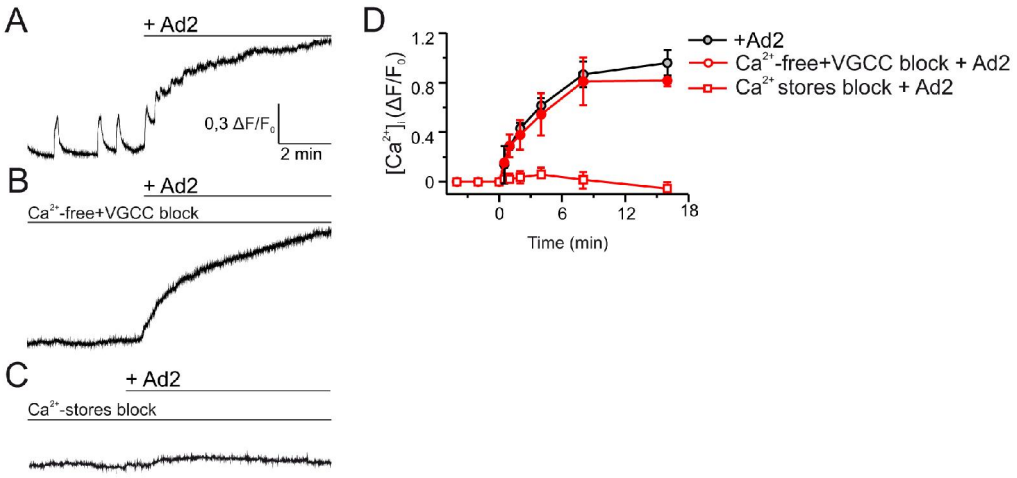

Fig. 54: Ad2 induces Ca^{2+} release from intracellular Ca^{2+} stores. (A) Ad2 increases intracellular Ca^{2+} concentration. (B) Blockage of VGCCs (Table 11) and Ca^{2+}-free EC solution did not prevent an increase of Ca^{2+} due to Ad2 (n = 44 cells). (C) Block of Ca^{2+} release (and refill) from intracellular stores (Table 14) abolished the effect of Ad2, indicating that intracellular Ca^{2+} stores are required in the process induced by Ad2 (n = 56 cells). (D) Quantification of the Ad2 effect presented as the ratio of ΔF (difference between maximal Ca^{2+} increase at given time) to F_0 (the base Ca^{2+} concentration) plotted against time (min). Ad2 was added at time 0.

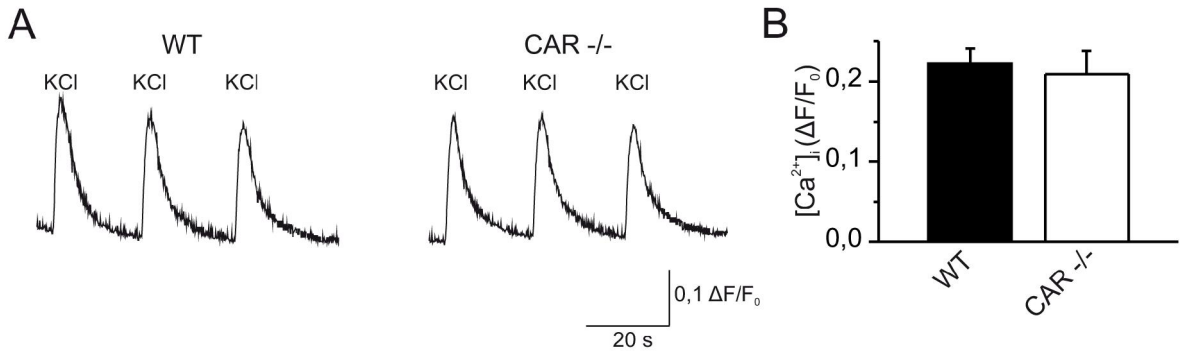

Fig. 55: VGCCs are not affected in CAR-/- cells. (A) Short application of 40 mM KCl to CAR KO and WT cells resulted in a similar increase in intracellular Ca^{2+}, suggesting that function of VGCCs is not impaired in CAR KO cells. (B) Quantification of the Ca^{2+} increase due to application of KCl (WT n = 44 cells; CAR KO n = 48 cells).

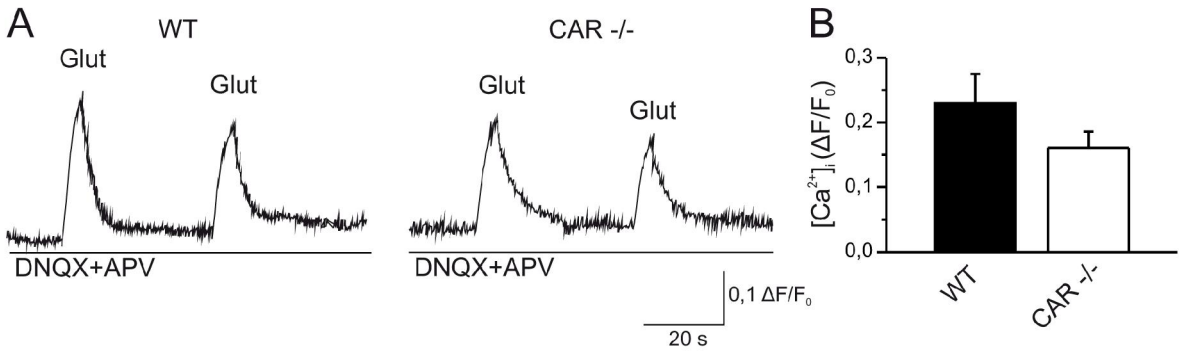

Fig. 56: Activation of intracellular Ca^{2+} stores in CAR KO and WT cells. (A) Example traces of increasing $[Ca^{2+}]_i$ after application of 1mM glutamate in CAR KO (right trace) and WT cells (left trace). (B) Glutamate-induced Ca^{2+} responses were smaller in CAR-deficient neurons, which, however, did not reach statistical significance (WT n = 18 cells; CAR KO n = 22 cells).

Target	Blocker	Final concentration	Reference	Activation
IP3Rs	U73122	20 µM	(Hoesch et al., 2002) (Simpson et al., 1996) (Sakaki et al., 1996)	IP3, PCL, mAChR, mGluR, ATP
	2-aminoethoxydiphenyl borate (2-APB)	100 µM	(Ascher-Landsberg et al., 1999) (Missiaen et al., 2001) (Lievremont et al., 2005) (Jaimovich and Carrasco, 2002)	
RyRs	Ryanodine	25 µM	(Hoesch et al., 2002) (Irving et al., 1992) (Sandler and Barbara, 1999)	Increase in $[Ca^{2+}]_i$
	Dandrolene	30 µM	(Kato and Rubel, 1999) (Simpson et al., 1996) (Fohrman et al., 1993)	
Ca^{2+}-ATPase	Thapsigargin (TG)	1 µM	(Poulsen et al., 1995) (Simpson et al., 1996) (Sandler and Barbara, 1999) (Svichar et al., 1997) (Sakaki et al., 1996)	

Table 14: Modulators of intracellular Ca^{2+} stores.

In addition to VGCCs and intracellular Ca^{2+} stores, intracellular Ca^{2+} could change due the activity of gap junctions. These channels allow the passage of ions or small molecules such as short peptides or second messengers e.g. cAMP or IP3 (Bruzzone and Dermietzel, 2006; Charles et al., 1991; Christ et al., 1992; Lampe and Lau, 2004; Rozental et al., 2001; Saez et al., 1989; Sanderson et al., 1990). Gap junctions have also been shown to be essential for spreading of Ca^{2+} waves and the coordination of Ca^{2+} oscillations (Boitano et al., 1992; Bruzzone et al., 1996; Bruzzone and Dermietzel, 2006; Charles et al., 1991; Stauffer et al., 1991). Since the movement of IP3 seems to be very frequent rather than Ca^{2+} itself, IP3 may activate a Ca^{2+} release from intracellular stores by gap junction communication (Bruzzone et al., 1996;Charles et al., 1991). However, application of the commonly used blocker for gap junctions CBX (Table 12), did not inhibit the Ca^{2+} increase evoked Ad2 (Fig. 57 B, C). This result suggests that connexins do not participate in the Ad2 induced Ca^{2+} elevation, which is in agreement with results presented in chapter 3.5.1, showing no modulation of gap junctional communication by Ad2.

Furthermore, the influence of different synaptic blockers on the Ad2 induced Ca^{2+} increase was analyzed. Application of TTX (100 µM), a blocker for voltage-gated Na^{+} channels, which are essential for action potentials, did not affect the Ca^{2+} increase induced by Ad2 (Fig. 57 D, E), further indicating that Na^{+} channels are not involved in Ad2-mediated effects (see also chapters 3.4.2).

The influence of blockers of $GABA_A$ and glycine receptors on Ad2-mediated changes was also studied. The application of the $GABA_A$ receptor antagonists biccuculine and picrotoxin as well as the glycine receptor antagonist strychnine, did not influence changes in intracellular Ca^{2+} caused by treatment with Ad2 (Fig. 57 F, G). This result suggests that synaptic activity mediated by $GABA_A$ or glycine channels do not participate in Ad2 induced Ca^{2+} increase. This finding is consistent with data presented in chapter 3.5.2, on Ad2-mediated changes in membrane conductance.

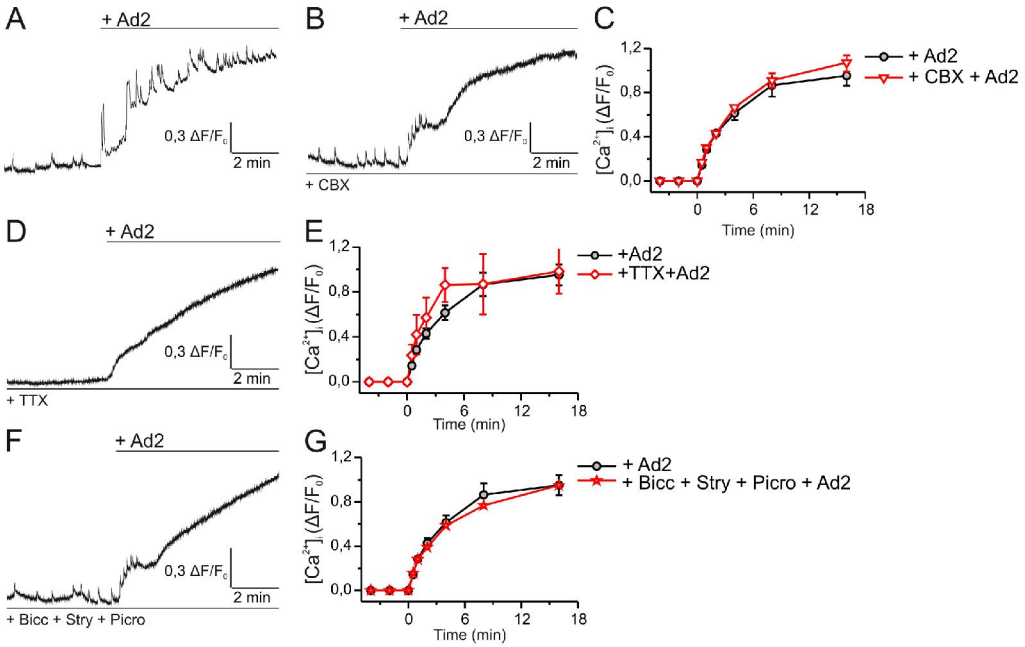

Fig. 57: Effects of different modulators on intracellular Ca^{2+} increase induced by Ad2. (A) Increase in intracellular Ca^{2+} due to the acute application of Ad2. (B) Treatment of cells with the gap junction blocker CBX did not prevent Ad2-induced Ca^{2+} increase. (C) Quantification of the Ca^{2+} increase caused by Ad2, before and after CBX treatment (n = 5 cells). The ratio of $\Delta F/F_0$ plotted versus time (min) is shown. Ad2 was added at time 0. (D, F) Application of TTX (D) and $GABA_A$ and gylcine receptor blockers (F) did not influence the effect of Ad2 on intracellular Ca^{2+}. (E, G) Quantification of the Ca^{2+} increase due to Ad2 before and after treatment with TTX (E, n = 27 cells) and blockers for $GABA_A$ and glycine receptors (G, n = 34 cells). Ratio of $\Delta F/F_0$ plotted against time (min). Ad2 was added at time 0.

3.7.3 CAR-CAR mediated increase in intracellular Ca^{2+}

In order to test whether homophilic CAR-CAR binding, may influence the intracellular Ca^{2+} concentration, Ca^{2+} imaging experiments using extracellular CAR domains were performed. Application of 250 µg/ml of CAR-D1D2 to cultivated cortical neurons (WT, E15, DIV 14) resulted in an increase of intracellular Ca^{2+} (Fig. 58 A, B; n = 32 cells). Application of CAR-D1D2 evoked a weaker Ca^{2+} response compared to Ad2 (compare Fig. 53 B or 54 D with Fig. 58 B).

Nonetheless, this result suggests that homophilic CAR-CAR interaction might mediate Ca^{2+} signals between cells and thus might influence intracellular Ca^{2+}-dependent pathways.

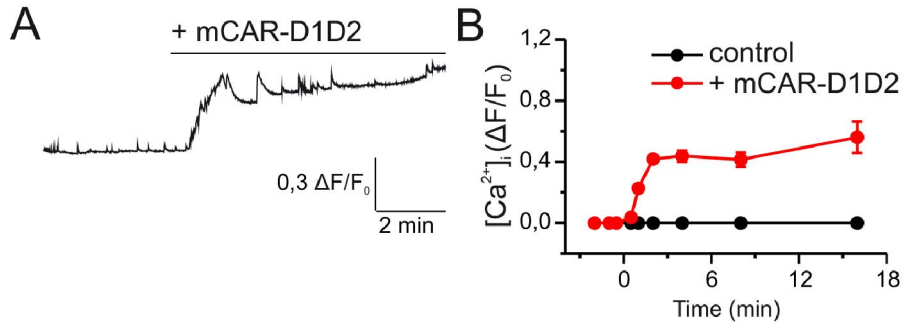

Fig. 58: Application of an extracellular CAR fragment increases intracellular Ca^{2+}. (A) Application of 250 µg/ml of CAR-D1D2 to cortical neurons (WT, E15, DIV 14) increased intracellular Ca^{2+} concentration. (B) Quantification of Ca^{2+} increase due to CAR-D1D2 (DIV 14, n = 32 cells). Ratio of $\Delta F/F_0$ plotted against time (min).

3.8 Ad2 disturbs homophilic CAR-CAR interaction

Ad2 binds to the first Ig domain of CAR (D1; Bewley et al., 1999; Xia et al., 1994; Xia et al., 1995) with a higher affinity than CAR to itself (Freimuth et al., 1999; van Raaij et al., 2000; Walters et al., 2002). Binding of Ad2 to CAR inhibits CAR-CAR homotypic interaction (Walters et al., 2002), resulting in a disruption of CAR-mediated cell-cell contacts.

In order to test long-lasting effects of Ad2 on cultivated neurons, 500 µg/ml of Ad2 was added to dissociated chick telencephalic and tectal chick neurons and then cultivated for 48 hours. Application of Ad2 resulted in the formation of less aggregates compared to control conditions (cells cultivated without Ad2; Fig. 59 A). The number of cells in aggregates was significantly lower in cultures treated with Ad2 (Fig. 59 B). Furthermore, the total sum of neurite length measured per view field significantly increased in Ad2 treated cells in comparison to control cultures (Fig. 59 A, C). These results suggest that Ad2 might disrupt homophilic CAR-CAR interaction between neurons. The increased neurite length might be a result of an Ad2-specific induced neurite outgrowth mechanism or of an inhibited cell-cell adhesion, allowing neurites to extend on the immobilized laminin.

A similar observation was made after application of Ad2 (500µg/ml) to cultivated cortical mouse neurons (E15, WT, 48 hours in culture). Ad2 treated cells showed a significantly lower number of aggregates (Fig. 59 D, E) and a higher total number of measured neurite length (not significant, Fig. 59 D, F).

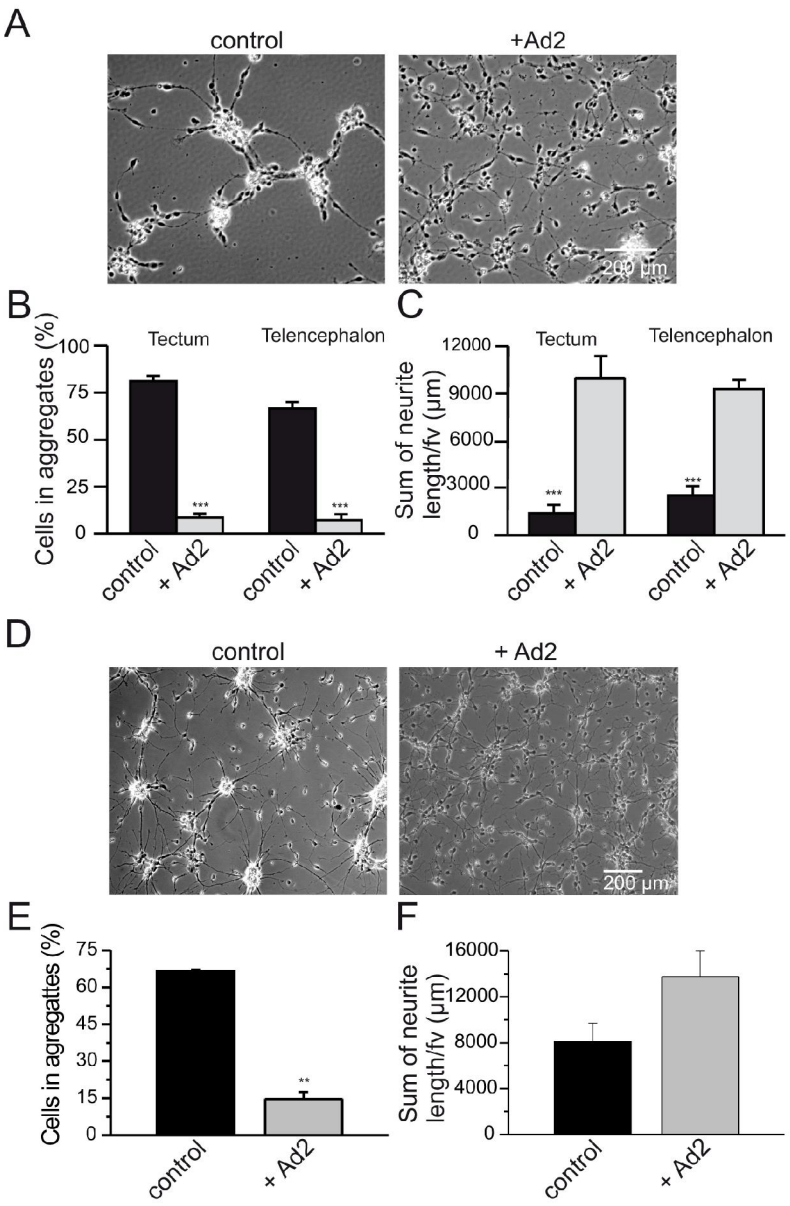

Fig. 59: Disruption of homophilic CAR-CAR binding by treatment with Ad2. Application of 500 µg/ml of Ad2 to the chick (A-C) or to the mouse (D-F) neuronal cell culture resulted in a significantly lower number of cells forming aggregates (chick: A, B, mouse: D, E) and a significantly higher sum of total length of measured neurites in chick neurons (C) and a higher, however, not significantly, sum of total neurite length in mouse neurons (F). Abbreviation: fv – field of view

3.9 Consequences of the absence of CAR on synaptic activity and on action potential generation

3.9.1 Changes in passive membrane properties in CAR-deficient neurons and Ad2 treated cells affect action potential generation

Neurotransmitter release at synapses is caused by APs and therefore APs are important for fast communication between neurons. The properties, as well as the density of voltage-gated

Na^+ and K^+ channels have been reported to play an essential role in the generation and propagation of APs (Kole et al., 2008; Rothe et al., 1999; Viswanathan and Balser, 2004). Passive membrane properties play an important role in the establishment and maintenance of the RMP and thus determine whether membrane depolarization due to synaptic input reaches a critical threshold voltage, resulting in an AP or not. Thus, considering the changes in membrane resistance in the absence of CAR, changes in the electrotonic membrane properties and a change in firing pattern of neurons could be expected.

The generation and the firing frequency of APs in CAR-deficient neurons and in Ad2 treated neurons were therefore investigated. Two different approaches were chosen. Spontaneous APs were recorded in the current-clamp mode at the physiological V_m or alternatively APs were evoked by prolonged square pulse current injections (20 steps, each 20 pA for 200 ms). A significantly higher frequency of spontaneous APs was observed in CAR KO cells than in WT cells (Fig. 60 A, B, n = 34-36; $p < 0.05$). Similar to this result, the frequency of APs evoked by current injection was also significantly higher in CAR-deficient neurons (Fig. 60 E, F). In contrast, cells treated with Ad2 showed a significantly lower firing frequency of spontaneous APs compared to controls (Fig. 60 C, D; n = 27-28) as well as a significantly lower frequency of evoked APs by current injection (Fig. 60 G, H; $p < 0.05$). Thus, cells with higher R_m and lower membrane conductance (CAR KO cells) showed higher frequency of recorded APs, whereas cells with low R_m and larger membrane conductance (Ad2 treated cells) yielded a lower frequency of APs. These data suggest that a higher R_m and a less leaky cell membrane results in a higher frequency of APs (Barrett and Crill, 1974; Yang et al., 2005). Enhanced membrane conductance, through passive ion channels, causes a decrease in depolarization magnitude due to the loss of current through the membrane, and thus does not allow reaching the threshold potential required for the generation of action potentials. Moreover, as mentioned in chapter 3.4.1 and 3.4.2, the properties of voltage-gated Na^+ and K^+ ion channels, which are essential for the generation of APs, were neither changed in CAR-deficient neurons nor in Ad2 treated cells, suggesting that the observed differences in frequency of APs were indeed due to changes in passive membrane conductance and not due to properties of voltage-gated ion channels.

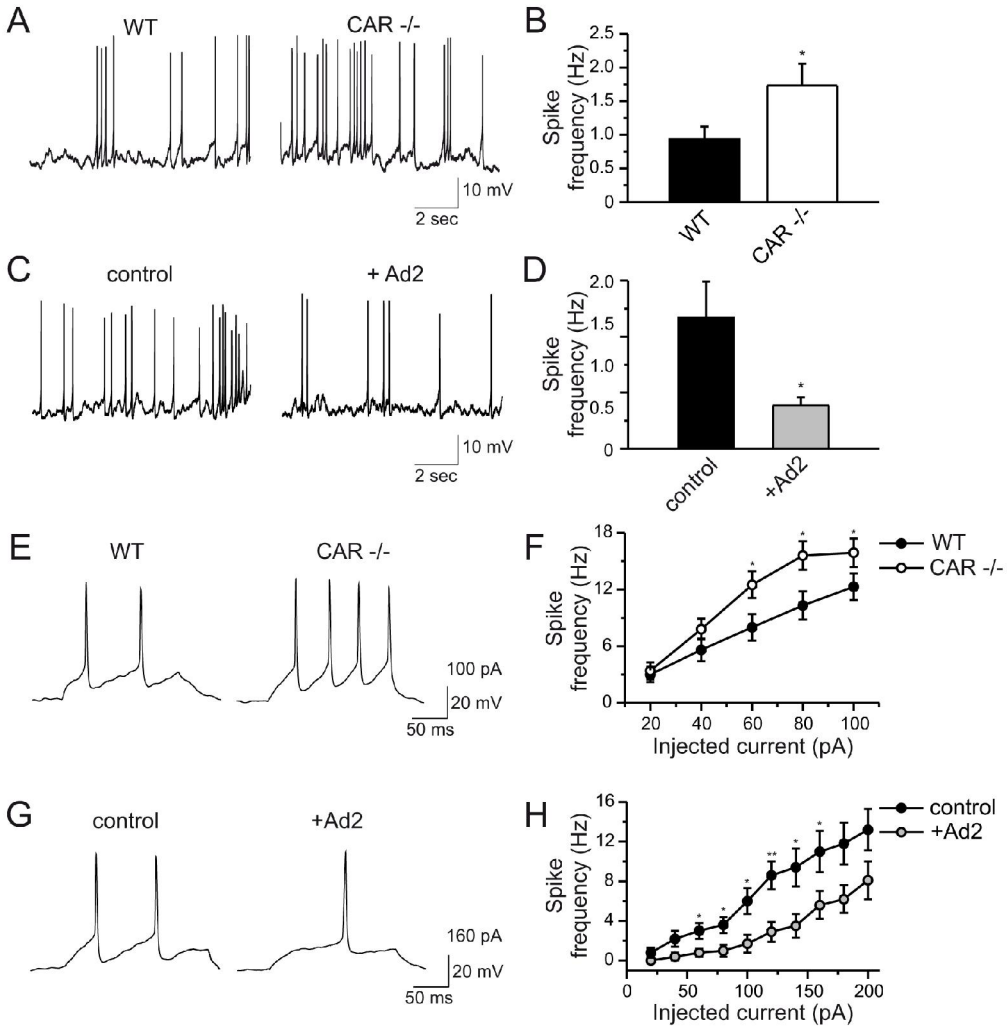

Fig. 60: CAR-deficient neurons showed higher firing frequency than WT cells, whereas in Ad2 treated cells a lower number of APs could be recorded. (A, E) Example traces of spontaneous APs (A) and injected APs (E) recorded in CAR-deficient neurons (right trace) and WT cells (left trace) are shown. (B, F) CAR KO cells showed a significantly higher firing frequency of both spontaneous APs (B) and injected APs (F) than WT cells (DIV 16-18, n = 34-36). (C, G) Example traces of spontaneous APs (C) and injected APs (G) recorded in Ad2 treated neurons (right trace) and control cells (left trace) are shown. (D, H) Firing frequency of spontaneous APs (D) and injected APs (H) recorded in Ad2 treated cells was significantly lower compared to the control cells (DIV 14, n = 27-28).

3.9.2. The absence of CAR influences neuronal network activity

To address the question of whether the absence of CAR might influence synaptic communication, cultivated CAR-deficient neurons were used to study the development of synaptic activity that might reflect the maturation of the neuronal networks and the properties of postsynaptic currents. Synaptic events recorded by whole-cell patch-clamp recordings in the voltage-clamp mode, represent neurotransmitter-mediated intercellular communication. Inhibitory and excitatory postsynaptic current as well as spontaneous (AP- dependent and -independent) or miniature (AP-independent) postsynaptic currents and their properties were

analyzed in CAR-deficient neurons at different cultivation periods and compared with WT cells.

Current amplitudes, frequency and kinetic properties (10-90 % rise time and decay time constant) of synaptic events were measured and analyzed. The amplitude and the frequency of synaptic currents indicates the amount and at which rate the neurotransmitter or vesicle is released from the presynapse as well as giving hints about the functionality of postsynaptic receptors.

Kinetic properties of synaptic events were investigated to test whether the structure and/or composition (organization) and sensitivity of channels mediating recorded synaptic currents might be affected in CAR KO cells (Clements et al., 1992; Gardner et al., 1999; Hollmann et al., 1991; Jones and Westbrook, 1997; Maconochie et al., 1994; Magleby and Stevens, 1972; Melnick, 1993; Melnick and Baev, 1993; Rubio and Wenthold, 1997; Trussell and Fischbach, 1989).

Recorded postsynaptic currents were distinguished by application of appropriate synaptic receptor blockers (Table 9, 15).

3.9.2.1 Excitatory postsynaptic currents show a higher frequency in CAR-deficient neurons

After 10 DIV cultivated neurons (E10.5) began to display spontaneous excitatory postsynaptic activity (sEPSCs; Fig. 61 A, B). In order to distinguish spontaneous excitatory events from inhibitory currents, recordings were performed in the presence of biccuculine, a $GABA_A$ receptor antagonist (Table 15). Recorded currents were inward at a negative holding potential (V_h=-70 mV), having a rapid rising phase (rise time) followed by a slower decay with the time constant (tau) of a few milliseconds (Fig. 61 C, D).

The averaged peak amplitudes of recorded sEPSCs were very similar in CAR KO and WT cells (Fig. 61 A). The mean amplitudes, which appeared at DIV 10, resembled those of more mature neurons at DIV 24 (Fig. 61 A). In contrast to the developmental stability of sEPSC amplitudes, the sEPSC frequency showed an explicit change, increasing progressively during the cultivation period. Moreover, the frequencies of recorded sEPSCs were significantly higher in CAR-deficient neurons than in WT cells (Fig. 61 B). At prolonged cultivation periods, a characteristic burst pattern of recorded currents was often observed (Fig. 61 G). The burst activity occurred more frequently in CAR KO cells than in WT neurons.

Furthermore, the kinetic properties of recorded sEPSCs were investigated. A 10-90 % rise time and the decay time constant (tau) revealed no significant differences between CAR KO

and WT neurons (Fig. 61 C, D), suggesting that there are no changes in the channel properties between both genotypes. Both, the rise time and tau of sEPSCs increased to a similar extent during the cultivation period.

Synaptic currents	Blocker	Blockage of	Final concentration
spontaneous Excitatory Postsynaptic Currents (sEPSCs)	Biccuculine	$GABA_A$ receptors	20 µM
miniature Excitatory Postsynaptic Currents (mEPSCs)	TTX Biccuculine	Voltage-gated Na^+ channels $GABA_A$ receptors	100 µM 20 µM
spontaneous Inhibitory Postsynaptic Currents (sIPSCs)	DNQX	AMPA/kainate receptors	10 µM
miniature Inhibitory Postsynaptic Currents (mIPSCs)	TTX DNQX	Voltage-gated Na^+ channels AMPA/kainate receptors	100 µM 10 µM

Table 15: Blockers for synaptic receptors.

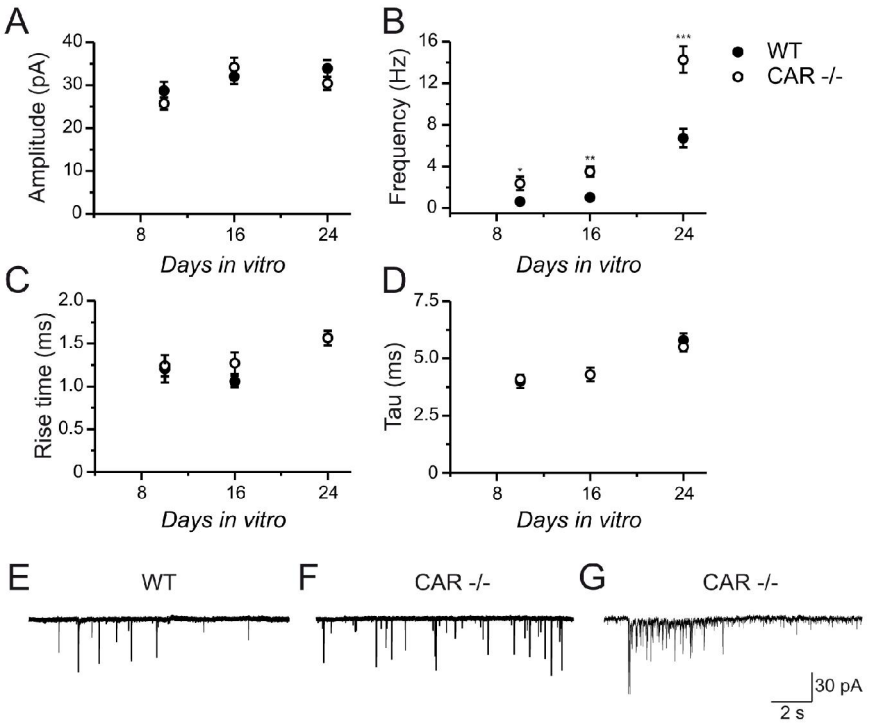

Fig. 61: Spontaneous excitatory postsynaptic currents (sEPSCs) showed a higher frequency in CAR KO cells compared to WT cells. (A) Amplitudes of recorded currents were similar in both genotypes. (B) CAR-deficient neurons showed a significantly higher frequency of sEPSCs compared to WT cells throughout the cultivation period. The frequency of recorded currents increased progressively during the cultivation period. (C, D) The kinetic properties of measured sEPSCs events were similar in both WT and KO cells. Both, the rise time value (C) and tau (D) increased during the cultivation period. (E, F) Example traces of recorded sEPSC in CAR-deficient neurons (F) and WT neurons (E). (G) Example traces of burst activity of sEPSCs recorded in CAR KO cells (A-D: DIV 10-2 n = 20-21, DIV 14-16 n = 20-22, DIV 20-25 n = 25-34).

Similar to results obtained for sEPCSs, recordings of miniature postsynaptic currents (mEPSCc) revealed a significantly higher frequency in CAR KO cells compared to WT cells (Fig. 62 B). Although the frequency of mEPSCs progressively increased during the cultivation period (Fig. 62 B), mEPSCs showed a lower frequency than sEPSCs, since mEPSCs contain only AP-independent events, whereas sEPSCs consist of both AP-dependent and independent currents (Table 15).

The averaged amplitude, rise time and decay time revealed no differences between CAR KO and WT cells (Fig. 62 A, C, D). Similar to sEPSCs, the rise time and tau of mEPSCs increased, whereas the amplitude remained stable during the cultivation period.

The obtained results, which reveal an increase in the frequency and changes in the kinetic properties, but no increase in the amplitude, were in agreement with published reports (Blanton et al., 1989; Blanton and Kriegstein, 1991b; Brown and Johnston, 1983; Johnston and Brown, 1983; McCormick and Prince, 1987; Sommer et al., 1990).

Table 16 presents the success rate of recorded currents (% of cells with synaptic activity in proportion to all recorded cells) in both cell types. No significant differences were observed.

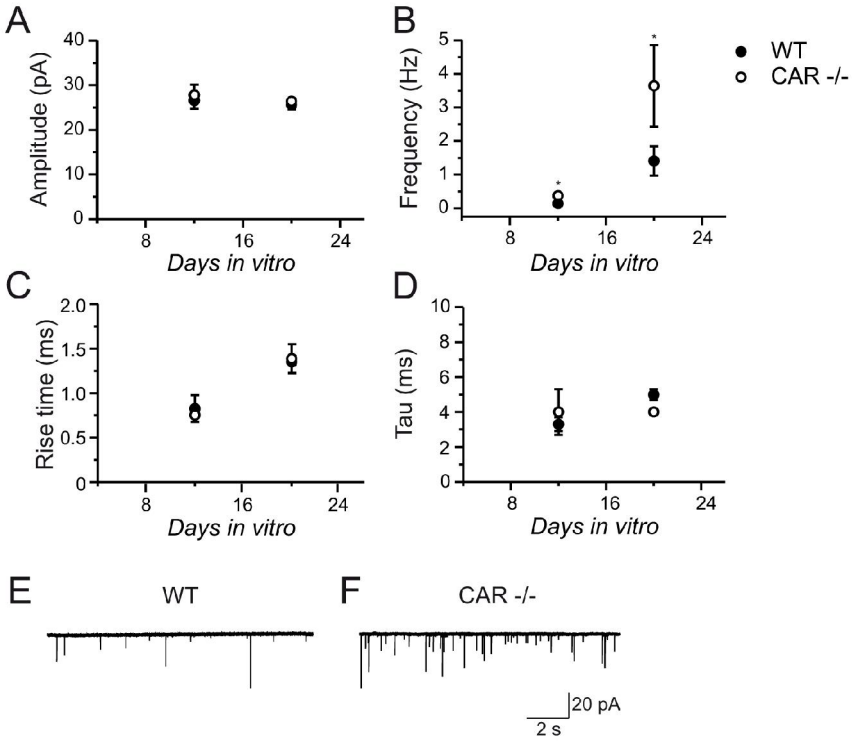

Fig. 62: The frequency of mEPSCs was significantly higher in CAR KO cells. (A) Amplitudes of recorded currents were similar in both types of cells. (B) CAR-deficient neurons showed a significantly higher frequency of mEPSCs. The frequency of recorded currents increased during the cultivation period. (C, D) Kinetic properties of recorded mEPSCs events were similar in both WT and KO cells. Both the rise time value (C) and tau (D) increased during the cultivation period. (E, F) A burst pattern of sEPSCs was often observed in CAR KO cells (F), but only rarely in WT cells (E; A-D: DIV 10-25 n = 20-25).

	mEPSCs		sEPSCs		mIPSCs		sIPSCs	
DIV	**WT**	**CAR -/-**	**WT**	**CAR -/-**	**WT**	**CAR -/-**	**WT**	**CAR -/-**
7-8					41 %	50 %	54 %	39 %
10-14	25 %	28 %	28 %	25 %	82 %	40 % (*)	77 %	65 %
16-20	45 %	48 %	47 %	48 %	90 %	75 %	89 %	72 %
20-24			58 %	60 %				

Table 16: Success rate of cells with synaptic currents (** $p < 0.05$ chi^2 test)

3.9.2.2 Inhibitory postsynaptic currents show a lower frequency in CAR-deficient neurons

Spontaneous inhibitory postsynaptic currents (sIPSCs) appeared after 7 days in culture, earlier than sEPSCs. Recorded currents at V_h = -70 mV were inward and showed a rapid rise time, but a much longer decay time compared to sEPSCs (Fig. 61 D compared to 63 D). In contrast to sEPSCs, the sIPSCs showed a change in the mean amplitude during the cultivation period (Fig. 61 A, B compared to Fig. 63 A, B). The decay time constant (tau) decreased within time (Fig. 63 D). These results were in accordance with published reports (Blanton et al., 1987; Blanton and Kriegstein, 1991a; Blanton and Kriegstein, 1991b; Hahm et al., 2005;Melnick, 1993).

The amplitude (Fig. 63 A) and frequency (Fig. 63 B) of recorded sIPSCs were significantly higher in WT cells compared to CAR-deficient neurons. These findings might be a result of impaired synaptic properties, or of a lower success rate of recorded currents in CAR KO cells (Table 16). Rise time (Fig. 63 C) and tau (Fig. 63 D) of recorded sIPSCs yielded no differences between CAR KO and WT cells.

Similar to results obtained for sIPSCs, recordings of miniature inhibitory postsynaptic currents (mIPSCs) revealed a higher amplitude and frequency in WT cells compared to CAR-deficient neurons (Fig. 64 A, B) whereas the kinetic properties of recorded currents were similar in both cell types (Fig. 64 C, D).

No differences in the kinetic properties of either IPSCs or EPSCs between CAR KO cells and WT cells could be observed, suggesting no changes in the properties of ion channels mediating these currents. Tau was much shorter in EPSCs than in IPSCs and increased during cultivation period in contrast to IPSCs (Fig. 61-64).

The frequency of recorded EPCS, in both CAR KO and WT cells, was much higher than that of IPSCs although IPSCs occurred earlier in the culture. Interestingly, the frequency

of recorded EPSCs in CAR-deficient neurons was significantly higher than in WT cells, while the frequency of recorded IPSCs was significantly lower, suggesting that the absence of CAR causes an imbalance in the ratio of inhibitory and excitatory synaptic activity.

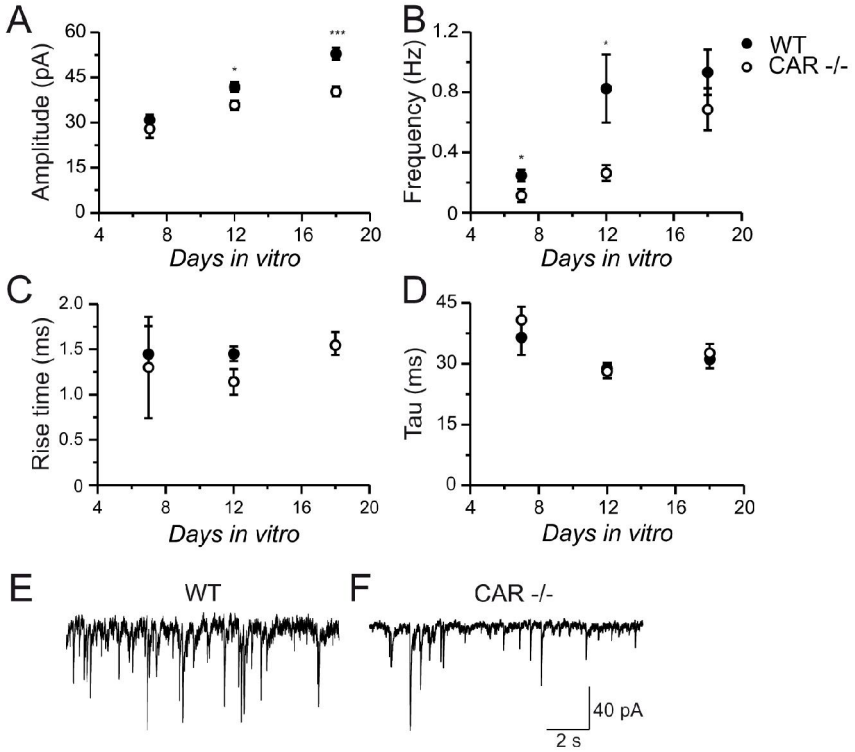

Fig. 63: CAR-deficient neurons revealed lower amplitude and frequency of sIPSCs. (A, B) Averaged amplitudes (A) and frequency (B) of recorded sIPSC were smaller in CAR-deficient neurons compared to WT cells. (C, D) No significant differences were observed in kinetic properties. The rise time (C) showed a slightly increasing trend during cultivation period, while tau (D) decreased. (*t* test: * for $p < 0.05$, DIV 7-8 n = 18-20, DIV 10-14 n = 34-35, DIV 16-20 n = 46)

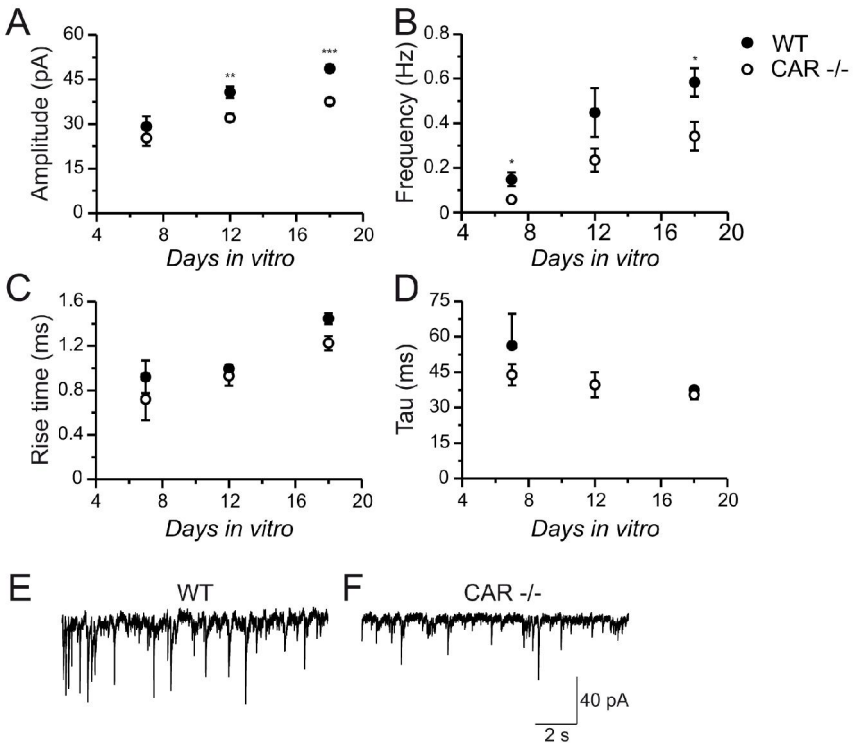

Fig. 64: CAR-deficient neurons revealed a lower amplitude and frequency of mIPSCs. (A, B) Averaged amplitudes (A) and frequency (B) of recorded mIPSC were smaller in CAR-deficient neurons compared to WT cells. Amplitude and frequency increased within the cultivation period in both cell types. (C, D) No significant differences were observed in kinetic properties: rise time (C) and tau (D) were similar in both genotypes (DIV 7-8 n = 20-21, DIV 10-14 n = 35-36, DIV 16-20 n = 59-75).

4. Discussion

The aim of this study was to investigate the physiological function of CAR in cultivated neurons. The CAR protein was identified as a cell surface protein enabling coxsackie viruses B and a number of adenoviruses to attach to host cells (Bergelson et al., 1997; Carson and Chapman, 2001; Mapoles et al., 1985; Tomko et al., 1997), however its physiological function is largely unknown, especially in the developing nervous system. CAR seems to be involved in many different cellular processes (Anders et al., 2003; Bowles and Towbin, 1998; Coyne et al., 2004; Excoffon et al., 2004; Fuxe et al., 2003; Honda et al., 2000; Okegawa et al., 2001; Zen et al., 2005). CAR as a cell-cell adhesion molecule (Bruning and Runnebaum, 2003; Cohen et al., 2001; Honda et al., 2000; Mirza et al., 2006) plays an essential role in heart development (Asher et al., 2005; Chen et al., 2006; Dorner et al., 2005) and appears to be associated with TJs (Cohen et al., 2001; Raschperger et al., 2006). An important role of CAR during the development of the nervous system has also been suggested because of its strong, developmentally regulated expression pattern (Honda et al., 2000). However, no specific function of CAR has been characterized so far.

In the present work an electrophysiological approach was chosen to investigate the role of CAR in developing neurons. The aim was to characterize CAR-deficient telencephalic neurons prepared at E10.5 and compare them to WT neurons. Different passive and active membrane parameters and synaptic currents were investigated in order to test the consequences of CAR absence on neuronal membrane properties and network formation. In parallel the effects of proteins binding to CAR such as the fiber knob of adenovirus (Ad2) and antibodies against CAR were investigated. These proteins might modulate the function of CAR and thereby help to characterize its function.

4.1 The absence of CAR results in an increased R_m

Whole-cell patch-clamp recordings revealed a significantly higher R_m in CAR-deficient neurons than in WT cells (E10.5; Fig. 18). This result suggests that the absence of CAR, and thus CAR-mediated interactions, influences passive membrane properties such as leak conductance at the RMP.

On the other hand, treatment of cortical neurons with Ad2 which binds directly to CAR, showed an opposite effect and resulted in a significantly lower R_m (Fig. 19). The Ad2 effect is CAR-dependent, because Ad2 influenced the R_m in WT cells, but not in CAR KO cells (Fig. 20). These results suggest that specific binding of Ad2 to CAR induces an intracellular mechanism which results in a lower R_m, whereas in the absence of CAR this intracellular

process can not be induced (does not exist). Differences in R_m in both CAR-deficient neurons and Ad2 treated cells remained significant during all analyzed cultivation periods, even though R_m decreased over the cultivation periods. This general decrease of R_m, due to the maturation of cells during the cultivation period is in agreement with published reports (Cameron and Nunez-Abades, 2000; Hohnke and Sur, 1999; McCormick and Prince, 1987; Ramoa and McCormick, 1994; Tepper and Trent, 1993). Other parameters such as capacitance and properties of voltage-gated ion channels were not affected, suggesting that changes in R_m were not due to delayed (e.g. in CAR KO cells) or accelerated (e.g. by Ad2) differentiation of cells. Furthermore, differences in the calculated specific R_m (R_m *specific;* Fig. 19, 20), representing R_m in relation to cell size (capacitance, C_m), indicate that changes in R_m were not due to different cell size (Kandel et al., 1996; Zomorrodi et al., 2008). The affected R_m in CAR KO and Ad2 treated neurons represents changes in passive membrane properties (see chapter 4.2).

As mentioned in the introduction, Ad2, the most distal part of adenovirus, binds directly to D1, the membrane distal Ig domain of CAR, and initiates CAR-mediated internalization of the virus into the host cell (Bewley et al., 1999; Freimuth et al., 1999; Kirby et al., 2000; Roelvink et al., 1999; Wang and Bergelson, 1999). At normal physiological conditions, without virus infection, D1 mediates homotypic CAR-CAR interaction between two adjacent cells (Excoffon et al., 2005; Jiang et al., 2004; van Raaij et al., 2000, Patzke et al., 2009, submitted). Thus, the fiber knob of adenovirus (Ad2) uses the same surface of the D1 domain for binding CAR as CAR uses for the formation of a CAR homodimer (Excoffon et al., 2005; van Raaij et al., 2000). Binding of Ad2 to CAR might therefore mimic homophilic CAR binding. Surprisingly, application of extracellular CAR domains D1 and/or D2, to cortical neurons did not influence the R_m (Fig. 23). This could be explained by the fact that Ad2 binds with 1000-fold greater affinity to CAR than CAR does to itself (van Raaij et al., 2000) and the effect of Ad2 might be much stronger and thus more easily detectable in contrast to CAR domains. Additionally, fiber knob is a trimetric protein and has three identical binding sites for CAR D1 which can be occupied simultaneously (Bewley et al., 1999; Lortat-Jacob et al., 2001; Xia et al., 1995) and therefore might result in a clustering of CAR polypeptides on the same membrane. Nevertheless, it is also possible, although Ad2 and CAR bind to the same D1 domain, that both proteins evoke different intracellular effects. Under normal physiological conditions CAR domains are involved in contact formation between cells, whereas Ad2 disrupts cell-cell contacts. Thus, the effects mediated by Ad2 or by CAR

domains may be different or may show a different magnitude and may therefore not be detectable by the same method.
Furthermore, antibodies against CAR (Rb80; Fig. 22) were applied to cortical neurons in order to test their effect on passive membrane properties. After 1h pre-incubation with anti-CAR ABs, neurons showed a significantly higher R_m and higher R_m *specific* compared to control cells (Fig. 22 D, F). The effect of anti-CAR ABs was similar to the observation made in CAR-deficient neurons (Fig. 18), suggesting that the anti-CAR ABs block the interaction of CAR with other proteins and thus might prevent the induction of CAR-mediated intracellular signaling pathways, which would be activated by binding of physiological interaction partners (e.g. D1, Ad2). Similarly, the absence of CAR also prevents all CAR-mediated processes. In both cases, blockage of CAR-mediated intracellular cascades resulted in changes of passive membrane properties and an increased R_m. Alternatively, binding of Ad2 to CAR might induce an intracellular pathway resulting in the decrease of R_m. Thus, interaction of Ad2 with CAR would evoke opposite effects compared to these observed in absence or blockage of CAR.
In addition, the effect of fibronectin – also a ligand of CAR (Patzke et al., 2009, submitted) - on R_m was investigated (500 µg/ml, 1h preincubation, data not shown). Fibronectin binds to the D2 domain of CAR (Patzke et al., 2009, submitted). As observed for D1 or D2, no differences in the R_m could be observed in the presence of fibronectin.
These results suggest that an Ad2-induced decrease in R_m is an Ad2-specific effect.

4.2 Possible reasons for the measured changes in R_m in the absence of CAR or after treatment with Ad2

The membrane resistance (R_m; input resistance) represents the relationship between current (I) flowing through the membrane and the voltage (V, potential) across the membrane. How much current flows through the membrane at a given potential depends on the number of ion channels and transport proteins, which are incorporated in the neuronal membrane. The higher the number of active channels, the more current will flow and the lower R_m will be (and R_m *specific*). Thus the R_m is inversely proportional to membrane conductance (*g*; $R_m = 1/g$, chapter 1.6.2; Hammond, 2001; Kandel et al., 2000).

A significantly higher R_m (and R_m *specific*) in CAR-deficient neurons indicates a lower membrane conductance, suggesting a lower number of ion channels in the membrane or altered properties of ion channels. On the other hand, the significantly lower R_m in Ad2

treated cells suggests enhanced membrane conductance and might indicate a positive effect of Ad2 on ion channel activation (opening probability).

Changes in R_m were observed at the RMP, when no voltage-gated ion channels are activate (linear I-V plot in Fig. 18 C and 19 C), suggesting that the difference in R_m represents altered leak (resting) membrane conductance. Therefore, to characterize the increased R_m in the absence of CAR I investigated the ionic conductance (Na^+, K^+, Cl^- and Ca^{2+}) across the neuronal membrane and I characterized specific ion channels, transport proteins and pumps, which are directly and non-directly involved in the establishment and maintenance of the RMP.

4.2.1 Voltage-gated and neurotransmitter-gated channels are not modulated by CAR

Voltage-gated K^+, Na^+ and Ca^{2+} channel properties were investigated in WT and CAR KO neurons as well as in control and Ad2 treated cells. No differences in the maximal voltage-gated K^+, Na^+ or Ca^{2+} currents, their current density or their activation voltages could be observed between CAR-deficient and WT neurons, as well as between Ad2 treated and control cells (Fig. 24-32). Furthermore, the blockage of these currents did not influence the differences in R_m in CAR-deficient and Ad2 treated cells (Fig. 28; 45). These results suggest that voltage-gated K^+, Na^+ and Ca^{2+} channels are not involved in the observed R_m changes. Similar to voltage-gated ion channels, neurotransmitter–gated receptors (ionotropic and metabotropic receptors) are, most probably, also not implicated in R_m differences between CAR KO and WT neurons, and Ad2 treated and control cells (blockage of $GABA_A$ receptors did not influence R_m differences, Fig. 39). Neurotransmitter-gated channels open only when a neurotransmitter is bound; otherwise they are closed at the RMP. In none of the experiments conducted neurotransmitters were applied and therefore no activation was evoked. If there was a spontaneous release of neurotransmitters in cultivated neurons, it occurred uncontrolled and independently in WT, but also in CAR-deficient neurons (see chapter 3.9.2). Furthermore, spontaneous synaptic activity at DIV 7 is very rare, but the observed differences in R_m at this stage are highly significant, suggesting that spontaneous synaptic activity is not implicated in the modulation of R_m. In addition, neurotransmitter-gated channels open only for a very short time (ms). This time scale is too short to permanently influence (change) R_m. Thus, neurotransmitter-gated channels seem not to be able to determine passive membrane properties (Kandel et al., 2000; Purves et al., 2008).

4.2.2 Gap junctions are not involved in observed changes in R_m in CAR-deficient neurons and Ad2 treated cells

As mentioned in chapter 3.5.1 gap junction proteins were investigated because of several reasons pointing towards a possible interaction between CAR and connexins. Pharmacological treatment with several gap junction blockers (Table 12) increased R_m in WT but not in CAR KO cells (Fig. 33 A, B). Furthermore, carbenoxolone (a gap junction blocker) was able to partly abolish the effect that Ad2 had on R_m (Fig. 33 C). These results suggest that connexins might be absent or not functional in CAR KO cells and that they might be involved in the Ad2 induced effect on R_m. However, aside from these pharmacological findings, no further evidence for gap junction implication in the function of CAR could be found. Western blot analysis and immunocytochemical stainings showed similar expression patterns of different connexins (Cx32, Cx36, Cx43) in CAR KO and WT tissues and cultivated neurons, suggesting that connexins are also present in CAR-deficient cells (Fig. 33). Dye spreading and electrical coupling performed in parental HeLa cells and stably transfected HeLa cells with connexin 36 or 43 were not influenced by Ad2 (Fig. 34-38). Additionally, several side effects of gap junction blockers have been reported, describing their influence on e.g. Ca^{2+} or Cl^- channels (Leshchenko et al., 2006; Marcet et al., 2004; Reyes et al., 2009; Ross et al., 2000; Rouach et al., 2003; Vapaatalo et al., 1978; Vessey et al., 2004; Yang and Ling, 2007). Therefore, the results obtained using gap junction blockers may be due to blockage of different channels and/or conductance and do not give sufficient evidence for implication of gap junction in the function of CAR. The involvement of connexins in CAR-mediated processes in cultivated neurons thus seems to be unlikely.

4.2.3 The Na^+/K^+-ATPase pump is functional in CAR KO cells

As mentioned in chapter 3.5.3 the Na^+/K^+-ATPase pump was considered in this study for several reasons including the possibility that CAR might indirectly modulate the Na^+/K^+-ATPase pump via agrin. Therefore the expression pattern of the Na^+/K^+-ATPase pump and its functionality in CAR-deficient neurons was studied. Immunocytochemical staining with antibodies against the α3 subunit of the Na^+/K^+-ATPase pump (expressed in neurons, Hilgenberg et al., 2006; Peng et al., 1997) revealed an abundant expression and a similar distribution in cultivated CAR KO and WT neurons (Fig. 40). Treatment of cells with ouabain, a common blocker of the Na^+/K^+-ATPase pump (Michael et al., 1978; Saghian et al., 1996; Schwartz et al., 1975) increased R_m in WT, but not in CAR KO cells (Fig. 41 D), suggesting that, although the Na^+/K^+-ATPase is expressed, it may not be functional in CAR-

deficient neurons. However, application of ouabain to CAR KO and WT cells increased the frequency of spontaneous postsynaptic currents in both genotypes, suggesting that the protein is also active in CAR-deficient neurons (Fig. 41 E). These results indicate that the Na^+/K^+-ATPase pump is expressed and moreover functional in CAR KO cells. The Na^+/K^+-ATPase pump is thus unlikely to be the reason for the significantly higher R_m in CAR-deficient neurons. Additionally, although an ouabain induced increase of the R_m has been reported (Matsumoto et al., 2008; Planelles and Anagnostopoulos, 1987), other reports describe an opposite effect on R_m or a dose-dependent effect of ouabain (Albrecht et al., 2005; Bonsi et al., 2004; Molnar et al., 1999; Saghian et al., 1996). These discrepancies may be due to the fact that the Na^+/K^+-ATPase pump triggers a complex scenario of cellular events and thereby affects numerous physiological functions. Blockage of the Na^+/K^+-ATPase pump leads to an imbalance in Na^+ and K^+ concentrations across the membrane and thus to an increase in V_m (Matsumoto et al., 2008; Molnar et al., 1999), which in turn influences synaptic activity (Glushchenko and Izvarina, 1997; Reich et al., 2004; Scuri et al., 2007; Wyse et al., 2004) and membrane conductance e.g. of Cl^- (Dierkes et al., 2006; Sacchi et al., 2007; Saghian et al., 1996). Thus, the observed effect of ouabain on R_m in WT cells may actually be a secondary effect of ouabain resulting from altered membrane conductance due to blockage of the pump.

4.2.4 Hyperpolarization-activated currents are altered in CAR KO cells and Ad2 treated cells

The electrophysiological identification of HCN channels is not simple due to their complex and unspecific properties. In order to test whether HCN channels may be altered in CAR-deficient neurons or in Ad2 treated cells hyperpolarizing voltage steps were applied to the membrane of CAR-deficient and WT neurons and Ad2 treated cells. HCN current recorded in CAR-deficient neurons revealed lower amplitudes compared to WT cells (Fig. 43), whereas the HCN current recorded in Ad2 treated cells showed higher amplitudes compared to control cells (Fig. 44). Only maximal currents were significantly different between both genotypes and between Ad2 treated and untreated cells. Application of the commonly used blocker ZD7288 (Bedner et al., 2006; Felix et al., 2003; Gasparini and DiFrancesco, 1997; Gonzalez-Iglesias et al., 2006) reduced the current in WT, but not in CAR KO cells (Fig. 43). After treatment with the commonly used HCN channel enhancer, gabapentin (Lin et al., 2009; Wickenden et al., 2009), only a slight increase in the current amplitude in control cells (E15) was observed (Fig. 42). These results are not sufficient to conclude whether HCN channel function is impaired in CAR KO cells or whether it is directly influenced by Ad2.

Application of ZD7288 blocked 52.2% of the measured current, whereas gabapentin could only slightly increase the amplitude (6.6%), suggesting that, most probably, the measured current consisted also of other currents. Thus, the observed differences in the recorded current between CAR KO and WT cells or control and Ad2 treated cells might not be due to differences in HCN channel properties. Besides HCN channels, other channels have been reported to become activated at highly negative membrane potentials: e.g. members of the KIR superfamily, inwardly rectifying potassium channels (Abraham et al., 1999; Clark et al., 1998) or hyperpolarization-activated Cl^- channels (Clark et al., 1998; Smith et al., 1995; Tarran et al., 2000). Therefore, it is difficult to conclude whether HCN channels are involved in CAR-mediated changes in membrane properties or whether the observed differences in membrane conductance at high negative membrane potentials, in CAR KO cells and Ad2 treated cells, result from current flowing through other ion channels.

4.2.5 Analysis of ion flow across the neuronal membrane in the absence of CAR

Investigating particular ion channels and transport proteins may be helpful to characterize neuronal properties of CAR-deficient neurons and Ad2 treated cells. However, the high diversity of these proteins, their complexity, unspecific ionic properties and an often unspecific pharmacology make it difficult to electrophysiologically identify the protein which is responsible for observed changes in R_m. Therefore, another approach for further investigation was chosen. Using different intra- and extracellular solutions during patch-clamp recordings, conductance of a single ion type through the membrane was investigated.

4.2.5.1 K^+ conductance is not responsible for higher R_m in CAR KO cells

The neuronal membrane at the RMP is most permeable for K^+ ions (Hammond, 2001; Kandel et al., 2000) and therefore K^+ conductance was investigated. Blockage of K^+ conductance, by removal of K^+ ions from the IC solution, resulted in a slight increase in R_m in both CAR-deficient and WT cells, as well in Ad2 treated and untreated cells, indicating that K^+ conductance was efficiently blocked and plays an important role in the establishment of the R_m (Cameron et al., 2000; Crill and Schwindt, 1983). However, after removal of K^+ from the cell, the differences in R_m between CAR KO and WT, cells as well as between Ad2 treated and control cells, still remained significant (Fig. 45). This suggests that K^+, although generally implicated in the establishment of the R_m, is not responsible for CAR-mediated differences in R_m.

These results would also suggest that the afore mentioned HCN channels, permeable for K^+ ions, are unlikely to be involved in the observed changes in R_m.

4.2.5.2 Cl^- conductance is impaired in CAR KO cells and enhanced in Ad2 treated cells

Experiments presented in chapter 3.6.2 provide evidence that Cl^- conductance is responsible for the observed changes in R_m. Recordings made under Cl^- free conditions (removal of Cl^- from IC solution) revealed no difference in R_m between CAR KO and WT cells (Fig. 46 A, B) and no reduction of R_m after treatment with Ad2 (Fig. 46 C, D). On the other hand, under conditions when mainly Cl^- conductance was measured (blockage of other conductances by application of blockers) CAR-deficient neurons showed significantly lower current amplitudes compared to WT cells (Fig. 47 A-C), whereas currents measured in Ad2 treated cells were significantly larger than in control cells (Fig. 47 D-F). Blockage of Cl^- currents, by application of commonly used Cl^- channel blockers (DIDS, NPPB), reduced the current in WT, but not in CAR KO neurons (Fig. 48 C, D). Furthermore, under conditions when all ion conductances were possible, subtraction of the measured current in WT neurons, from the current recorded in CAR KO neurons, resulted in electrophysiological identification of a current, which does not exist in CAR-deficient neurons and whose E*rev* was very similar to the calculated E*rev* of Cl^- (Fig. 49 A-C; Table 13). A similar result was obtained by subtraction of the current recorded in Ad2 treated cells, from the current measured in control cells, indicating that the additional current measured after treatment with Ad2 was due to enhanced Cl^- conductance (Fig. 49 D-F). The strongest result pointing to an implication of Cl^- in CAR-mediated changes in membrane conductance resulted from an experiment where E*rev* of different ions was shifted. By simultaneously lowering concentrations of Cl^- and Na^+ ions in the recording solutions, E*rev* of both Na^+ and Cl^- shifted in two different directions. E*rev* of Cl^- shifted to a more positive direction and E*rev* of Na^+ to a more negative direction (Table 13). Under these experimental conditions the E*rev* of the additional current recorded in Ad2 treated neurons and E*rev* of the current lacking in CAR KO neurons, were both shifted in a more positive direction, towards the E*rev* of Cl^- (Fig. 50). Results of all these experiments suggest that Cl^- conductance, which is enhanced in Ad2 treated cells, but impaired in CAR-deficient neurons, is responsible for the observed differences in R_m.
Additionally, the results from the E*rev* shift experiment exclude Na^+ ions to be implicated in the observed changes in membrane conductance.

It is important to mention that some blockers commonly used for blocking Cl^- currents also block gap junctions e.g. NPPB (Eskandari et al., 2002; Kotsias and Peracchia, 2005) or conversely, that common gap junction blockers: carbenoxolone and alcohol-based blockers were reported to influence Cl^- currents (Leshchenko et al., 2006; Marcet et al., 2004; Reyes et al., 2009; Ross et al., 2000; Rouach et al., 2003; Vapaatalo et al., 1978; Vessey et al., 2004; Yang and Ling, 2007). This fact would explain why, after application of several gap junction blockers, the R_m increased in WT neurons, but not in CAR KO neurons, suggesting that the applied gap junction blockers at least partly blocked Cl^- conductance in WT cells.
Furthermore, although Ad2 was able to reduce R_m in HeLa and HeLaCx36 cell (Fig. 35 A, C), the presence of Cl^- currents in HeLa cells has been reported (Diaz et al., 1993; Shibata et al., 2005; Stutzin et al., 1998), suggesting that the effect of Ad2 on R_m could be due to enhanced Cl^- conductance and not due to changes in connexin properties.
Regarding the unclear situation of HCN channels, the results on Cl^- ions showed that neither K^+ nor Na^+ seems to be involved in the observed changes in R_m, suggesting that HCN channels are not implicated in CAR-mediated processes. Another channel which is activated at negative membrane potentials is the hyperpolarization-activated inwardly rectifying chloride channel (Clark et al., 1998). This channel has been identified in different neuron types (Madison et al., 1986; Staley, 1994) and belongs to the voltage-gated chloride channel family (Thiemann et al., 1992). It is therefore possible that the application of negative potentials to neurons activated both HCN and hyperpolarization-activated chloride channels. Consequently the differences measured between CAR KO and WT cells, and Ad2 treated and untreated cells, where rather due to Cl^- conductance than to K^+ and/or Na^+ currents.
The differences in R_m in WT, but not in CAR KO neurons after application of ouabain (blockage of the Na^+/K^+-ATPase pump) could also be the reason for the secondary effect of the blockage of the Na^+/K^+ ATPase on Cl^- conductance (Dierkes et al., 2006; Sacchi et al., 2007; Saghian et al., 1996).

As mentioned in chapter 3.6.2, the recorded Cl^- current I-V relationship is outwardly rectifying. Such characteristic outward rectification has been reported for two different Cl^- currents: Ca^{2+}- activated Cl^- current ($I_{Cl(Ca)}$; Ca^{2+}-activated Cl^- channels (CaCCs; Arreola et al., 2002; Eder et al., 1998; Herness and Sun, 1999; Matchkov et al., 2004; Mignen et al., 2000;Nilius et al., 1997b; Schroeder et al., 2008; Zholos et al., 2005; Kotlikoff and Wang, 1998) and volume-regulated Cl^- current ($I_{(Cl-)vol}$; volume-regulated Cl^- channels (VRCCs); Diaz et al., 1993; Kelly et al., 1994). VRCCs are activated by hypoosmotic stress e.g. by application of hypotonic solution and have an essential role in fluid transport and volume

regulation in a number of non-excitable cells e.g. renal cells, osteoclasts and epithelia cells (Braun and Schulman, 1996; Chan et al., 1994; Kelly et al., 1994; Kubo and Okada, 1992; Solc and Wine, 1991; Worrell et al., 1989), but also in excitable cells such as cardiac myocytes (Sorota, 1992; Tseng, 1992).

Activation of CaCCs may occur by direct binding of Ca^{2+} (Arreola et al., 2002; Hartzell et al., 2005; Kuruma and Hartzell, 2000; Reisert et al., 2003) or via activation of Ca^{2+}-binding proteins (e.g. CaMKII). Activation of CaCCs requires a rise $[Ca^{2+}]_i$, which can occur either by Ca^{2+} influx through VGCCs or through the release of Ca^{2+} from intracellular Ca^{2+} stores (mobilization through IP3 receptors and another store-operated calcium entry; Frings et al., 2000; Zholos et al., 2005). Ca^{2+} binding to CaCCs seems to be voltage-dependent and $[Ca^{2+}]_i$-dependent. Ca^{2+} appears to bind more efficient to CaCCs at high positive membrane potentials (e.g. at + 50 mV) than at low negative potentials (e.g. at -100 mV). The resulting I-V relationship shows outward rectification at physiologically low $[Ca^{2+}]_i$ (< 500 nM). This rectification decreases (or is lost) by raising $[Ca^{2+}]_i$ to > 1µM. At a higher $[Ca^{2+}]_i$, Ca^{2+}-dependent opening predominates, even at a negative potentials (Arreola et al., 1996; Arreola et al., 2002; Eggermont, 2004; Evans and Marty, 1986; Hartzell, 2008; Kuruma and Hartzell, 2000; Qu et al., 2003; Reisert et al., 2003).

The Cl^- current identified in this study showed outward rectification and thus, could belong to either one of these two channel groups. VRCCs are unlikely to be involved because the osmotic stress (or hypotonic solution application) activating VRCCs, was avoided during all electrophysiological experiments, by adjusting the osmolality of the recording solutions and pH values carefully. Thus, stable osmotic conditions during recordings reduced the possibility of evoking volume-activated (swelling-activated) Cl^- currents.

Based on the following interesting observation further investigations focused on CaCCs: recordings, under conditions when mainly Cl^- conductance was measured, resulted in an enhanced Cl^- current in Ad2 treated cells and a loss of outward rectification (Fig. 46 E, F). Ca^{2+}-dependency of the measured outward rectification could be shown by increasing or decreasing the $[Ca^{2+}]_i$, which resulted in a decrease and increase in outward rectification, respectively (Fig. 51 A, B). Further evidence suggesting that the recorded Cl^- current belongs to CaCCs, was the observation of a higher permeability of Cl^- channels for different halides (Br^-, I^-; Fig. 51 C-E; Eggermont, 2004; Frings et al., 2000; Greenwood and Large, 1999; Matchkov et al., 2004; Mignen et al., 2000; Rychkov et al., 1998). Substitution of Cl^- by Br-ions significantly increased current in WT cells, but not in CAR KO neurons (Fig. 52 A-D),

indicating that impaired Cl^- conductance in CAR-deficient neurons may indeed be due to impaired CaCCs function.
The observed loss of outward rectification after treatment with Ad2 suggests also that Ad2 might be able to modulate the $[Ca^{2+}]_i$.

4.3 CAR-mediated increase in intracellular Ca^{2+}

Two independent methods, calcium imaging and whole-cell patch-clamp recordings, revealed the ability of Ad2 to increase the $[Ca^{2+}]_i$ (Fig. 53). The effect of Ad2 occurred within seconds and lasted for over 10 min, gradually increasing, if Ad2 was not washed out (data not shown). The Ad2-induced increase in $[Ca^{2+}]_i$ was independent of blocking different voltage-gated ion channels, synaptic receptors or gap junctions (Fig. 54 A, D, Fig. 57), confirming data obtained by means of whole-cell patch-clamp recordings (see chapters 3.4, 3.5.1, 3.5.2). In addition, this effect was independent of extracellular Ca^{2+}, EC-Ca^{2+}-free solution and blockage of different VGCCs did not prevent the Ad2-induced increase of Ca^{2+}. Ad2 appears to trigger a release of Ca^{2+} from intracellular stores (Fig. 54), because blockage of IP3Ry and RyRs completely abolished its effect. Several types of intracellular organelles are currently believed to serve as intracellular Ca^{2+} storage compartments including the endoplasmic reticulum (ER), mitochondria and the nuclear envelope (Gerasimenko et al., 2003; Verkhratsky and Petersen, 1998). Ca^{2+} flux into the cytosol from calcium stores is mediated by two important Ca^{2+} permeable channels: IP3Rs (Hoesch et al., 2002; Kato and Rubel, 1999; Nakamura et al., 2000; Poulsen et al., 1995; Yamamoto et al., 2000) and RyRs (Hoesch et al., 2002; Kato and Rubel, 1999; Poulsen et al., 1995; Sandler and Barbara, 1999). The endoplasmic reticulum Ca^{2+}-ATPase pump (SERCA) is subsequently responsible for the refilling of intracellular Ca^{2+} stores with cytosolic Ca^{2+} (Kato and Rubel, 1999; Krizaj et al., 1999; Nakamura et al., 2000; Poulsen et al., 1995; Sandler and Barbara, 1999; Shmigol et al., 1995). Release of Ca^{2+} from stores requires activation of at least one of the mentioned channels, IP3Rs may be activated by binding of IP3, whose formation can be stimulated by activation of metabotropic glutamate (mGluRs) and M_3-muscarinic cholinoergicreceptors (M_3-mAChRs; Milani et al., 1993; Simpson et al., 1996; Whitham et al., 1991). Ca^{2+} release via RyRs is activated by an increase in $[Ca^{2+}]_i$ (Ca^{2+} induced Ca^{2+} release (CICR)).
In cultivated cortical neurons (E15), Ca^{2+} could be released from intracellular Ca^{2+} stores by application of 1 mM glutamate (Fig. 56) or 100 µM acetylcholine (data not shown) by activation of mGluRs or mAChRs respectively (in the presence of blockers for ionotropic receptors for these neurotransmitters), suggesting that IP3Rs are, most probably, present in

these neurons (WT, E15). In contrast, application of caffeine, a commonly used RyRs activator (Friel and Tsien, 1992; Sandler and Barbara, 1999; Sitsapesan and Williams, 1990), did not evoke a Ca^{2+} increase (data not shown), leaving the presence of RyRs in these neurons unclear. Nevertheless, it is possible that Ad2 may activate only one type of Ca^{2+} store e.g. IP3-gated stores, and that Ca^{2+}released from this store subsequently activates other stores by CICR. This fact may be a reason for the gradually increasing $[Ca^{2+}]_i$ after Ad2 application that lasted for at least 10 min (Fig. 53, 54, 57).

Two questions arise: 1) which intracellular pathway is affected by the Ad2-CAR-mediated mechanism to activate Ca^{2+} receptors on intracellular Ca^{2+} stores, and 2) are the intracellular Ca^{2+} stores affected in CAR KO neurons. Application of glutamate to CAR KO and WT neurons revealed lower Ca^{2+} responses in CAR KO neurons (not significant, Fig. 56), suggesting that Ca^{2+} stores in CAR KO cells might be affected and could contain either less Ca^{2+} or alternatively less Ca^{2+}-releasing receptors. However, to confirm this, further experiments are required.

Activation of mGluRs e.g. mGluR1, leads to activation of G-proteins, which are coupled to the receptor (e.g. Gaq, Ga11). This is followed by the activation of the phospholipase Cb (PLCb), which cleaves phosphatidyl-4,5-bisphosphate (PIP2) into IP3 and DAG (diacylglycerol). By binding to its receptor (IP3R) in the endoplasmic reticulum membrane, IP3 releases Ca^{2+}-ions from this intracellular Ca^{2+}-store (Fagni et al., 2000; Hartmann and Konnerth, 2008; Hermans and Challiss, 2001). The same pathway for activation of IP3Rs on intracellular Ca^{2+} stores has been reported for different receptors e.g. purinergic receptors (Parikh et al., 1997; Sakaki et al., 1996) and muscarinic receptors (Clapham et al., 2001; Tobin et al., 2009; Whitham et al., 1991). Thus, Ad2-binding to CAR could also activate or influence this, or similar pathways, to release Ca^{2+} from intracellular stores. The blocker U-73122 (Table 14, Fig. 54) was applied to inhibit agonist-induced IP3 formation by suppressing the activity of PLC (Alter et al., 1994; Bleasdale et al., 1990; Pulcinelli et al., 1998; Smith et al., 1990), suggesting that PLC-activated Ca^{2+} release from intracellular stores may be involved in the Ad2-induced increase of $[Ca^{2+}]_i$. However, to clarify this aspect further experiments are required.

In addition to the Ad2-mediated increase of Ca^{2+}, application of extracellular CAR domains also resulted in an increase of $[Ca^{2+}]_i$ (Fig. 58), although the effect was only half as strong as that caused by Ad2.

The weaker effect of CAR domains might provide an explanation for there being no effect of CAR domains on the R_m. For example, either the increase in $[Ca^{2+}]_i$ due to CAR domains is not sufficient to induce changes in membrane conductance e.g. to activate the CaCCs or that both proteins (Ad2 and CAR domains) influence different Ca^{2+}-dependent processes in the cell. Nevertheless, these results suggest that both Ad2 and extracellular CAR domains, by binding to CAR, induce an increase in $[Ca^{2+}]_i$. These results suggest that CAR may play an important role in intracellular Ca^{2+}-mediated mechanisms as e.g. modulation of chloride conductance by influencing the CaCCs. Ad2 induces a Ca^{2+} release from intracellular Ca^{2+} stores and so leads to the activation of CaCCs, resulting in enhanced membrane conductance and therefore lower R_m. Ca^{2+} released from intracellular stores has been reported to activated CaCCs (Zholos et al., 2005). However, since Ca^{2+} triggers many different processes in the cell, changes in the Cl^- conductance due to an Ad2-induced increase of Ca^{2+}, may be one of many possible effects.

Several other cell adhesion molecules such as neural cell adhesion molecule (NCAM) or L1, have also been reported to mediate intracellular signaling pathways via multiple Ca^{2+}-dependent mechanisms (Doherty et al., 1991b; Kiryushko et al., 2006; Walmod et al., 2004; Zhukareva et al., 1997). This suggests that CAR-mediated intracellular mechanisms presented in this work are not uncommon properties for cell adhesion molecules. Being a cell adhesion molecule may be the key to being a mediator in intracellular signaling pathways. This ability of cell adhesion molecules to transduce cell surface signals into intracellular responses is thought to be critical for developing neurons, particularly for axonal pathfinding and targeting as well as neurite outgrowth (Doherty and Walsh, 1994; Green et al., 1997; Zhukareva et al., 1997).

4.4 CAR as an adhesion molecule

CAR is an adhesion molecule and due to its homo- and heterophilic interactions mediates cell-cell contacts and cell-extracellular matrix (ECM) protein contacts (Bruning and Runnebaum, 2003; Cohen et al., 2001; Honda et al., 2000; Mirza et al., 2006; Patzke et al., 2009, submitted).

In the present work several observations were made confirming the ability of CAR to form contacts between cells and between cells and ECM proteins.

Treatment of cortical neurons with anti-CAR ABs for several days resulted in cell detachment from the substrate and cell death of detached cells (Fig. 21). This result suggests that ABs disrupt CAR-mediated cell-substrate interaction. A similar observation was made in HeLa

cells, where application of anti-CAR ABs to the cultivated CAR-positive HeLa cells resulted in detachment of these cells from the substrate (fibronectin; fibulin; Patzke et al., 2009, submitted). Anti-chick CAR antibodies also blocked the adhesion of retinal and tectal chick neurons on fibronectin and laminin (Patzke et al, 2009, submitted). Another report showed that C6 cells transfected with CAR cDNA aggregated homophilically, and this aggregation was inhibited by specific antibodies against the extracellular domain of CAR (Honda et al., 2000). These data suggest that antibodies against CAR are able to disturb CAR-mediated homophilic and heterophilic (with ECM gylocproteins) interactions. Binding of ABs to CAR prevents CAR interaction with other molecules e.g. D1, another CAR, Ad2 or ECM proteins. Furthermore, application of Ad2 to tectal and telencephalic chick or cortical mouse neurons resulted in a significantly lower number of cell aggregates and a significantly higher sum of neurite length (Fig. 59). These results suggest that Ad2 was able to disrupt the homophilic CAR:CAR interaction between cells. This may be explained by the assumption that fiber knob binding is predicted to have a ~1,000-fold greater affinity allowing viral disruption of CAR D1:D1 dimers (van Raaij et al., 2000). Interactions between CAR and ECM proteins seemed not to be affected and all cells stayed attached to the substrate.

These results confirm the role of CAR as a cell-adhesion molecule, suggesting its important role in the development of the nervous system, where formation of contacts between cells and cell-ECM proteins appears to be essential.

Although a significantly lower number of cells forming aggregates due to Ad2 is clearly a result of disturbed homophilic CAR interactions, a significantly higher sum of neurite length is not that evident. From this experiment it is difficult to conclude whether longer neurites are due to an Ad2-specific induced process or due to disruption of cell-cell contacts, which itself could promote neuronal outgrowth in order to stay in contact with other cells. To answer this question an experiment would be necessary, where the neurite length of a single neuron before and after Ad2 treatment would have to be measured.

4.4.1 Ad2-induced Ca^{2+} increase might stimulate neurite outgrowth

Ca^{2+} is an important second messenger that is involved in the triggering and regulation of many neuronal processes, including neurotransmitter release (Borst and Sakmann, 1996; Mulkey and Zucker, 1991), synaptic plasticity (Bear and Malenka, 1994), transcription control (Hardingham et al., 1997) and neurite outgrowth (Ciccolini et al., 2003; Kocsis et al., 1994; Ronn et al., 2002; Williams et al., 1992). The process of neurite outgrowth depends upon the functional interplay between a vast array of environmental cues provided by components of the ECM, different molecules present on the surface and numerous

intracellular processes (Bixby and Harris, 1991; Doherty and Walsh, 1989; Lumsden and Cohen, 1991). Several cell adhesion molecules have been reported to be involved in this process e.g. L1 (Schuch et al., 1989; Williams et al., 1992), neuronal-cell adhesion molecules (NCAM; Doherty et al., 1991a; Kiryushko et al., 2004; Ronn et al., 2002; Schuch et al., 1989) or synaptic adhesion-like molecules (SALMs; Wang et al., 2008) by activation of diverse intracellular signaling pathways leading to an increase in intracellular Ca^{2+} concentration (Kiryushko et al., 2006; Kolkova et al., 2000; Schuch et al., 1989). Therefore, CAR as an adhesion molecule with the ability to modulate intracellular Ca^{2+} concentration might also be a good candidate for inducing intracellular signals promoting neuronal outgrowth. Ad2-mediated increase of $[Ca^{2+}]_i$ and neuronal outgrowth might involve a PLC-dependent pathway (see chapter 3.7.2 and 4.3).

An Ad2-induced intracellular increase of Ca^{2+} and a significantly higher sum of neurites in Ad2 treated cells may suggest that CAR could play a role in the development of neuronal cells and in neurite formation and/or outgrowth. However, the presented data (Fig. 59) are not sufficient to confirm this assumption and further experiments are required to clarify this aspect.

4.5 Changes in membrane conductance influence network activity and action potential generation

Synaptic potentials arriving at neurons must propagate from their synaptic input sites to the axon hillock to participate in the generation of APs. This passive potential propagation depends on passive electrical properties of the neuronal membrane (Elmslie, 2005). Thus, passive membrane properties play an important role in the integration of synaptic and intrinsic neuronal input as well as in the generation and propagation of synaptic output – APs (Ruben, 2001; Surges et al., 2004; Waters and Helmchen, 2006). Changes in membrane resistance and membrane conductance may affect network activity and generation of APs. Therefore, consequences of altered membrane properties on synaptic activity in CAR-deficient neurons and in Ad2 treated cells were investigated.

Recordings of spontaneous and induced action potentials (APs) revealed a significantly higher frequency in CAR KO cells compared to WT neurons (Fig. 60 A, B, E, F). In contrast, APs recorded in Ad2 treated cells showed a significantly lower frequency (Fig. 60 C, D, G, H). These results suggest that passive membrane properties indeed play an important role in the generation of APs. The higher the R_m and the less leaky the cell membrane (the lower the conductance through the membrane), the larger fraction of the

currents from distant dendritic synapses will be transmitted electrically to the spike-initiating zone. This results in a higher probability of APs arising and thus in a higher frequency of APs. In contrast, when the R_m is low, very little of the current from distant synapses will reach the soma and the initial AP generation-segment, resulting in a low probability to induce APs and thus lower firing frequency (Barrett and Crill, 1974; Yang et al., 2005). Thus, the higher R_m in CAR KO neurons results in a higher excitability compared to WT cells. In contrast, enhanced membrane conductance induced by Ad2 causes a slight decrease in the magnitude of depolarization due to the loss of ions through the membrane, and thus does not allow the threshold potential required for the generation of APs to be reached, resulting in a lower AP frequency than in control cells.

In addition, an interesting observation was made in CAR-deficient cultivated cardiomyocytes, which showed a significantly higher beating frequency compared to WT cells, (Patzke, 2009). This hyperexcitability of CAR-deficient cardiomyocytes might suggest similar properties of these cells compared to CAR KO neurons.

Similar membrane properties as presented in this work for CAR-deficient neurons have been previously reported for muscle cells affected by myotonia diseases. Myotonia reflects a state of muscle fiber hyperexcitability (Mankodi, 2008). Clinical symptoms in myotonia are stiffness and delayed relaxation of muscles after sustained contraction. Genetic and physiological studies have shown that myotonia is caused by mutations in the gene encoding ClC-1, a chloride channel that is highly expressed and specific to skeletal muscle. Thomsen's and Becker's congenital myotonias are the most common chloride channel disorders (Koch et al., 1992; Zhang et al., 1996). A mutation in ClC-1 leads to impaired Cl^- conductance across the membrane (Barchi, 1975; de Diego et al., 1999; Gurnett et al., 1995; Liu and Lin-Shiau, 1992; Mankodi and Thornton, 2002; Torbergsen et al., 2003). Furthermore, myotonia has been associated with an increase in membrane (input) resistance (R_m) of muscle cells (Barchi, 1975; Barchi, 1978; Gruener et al., 1979; Liu and Lin-Shiau, 1992).

In addition to APs, neuronal network activity in CAR-deficient neurons was investigated and compared to WT cells. It has been reported that different adhesion proteins might be involved in synaptogenesis, formation and maturation of neuronal networks (Biederer et al., 2002; Bredt and Nicoll, 2003; Brose, 1999; Cotman et al., 1998; Fannon and Colman, 1996; Fields and Itoh, 1996; Hoffman, 1998; Husi et al., 2000; Kim and Sheng, 2004; Kohmura et al., 1998; Lin et al., 2003;Luthi et al., 1996; Scheiffele et al., 2000; Uchida et al., 1996). Thus, in order to test whether CAR, as an adhesion molecule, might also

influence synaptic activity and network formation, inhibitory and excitatory postsynaptic currents were recorded and compared between CAR KO and WT neurons.
The frequency of recorded EPSCs (spontaneous Fig. 61 and miniature Fig. 62) in CAR-deficient neurons was significantly higher than in WT cells, while the frequency of recorded IPSCs (spontaneous Fig. 63 and miniature Fig. 64) was significantly lower. These results suggest an imbalance in the inhibitory to excitatory synaptic input ratio. The relative balance between excitatory and inhibitory (E/I) system is an important determinate of functional neuronal circuits (Blanton and Kriegstein, 1991b;Kirkwood and Bear, 1994; Levinson and El Husseini, 2005; Schummers et al., 2002; Somers et al., 1995; Traub et al., 1987a; Traub et al., 1987b; van Vreeswijk and Sompolinsky, 1996). The total number of formed synapses and the ratio of excitatory-to-inhibitory synaptic inputs a neuron receives, are critical factors for determining neuronal excitability and function (Chih et al., 2005; Levinson et al., 2005; Levinson and El Husseini, 2005; Schummers et al., 2002). Different adhesion molecules are involved in synaptogenesis and circuit formation and are thought to bridge the pre- and postsynaptic compartments of synapses in the central nervous system. Adhesion proteins such as neuroligin1, SynCAM or L1 have been reported to be involved in balancing of the excitatory and inhibitory ratio (Biederer et al., 2002; Levinson et al., 2005; Levinson and El Husseini, 2005; Prange et al., 2004; Scheiffele et al., 2000). According to the results presented here, CAR might also be implicated in regulating the balance between the E/I system. Additionally, an epileptic activity has been described to be a common outcome of synaptic E/I imbalance (Abegg et al., 2004;Chagnac-Amitai and Connors, 1989; Dalby and Mody, 2001; Sutula and Steward, 1986; Yang et al., 2005a). Epileptic neurons are thought to have abnormal intrinsic properties, e.g. intrinsic hyperexcitability, that are released or triggered by several extrinsic factors and are based on disruption of the balance between depolarizing and hyperpolarizing factors (Schwartzkroin and Wyler, 1980). Moreover, a correlation between epileptogenesis, imbalance in synaptic E/I ratio, changes in intrinsic membrane properties, as well Ca^{2+}- activated currents have been reported (Schwartzkroin and Wyler, 1980; Yang et al., 2005). This suggests that higher R_m, higher frequency of APs and EPSCs as well as lower inhibitory synaptic input in CAR-deficient neurons may also lead to the generation of epileptiform activity. However, CAR KO animals die at an embryonic stage and the consequences of CAR absence for animal behavior can not be investigated.
Observed changes in CAR-deficient neurons including higher R_m, higher excitability (hyperexcitability) and impaired Cl^- conductance are all related to each other and seem to play an essential role in neuronal development and network formation.

4.6 Conclusions

In the present work mainly electrophysiological approaches were taken to investigate the role of CAR in developing neurons. Consequences of the absence of CAR in neurons and CAR interactions with different CAR-binding molecules (Ad2, D1, CAR-D1D2, Rb80) on neuronal passive and active membrane properties, membrane conductance, synaptic activity (intrinsic and extrinsic inputs) and Ca^{2+} signaling were studied. Several interesting observations were made leading to a model, which is schematically presented in Fig. 65. The absence of CAR results in a significantly higher R_m due to impaired Cl^- conductance across the membrane. Reduced Cl^- conductance in CAR KO neurons is, most probably, a reason for a higher excitability and an imbalance of the E/I ratio in these cells. Lower Cl^- conductance in CAR KO cells might be caused by impaired Ca^{2+} release from intracellular Ca^{2+} stores leading to inhibition of e.g. CaCCs and thus lower Cl^- conductance. However, independent of Ca^{2+} signaling, a lower number of Cl^- channels or their impaired functionality in CAR-deficient neurons is also possible.

On the other hand, binding of Ad2, the fiber knob of adenovirus, to the membrane distal Ig domain of CAR (D1), results in a significantly lower R_m due to enhanced Cl^- conductance across the membrane. This change in membrane permeability is caused, most probably, by activation of Ca^{2+} release from intracellular Ca^{2+} stores that leads to an Ad2-induced increase in $[Ca^{2+}]_i$ and an activation of $I_{Cl^-(Ca)}$. Ad2 may activate Ca^{2+} release from intracellular stores by activation of a similar pathway, as described for different metabotropic receptors or by influencing a particular step in such a pathway (intracellular pathway leading to release of Ca^{2+} is presented as X in Fig. 65). Enhanced membrane conductance due to Ad2 also results in lower excitability of Ad2 treated cells.

Extracellular CAR domains simulate homophilic CAR binding and are also able to induce intracellular Ca^{2+} increase. Although CAR domains did not influence membrane conductance, homophilic CAR-mediated pathways might be similar to these specifically induced by Ad2 but with lower amplification or they may activate other Ca^{2+}-dependent mechanisms (presented as Y in Fig. 65). In contrast, antibodies against CAR block homo- and heterophilic interactions and thus block all CAR-mediated processes in the cell.

Results presented in this work suggest that CAR may play an important role in the development of neurons, influencing intracellular Ca^{2+} homeostasis and thus e.g. Cl^- conductance across the membrane, the excitability of neurons and the formation of balanced synaptic circuits. CAR as an adhesion molecule mediating cell-cell contacts appears to be involved in transduction of intracellular signaling pathways.

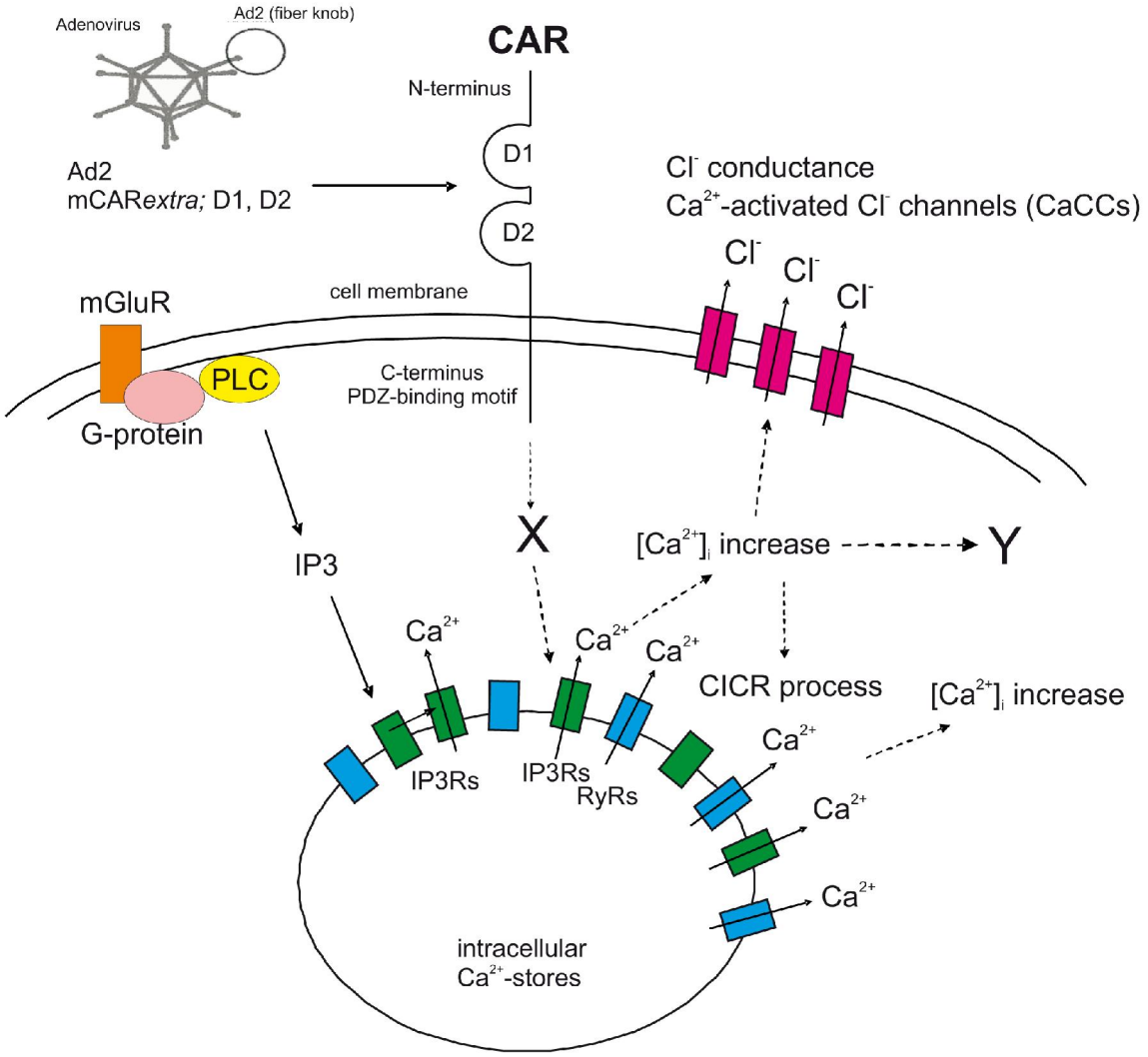

Fig. 65: Schematic model of CAR-mediated intracellular pathway. Binding of Ad2 to D1 of CAR induces Ca^{2+} release from intracellular Ca^{2+} stores. This Ad2-induced Ca^{2+} increase leads to enhanced Cl^- conductance across the membrane, most probably, by activation of CaCCs. Ad2-induced activation of Ca^{2+} stores may be direct or via activation of intracellular pathway (presented as X). Homophilic CAR interaction also seems to mediate Ca^{2+} signals with either lower amplification compared to Ad2 or to other intracellular targets (presented as Y). Ad2-dependent pathway presented as X may be similar to this described for mGluRs. Ca^{2+} can be released from intracellular Ca^{2+} stores via G-protein and PLC-dependent pathway. Activation of metabotropic glutamate receptor (mGluR), which is coupled to G-protein, leads via PLC, to the synthesis of IP3. Binding o IP3 to IP3Rs releases Ca^{2+} from intracellular Ca^{2+} stores. Abbreviation; PLC – phospholipase C.

5. Summary

How cell adhesion proteins of the Ig superfamily modulate intracellular signaling cascades and thereby influence neuronal communication is not well understood. In contrast to other CAMs, the coxsackie virus and adenovirus receptor (CAR) is strongly expressed in the embryonic and early postnatal brain. Initially it is found on all neural cells but becomes concentrated in axon- and dendrite-rich areas, suggesting that it might play a role in the development of neuronal circuits.

Here, I investigated the function of CAR by patch-clamp recordings using CAR-deficient neurons or reagents binding to CAR (fiber knob Ad2, anti-CAR antibodies, recombinant extracellular CAR domains). Initially I studied passive membrane properties of cultivated neurons. Unexpectedly, I observed an increased R_m in CAR-deficient neurons. In parallel, a decrease of R_m was measured in wild type neurons in the presence of the fiber knob Ad2 – a trimeric protein binding to CAR that disrupts cell-cell contacts.

Most likely CAR-mediated changes in membrane resistance (R_m) are the result of an altered Cl^- conductance across the membrane, which is impaired in CAR-deficient neurons and enhanced in Ad2 treated neurons. This conclusion is based on several electrophysiological recordings including the comparison of the Cl^- conductance between CAR-deficient and WT neurons, the Cl^- ion substitution in the recording solution, the pharmacological block of the Cl^- current as well as shifting the reversal potential of Cl^-. In addition, investigations on the conductance of other ions such as Na^+ and K^+ across the membrane as well as investigations on gap junctions or on Na^+/K^+-ATPase, HCN or voltage-gated Na^+, K^+, Ca^{2+} channels revealed no evidence for their implication in the deficits observed in CAR KO neurons. Furthermore, it could be shown that Ad2 is able to increase the $[Ca^{2+}]_i$, by releasing Ca^{2+} from intracellular Ca^{2+} stores. An Ad2-mediated increase in the $[Ca^{2+}]_i$ leads, most probably, to activation of the Ca^{2+}-activated Cl^- channels (CaCCs). Several characteristical properties for the CaCCs could be observed including outward rectification, voltage- and Ca^{2+}-dependency and specific halide selectivity for these channels. This enhanced Cl^- conductance in Ad2 treated neurons results in a significantly lower R_m.

The absence of CAR and the Ad2-mediated changes in the membrane conductance influence also neuronal network activity. CAR-deficient neurons showed a significantly higher frequency of action potentials (APs) compared to WT cells, whereas Ad2 treated neurons revealed a significantly lower frequency of APs than control cells. Furthermore, investigation of neuronal network formation and synaptic activity in CAR-deficient neurons revealed an

imbalance in the excitatory and inhibitory input ratio, suggesting a function of CAR in the formation of neuronal networks.

The data presented in this work lead to the conclusions that CAR plays an important role during the development of neurons by modulating the $[Ca^{2+}]_i$, the membrane conductance as well as synaptic activity and action potential generation.

6. Zusammenfassung

Wie die Zelladhesionsproteine der Ig Superfamilie intrazelluläre Signalkaskaden modulieren und dabei neuronale Kommunikation beeinflussen, ist gegenwärtig nicht gut verstanden. In Gegensatz zu anderen CAMs (cell adhesion molecules) ist der Coxsackie- und Adenovirus-rezeptor (CAR) intensiv im embryonalen und postnatalen Gehirn exprimiert. Anfänglich ist es auf allen neuronalen Zellen zu finden, dann aber vorwiegend in Axon- und Dendriten-reichen Regionen exprimiert. Dies lässt sich vermuten, dass CAR bei Bildung von neuronalen Schaltkreisen von Bedeutung ist.

In dieser Arbeit habe ich die Funktion von CAR mittels elektrophysiologischer Techniken untersucht. Dabei habe ich sowohl CAR-defiziente Neurone als auch Reagenzien, die an CAR binden (fiber knob Ad2, Anti-CAR Antikörper, rekombinante extrazelluläre Domänen von CAR), verwendet.

Anfänglich habe ich passive Membraneigenschaften von kultivierten Neuronen untersucht. Dabei beobachtete ich unerwarteterweise eine Zunahme des Membranwiderstandes (R_m) in CAR-defizienten Neuronen. In parallelen Experimenten konnte ich eine Abnahme von R_m nach Applikation von Ad2 beobachten. Ad2 ist ein trimeres Protein, das an CAR bindet und Zell-Zellkontakte unterbricht.

Elektrophysiologische Untersuchungen an CAR-defizienten Neuronen zeigten, dass CAR in die Regulation der Cl^- Leitfähigkeit neuronaler Membrane involviert ist. CAR-defiziente Neurone zeigten im Vergleich zu Wildtyp Zellen eine verminderte Cl^- Leitfähigkeit, und dadurch einen signifikant höheren R_m. Zusätzlich zu dem Ergebnis in CAR-defizienten Neuronen, wiesen Ad2 behandelte Neurone, einen signifikant niedrigeren R_m auf, was auf eine erhöhte Cl^- Leitfähigkeit in diesen Zellen schließen lässt. Dieser Befund wurde durch verschiedene elektrophysiologische Messungen unterstützt, wie z.B. Cl^- Ionen Substitution, pharmakologischer Block von Cl^- Strömen oder Verschiebung von Cl^- Umkehrpotentialen. Zusätzlich wurden andere Ionen wie K^+ und Na^+, gap junctions, HCN Kanäle oder die Na^+/K^+-ATPase untersucht. Keines dieser Proteine oder Ionen ist danach an den CAR-vermittelten Effekten beteiligt.

Der Cl^- Strom, der in CAR-defizienten und Ad2 behandelten Zellen identifiziert wurde, zeigte charakteristische Merkmale eines Ca^{2+}-aktivierten Cl^- Stromes: Ca^{2+}-Abhängigkeit, nach außen gerichtete Leitfähigkeit und höhere Permeabilität für verschiedene Halogenid Ionen. Im Einklang mit diesen Ergebnissen steht, dass, wie mittels Ca^{2+}-Imaging festgestellt wurde, die Applikation von Ad2 die intrazelluläre Ca^{2+} Konzentration erhöht, indem Ca^{2+} aus intrazellulären Ca^{2+} Speichern freigesetzt wird. Die durch Ad2 Applikation erhöhte $[Ca^{2+}]_i$ Konzentration stimuliert Ca^{2+}aktivierte Cl^- Kanäle, wodurch die Cl^- Leitfähigkeit in Ad2 behandelten Zellen steigt und der R_m sich verringert.
Die Abwesenheit von CAR und die dadurch veränderte Cl^- Leitfähigkeit beeinflusst die Generierung von Aktionspotentialen und die Entstehung von neuronalen Netzwerken. Es kommt zu einer Störung der exzitatorisch-inhibitorisch Balance.
In dieser Arbeit konnte gezeigt werden, dass CAR eine wichtige Rolle während der Entwicklung embryonaler Neurone spielt, indem es in Ca^{2+}-ahbängiger Weise die Cl^- Leitfähigkeit durch die Membran und somit die synaptische Aktivität und Generierung von Aktionspotentialen beeinflusst.

7. Reference List

Abegg,M.H., Savic,N., Ehrengruber,M.U., McKinney,R.A., and Gahwiler,B.H. (2004). Epileptiform activity in rat hippocampus strengthens excitatory synapses. J.Physiol 554, 439-448.

Abraham,M.R., Jahangir,A., Alekseev,A.E., and Terzic,A. (1999). Channelopathies of inwardly rectifying potassium channels. FASEB J. 13, 1901-1910.

Aguado,F., Espinosa-Parrilla,J.F., Carmona,M.A., and Soriano,E. (2002). Neuronal activity regulates correlated network properties of spontaneous calcium transients in astrocytes in situ. J.Neurosci 22, 9430-9444.

Akasu,T., Nishimura,T., and Tokimasa,T. (1990). Calcium-dependent chloride current in neurones of the rabbit pelvic parasympathetic ganglia. J.Physiol 422, 303-320.

Alberts,B., Bray,D., Johnson,A., Lewis,J., Raff,M., Roberts,K., and Walter,P. (2002). Molecular biology of the cell. (New York, USA: Garland Science).

Albrecht,J., Hanganu,I.L., Heck,N., and Luhmann,H.J. (2005). Oxygen and glucose deprivation induces major dysfunction in the somatosensory cortex of the newborn rat. Eur.J.Neurosci. 22, 2295-2305.

Alter,C.A., Amagasu,M., Shah,K., Jolly,Y.C., Major,C., and Wolf,B.A. (1994). U-73122 does not specifically inhibit phospholipase C in rat pancreatic islets and insulin-secreting beta-cell lines. Life Sci. 54, L107-L112.

Alvarez-Leefmans,F.J., Gamino,S.M., Giraldez,F., and Nogueron,I. (1988). Intracellular chloride regulation in amphibian dorsal root ganglion neurones studied with ion-selective microelectrodes. J.Physiol 406, 225-246.

Anders,M., Christian,C., McMahon,M., McCormick,F., and Korn,W.M. (2003). Inhibition of the Raf/MEK/ERK pathway up-regulates expression of the coxsackievirus and adenovirus receptor in cancer cells. Cancer Res. 63, 2088-2095.

Anderson,J.M., Stevenson,B.R., Jesaitis,L.A., Goodenough,D.A., and Mooseker,M.S. (1988). Characterization of ZO-1, a protein component of the tight junction from mouse liver and Madin-Darby canine kidney cells. J.Cell Biol. 106, 1141-1149.

Antic,S.D. (2003). Action potentials in basal and oblique dendrites of rat neocortical pyramidal neurons. J.Physiol 550, 35-50.

Aponte,Y., Lien,C.C., Reisinger,E., and Jonas,P. (2006). Hyperpolarization-activated cation channels in fast-spiking interneurons of rat hippocampus. J.Physiol 574, 229-243.

Arreola,J., Begenisich,T., and Melvin,J.E. (2002). Conformation-dependent regulation of inward rectifier chloride channel gating by extracellular protons. J.Physiol 541, 103-112.

Arreola,J., Melvin,J.E., and Begenisich,T. (1996). Activation of calcium-dependent chloride channels in rat parotid acinar cells. J.Gen.Physiol 108, 35-47.

Ascher-Landsberg,J., Saunders,T., Elovitz,M., and Phillippe,M. (1999). The effects of 2-aminoethoxydiphenyl borate, a novel inositol 1,4, 5-trisphosphate receptor modulator on myometrial contractions. Biochem.Biophys.Res.Commun. 264, 979-982.

Asher,D.R., Cerny,A.M., Weiler,S.R., Horner,J.W., Keeler,M.L., Neptune,M.A., Jones,S.N., Bronson,R.T., Depinho,R.A., and Finberg,R.W. (2005). Coxsackievirus and adenovirus receptor is essential for cardiomyocyte development. Genesis. 42, 77-85.

Bading,H., Ginty,D.D., and Greenberg,M.E. (1993). Regulation of gene expression in hippocampal neurons by distinct calcium signaling pathways. Science 260, 181-186.

Bai,M., Harfe,B., and Freimuth,P. (1993). Mutations that alter an Arg-Gly-Asp (RGD) sequence in the adenovirus type 2 penton base protein abolish its cell-rounding activity and delay virus reproduction in flat cells. J.Virol. 67, 5198-5205.

Bailey,A. and Mautner,V. (1994). Phylogenetic relationships among adenovirus serotypes. Virology 205, 438-452.

Banach,K. and Weingart,R. (2000). Voltage gating of Cx43 gap junction channels involves fast and slow current transitions. Pflugers Arch. 439, 248-250.

Bao,L., Samuels,S., Locovei,S., Macagno,E.R., Muller,K.J., and Dahl,G. (2007). Innexins form two types of channels. FEBS Lett. 581, 5703-5708.

Barchi,R.L. (1975). Myotonia. An evaluation of the chloride hypothesis. Arch.Neurol. 32, 175-180.

Barchi,R.L. (1978). Muscle membrane chloride conductance and the myotonic syndromes. Electroencephalogr.Clin.Neurophysiol.Suppl 559-570.

Baron,A., Pacaud,P., Loirand,G., Mironneau,C., and Mironneau,J. (1991). Pharmacological block of Ca(2+)-activated Cl- current in rat vascular smooth muscle cells in short-term primary culture. Pflugers Arch. 419, 553-558.

Barrett,J.N. and Crill,W.E. (1974). Specific membrane properties of cat motoneurones. J.Physiol 239, 301-324.

Barry,P.H. (1994). JPCalc, a software package for calculating liquid junction potential corrections in patch-clamp, intracellular, epithelial and bilayer measurements and for correcting junction potential measurements. J.Neurosci.Methods 51, 107-116.

Barry,P.H. and Lynch,J.W. (1991). Liquid junction potentials and small cell effects in patch-clamp analysis. J.Membr.Biol. 121, 101-117.

Bazzoni,G. (2003). The JAM family of junctional adhesion molecules. Curr.Opin.Cell Biol. 15, 525-530.

Bear,M.F. and Malenka,R.C. (1994). Synaptic plasticity: LTP and LTD. Curr.Opin.Neurobiol. 4, 389-399.

Bedner,P., Niessen,H., Odermatt,B., Kretz,M., Willecke,K., and Harz,H. (2006). Selective permeability of different connexin channels to the second messenger cyclic AMP. J.Biol.Chem. 281, 6673-6681.

Bennett,M.V., Contreras,J.E., Bukauskas,F.F., and Saez,J.C. (2003). New roles for astrocytes: gap junction hemichannels have something to communicate. Trends Neurosci. 26, 610-617.

Bennett,M.V. and Zukin,R.S. (2004). Electrical coupling and neuronal synchronization in the Mammalian brain. Neuron 41, 495-511.

Bennett,M.V.L., Spray,D.C., and HARRIS,A.L. Electrical coupling in development. 1981.

Bergelson,J.M., Cunningham,J.A., Droguett,G., Kurt-Jones,E.A., Krithivas,A., Hong,J.S., Horwitz,M.S., Crowell,R.L., and Finberg,R.W. (1997). Isolation of a common receptor for Coxsackie B viruses and adenoviruses 2 and 5. Science 275, 1320-1323.

Bergelson,J.M., Krithivas,A., Celi,L., Droguett,G., Horwitz,M.S., Wickham,T., Crowell,R.L., and Finberg,R.W. (1998). The murine CAR homolog is a receptor for coxsackie B viruses and adenoviruses. J.Virol. 72, 415-419.

Berridge,M.J. (1993). Inositol trisphosphate and calcium signalling. Nature 361, 315-325.

Berridge,M.J., Bootman,M.D., and Roderick,H.L. (2003). Calcium signalling: dynamics, homeostasis and remodelling. Nat.Rev.Mol.Cell Biol. 4, 517-529.

Berridge,M.J., Lipp,P., and Bootman,M.D. (2000). The versatility and universality of calcium signalling. Nat.Rev.Mol.Cell Biol. 1, 11-21.

Bewley,M.C., Springer,K., Zhang,Y.B., Freimuth,P., and Flanagan,J.M. (1999). Structural analysis of the mechanism of adenovirus binding to its human cellular receptor, CAR. Science 286, 1579-1583.

Bianchi,R., Young,S.R., and Wong,R.K. (1999). Group I mGluR activation causes voltage-dependent and -independent Ca2+ rises in hippocampal pyramidal cells. J.Neurophysiol. 81, 2903-2913.

Biederer,T., Sara,Y., Mozhayeva,M., Atasoy,D., Liu,X., Kavalali,E.T., and Sudhof,T.C. (2002). SynCAM, a synaptic adhesion molecule that drives synapse assembly. Science 297, 1525-1531.

Bittman,K., Owens,D.F., Kriegstein,A.R., and LoTurco,J.J. (1997). Cell coupling and uncoupling in the ventricular zone of developing neocortex. J.Neurosci. 17, 7037-7044.

Bixby,J.L. and Harris,W.A. (1991). Molecular mechanisms of axon growth and guidance. Annu.Rev.Cell Biol. 7, 117-159.

Blanton,M.G. and Kriegstein,A.R. (1991a). Appearance of putative amino acid neurotransmitters during differentiation of neurons in embryonic turtle cerebral cortex. J.Comp Neurol. 310, 571-592.

Blanton,M.G. and Kriegstein,A.R. (1991b). Spontaneous action potential activity and synaptic currents in the embryonic turtle cerebral cortex. J.Neurosci. 11, 3907-3923.

Blanton,M.G., Lo Turco,J.J., and Kriegstein,A.R. (1989). Whole cell recording from neurons in slices of reptilian and mammalian cerebral cortex. J.Neurosci.Methods 30, 203-210.

Blanton,M.G., Shen,J.M., and Kriegstein,A.R. (1987). Evidence for the inhibitory neurotransmitter gamma-aminobutyric acid in aspiny and sparsely spiny nonpyramidal neurons of the turtle dorsal cortex. J.Comp Neurol. 259, 277-297.

Blatz,A.L. and Magleby,K.L. (1986). Single apamin-blocked Ca-activated K+ channels of small conductance in cultured rat skeletal muscle. Nature 323, 718-720.

Blaustein,M.P., Goldman,W.F., Fontana,G., Krueger,B.K., Santiago,E.M., Steele,T.D., Weiss,D.N., and Yarowsky,P.J. (1991). Physiological roles of the sodium-calcium exchanger in nerve and muscle. Ann.N.Y.Acad.Sci. 639, 254-274.

Blaustein,M.P. and Golovina,V.A. (2001). Structural complexity and functional diversity of endoplasmic reticulum Ca(2+) stores. Trends Neurosci 24, 602-608.

Bleasdale,J.E., Thakur,N.R., Gremban,R.S., Bundy,G.L., Fitzpatrick,F.A., Smith,R.J., and Bunting,S. (1990). Selective inhibition of receptor-coupled phospholipase C-dependent processes in human platelets and polymorphonuclear neutrophils. J.Pharmacol.Exp.Ther. 255, 756-768.

Boitano,S., Dirksen,E.R., and Sanderson,M.J. (1992). Intercellular propagation of calcium waves mediated by inositol trisphosphate. Science 258, 292-295.

Bolivar,J.J., Tapia,D., Arenas,G., Castanon-Arreola,M., Torres,H., and Galarraga,E. (2008). A hyperpolarization-activated, cyclic nucleotide-gated, (Ih-like) cationic current and HCN gene expression in renal inner medullary collecting duct cells. Am.J.Physiol Cell Physiol 294, C893-C906.

Bonsi,P., Calabresi,P., De Persis,C., Papa,M., Centonze,D., Bernardi,G., and Pisani,A. (2004). Early ionic and membrane potential changes caused by the pesticide rotenone in striatal cholinergic interneurons. Exp.Neurol. 185, 169-181.

Borst,J.G. and Sakmann,B. (1996). Calcium influx and transmitter release in a fast CNS synapse. Nature 383, 431-434.

Bossinger,O. and Schierenberg,E. (1996). The use of fluorescent marker dyes for studying intercellular communication in nematode embryos. Int.J.Dev.Biol. 40, 431-439.

Boudin,M.L. and Boulanger,P. (1982). Assembly of adenovirus penton base and fiber. Virology 116, 589-604.

Bowles,K.R., Gibson,J., Wu,J., Shaffer,L.G., Towbin,J.A., and Bowles,N.E. (1999). Genomic organization and chromosomal localization of the human Coxsackievirus B-adenovirus receptor gene. Hum.Genet. 105, 354-359.

Bowles,N.E., Dubowitz,V., Sewry,C.A., and Archard,L.C. (1987). Dermatomyositis, polymyositis, and Coxsackie-B-virus infection. Lancet 1, 1004-1007.

Bowles,N.E. and Towbin,J.A. (1998). Molecular aspects of myocarditis. Curr.Opin.Cardiol. 13, 179-184.

Braet,K., Aspeslagh,S., Vandamme,W., Willecke,K., Martin,P.E., Evans,W.H., and Leybaert,L. (2003). Pharmacological sensitivity of ATP release triggered by photoliberation of inositol-1,4,5-trisphosphate and zero extracellular calcium in brain endothelial cells. J.Cell Physiol 197, 205-213.

Brandt,C.D., Kim,H.W., Vargosko,A.J., Jeffries,B.C., Arrobio,J.O., Rindge,B., Parrott,R.H., and Chanock,R.M. (1969). Infections in 18,000 infants and children in a controlled study of respiratory tract disease. I. Adenovirus pathogenicity in relation to serologic type and illness syndrome. Am.J.Epidemiol. 90, 484-500.

Braun,A.P. and Schulman,H. (1996). Distinct voltage-dependent gating behaviours of a swelling-activated chloride current in human epithelial cells. J.Physiol 495 (Pt 3), 743-753.

Bray,J.J., Hawken,M.J., Hubbard,J.I., Pockett,S., and Wilson,L. (1976). The membrane potential of rat diaphragm muscle fibres and the effect of denervation. J.Physiol 255, 651-667.

Bredt,D.S. and Nicoll,R.A. (2003). AMPA receptor trafficking at excitatory synapses. Neuron 40, 361-379.

Brodie,C., Bak,A., Shainberg,A., and Sampson,S.R. (1987). Role of Na-K ATPase in regulation of resting membrane potential of cultured rat skeletal myotubes. J.Cell Physiol 130, 191-198.

Brodie,C. and Sampson,S.R. (1985). Contribution of electrogenic sodium-potassium ATPase to resting membrane potential of cultured rat skeletal myotubes. Brain Res. 347, 28-35.

Brose,N. (1999). Synaptic cell adhesion proteins and synaptogenesis in the mammalian central nervous system. Naturwissenschaften 86, 516-524.

Brown,T.H. and Johnston,D. (1983). Voltage-clamp analysis of mossy fiber synaptic input to hippocampal neurons. J.Neurophysiol. 50, 487-507.

Bruning,A. and Runnebaum,I.B. (2003). CAR is a cell-cell adhesion protein in human cancer cells and is expressionally modulated by dexamethasone, TNFalpha, and TGFbeta. Gene Ther. 10, 198-205.

Bruzzone,R. and Dermietzel,R. (2006). Structure and function of gap junctions in the developing brain. Cell Tissue Res. 326, 239-248.

Bruzzone,R., White,T.W., and Paul,D.L. (1996). Connections with connexins: the molecular basis of direct intercellular signaling. Eur.J.Biochem. 238, 1-27.

Bruzzone,S., Guida,L., Zocchi,E., Franco,L., and De Flora,A. (2001). Connexin 43 hemi channels mediate Ca2+-regulated transmembrane NAD+ fluxes in intact cells. FASEB J. 15, 10-12.

Bukauskas,F.F., Elfgang,C., Willecke,K., and Weingart,R. (1995). Biophysical properties of gap junction channels formed by mouse connexin40 in induced pairs of transfected human HeLa cells. Biophys.J. 68, 2289-2298.

Bukauskas,F.F. and Weingart,R. (1993). Temperature dependence of gap junction properties in neonatal rat heart cells. Pflugers Arch. 423, 133-139.

Burgoyne,R.D., O'Callaghan,D.W., Hasdemir,B., Haynes,L.P., and Tepikin,A.V. (2004). Neuronal Ca2+-sensor proteins: multitalented regulators of neuronal function. Trends Neurosci 27, 203-209.

Burgoyne,R.D. and Weiss,J.L. (2001). The neuronal calcium sensor family of Ca2+-binding proteins. Biochem.J. 353, 1-12.

Cameron,W.E. and Nunez-Abades,P.A. (2000). Physiological changes accompanying anatomical remodeling of mammalian motoneurons during postnatal development. Brain Res.Bull. 53, 523-527.

Cameron,W.E., Nunez-Abades,P.A., Kerman,I.A., and Hodgson,T.M. (2000). Role of potassium conductances in determining input resistance of developing brain stem motoneurons. J.Neurophysiol. 84, 2330-2339.

Cao,F., Eckert,R., Elfgang,C., Nitsche,J.M., Snyder,S.A., ulser,D.F., Willecke,K., and Nicholson,B.J. (1998). A quantitative analysis of connexin-specific permeability differences of gap junctions expressed in HeLa transfectants and Xenopus oocytes. J.Cell Sci. 111 (Pt 1), 31-43.

Carson,S.D. and Chapman,N.M. (2001). Coxsackievirus and adenovirus receptor (CAR) binds immunoglobulins. Biochemistry 40, 14324-14329.

Catterall,W.A. and Few,A.P. (2008). Calcium channel regulation and presynaptic plasticity. Neuron 59, 882-901.

Caveney,S. (1985). The role of gap junctions in development. Annu.Rev.Physiol 47, 319-335.

Chagnac-Amitai,Y. and Connors,B.W. (1989). Synchronized excitation and inhibition driven by intrinsically bursting neurons in neocortex. J.Neurophysiol. 62, 1149-1162.

Chan,H.C., Fu,W.O., Chung,Y.W., Huang,S.J., Chan,P.S., and Wong,P.Y. (1994). Swelling-induced anion and cation conductances in human epididymal cells. J.Physiol 478 Pt 3, 449-460.

Chanson,M., Berclaz,P.Y., Scerri,I., Dudez,T., Wernke-Dollries,K., Pizurki,L., Pavirani,A., Fiedler,M.A., and Suter,S. (2001). Regulation of gap junctional communication by a pro-inflammatory cytokine in cystic fibrosis transmembrane conductance regulator-expressing but not cystic fibrosis airway cells. Am.J.Pathol. 158, 1775-1784.

Chardonnet,Y. and Dales,S. (1970). Early events in the interaction of adenoviruses with HeLa cells. I. Penetration of type 5 and intracellular release of the DNA genome. Virology 40, 462-477.

Charles,A.C., Merrill,J.E., Dirksen,E.R., and Sanderson,M.J. (1991). Intercellular signaling in glial cells: calcium waves and oscillations in response to mechanical stimulation and glutamate. Neuron 6, 983-992.

Charpantier,E., Cancela,J., and Meda,P. (2007). Beta cells preferentially exchange cationic molecules via connexin 36 gap junction channels. Diabetologia 50, 2332-2341.

Chaytor,A.T., Martin,P.E., Evans,W.H., Randall,M.D., and Griffith,T.M. (1999). The endothelial component of cannabinoid-induced relaxation in rabbit mesenteric artery depends on gap junctional communication. J.Physiol 520 Pt 2, 539-550.

Chen,J.W., Zhou,B., Yu,Q.C., Shin,S.J., Jiao,K., Schneider,M.D., Baldwin,H.S., and Bergelson,J.M. (2006). Cardiomyocyte-specific deletion of the coxsackievirus and adenovirus receptor results in hyperplasia of the embryonic left ventricle and abnormalities of sinuatrial valves. Circ.Res. 98, 923-930.

Chih,B., Engelman,H., and Scheiffele,P. (2005). Control of excitatory and inhibitory synapse formation by neuroligins. Science 307, 1324-1328.

Chin,D. and Means,A.R. (2000). Calmodulin: a prototypical calcium sensor. Trends Cell Biol. 10, 322-328.

Chretien,I., Marcuz,A., Courtet,M., Katevuo,K., Vainio,O., Heath,J.K., White,S.J., and Du,P.L. (1998). CTX, a Xenopus thymocyte receptor, defines a molecular family conserved throughout vertebrates. Eur.J.Immunol. 28, 4094-4104.

Christ,G.J., Moreno,A.P., Melman,A., and Spray,D.C. (1992). Gap junction-mediated intercellular diffusion of Ca2+ in cultured human corporal smooth muscle cells. Am.J.Physiol 263, C373-C383.

Ciccolini,F., Collins,T.J., Sudhoelter,J., Lipp,P., Berridge,M.J., and Bootman,M.D. (2003). Local and global spontaneous calcium events regulate neurite outgrowth and onset of GABAergic phenotype during neural precursor differentiation. J.Neurosci 23, 103-111.

Ciolofan,C., Li,X.B., Olson,C., Kamasawa,N., Gebhardt,B.R., Yasumura,T., Morita,M., Rash,J.E., and Nagy,J.I. (2006). Association of connexin36 and zonula occludens-1 with zonula occludens-2 and the transcription factor zonula occludens-1-associated nucleic acid-binding protein at neuronal gap junctions in rodent retina. Neuroscience 140, 433-451.

Clapham,D.E. (1995). Calcium signaling. Cell 80, 259-268.

Clapham,D.E., Runnels,L.W., and Strubing,C. (2001). The TRP ion channel family. Nat.Rev.Neurosci 2, 387-396.

Clark,S., Jordt,S.E., Jentsch,T.J., and Mathie,A. (1998). Characterization of the hyperpolarization-activated chloride current in dissociated rat sympathetic neurons. J.Physiol 506 (Pt 3), 665-678.

Clements,J.D., Lester,R.A., Tong,G., Jahr,C.E., and Westbrook,G.L. (1992). The time course of glutamate in the synaptic cleft. Science 258, 1498-1501.

Cohen,C.J., Shieh,J.T., Pickles,R.J., Okegawa,T., Hsieh,J.T., and Bergelson,J.M. (2001). The coxsackievirus and adenovirus receptor is a transmembrane component of the tight junction. Proc.Natl.Acad.Sci.U.S.A 98, 15191-15196.

Cole,K.S. (1968). Membranes, Ions and Impulses: A Chapter of Classical Biophysics…. (Berkeley, University of California USA: Berkeley University of California Press).

Condorelli,D.F., Belluardo,N., Trovato-Salinaro,A., and Mudo,G. (2000). Expression of Cx36 in mammalian neurons. Brain Res.Brain Res.Rev. 32, 72-85.

Congar,P., Leinekugel,X., Ben Ari,Y., and Crepel,V. (1997). A long-lasting calcium-activated nonselective cationic current is generated by synaptic stimulation or exogenous activation of group I metabotropic glutamate receptors in CA1 pyramidal neurons. J.Neurosci. 17, 5366-5379.

Contreras,J.E., Sanchez,H.A., Eugenin,E.A., Speidel,D., Theis,M., Willecke,K., Bukauskas,F.F., Bennett,M.V., and Saez,J.C. (2002). Metabolic inhibition induces opening of unapposed connexin 43 gap junction hemichannels and reduces gap junctional communication in cortical astrocytes in culture. Proc.Natl.Acad.Sci.U.S.A 99, 495-500.

Cotman,C.W., Hailer,N.P., Pfister,K.K., Soltesz,I., and Schachner,M. (1998). Cell adhesion molecules in neural plasticity and pathology: similar mechanisms, distinct organizations? Prog.Neurobiol. 55, 659-669.

Coyne,C.B. and Bergelson,J.M. (2005). CAR: a virus receptor within the tight junction. Adv.Drug Deliv.Rev. 57, 869-882.

Coyne,C.B., Voelker,T., Pichla,S.L., and Bergelson,J.M. (2004). The coxsackievirus and adenovirus receptor interacts with the multi-PDZ domain protein-1 (MUPP-1) within the tight junction. J.Biol.Chem. 279, 48079-48084.

Craig,A.M., Graf,E.R., and Linhoff,M.W. (2006). How to build a central synapse: clues from cell culture. Trends Neurosci. 29, 8-20.

Crill,W.E. and Schwindt,P.C. (1983). Active currents in mammalian central neurons. Trends Neurosci.

Crossin,K.L. and Krushel,L.A. (2000). Cellular signaling by neural cell adhesion molecules of the immunoglobulin superfamily. Dev.Dyn. 218, 260-279.

Cusack,S. (2005). Adenovirus complex structures. Curr.Opin.Struct.Biol. 15, 237-243.

Dalby,N.O. and Mody,I. (2001). The process of epileptogenesis: a pathophysiological approach. Curr.Opin.Neurol. 14, 187-192.

de Diego,C., Gamez,J., Plassart-Schiess,E., Lasa,A., Del Rio,E., Cervera,C., Baiget,M., Gallano,P., and Fontaine,B. (1999). Novel mutations in the muscle chloride channel CLCN1 gene causing myotonia congenita in Spanish families. J.Neurol. 246, 825-829.

Dean,C. and Dresbach,T. (2006). Neuroligins and neurexins: linking cell adhesion, synapse formation and cognitive function. Trends Neurosci. 29, 21-29.

Deleze,J. (1960). Possible reasons for drop of resting potential of mammalian heart preparations during hypothermia. Circ.Res. 8, 553-557.

Dermietzel,R., Hertberg,E.L., Kessler,J.A., and Spray,D.C. (1991). Gap junctions between cultured astrocytes: immunocytochemical, molecular, and electrophysiological analysis. J.Neurosci. 11, 1421-1432.

Dermietzel,R. and Spray,D.C. (1993). Gap junctions in the brain: where, what type, how many and why? Trends Neurosci. 16, 186-192.

Dermietzel,R., Traub,O., Hwang,T.K., Beyer,E., Bennett,M.V., Spray,D.C., and Willecke,K. (1989). Differential expression of three gap junction proteins in developing and mature brain tissues. Proc.Natl.Acad.Sci.U.S.A 86, 10148-10152.

Deumens,R., Koopmans,G.C., Lemmens,M., Mollers,S., Honig,W.M., Steinbusch,H.W., Brook,G., and Joosten,E.A. (2006). Neurite outgrowth promoting effects of enriched and mixed OEC/ONF cultures. Neurosci.Lett. 397, 20-24.

Devaux,C., Adrian,M., Berthet-Colominas,C., Cusack,S., and Jacrot,B. (1990). Structure of adenovirus fibre. I. Analysis of crystals of fibre from adenovirus serotypes 2 and 5 by electron microscopy and X-ray crystallography. J.Mol.Biol. 215, 567-588.

Devaux,C., Caillet-Boudin,M.L., Jacrot,B., and Boulanger,P. (1987). Crystallization, enzymatic cleavage, and the polarity of the adenovirus type 2 fiber. Virology 161, 121-128.

Diaz,M., Valverde,M.A., Higgins,C.F., Rucareanu,C., and Sepulveda,F.V. (1993). Volume-activated chloride channels in HeLa cells are blocked by verapamil and dideoxyforskolin. Pflugers Arch. 422, 347-353.

Dierkes,P.W., Wusten,H.J., Klees,G., Muller,A., and Hochstrate,P. (2006). Ionic mechanism of ouabain-induced swelling of leech Retzius neurons. Pflugers Arch. 452, 25-35.

DiFrancesco,D. (1993). Pacemaker mechanisms in cardiac tissue. Annu.Rev.Physiol 55, 455-472.

DiPolo,R. and Beauge,L. (2006). Sodium/calcium exchanger: influence of metabolic regulation on ion carrier interactions. Physiol Rev. 86, 155-203.

Dobrowolski,R., Sommershof,A., and Willecke,K. (2007). Some oculodentodigital dysplasia-associated Cx43 mutations cause increased hemichannel activity in addition to deficient gap junction channels. J.Membr.Biol. 219, 9-17.

Doherty,P., Ashton,S.V., Moore,S.E., and Walsh,F.S. (1991). Morphoregulatory activities of NCAM and N-cadherin can be accounted for by G protein-dependent activation of L- and N-type neuronal Ca2+ channels. Cell 67, 21-33.

Doherty,P. and Walsh,F.S. (1989). Neurite guidance molecules. Curr.Opin.Cell Biol. 1, 1102-1106.

Doherty,P. and Walsh,F.S. (1992). Cell adhesion molecules, second messengers and axonal growth. Curr.Opin.Neurobiol. 2, 595-601.

Doherty,P. and Walsh,F.S. (1994). Signal transduction events underlying neurite outgrowth stimulated by cell adhesion molecules. Curr.Opin.Neurobiol. 4, 49-55.

Doherty,P., Williams,G., and Williams,E.J. (2000). CAMs and axonal growth: a critical evaluation of the role of calcium and the MAPK cascade. Mol.Cell Neurosci 16, 283-295.

Dorner,A.A., Wegmann,F., Butz,S., Wolburg-Buchholz,K., Wolburg,H., Mack,A., Nasdala,I., August,B., Westermann,J., Rathjen,F.G., and Vestweber,D. (2005). Coxsackievirus-adenovirus receptor (CAR) is essential for early embryonic cardiac development. J.Cell Sci. 118, 3509-3521.

Dunlap,K., Luebke,J.I., and Turner,T.J. (1995). Exocytotic Ca2+ channels in mammalian central neurons. Trends Neurosci 18, 89-98.

Ebihara,L. (2003). Physiology and biophysics of hemi-gap-junctional channels expressed in Xenopus oocytes. Acta Physiol Scand. 179, 5-8.

Ebnet,K., Aurrand-Lions,M., Kuhn,A., Kiefer,F., Butz,S., Zander,K., Meyer zu Brickwedde,M.K., Suzuki,A., Imhof,B.A., and Vestweber,D. (2003). The junctional adhesion molecule (JAM) family members JAM-2 and JAM-3 associate with the cell polarity protein PAR-3: a possible role for JAMs in endothelial cell polarity. J.Cell Sci. 116, 3879-3891.

Eckert,R., Dunina-Barkovskaya,A., and Hulser,D.F. (1993). Biophysical characterization of gap-junction channels in HeLa cells. Pflugers Arch. 424, 335-342.

Eder,C., Klee,R., and Heinemann,U. (1998). Involvement of stretch-activated Cl- channels in ramification of murine microglia. J.Neurosci. 18, 7127-7137.

Edman,A., Gestrelius,S., and Grampp,W. (1986). Transmembrane ion balance in slowly and rapidly adapting lobster stretch receptor neurones. J.Physiol 377, 171-191.

Eggermont,J. (2004). Calcium-activated chloride channels: (un)known, (un)loved? Proc.Am.Thorac.Soc. 1, 22-27.

Eide,F.F., Lowenstein,D.H., and Reichardt,L.F. (1993). Neurotrophins and their receptors--current concepts and implications for neurologic disease. Exp.Neurol. 121, 200-214.

Elfgang,C., Eckert,R., Lichtenberg-Frate,H., Butterweck,A., Traub,O., Klein,R.A., Hulser,D.F., and Willecke,K. (1995). Specific permeability and selective formation of gap junction channels in connexin-transfected HeLa cells. J.Cell Biol. 129, 805-817.

Elmslie. Passive propagation of electrical signals. 2005.

Eskandari,S., Zampighi,G.A., Leung,D.W., Wright,E.M., and Loo,D.D. (2002). Inhibition of gap junction hemichannels by chloride channel blockers. J.Membr.Biol. 185, 93-102.

Evans,M.G. and Marty,A. (1986). Calcium-dependent chloride currents in isolated cells from rat lacrimal glands. J.Physiol 378, 437-460.

Excoffon,K.J., Gansemer,N., Traver,G., and Zabner,J. (2007). Functional effects of coxsackievirus and adenovirus receptor glycosylation on homophilic adhesion and adenoviral infection. J.Virol. 81, 5573-5578.

Excoffon,K.J., Hruska-Hageman,A., Klotz,M., Traver,G.L., and Zabner,J. (2004). A role for the PDZ-binding domain of the coxsackie B virus and adenovirus receptor (CAR) in cell adhesion and growth. J.Cell Sci. 117, 4401-4409.

Excoffon,K.J., Traver,G.L., and Zabner,J. (2005). The role of the extracellular domain in the biology of the coxsackievirus and adenovirus receptor. Am.J.Respir.Cell Mol.Biol. 32, 498-503.

Fagni,L., Chavis,P., Ango,F., and Bockaert,J. (2000). Complex interactions between mGluRs, intracellular Ca2+ stores and ion channels in neurons. Trends Neurosci. 23, 80-88.

Fannon,A.M. and Colman,D.R. (1996). A model for central synaptic junctional complex formation based on the differential adhesive specificities of the cadherins. Neuron 17, 423-434.

Fechner,H., Haack,A., Wang,H., Wang,X., Eizema,K., Pauschinger,M., Schoemaker,R., Veghel,R., Houtsmuller,A., Schultheiss,H.P., Lamers,J., and Poller,W. (1999). Expression of coxsackie adenovirus receptor and alphav-integrin does not correlate with adenovector targeting in vivo indicating anatomical vector barriers. Gene Ther. 6, 1520-1535.

Fechner,H., Noutsias,M., Tschoepe,C., Hinze,K., Wang,X., Escher,F., Pauschinger,M., Dekkers,D., Vetter,R., Paul,M., Lamers,J., Schultheiss,H.P., and Poller,W. (2003). Induction of coxsackievirus-adenovirus-receptor expression during myocardial tissue formation and remodeling: identification of a cell-to-cell contact-dependent regulatory mechanism. Circulation 107, 876-882.

Felix,R., Sandoval,A., Sanchez,D., Gomora,J.C., De la Vega-Beltran JL, Trevino,C.L., and Darszon,A. (2003). ZD7288 inhibits low-threshold Ca(2+) channel activity and regulates sperm function. Biochem.Biophys.Res.Commun. 311, 187-192.

Fernandez-Chacon,R., Konigstorfer,A., Gerber,S.H., Garcia,J., Matos,M.F., Stevens,C.F., Brose,N., Rizo,J., Rosenmund,C., and Sudhof,T.C. (2001). Synaptotagmin I functions as a calcium regulator of release probability. Nature 410, 41-49.

Fields,R.D. and Itoh,K. (1996). Neural cell adhesion molecules in activity-dependent development and synaptic plasticity. Trends Neurosci. 19, 473-480.

Fioretti,B., Castigli,E., Calzuola,I., Harper,A.A., Franciolini,F., and Catacuzzeno,L. (2004). NPPB block of the intermediate-conductance Ca2+-activated K+ channel. Eur.J.Pharmacol. 497, 1-6.

FitzGerald,D.J., Padmanabhan,R., Pastan,I., and Willingham,M.C. (1983). Adenovirus-induced release of epidermal growth factor and pseudomonas toxin into the cytosol of KB cells during receptor-mediated endocytosis. Cell 32, 607-617.

Fohrman,E.B., de Erausquin,G., Costa,E., and Wojcik,W.J. (1993). Muscarinic m3 receptors and dynamics of intracellular Ca2+ cerebellar granule neurons. Eur.J.Pharmacol. 245, 263-271.

Frace,A.M., Maruoka,F., and Noma,A. (1992). External K+ increases Na+ conductance of the hyperpolarization-activated current in rabbit cardiac pacemaker cells. Pflugers Arch. 421, 97-99.

Freimuth,P., Philipson,L., and Carson,S.D. (2008). The coxsackievirus and adenovirus receptor. Curr.Top.Microbiol.Immunol. 323, 67-87.

Freimuth,P., Springer,K., Berard,C., Hainfeld,J., Bewley,M., and Flanagan,J. (1999). Coxsackievirus and adenovirus receptor amino-terminal immunoglobulin V-related domain binds adenovirus type 2 and fiber knob from adenovirus type 12. J.Virol. 73, 1392-1398.

Friel,D.D. and Tsien,R.W. (1992). Phase-dependent contributions from Ca2+ entry and Ca2+ release to caffeine-induced [Ca2+]i oscillations in bullfrog sympathetic neurons. Neuron 8, 1109-1125.

Frings,S., Reuter,D., and Kleene,S.J. (2000). Neuronal Ca2+ -activated Cl- channels--homing in on an elusive channel species. Prog.Neurobiol. 60, 247-289.

Fuxe,J., Liu,L., Malin,S., Philipson,L., Collins,V.P., and Pettersson,R.F. (2003). Expression of the coxsackie and adenovirus receptor in human astrocytic tumors and xenografts. Int.J.Cancer 103, 723-729.

Gallin,W.J. and Greenberg,M.E. (1995). Calcium regulation of gene expression in neurons: the mode of entry matters. Curr.Opin.Neurobiol. 5, 367-374.

Garashchuk,O.V. and . Calcium entrance through the NMDA-gated receptor-channel complexes in central neurons. Neurophysiology 30[3]. 1998.

Garcia,M.L. and Strehler,E.E. (1999). Plasma membrane calcium ATPases as critical regulators of calcium homeostasis during neuronal cell function. Front Biosci. 4, D869-D882.

Gardner,S.M., Trussell,L.O., and Oertel,D. (1999). Time course and permeation of synaptic AMPA receptors in cochlear nuclear neurons correlate with input. J.Neurosci. 19, 8721-8729.

Gasparini,S. and DiFrancesco,D. (1997). Action of the hyperpolarization-activated current (Ih) blocker ZD 7288 in hippocampal CA1 neurons. Pflugers Arch. 435, 99-106.

Gerasimenko,J.V., Maruyama,Y., Yano,K., Dolman,N.J., Tepikin,A.V., Petersen,O.H., and Gerasimenko,O.V. (2003). NAADP mobilizes Ca2+ from a thapsigargin-sensitive store in the nuclear envelope by activating ryanodine receptors. J.Cell Biol. 163, 271-282.

Gerencser,G.A. and Zhang,J. (2003). Chloride ATPase pumps in nature: do they exist? Biol.Rev.Camb.Philos.Soc. 78, 197-218.

Gerrow,K. and El Husseini,A. (2006). Cell adhesion molecules at the synapse. Front Biosci. 11, 2400-2419.

Gestrelius,S., Grampp,W., and Sjolin,L. (1981). Subthreshold and near-threshold membrane currents in lobster stretch receptor neurones. J.Physiol 310, 191-203.

Giaume,C., Fromaget,C., el Aoumari,A., Cordier,J., Glowinski,J., and Gros,D. (1991). Gap junctions in cultured astrocytes: single-channel currents and characterization of channel-forming protein. Neuron 6, 133-143.

Glasgow,J.N., Everts,M., and Curiel,D.T. (2006). Transductional targeting of adenovirus vectors for gene therapy. Cancer Gene Ther. 13, 830-844.

Glitsch,H.G. (2001). Electrophysiology of the sodium-potassium-ATPase in cardiac cells. Physiol Rev. 81, 1791-1826.

Glushchenko,T.S. and Izvarina,N.L. (1997). Na+,K(+)-ATPase activity in neurons and glial cells of the olfactory cortex of the rat brain during the development of long-term potentiation. Neurosci.Behav.Physiol 27, 49-52.

Goda,Y. and Davis,G.W. (2003). Mechanisms of synapse assembly and disassembly. Neuron 40, 243-264.

Goldshleger,R., Shahak,Y., and Karlish,S.J. (1990). Electrogenic and electroneutral transport modes of renal Na/K ATPase reconstituted into proteoliposomes. J.Membr.Biol. 113, 139-154.

Goldstein,S.A., Bockenhauer,D., O'Kelly,I., and Zilberberg,N. (2001). Potassium leak channels and the KCNK family of two-P-domain subunits. Nat.Rev.Neurosci. 2, 175-184.

Gomez,T.M. and Spitzer,N.C. (1999). In vivo regulation of axon extension and pathfinding by growth-cone calcium transients. Nature 397, 350-355.

Gonzalez-Iglesias,A.E., Kretschmannova,K., Tomic,M., and Stojilkovic,S.S. (2006). ZD7288 inhibits exocytosis in an HCN-independent manner and downstream of voltage-gated calcium influx in pituitary lactotrophs. Biochem.Biophys.Res.Commun. 346, 845-850.

Goodenough,D.A. and Paul,D.L. (2003). Beyond the gap: functions of unpaired connexon channels. Nat.Rev.Mol.Cell Biol. 4, 285-294.

Gopinath,G., Sable,V., Sailaja,K., and Tandon,P.N. (1996). Cell surface molecules (NCAM and L1) in intrastriatal transplants of embryonic mesencephalon in rats. Neuroscience 73, 161-169.

Green,P.J., Walsh,F.S., and Doherty,P. (1997). Signal transduction mechanisms underlying axonal growth responses stimulated by cell adhesion molecules. Rev.Neurol.(Paris) 153, 509-514.

Greenwood,I.A., Helliwell,R.M., and Large,W.A. (1997). Modulation of Ca(2+)-activated Cl-currents in rabbit portal vein smooth muscle by an inhibitor of mitochondrial Ca2+ uptake. J.Physiol 505 (Pt 1), 53-64.

Greenwood,I.A., Hogg,R.C., and Large,W.A. (1995). Effect of frusemide, ethacrynic acid and indanyloxyacetic acid on spontaneous Ca-activated currents in rabbit portal vein smooth muscle cells. Br.J.Pharmacol. 115, 733-738.

Greenwood,I.A. and Large,W.A. (1999). Modulation of the decay of Ca2+-activated Cl- currents in rabbit portal vein smooth muscle cells by external anions. J.Physiol 516 (Pt 2), 365-376.

Greer,P.L. and Greenberg,M.E. (2008). From synapse to nucleus: calcium-dependent gene transcription in the control of synapse development and function. Neuron 59, 846-860.

Grist,N.R., Bell,E.J., and Reid,D. (1975). The epidemiology of enteroviruses. Scott.Med.J. 20, 27-31.

Gruener,R., Stern,L.Z., Markovitz,D., and Gerdes,C. (1979). Electrophysiologic properties of intercostal muscle fibers in human neuromuscular diseases. Muscle Nerve 2, 165-172.

Grynkiewicz,G., Poenie,M., and Tsien,R.Y. (1985). A new generation of Ca2+ indicators with greatly improved fluorescence properties. J.Biol.Chem. 260, 3440-3450.

Gu,X. and Spitzer,N.C. (1995). Distinct aspects of neuronal differentiation encoded by frequency of spontaneous Ca2+ transients. Nature 375, 784-787.

Guerini,D., Garcia-Martin,E., Gerber,A., Volbracht,C., Leist,M., Merino,C.G., and Carafoli,E. (1999). The expression of plasma membrane Ca2+ pump isoforms in cerebellar granule neurons is modulated by Ca2+. J.Biol.Chem. 274, 1667-1676.

Gurnett,C.A., Kahl,S.D., Anderson,R.D., and Campbell,K.P. (1995). Absence of the skeletal muscle sarcolemma chloride channel ClC-1 in myotonic mice. J.Biol.Chem. 270, 9035-9038.

Hahm,E.T., Lee,J.J., Min,B.I., and Cho,Y.W. (2005). Developmental change of GABAergic postsynaptic current in rat periaqueductal gray. Neurosci.Lett. 380, 187-192.

Halm,D.R. and Frizzell,R.A. (1992). Anion Permeation in an Apical Membrane Chloride Channel of a Secretory Epithelial Cell. J.Gen.Physiol.

Hamill,O.P., Marty,A., Neher,E., Sakmann,B., and Sigworth,F.J. (1981). Improved patch-clamp techniques for high-resolution current recording from cells and cell-free membrane patches. Pflugers Arch. 391, 85-100.

Hammond,C. (2001). Cellular and Molecular Neurobiology. (France.

Hardingham,G.E., Chawla,S., Johnson,C.M., and Bading,H. (1997). Distinct functions of nuclear and cytoplasmic calcium in the control of gene expression. Nature 385, 260-265.

Hartmann,J. and Konnerth,A. (2008). Mechanisms of metabotropic glutamate receptor-mediated synaptic signaling in cerebellar Purkinje cells. Acta Physiol (Oxf).

Hartzell,C., Putzier,I., and Arreola,J. (2005). Calcium-activated chloride channels. Annu.Rev.Physiol 67, 719-758.

Hartzell,H.C. (2008). Physiology. CaCl-ing channels get the last laugh. Science 322, 534-535.

Haubrich,S., Schwarz,H.J., Bukauskas,F., Lichtenberg-Frate,H., Traub,O., Weingart,R., and Willecke,K. (1996). Incompatibility of connexin 40 and 43 Hemichannels in gap junctions between mammalian cells is determined by intracellular domains. Mol.Biol.Cell 7, 1995-2006.

Henke,W., Cetinsoy,C., Jung,K., and Loening,S. (1996). Non-hyperbolic calcium calibration curve of Fura-2: implications for the reliability of quantitative Ca2+ measurements. Cell Calcium 20, 287-292.

Henry,L.J., Xia,D., Wilke,M.E., Deisenhofer,J., and Gerard,R.D. (1994). Characterization of the knob domain of the adenovirus type 5 fiber protein expressed in Escherichia coli. J.Virol. 68, 5239-5246.

Hermans,E. and Challiss,R.A. (2001). Structural, signalling and regulatory properties of the group I metabotropic glutamate receptors: prototypic family C G-protein-coupled receptors. Biochem.J. 359, 465-484.

Herms,J., Schneider,I., Dewachter,I., Caluwaerts,N., Kretzschmar,H., and Van Leuven,F. (2003). Capacitive calcium entry is directly attenuated by mutant presenilin-1, independent of the expression of the amyloid precursor protein. J.Biol.Chem. 278, 2484-2489.

Herness,M.S. and Sun,X.D. (1999). Characterization of chloride currents and their noradrenergic modulation in rat taste receptor cells. J.Neurophysiol. 82, 260-271.

Hilgenberg,L.G. and Smith,M.A. (2004). Agrin signaling in cortical neurons is mediated by a tyrosine kinase-dependent increase in intracellular Ca2+ that engages both CaMKII and MAPK signal pathways. J.Neurobiol. 61, 289-300.

Hilgenberg,L.G., Su,H., Gu,H., O'Dowd,D.K., and Smith,M.A. (2006). Alpha3Na+/K+-ATPase is a neuronal receptor for agrin. Cell 125, 359-369.

Hodgkin,A.L. and Huxley,A.F. (1990). A quantitative description of membrane current and its application to conduction and excitation in nerve. 1952. Bull.Math.Biol. 52, 25-71.

Hoesch,R.E., Yienger,K., Weinreich,D., and Kao,J.P. (2002). Coexistence of functional IP(3) and ryanodine receptors in vagal sensory neurons and their activation by ATP. J.Neurophysiol. 88, 1212-1219.

Hoffman,K.B. (1998). The relationship between adhesion molecules and neuronal plasticity. Cell Mol.Neurobiol. 18, 461-475.

Hogg,R.C., Wang,Q., and Large,W.A. (1994). Effects of Cl channel blockers on Ca-activated chloride and potassium currents in smooth muscle cells from rabbit portal vein. Br.J.Pharmacol. 111, 1333-1341.

Hohnke,C.D. and Sur,M. (1999). Stable properties of spontaneous EPSCs and miniature retinal EPSCs during the development of ON/OFF sublamination in the ferret lateral geniculate nucleus. J.Neurosci. 19, 236-247.

Hollmann,M., Hartley,M., and Heinemann,S. (1991). Ca2+ permeability of KA-AMPA--gated glutamate receptor channels depends on subunit composition. Science 252, 851-853.

Honda,T., Saitoh,H., Masuko,M., Katagiri-Abe,T., Tominaga,K., Kozakai,I., Kobayashi,K., Kumanishi,T., Watanabe,Y.G., Odani,S., and Kuwano,R. (2000). The coxsackievirus-adenovirus receptor protein as a cell adhesion molecule in the developing mouse brain. Brain Res.Mol.Brain Res. 77, 19-28.

Hormuzdi,S.G., Filippov,M.A., Mitropoulou,G., Monyer,H., and Bruzzone,R. (2004). Electrical synapses: a dynamic signaling system that shapes the activity of neuronal networks. Biochim.Biophys.Acta 1662, 113-137.

Hormuzdi,S.G., Pais,I., LeBeau,F.E., Towers,S.K., Rozov,A., Buhl,E.H., Whittington,M.A., and Monyer,H. (2001). Impaired electrical signaling disrupts gamma frequency oscillations in connexin 36-deficient mice. Neuron 31, 487-495.

Hotta,Y., Honda,T., Naito,M., and Kuwano,R. (2003). Developmental distribution of coxsackie virus and adenovirus receptor localized in the nervous system. Brain Res.Dev.Brain Res. 143, 1-13.

Howitt,J., Bewley,M.C., Graziano,V., Flanagan,J.M., and Freimuth,P. (2003). Structural basis for variation in adenovirus affinity for the cellular coxsackievirus and adenovirus receptor. J.Biol.Chem. 278, 26208-26215.

Huang,E.J. and Reichardt,L.F. (2001). Neurotrophins: roles in neuronal development and function. Annu.Rev.Neurosci. 24, 677-736.

Husi,H., Ward,M.A., Choudhary,J.S., Blackstock,W.P., and Grant,S.G. (2000). Proteomic analysis of NMDA receptor-adhesion protein signaling complexes. Nat.Neurosci. 3, 661-669.

Imrie,C.W., Ferguson,J.C., and Sommerville,R.G. (1977). Coxsackie and mumpsvirus infection in a prospective study of acute pancreatitis. Gut 18, 53-56.

Inagaki,C., Hara,M., and Zeng,X.T. (1996). A Cl- pump in rat brain neurons. J.Exp.Zool. 275, 262-268.

Irving,A.J., Collingridge,G.L., and Schofield,J.G. (1992). L-glutamate and acetylcholine mobilise Ca2+ from the same intracellular pool in cerebellar granule cells using transduction mechanisms with different Ca2+ sensitivities. Cell Calcium 13, 293-301.

Ishii,T.M., Silvia,C., Hirschberg,B., Bond,C.T., Adelman,J.P., and Maylie,J. (1997). A human intermediate conductance calcium-activated potassium channel. Proc.Natl.Acad.Sci.U.S.A 94, 11651-11656.

Ito,M., Kodama,M., Masuko,M., Yamaura,M., Fuse,K., Uesugi,Y., Hirono,S., Okura,Y., Kato,K., Hotta,Y., Honda,T., Kuwano,R., and Aizawa,Y. (2000). Expression of coxsackievirus and adenovirus receptor in hearts of rats with experimental autoimmune myocarditis. Circ.Res. 86, 275-280.

Jaimovich,E. and Carrasco,M.A. (2002). IP3 dependent Ca2+ signals in muscle cells are involved in regulation of gene expression. Biol.Res. 35, 195-202.

Jiang,S., Jacobs,A., Laue,T.M., and Caffrey,M. (2004). Solution structure of the coxsackievirus and adenovirus receptor domain 1. Biochemistry 43, 1847-1853.

Johnston,D. and Brown,T.H. (1983). Interpretation of voltage-clamp measurements in hippocampal neurons. J.Neurophysiol. 50, 464-486.

Joiner,W.J., Tang,M.D., Wang,L.Y., Dworetzky,S.I., Boissard,C.G., Gan,L., Gribkoff,V.K., and Kaczmarek,L.K. (1998). Formation of intermediate-conductance calcium-activated potassium channels by interaction of Slack and Slo subunits. Nat.Neurosci 1, 462-469.

Jones,M.V. and Westbrook,G.L. (1997). Shaping of IPSCs by endogenous calcineurin activity. J.Neurosci. 17, 7626-7633.

Juszczak,G.R. and Swiergiel,A.H. (2009). Properties of gap junction blockers and their behavioural, cognitive and electrophysiological effects: animal and human studies. Prog.Neuropsychopharmacol.Biol.Psychiatry 33, 181-198.

Kaftan,E.J., Ehrlich,B.E., and Watras,J. (1997). Inositol 1,4,5-trisphosphate (InsP3) and calcium interact to increase the dynamic range of InsP3 receptor-dependent calcium signaling. J.Gen.Physiol 110, 529-538.

Kamermans,M., Fahrenfort,I., Schultz,K., Janssen-Bienhold,U., Sjoerdsma,T., and Weiler,R. (2001). Hemichannel-mediated inhibition in the outer retina. Science 292, 1178-1180.

Kanaka,C., Ohno,K., Okabe,A., Kuriyama,K., Itoh,T., Fukuda,A., and Sato,K. (2001). The differential expression patterns of messenger RNAs encoding K-Cl cotransporters (KCC1,2) and Na-K-2Cl cotransporter (NKCC1) in the rat nervous system. Neuroscience 104, 933-946.

Kandel,E.R., Schwartz,J.H., and Jessell,T.M. (1996). Essentials of Neural Science and Behavior.

Kandel,E.R., Schwartz,J.H., and Jessell,T.M. (2000). Principles of neural science. (fourth edition: MrGraw-Hill).

Kashimura,T., Kodama,M., Hotta,Y., Hosoya,J., Yoshida,K., Ozawa,T., Watanabe,R., Okura,Y., Kato,K., Hanawa,H., Kuwano,R., and Aizawa,Y. (2004). Spatiotemporal changes of coxsackievirus and adenovirus receptor in rat hearts during postnatal development and in cultured cardiomyocytes of neonatal rat. Virchows Arch. 444, 283-292.

Kato,B.M. and Rubel,E.W. (1999). Glutamate regulates IP3-type and CICR stores in the avian cochlear nucleus. J.Neurophysiol. 81, 1587-1596.

Kelly,M.E., Dixon,S.J., and Sims,S.M. (1994). Outwardly rectifying chloride current in rabbit osteoclasts is activated by hyposmotic stimulation. J.Physiol 475, 377-389.

Khazipov,R. and Luhmann,H.J. (2006). Early patterns of electrical activity in the developing cerebral cortex of humans and rodents. Trends Neurosci. 29, 414-418.

Khodorov,B., Pinelis,V., Vergun,O., Storozhevykh,T., Fajuk,D., Vinskaya,N., Arsenjeva,E., Khaspekov,L., Lyzin,A., Isaev,N., and . (1995). Dramatic effects of external alkalinity on

neuronal calcium recovery following a short-duration glutamate challenge: the role of the plasma membrane Ca2+/H+ pump. FEBS Lett. 371, 249-252.

Khodorov,B.I. (2000). Mechanisms of destabilization of Ca2+-homeostasis of brain neurons caused by toxic glutamate challenge. Membr.Cell Biol. 14, 149-162.

Kim,E. and Sheng,M. (2004). PDZ domain proteins of synapses. Nat.Rev.Neurosci. 5, 771-781.

Kim,M., Sumerel,L.A., Belousova,N., Lyons,G.R., Carey,D.E., Krasnykh,V., and Douglas,J.T. (2003). The coxsackievirus and adenovirus receptor acts as a tumour suppressor in malignant glioma cells. Br.J.Cancer 88, 1411-1416.

Kirby,I., Davison,E., Beavil,A.J., Soh,C.P., Wickham,T.J., Roelvink,P.W., Kovesdi,I., Sutton,B.J., and Santis,G. (2000). Identification of contact residues and definition of the CAR-binding site of adenovirus type 5 fiber protein. J.Virol. 74, 2804-2813.

Kirkwood,A. and Bear,M.F. (1994). Homosynaptic long-term depression in the visual cortex. J.Neurosci. 14, 3404-3412.

Kiryushko,D., Berezin,V., and Bock,E. (2004). Regulators of neurite outgrowth: role of cell adhesion molecules. Ann.N.Y.Acad.Sci. 1014, 140-154.

Kiryushko,D., Korshunova,I., Berezin,V., and Bock,E. (2006). Neural cell adhesion molecule induces intracellular signaling via multiple mechanisms of Ca2+ homeostasis. Mol.Biol.Cell 17, 2278-2286.

Koch,M.C., Steinmeyer,K., Lorenz,C., Ricker,K., Wolf,F., Otto,M., Zoll,B., Lehmann-Horn,F., Grzeschik,K.H., and Jentsch,T.J. (1992). The skeletal muscle chloride channel in dominant and recessive human myotonia. Science 257, 797-800.

Kocsis,J.D., Rand,M.N., Lankford,K.L., and Waxman,S.G. (1994). Intracellular calcium mobilization and neurite outgrowth in mammalian neurons. J.Neurobiol. 25, 252-264.

Kohmura,N., Senzaki,K., Hamada,S., Kai,N., Yasuda,R., Watanabe,M., Ishii,H., Yasuda,M., Mishina,M., and Yagi,T. (1998). Diversity revealed by a novel family of cadherins expressed in neurons at a synaptic complex. Neuron 20, 1137-1151.

Koike,T., Martin,D.P., and Johnson,E.M., Jr. (1989). Role of Ca2+ channels in the ability of membrane depolarization to prevent neuronal death induced by trophic-factor deprivation: evidence that levels of internal Ca2+ determine nerve growth factor dependence of sympathetic ganglion cells. Proc.Natl.Acad.Sci.U.S.A 86, 6421-6425.

Kole,M.H., Ilschner,S.U., Kampa,B.M., Williams,S.R., Ruben,P.C., and Stuart,G.J. (2008). Action potential generation requires a high sodium channel density in the axon initial segment. Nat.Neurosci. 11, 178-186.

Kolkova,K., Novitskaya,V., Pedersen,N., Berezin,V., and Bock,E. (2000). Neural cell adhesion molecule-stimulated neurite outgrowth depends on activation of protein kinase C and the Ras-mitogen-activated protein kinase pathway. J.Neurosci. 20, 2238-2246.

Kondo,R.P., Wang,S.Y., John,S.A., Weiss,J.N., and Goldhaber,J.I. (2000). Metabolic inhibition activates a non-selective current through connexin hemichannels in isolated ventricular myocytes. J.Mol.Cell Cardiol. 32, 1859-1872.

Korsching,S. (1993). The neurotrophic factor concept: a reexamination. J.Neurosci. 13, 2739-2748.

Kotlikoff,M.I. and Wang,Y.X. (1998). Calcium release and calcium-activated chloride channels in airway smooth muscle cells. Am.J.Respir.Crit Care Med. 158, S109-S114.

Kotsias,B.A. and Peracchia,C. (2005). Functional interaction between CFTR and Cx45 gap junction channels expressed in oocytes. J.Membr.Biol. 203, 143-150.

Krizaj,D., Bao,J.X., Schmitz,Y., Witkovsky,P., and Copenhagen,D.R. (1999). Caffeine-sensitive calcium stores regulate synaptic transmission from retinal rod photoreceptors. J.Neurosci. 19, 7249-7261.

Kroger,S., Horton,S.E., and Honig,L.S. (1996). The developing avian retina expresses agrin isoforms during synaptogenesis. J.Neurobiol. 29, 165-182.

Kubo,M. and Okada,Y. (1992). Volume-regulatory Cl- channel currents in cultured human epithelial cells. J.Physiol 456, 351-371.

Kuruma,A. and Hartzell,H.C. (2000). Bimodal control of a Ca(2+)-activated Cl(-) channel by different Ca(2+) signals. J.Gen.Physiol 115, 59-80.

Lalonde,M.R., Kelly,M.E., and Barnes,S. (2008). Calcium-activated chloride channels in the retina. Channels (Austin.) 2, 252-260.

Lampe,P.D. and Lau,A.F. (2004). The effects of connexin phosphorylation on gap junctional communication. Int.J.Biochem.Cell Biol. 36, 1171-1186.

Lang,D.G. and Ritchie,A.K. (1987). Large and small conductance calcium-activated potassium channels in the GH3 anterior pituitary cell line. Pflugers Arch. 410, 614-622.

Lankford,K., De Mello,F.G., and Klein,W.L. (1987). A transient embryonic dopamine receptor inhibits growth cone motility and neurite outgrowth in a subset of avian retina neurons. Neurosci.Lett. 75, 169-174.

Latorre,R., Oberhauser,A., Labarca,P., and Alvarez,O. (1989). Varieties of calcium-activated potassium channels. Annu.Rev.Physiol 51, 385-399.

Lavado,E., Sanchez-Abarca,L.I., Tabernero,A., Bolanos,J.P., and Medina,J.M. (1997). Oleic acid inhibits gap junction permeability and increases glucose uptake in cultured rat astrocytes. J.Neurochem. 69, 721-728.

Law,L.K. and Davidson,B.L. (2005). What does it take to bind CAR? Mol.Ther. 12, 599-609.

Leinders-Zufall,T., Rand,M.N., Shepherd,G.M., Greer,C.A., and Zufall,F. (1997). Calcium entry through cyclic nucleotide-gated channels in individual cilia of olfactory receptor cells: spatiotemporal dynamics. J.Neurosci 17, 4136-4148.

Lesage,F. (2003). Pharmacology of neuronal background potassium channels. Neuropharmacology 44, 1-7.

Leshchenko,Y., Likhodii,S., Yue,W., Burnham,W.M., and Perez Velazquez,J.L. (2006). Carbenoxolone does not cross the blood brain barrier: an HPLC study. BMC.Neurosci. 7, 3.

Levinson,J.N., Chery,N., Huang,K., Wong,T.P., Gerrow,K., Kang,R., Prange,O., Wang,Y.T., and El Husseini,A. (2005). Neuroligins mediate excitatory and inhibitory synapse formation: involvement of PSD-95 and neurexin-1beta in neuroligin-induced synaptic specificity. J.Biol.Chem. 280, 17312-17319.

Levinson,J.N. and El Husseini,A. (2005). Building excitatory and inhibitory synapses: balancing neuroligin partnerships. Neuron 48, 171-174.

Li,D., Duan,L., Freimuth,P., and O'Malley,B.W., Jr. (1999). Variability of adenovirus receptor density influences gene transfer efficiency and therapeutic response in head and neck cancer. Clin.Cancer Res. 5, 4175-4181.

Lievremont,J.P., Bird,G.S., and Putney,J.W., Jr. (2005). Mechanism of inhibition of TRPC cation channels by 2-aminoethoxydiphenylborane. Mol.Pharmacol. 68, 758-762.

Lin,B., Arai,A.C., Lynch,G., and Gall,C.M. (2003). Integrins regulate NMDA receptor-mediated synaptic currents. J.Neurophysiol. 89, 2874-2878.

Lin,C.F., Tsaur,M.L., Lin,C.S., Chen,C.C., Huang,Y.J., and Cheng,J.K. (2009). Intrathecal gabapentin does not act as a hyperpolarization-activated cyclic nucleotide-gated channel activator in the rat formalin test. Eur.J.Anaesthesiol.

Lisewski,U., Shi,Y., Wrackmeyer,U., Fischer,R., Chen,C., Schirdewan,A., Juttner,R., Rathjen,F., Poller,W., Radke,M.H., and Gotthardt,M. (2008). The tight junction protein CAR regulates cardiac conduction and cell-cell communication. J.Exp.Med. 205, 2369-2379.

Liu,S.H. and Lin-Shiau,S.Y. (1992). Studies on mercury-induced myotonia in the mouse diaphragm. Arch.Int.Pharmacodyn.Ther. 319, 86-100.

Locke,S. and Solomon,H.C. (1967). Relation of resting potential of rat gastrocnemius and soleus muscles to innervation, activity, and the Na-K pump. J.Exp.Zool. 166, 377-386.

Loewenstein. The cell-to-cell channel of gap junctions. 1987. Cell.

Lortat-Jacob,H., Chouin,E., Cusack,S., and van Raaij,M.J. (2001). Kinetic analysis of adenovirus fiber binding to its receptor reveals an avidity mechanism for trimeric receptor-ligand interactions. J.Biol.Chem. 276, 9009-9015.

Louis,N., Fender,P., Barge,A., Kitts,P., and Chroboczek,J. (1994). Cell-binding domain of adenovirus serotype 2 fiber. J.Virol. 68, 4104-4106.

Lu,B., Su,Y., Das,S., Liu,J., Xia,J., and Ren,D. (2007). The neuronal channel NALCN contributes resting sodium permeability and is required for normal respiratory rhythm. Cell 129, 371-383.

Ludwig,A., Zong,X., Hofmann,F., and Biel,M. (1999). Structure and function of cardiac pacemaker channels. Cell Physiol Biochem. 9, 179-186.

Ludwig,A., Zong,X., Jeglitsch,M., Hofmann,F., and Biel,M. (1998). A family of hyperpolarization-activated mammalian cation channels. Nature 393, 587-591.

Luissint,A.C., Lutz,P.G., Calderwood,D.A., Couraud,P.O., and Bourdoulous,S. (2008). JAM-L-mediated leukocyte adhesion to endothelial cells is regulated in cis by alpha4beta1 integrin activation. J.Cell Biol. 183, 1159-1173.

Lumsden,A. and Cohen,J. (1991). Axon guidance in the vertebrate central nervous system. Curr.Opin.Genet.Dev. 1, 230-235.

Luo,J., Wang,Y., Chen,H., Kintner,D.B., Cramer,S.W., Gerdts,J.K., Chen,X., Shull,G.E., Philipson,K.D., and Sun,D. (2008). A concerted role of Na+ -K+ -Cl- cotransporter and Na+/Ca2+ exchanger in ischemic damage. J.Cereb.Blood Flow Metab 28, 737-746.

Lurtz,M.M. and Louis,C.F. (2007). Intracellular calcium regulation of connexin43. Am.J.Physiol Cell Physiol 293, C1806-C1813.

Luthi,A. and McCormick,D.A. (1998). H-current: properties of a neuronal and network pacemaker. Neuron 21, 9-12.

Luthi,A., Mohajeri,H., Schachner,M., and Laurent,J.P. (1996). Reduction of hippocampal long-term potentiation in transgenic mice ectopically expressing the neural cell adhesion molecule L1 in astrocytes. J.Neurosci.Res. 46, 1-6.

Lyashchenko,A.K. and Tibbs,G.R. (2008). Ion binding in the open HCN pacemaker channel pore: fast mechanisms to shape "slow" channels. J.Gen.Physiol 131, 227-243.

Maconochie,D.J., Zempel,J.M., and Steinbach,J.H. (1994). How quickly can GABAA receptors open? Neuron 12, 61-71.

Madison,D.V., Malenka,R.C., and Nicoll,R.A. (1986). Phorbol esters block a voltage-sensitive chloride current in hippocampal pyramidal cells. Nature 321, 695-697.

Magleby,K.L. and Stevens,C.F. (1972). The effect of voltage on the time course of end-plate currents. J.Physiol 223, 151-171.

Mankodi,A. (2008). Myotonic disorders. Neurol.India 56, 298-304.

Mankodi,A. and Thornton,C.A. (2002). Myotonic syndromes. Curr.Opin.Neurol. 15, 545-552.

Mapoles,J.E., Krah,D.L., and Crowell,R.L. (1985). Purification of a HeLa cell receptor protein for group B coxsackieviruses. J.Virol. 55, 560-566.

Marcet,B., Becq,F., Norez,C., Delmas,P., and Verrier,B. (2004). General anesthetic octanol and related compounds activate wild-type and delF508 cystic fibrosis chloride channels. Br.J.Pharmacol. 141, 905-914.

Marshall,J., Dolan,B.M., Garcia,E.P., Sathe,S., Tang,X., Mao,Z., and Blair,L.A. (2003). Calcium channel and NMDA receptor activities differentially regulate nuclear C/EBPbeta levels to control neuronal survival. Neuron 39, 625-639.

Martin,D., Tawadros,T., Meylan,L., Abderrahmani,A., Condorelli,D.F., Waeber,G., and Haefliger,J.A. (2003). Critical role of the transcriptional repressor neuron-restrictive silencer factor in the specific control of connexin36 in insulin-producing cell lines. J.Biol.Chem. 278, 53082-53089.

Marty,A. (1981). Ca-dependent K channels with large unitary conductance in chromaffin cell membranes. Nature 291, 497-500.

Marty,A. (1989). The physiological role of calcium-dependent channels. Trends Neurosci 12, 420-424.

Matchkov,V.V., Aalkjaer,C., and Nilsson,H. (2004). A cyclic GMP-dependent calcium-activated chloride current in smooth-muscle cells from rat mesenteric resistance arteries. J.Gen.Physiol 123, 121-134.

Matsumoto,S., Kitagawa,J., and Takeda,M. (2008). The effects of ouabain on resting membrane potential and hyperpolarization-activated current in neonatal rat nodose ganglion neurons. Neurosci.Lett. 439, 241-244.

McClintock,T.S. and Ache,B.W. (1989). Ionic currents and ion channels of lobster olfactory receptor neurons. J.Gen.Physiol 94, 1085-1099.

McCormick,D.A. and Huguenard,J.R. (1992). A model of the electrophysiological properties of thalamocortical relay neurons. J.Neurophysiol. 68, 1384-1400.

McCormick,D.A. and Prince,D.A. (1987). Post-natal development of electrophysiological properties of rat cerebral cortical pyramidal neurones. J.Physiol 393, 743-762.

Melnick,I.V. (1993). Development of spontaneous synaptic activity in culture of the chick spinal cord neurons. Neuroscience 53, 509-518.

Melnick,I.V. and Baev,K.V. (1993). Glycine conductance changes in chick spinal cord neurons developing in culture. Neuroscience 52, 347-360.

Melnick,J.L. (1996). Current status of poliovirus infections. Clin.Microbiol.Rev. 9, 293-300.

Mennerick,S. and Zorumski,C.F. (2000). Neural activity and survival in the developing nervous system. Mol.Neurobiol. 22, 41-54.

Michael,L., Pitts,B.J., and Schwartz,A. (1978). Is pump stimulation associated with positive inotropy of the heart? Science 200, 1287-1289.

Mignen,O., Egee,S., Liberge,M., and Harvey,B.J. (2000). Basolateral outward rectifier chloride channel in isolated crypts of mouse colon. Am.J.Physiol Gastrointest.Liver Physiol 279, G277-G287.

Milani,D., Candeo,P., Favaron,M., Blackstone,C.D., and Manev,H. (1993). A subpopulation of cerebellar granule neurons in culture expresses a functional mGluR1 metabotropic glutamate receptor: effect of depolarizing growing conditions. Receptors.Channels 1, 243-250.

Miragall,F., Albiez,P., Bartels,H., de Vries,U., and Dermietzel,R. (1997). Expression of the gap junction protein connexin43 in the subependymal layer and the rostral migratory stream of the mouse: evidence for an inverse correlation between intensity of connexin43 expression and cell proliferation activity. Cell Tissue Res. 287, 243-253.

Mirza,M., Hreinsson,J., Strand,M.L., Hovatta,O., Soder,O., Philipson,L., Pettersson,R.F., and Sollerbrant,K. (2006). Coxsackievirus and adenovirus receptor (CAR) is expressed in male germ cells and forms a complex with the differentiation factor JAM-C in mouse testis. Exp.Cell Res. 312, 817-830.

Missiaen,L., Callewaert,G., De Smedt,H., and Parys,J.B. (2001). 2-Aminoethoxydiphenyl borate affects the inositol 1,4,5-trisphosphate receptor, the intracellular Ca2+ pump and the non-specific Ca2+ leak from the non-mitochondrial Ca2+ stores in permeabilized A7r5 cells. Cell Calcium 29, 111-116.

Molleman,A. (2002). Patch-Clamping-An Introductory Guide to Patch Clamp Electrophysiology. John Wiley & Sons).

Molnar,L.R., Thayne,K.A., Fleming,W.W., and Taylor,D.A. (1999). The role of the sodium pump in the developmental regulation of membrane electrical properties of cerebellar Purkinje neurons of the rat. Brain Res.Dev.Brain Res. 112, 287-291.

Montano,L.M. and Bazan-Perkins,B. (2005). Resting calcium influx in airway smooth muscle. Can.J.Physiol Pharmacol. 83, 717-723.

Moosmang,S., Stieber,J., Zong,X., Biel,M., Hofmann,F., and Ludwig,A. (2001). Cellular expression and functional characterization of four hyperpolarization-activated pacemaker channels in cardiac and neuronal tissues. Eur.J.Biochem. 268, 1646-1652.

Mulkey,R.M. and Zucker,R.S. (1991). Action potentials must admit calcium to evoke transmitter release. Nature 350, 153-155.

Musil,L.S. and Goodenough,D.A. (1991). Biochemical analysis of connexin43 intracellular transport, phosphorylation, and assembly into gap junctional plaques. J.Cell Biol. 115, 1357-1374.

Nadarajah,B., Makarenkova,H., Becker,D.L., Evans,W.H., and Parnavelas,J.G. (1998). Basic FGF increases communication between cells of the developing neocortex. J.Neurosci. 18, 7881-7890.

Nakamura,T., Nakamura,K., Lasser-Ross,N., Barbara,J.G., Sandler,V.M., and Ross,W.N. (2000). Inositol 1,4,5-trisphosphate (IP3)-mediated Ca2+ release evoked by metabotropic agonists and backpropagating action potentials in hippocampal CA1 pyramidal neurons. J.Neurosci. 20, 8365-8376.

Nalbantoglu,J., Pari,G., Karpati,G., and Holland,P.C. (1999). Expression of the primary coxsackie and adenovirus receptor is downregulated during skeletal muscle maturation and limits the efficacy of adenovirus-mediated gene delivery to muscle cells. Hum.Gene Ther. 10, 1009-1019.

Nassiri-Asl,M., Zamansoltani,F., and Zangivand,A.A. (2008). The inhibitory effect of trimethylamine on the anticonvulsant activities of quinine in the pentylenetetrazole model in rats. Prog.Neuropsychopharmacol.Biol.Psychiatry 32, 1496-1500.

Neher,E. (1995). The use of fura-2 for estimating Ca buffers and Ca fluxes. Neuropharmacology 34, 1423-1442.

Neher,E. and Sakmann,B. (1976). Single-channel currents recorded from membrane of denervated frog muscle fibres. Nature 260, 799-802.

Neher,E., Sakmann,B., and Steinbach,J.H. (1978). The extracellular patch clamp: a method for resolving currents through individual open channels in biological membranes. Pflugers Arch. 375, 219-228.

Nikonenko,I., Toni,N., Moosmayer,M., Shigeri,Y., Muller,D., and Sargent,J.L. (2003). Integrins are involved in synaptogenesis, cell spreading, and adhesion in the postnatal brain. Brain Res.Dev.Brain Res. 140, 185-194.

Nilius,B., Prenen,J., Kamouchi,M., Viana,F., Voets,T., and Droogmans,G. (1997a). Inhibition by mibefradil, a novel calcium channel antagonist, of Ca(2+)- and volume-activated Cl- channels in macrovascular endothelial cells. Br.J.Pharmacol. 121, 547-555.

Nilius,B., Prenen,J., Szucs,G., Wei,L., Tanzi,F., Voets,T., and Droogmans,G. (1997b). Calcium-activated chloride channels in bovine pulmonary artery endothelial cells. J.Physiol 498 (Pt 2), 381-396.

Niu,Y., Su,Z., Zhao,C., Song,B., Zhang,X., Zhao,N., Shen,X., and Gong,Y. (2009). Effect of amyloid beta on capacitive calcium entry in neural 2a cells. Brain Res.Bull. 78, 152-157.

Noutsias,M., Fechner,H., de Jonge,H., Wang,X., Dekkers,D., Houtsmuller,A.B., Pauschinger,M., Bergelson,J., Warraich,R., Yacoub,M., Hetzer,R., Lamers,J., Schultheiss,H.P., and Poller,W. (2001). Human coxsackie-adenovirus receptor is colocalized with integrins alpha(v)beta(3) and alpha(v)beta(5) on the cardiomyocyte sarcolemma and upregulated in dilated cardiomyopathy: implications for cardiotropic viral infections. Circulation 104, 275-280.

Ohta,T., Wakade,A.R., Yonekubo,K., and Ito,S. (2002). Functional relation between caffeine- and muscarine-sensitive Ca2+ stores and no Ca2+ releasing action of cyclic adenosine diphosphate-ribose in guinea-pig adrenal chromaffin cells. Neurosci.Lett. 326, 167-170.

Okegawa,T., Li,Y., Pong,R.C., Bergelson,J.M., Zhou,J., and Hsieh,J.T. (2000). The dual impact of coxsackie and adenovirus receptor expression on human prostate cancer gene therapy. Cancer Res. 60, 5031-5036.

Okegawa,T., Pong,R.C., Li,Y., Bergelson,J.M., Sagalowsky,A.I., and Hsieh,J.T. (2001). The mechanism of the growth-inhibitory effect of coxsackie and adenovirus receptor (CAR) on

human bladder cancer: a functional analysis of car protein structure. Cancer Res. 61, 6592-6600.

Pais,I., Hormuzdi,S.G., Monyer,H., Traub,R.D., Wood,I.C., Buhl,E.H., Whittington,M.A., and LeBeau,F.E. (2003). Sharp wave-like activity in the hippocampus in vitro in mice lacking the gap junction protein connexin 36. J.Neurophysiol. 89, 2046-2054.

Pape,H.C. (1996). Queer current and pacemaker: the hyperpolarization-activated cation current in neurons. Annu.Rev.Physiol 58, 299-327.

Parikh,H.N., Liu,L., and Chiodo,L.A. (1997). P2U Receptor Stimulation Increases Intracellular Ca2+ in Hybrid N18TG2 X Mesencephalon (MES-23.5) Cells Via Two Distinct Mechanisms. Neuroscience-Net.

Patzke,C. Untersuchung eines adhäsionshemmenden Effektes von gegen den Coxsackie-und Adenovirusrezeptor gerichteten Antikörpern in Bezug auf HeLa-Zellen und dessen Neutralisierung durch fötales Kälberserum. 2004. Thesis/Dissertation

Patzke,C., Max,K., Behlke,J., Schreiber,J., Schmidt, H., Dorner,A., Kröger,S., Henning,M., Otto,A., Heinemann,U., and Rathjen,F.G. Functional and structural characterization of the Coxsackievirus-adenovirus receptor (CAR): complex homophilic and heterophilic interactions on neural cells. Sumbitted . 2009.

Patzke,C. Der Coxsackie- und Adenovirus-Rezeptor im embryonalen Nervensystem: ein homophiles und heterophiles Zelladhäsionsmolekül. 2009. Thesis/Dissertation

Paulev,P.E. (2000). Medical Physiology and Pathophysiology, Essentials and clinical problems. Copenhagen Medical Publishers).

Pearson,M.M., Lu,J., Mount,D.B., and Delpire,E. (2001). Localization of the K(+)-Cl(-) cotransporter, KCC3, in the central and peripheral nervous systems: expression in the choroid plexus, large neurons and white matter tracts. Neuroscience 103, 481-491.

Pearson,R.G., Molino,Y., Williams,P.M., Tendler,S.J., Davies,M.C., Roberts,C.J., and Shakesheff,K.M. (2003). Spatial confinement of neurite regrowth from dorsal root ganglia within nonporous microconduits. Tissue Eng 9, 201-208.

Peng,L., Martin-Vasallo,P., and Sweadner,K.J. (1997). Isoforms of Na,K-ATPase alpha and beta subunits in the rat cerebellum and in granule cell cultures. J.Neurosci. 17, 3488-3502.

Perkins,G., Goodenough,D., and Sosinsky,G. (1997). Three-dimensional structure of the gap junction connexon. Biophys.J. 72, 533-544.

Petrella,J., Cohen,C.J., Gaetz,J., and Bergelson,J.M. (2002). A zebrafish coxsackievirus and adenovirus receptor homologue interacts with coxsackie B virus and adenovirus. J.Virol. 76, 10503-10506.

Philipson,L., Lonberg-Holm,K., and Pettersson,U. (1968). Virus-receptor interaction in an adenovirus system. J.Virol. 2, 1064-1075.

Philipson,L. and Pettersson,R.F. (2004). The coxsackie-adenovirus receptor--a new receptor in the immunoglobulin family involved in cell adhesion. Curr.Top.Microbiol.Immunol. 273, 87-111.

Pinilla,P.J., Hernandez,A.T., Camello,M.C., Pozo,M.J., Toescu,E.C., and Camello,P.J. (2005). Non-stimulated Ca2+ leak pathway in cerebellar granule neurones. Biochem.Pharmacol. 70, 786-793.

Planelles,G. and Anagnostopoulos,T. (1987). Effects of membrane potential changes on electrical cell-to-cell coupling in proximal tubule. Pflugers Arch. 408, 531-533.

Poolos,N.P. (2004). The Yin and Yang of the H-Channel and Its Role in Epilepsy. Epilepsy Curr. 4, 3-6.

Porter,N.M., Thibault,O., Thibault,V., Chen,K.C., and Landfield,P.W. (1997). Calcium channel density and hippocampal cell death with age in long-term culture. J.Neurosci 17, 5629-5639.

Pottek,M., Hoppenstedt,W., Janssen-Bienhold,U., Schultz,K., Perlman,I., and Weiler,R. (2003). Contribution of connexin26 to electrical feedback inhibition in the turtle retina. J.Comp Neurol. 466, 468-477.

Poulsen,J.C., Caspersen,C., Mathiasen,D., East,J.M., Tunwell,R.E., Lai,F.A., Maeda,N., Mikoshiba,K., and Treiman,M. (1995). Thapsigargin-sensitive Ca(2+)-ATPases account for Ca2+ uptake to inositol 1,4,5-trisphosphate-sensitive and caffeine-sensitive Ca2+ stores in adrenal chromaffin cells. Biochem.J. 307 (Pt 3), 749-758.

Prange,O., Wong,T.P., Gerrow,K., Wang,Y.T., and El Husseini,A. (2004). A balance between excitatory and inhibitory synapses is controlled by PSD-95 and neuroligin. Proc.Natl.Acad.Sci.U.S.A 101, 13915-13920.

Prole,D.L. and Yellen,G. (2006). Reversal of HCN channel voltage dependence via bridging of the S4-S5 linker and Post-S6. J.Gen.Physiol 128, 273-282.

Pulcinelli,F.M., Gresele,P., Bonuglia,M., and Gazzaniga,P.P. (1998). Evidence for separate effects of U73122 on phospholipase C and calcium channels in human platelets. Biochem.Pharmacol. 56, 1481-1484.

Purves,D., Augustine,G.J., Fitzpatrick,D., Hall,W.C., LaMantia,A.S., McNamara,J.O., and White,L.E. (2008). Neuroscience. (Sunderland, Massachusetts, USA: Sinauer Associates).

Qu,Z., Wei,R.W., and Hartzell,H.C. (2003). Characterization of Ca2+-activated Cl- currents in mouse kidney inner medullary collecting duct cells. Am.J.Physiol Renal Physiol 285, F326-F335.

Ramoa,A.S. and McCormick,D.A. (1994). Developmental changes in electrophysiological properties of LGNd neurons during reorganization of retinogeniculate connections. J.Neurosci. 14, 2089-2097.

Raschperger,E., Engstrom,U., Pettersson,R.F., and Fuxe,J. (2004). CLMP, a novel member of the CTX family and a new component of epithelial tight junctions. J.Biol.Chem. 279, 796-804.

Raschperger,E., Thyberg,J., Pettersson,S., Philipson,L., Fuxe,J., and Pettersson,R.F. (2006). The coxsackie- and adenovirus receptor (CAR) is an in vivo marker for epithelial tight junctions, with a potential role in regulating permeability and tissue homeostasis. Exp.Cell Res. 312, 1566-1580.

Rauen,K.A., Sudilovsky,D., Le,J.L., Chew,K.L., Hann,B., Weinberg,V., Schmitt,L.D., and McCormick,F. (2002). Expression of the coxsackie adenovirus receptor in normal prostate and in primary and metastatic prostate carcinoma: potential relevance to gene therapy. Cancer Res. 62, 3812-3818.

Reich,C.G., Mason,S.E., and Alger,B.E. (2004). Novel form of LTD induced by transient, partial inhibition of the Na,K-pump in rat hippocampal CA1 cells. J.Neurophysiol. 91, 239-247.

Reisert,J., Bauer,P.J., Yau,K.W., and Frings,S. (2003). The Ca-activated Cl channel and its control in rat olfactory receptor neurons. J.Gen.Physiol 122, 349-363.

Reyes,J.P., Hernandez-Carballo,C.Y., Perez-Flores,G., Perez-Cornejo,P., and Arreola,J. (2009). Lack of coupling between membrane stretching and pannexin-1 hemichannels. Biochem.Biophys.Res.Commun. 380, 50-53.

Roelvink,P.W., Lizonova,A., Lee,J.G., Li,Y., Bergelson,J.M., Finberg,R.W., Brough,D.E., Kovesdi,I., and Wickham,T.J. (1998). The coxsackievirus-adenovirus receptor protein can function as a cellular attachment protein for adenovirus serotypes from subgroups A, C, D, E, and F. J.Virol. 72, 7909-7915.

Roelvink,P.W., Mi,L.G., Einfeld,D.A., Kovesdi,I., and Wickham,T.J. (1999). Identification of a conserved receptor-binding site on the fiber proteins of CAR-recognizing adenoviridae. Science 286, 1568-1571.

Romanello,M. and D'Andrea,P. (2001). Dual mechanism of intercellular communication in HOBIT osteoblastic cells: a role for gap-junctional hemichannels. J.Bone Miner.Res. 16, 1465-1476.

Ronn,L.C., Dissing,S., Holm,A., Berezin,V., and Bock,E. (2002). Increased intracellular calcium is required for neurite outgrowth induced by a synthetic peptide ligand of NCAM. FEBS Lett. 518, 60-66.

Rose,C.R. and Konnerth,A. (2001). Stores not just for storage. intracellular calcium release and synaptic plasticity. Neuron 31, 519-522.

Ross,F.M., Gwyn,P., Spanswick,D., and Davies,S.N. (2000). Carbenoxolone depresses spontaneous epileptiform activity in the CA1 region of rat hippocampal slices. Neuroscience 100, 789-796.

Rothe,T., Juttner,R., Bahring,R., and Grantyn,R. (1999). Ion conductances related to development of repetitive firing in mouse retinal ganglion neurons in situ. J.Neurobiol. 38, 191-206.

Rouach,N., Segal,M., Koulakoff,A., Giaume,C., and Avignone,E. (2003). Carbenoxolone blockade of neuronal network activity in culture is not mediated by an action on gap junctions. J.Physiol 553, 729-745.

Rozental,R., Andrade-Rozental,A.F., Zheng,X., Urban,M., Spray,D.C., and Chiu,F.C. (2001). Gap junction-mediated bidirectional signaling between human fetal hippocampal neurons and astrocytes. Dev.Neurosci. 23, 420-431.

Rozental,R., Giaume,C., and Spray,D.C. (2000). Gap junctions in the nervous system. Brain Res.Brain Res.Rev. 32, 11-15.

Ruben. Action potentials: Generation and Propagation. 2001.

Rubio,M.E. and Wenthold,R.J. (1997). Glutamate receptors are selectively targeted to postsynaptic sites in neurons. Neuron 18, 939-950.

Russo,R.E., Reali,C., Radmilovich,M., Fernandez,A., and Trujillo-Cenoz,O. (2008). Connexin 43 delimits functional domains of neurogenic precursors in the spinal cord. J.Neurosci. 28, 3298-3309.

Rux,J.J. and Burnett,R.M. (2004). Adenovirus structure. Hum.Gene Ther. 15, 1167-1176.

Rychkov,G.Y., Pusch,M., Roberts,M.L., Jentsch,T.J., and Bretag,A.H. (1998). Permeation and block of the skeletal muscle chloride channel, ClC-1, by foreign anions. J.Gen.Physiol 111, 653-665.

Sacchi,O., Rossi,M.L., Canella,R., and Fesce,R. (2007). Regulation of the subthreshold chloride conductance in the rat sympathetic neuron. Eur.J.Neurosci. 25, 1112-1126.

Saez,J.C., Connor,J.A., Spray,D.C., and Bennett,M.V. (1989). Hepatocyte gap junctions are permeable to the second messenger, inositol 1,4,5-trisphosphate, and to calcium ions. Proc.Natl.Acad.Sci.U.S.A 86, 2708-2712.

Saffell,J.L., Williams,E.J., Mason,I.J., Walsh,F.S., and Doherty,P. (1997). Expression of a dominant negative FGF receptor inhibits axonal growth and FGF receptor phosphorylation stimulated by CAMs. Neuron 18, 231-242.

Saghian,A.A., Ayrapetyan,S.N., and Carpenter,D.O. (1996). Low concentrations of ouabain stimulate Na/Ca exchange in neurons. Cell Mol.Neurobiol. 16, 489-498.

Sakai,N., Tabb,T., and Garfield,R.E. (1992). Studies of connexin 43 and cell-to-cell coupling in cultured human uterine smooth muscle. Am.J.Obstet.Gynecol. 167, 1267-1277.

Sakaki,Y., Fukuda,Y., and Yamashita,M. (1996). Muscarinic and purinergic Ca2+ mobilizations in the neural retina of early embryonic chick. Int.J.Dev.Neurosci. 14, 691-699.

Salkoff,L., Butler,A., Fawcett,G., Kunkel,M., CARdle,C., Mino,G., Nonet,M., Walton,N., Wang,Z.W., Yuan,A., and Wei,A. (2001). Evolution tunes the excitability of individual neurons. Neuroscience 103, 853-859.

Sanderson,M.J., Charles,A.C., and Dirksen,E.R. (1990). Mechanical stimulation and intercellular communication increases intracellular Ca2+ in epithelial cells. Cell Regul. 1, 585-596.

Sandler,V.M. and Barbara,J.G. (1999). Calcium-induced calcium release contributes to action potential-evoked calcium transients in hippocampal CA1 pyramidal neurons. J.Neurosci. 19, 4325-4336.

Santoro,B., Liu,D.T., Yao,H., Bartsch,D., Kandel,E.R., Siegelbaum,S.A., and Tibbs,G.R. (1998). Identification of a gene encoding a hyperpolarization-activated pacemaker channel of brain. Cell 93, 717-729.

Scheiffele,P., Fan,J., Choih,J., Fetter,R., and Serafini,T. (2000). Neuroligin expressed in nonneuronal cells triggers presynaptic development in contacting axons. Cell 101, 657-669.

Schmid,R.S. and Maness,P.F. (2008). L1 and NCAM adhesion molecules as signaling coreceptors in neuronal migration and process outgrowth. Curr.Opin.Neurobiol. 18, 245-250.

Schomberg,S.L., Su,G., Haworth,R.A., and Sun,D. (2001). Stimulation of Na-K-2Cl cotransporter in neurons by activation of Non-NMDA ionotropic receptor and group-I mGluRs. J.Neurophysiol. 85, 2563-2575.

Schroeder,B.C., Cheng,T., Jan,Y.N., and Jan,L.Y. (2008). Expression cloning of TMEM16A as a calcium-activated chloride channel subunit. Cell 134, 1019-1029.

Schuch,U., Lohse,M.J., and Schachner,M. (1989). Neural cell adhesion molecules influence second messenger systems. Neuron 3, 13-20.

Schummers,J., Marino,J., and Sur,M. (2002). Synaptic integration by V1 neurons depends on location within the orientation map. Neuron 36, 969-978.

Schwartz,A., Lindenmayer,G.E., and Allen,J.C. (1975). The sodium-potassium adenosine triphosphatase: pharmacological, physiological and biochemical aspects. Pharmacol.Rev. 27, 3-134.

Schwartzkroin,P.A. and Wyler,A.R. (1980). Mechanisms underlying epileptiform burst discharge. Ann.Neurol. 7, 95-107.

Scuri,R., Lombardo,P., Cataldo,E., Ristori,C., and Brunelli,M. (2007). Inhibition of Na+/K+ ATPase potentiates synaptic transmission in tactile sensory neurons of the leech. Eur.J.Neurosci. 25, 159-167.

Shah,M. and Haylett,D.G. (2000). The pharmacology of hSK1 Ca2+-activated K+ channels expressed in mammalian cell lines. Br.J.Pharmacol. 129, 627-630.

Shao,X.M. and Feldman,J.L. (2007). Micro-agar salt bridge in patch-clamp electrode holder stabilizes electrode potentials. J.Neurosci.Methods 159, 108-115.

Shaw,C.A., Holland,P.C., Sinnreich,M., Allen,C., Sollerbrant,K., Karpati,G., and Nalbantoglu,J. (2004). Isoform-specific expression of the Coxsackie and adenovirus receptor (CAR) in neuromuscular junction and cardiac intercalated discs. BMC.Cell Biol. 5, 42.

Shelley,J., Dedek,K., Schubert,T., Feigenspan,A., Schultz,K., Hombach,S., Willecke,K., and Weiler,R. (2006). Horizontal cell receptive fields are reduced in connexin57-deficient mice. Eur.J.Neurosci. 23, 3176-3186.

Shibata,H., Satoh,T.O., Ugawa,T., Masuda,N., Yanai-Inamura,H., Abe,A., Kondo,Y., Kuramochi,T., Akamatsu,S., and Uchida,W. (2005). Characterization of the pharmacology of YM-198313 on volume-regulated anion channels. Biol.Pharm.Bull. 28, 1187-1191.

Shmigol,A., Kostyuk,P., and Verkhratsky,A. (1995). Dual action of thapsigargin on calcium mobilization in sensory neurons: inhibition of Ca2+ uptake by caffeine-sensitive pools and blockade of plasmalemmal Ca2+ channels. Neuroscience 65, 1109-1118.

Simpson,J.E., Gawenis,L.R., Walker,N.M., Boyle,K.T., and Clarke,L.L. (2005). Chloride conductance of CFTR facilitates basal Cl-/. Am.J.Physiol Gastrointest.Liver Physiol 288, G1241-G1251.

Simpson,P.B., Nahorski,S.R., and Challiss,R.A. (1996). Agonist-evoked Ca2+ mobilization from stores expressing inositol 1,4,5-trisphosphate receptors and ryanodine receptors in cerebellar granule neurones. J.Neurochem. 67, 364-373.

Sitsapesan,R. and Williams,A.J. (1990). Mechanisms of caffeine activation of single calcium-release channels of sheep cardiac sarcoplasmic reticulum. J.Physiol 423, 425-439.

Sjodin,R.A. (1982). Transport of electrolytes in muscle. J.Membr.Biol. 68, 161-178.

Smith,R.J., Sam,L.M., Justen,J.M., Bundy,G.L., Bala,G.A., and Bleasdale,J.E. (1990). Receptor-coupled signal transduction in human polymorphonuclear neutrophils: effects of a novel inhibitor of phospholipase C-dependent processes on cell responsiveness. J.Pharmacol.Exp.Ther. 253, 688-697.

Smith,R.L., Clayton,G.H., Wilcox,C.L., Escudero,K.W., and Staley,K.J. (1995). Differential expression of an inwardly rectifying chloride conductance in rat brain neurons: a potential mechanism for cell-specific modulation of postsynaptic inhibition. J.Neurosci 15, 4057-4067.

Snutch,T.P. and Reiner,P.B. (1992). Ca2+ channels: diversity of form and function. Curr.Opin.Neurobiol. 2, 247-253.

Solc,C.K. and Wine,J.J. (1991). Swelling-induced and depolarization-induced C1-channels in normal and cystic fibrosis epithelial cells. Am.J.Physiol 261, C658-C674.

Sollerbrant,K., Raschperger,E., Mirza,M., Engstrom,U., Philipson,L., Ljungdahl,P.O., and Pettersson,R.F. (2003). The Coxsackievirus and adenovirus receptor (CAR) forms a complex with the PDZ domain-containing protein ligand-of-numb protein-X (LNX). J.Biol.Chem. 278, 7439-7444.

Somers,D.C., Nelson,S.B., and Sur,M. (1995). An emergent model of orientation selectivity in cat visual cortical simple cells. J.Neurosci. 15, 5448-5465.

Sommer,B., Keinanen,K., Verdoorn,T.A., Wisden,W., Burnashev,N., Herb,A., Kohler,M., Takagi,T., Sakmann,B., and Seeburg,P.H. (1990). Flip and flop: a cell-specific functional switch in glutamate-operated channels of the CNS. Science 249, 1580-1585.

Sorota,S. (1992). Swelling-induced chloride-sensitive current in canine atrial cells revealed by whole-cell patch-clamp method. Circ.Res. 70, 679-687.

Sosinsky,G.E. and Nicholson,B.J. (2005). Structural organization of gap junction channels. Biochim.Biophys.Acta 1711, 99-125.

Spitzer,N.C. (2006). Electrical activity in early neuronal development. Nature 444, 707-712.

Spray,D.C., Harris,A.L., and Bennett,M.V. (1981). Equilibrium properties of a voltage-dependent junctional conductance. J.Gen.Physiol 77, 77-93.

Srinivas,M. and Spray,D.C. (2003). Closure of gap junction channels by arylaminobenzoates. Mol.Pharmacol. 63, 1389-1397.

Staley,K. (1994). The role of an inwardly rectifying chloride conductance in postsynaptic inhibition. J.Neurophysiol. 72, 273-284.

Stauffer,K.A., Kumar,N.M., Gilula,N.B., and Unwin,N. (1991). Isolation and purification of gap junction channels. J.Cell Biol. 115, 141-150.

Stevenson,B.R., Siliciano,J.D., Mooseker,M.S., and Goodenough,D.A. (1986). Identification of ZO-1: a high molecular weight polypeptide associated with the tight junction (zonula occludens) in a variety of epithelia. J.Cell Biol. 103, 755-766.

Stewart,P.L., Burnett,R.M., Cyrklaff,M., and Fuller,S.D. (1991). Image reconstruction reveals the complex molecular organization of adenovirus. Cell 67, 145-154.

Stout,C.E., Costantin,J.L., Naus,C.C., and Charles,A.C. (2002). Intercellular calcium signaling in astrocytes via ATP release through connexin hemichannels. J.Biol.Chem. 277, 10482-10488.

Stutzin,A., Eguiguren,A.L., Montes,N., and Sepulveda,F.V. (1998). Modulation by extracellular and intracellular iodide of volume-activated Cl- current in HeLa cells. Pflugers Arch. 436, 152-154.

Surges,R., Freiman,T.M., and Feuerstein,T.J. (2003). Gabapentin increases the hyperpolarization-activated cation current Ih in rat CA1 pyramidal cells. Epilepsia 44, 150-156.

Surges,R., Freiman,T.M., and Feuerstein,T.J. (2004). Input resistance is voltage dependent due to activation of Ih channels in rat CA1 pyramidal cells. J.Neurosci.Res. 76, 475-480.

Sutor,B., Schmolke,C., Teubner,B., Schirmer,C., and Willecke,K. (2000). Myelination defects and neuronal hyperexcitability in the neocortex of connexin 32-deficient mice. Cereb.Cortex 10, 684-697.

Sutula,T. and Steward,O. (1986). Quantitative analysis of synaptic potentiation during kindling of the perforant path. J.Neurophysiol. 56, 732-746.

Suzu,S., Hayashi,Y., Harumi,T., Nomaguchi,K., Yamada,M., Hayasawa,H., and Motoyoshi,K. (2002). Molecular cloning of a novel immunoglobulin superfamily gene preferentially expressed by brain and testis. Biochem.Biophys.Res.Commun. 296, 1215-1221.

Suzuki,S.C., Inoue,T., Kimura,Y., Tanaka,T., and Takeichi,M. (1997). Neuronal circuits are subdivided by differential expression of type-II classic cadherins in postnatal mouse brains. Mol.Cell Neurosci. 9, 433-447.

Svichar,N., Shmigol,A., Verkhratsky,A., and Kostyuk,P. (1997). ATP induces Ca2+ release from IP3-sensitive Ca2+ stores exclusively in large DRG neurones. Neuroreport 8, 1555-1559.

Takahashi,A., Camacho,P., Lechleiter,J.D., and Herman,B. (1999). Measurement of intracellular calcium. Physiol Rev. 79, 1089-1125.

Talley,E.M., Sirois,J.E., Lei,Q., and Bayliss,D.A. (2003). Two-pore-Domain (KCNK) potassium channels: dynamic roles in neuronal function. Neuroscientist. 9, 46-56.

Talley,E.M., Solorzano,G., Lei,Q., Kim,D., and Bayliss,D.A. (2001). Cns distribution of members of the two-pore-domain (KCNK) potassium channel family. J.Neurosci. 21, 7491-7505.

Tan,M.L., Theeuwes,H.P., Feenstra,L., and Borst,J.G. (2007). Membrane properties and firing patterns of inferior colliculus neurons: an in vivo patch-clamp study in rodents. J.Neurophysiol. 98, 443-453.

Tarran,R., Argent,B.E., and Gray,M.A. (2000). Regulation of a hyperpolarization-activated chloride current in murine respiratory ciliated cells. J.Physiol 524 Pt 2, 353-364.

Tepper,J.M. and Trent,F. (1993). In vivo studies of the postnatal development of rat neostriatal neurons. Prog Brain Res. 99, 35-50.

Theander,S., Fahraeus,C., and Grampp,W. (1996). Analysis of leak current properties in the lobster stretch receptor neurone. Acta Physiol Scand. 157, 493-509.

Theis,M., Sohl,G., Eiberger,J., and Willecke,K. (2005). Emerging complexities in identity and function of glial connexins. Trends Neurosci. 28, 188-195.

Thiemann,A., Grunder,S., Pusch,M., and Jentsch,T.J. (1992). A chloride channel widely expressed in epithelial and non-epithelial cells. Nature 356, 57-60.

Thomas,R.C. (1972). Electrogenic sodium pump in nerve and muscle cells. Physiol Rev. 52, 563-594.

Tobin,G., Giglio,D., and Lundgren,O. (2009). Muscarinic receptor subtypes in the alimentary tract. J.Physiol Pharmacol. 60, 3-21.

Tomko,R.P., Johansson,C.B., Totrov,M., Abagyan,R., Frisen,J., and Philipson,L. (2000). Expression of the adenovirus receptor and its interaction with the fiber knob. Exp.Cell Res. 255, 47-55.

Tomko,R.P., Xu,R., and Philipson,L. (1997). HCAR and CAR: the human and mouse cellular receptors for subgroup C adenoviruses and group B coxsackieviruses. Proc.Natl.Acad.Sci.U.S A 94, 3352-3356.

Torbergsen,T., Hodnebo,A., Brautaset,N.J., Loseth,S., and Stalberg,E. (2003). A rare form of painful nondystrophic myotonia. Clin.Neurophysiol. 114, 2347-2354.

Török TL (2007). Electrogenic Na+/Ca2+-exchange of nerve and muscle cells. Prog Neurobiol.

Traub,R.D., Miles,R., and Wong,R.K. (1987a). Models of synchronized hippocampal bursts in the presence of inhibition. I. Single population events. J.Neurophysiol. 58, 739-751.

Traub,R.D., Miles,R., Wong,R.K., Schulman,L.S., and Schneiderman,J.H. (1987b). Models of synchronized hippocampal bursts in the presence of inhibition. II. Ongoing spontaneous population events. J.Neurophysiol. 58, 752-764.

Trump,B.F. and Berezesky,I.K. (1996). The mechanisms of calcium-mediated cell injury and cell death [correcgted]. New Horiz. 4, 139-150.

Trussell,L.O. and Fischbach,G.D. (1989). Glutamate receptor desensitization and its role in synaptic transmission. Neuron 3, 209-218.

Tseng,G.N. (1992). Cell swelling increases membrane conductance of canine cardiac cells: evidence for a volume-sensitive Cl channel. Am.J.Physiol 262, C1056-C1068.

Tu,H., Nelson,O., Bezprozvanny,A., Wang,Z., Lee,S.F., Hao,Y.H., Serneels,L., de Strooper,B., Yu,G., and Bezprozvanny,I. (2006). Presenilins form ER Ca2+ leak channels, a function disrupted by familial Alzheimer's disease-linked mutations. Cell 126, 981-993.

Uchida,N., Honjo,Y., Johnson,K.R., Wheelock,M.J., and Takeichi,M. (1996). The catenin/cadherin adhesion system is localized in synaptic junctions bordering transmitter release zones. J.Cell Biol. 135, 767-779.

Ueno,T., Okabe,A., Akaike,N., Fukuda,A., and Nabekura,J. (2002). Diversity of neuron-specific K+-Cl- cotransporter expression and inhibitory postsynaptic potential depression in rat motoneurons. J.Biol.Chem. 277, 4945-4950.

Valiunas,V., Mui,R., McLachlan,E., Valdimarsson,G., Brink,P.R., and White,T.W. (2004). Biophysical characterization of zebrafish connexin35 hemichannels. Am.J.Physiol Cell Physiol 287, C1596-C1604.

van Raaij,M.J., Chouin,E., van der,Z.H., Bergelson,J.M., and Cusack,S. (2000). Dimeric structure of the coxsackievirus and adenovirus receptor D1 domain at 1.7 A resolution. Structure. 8, 1147-1155.

van Vreeswijk,C. and Sompolinsky,H. (1996). Chaos in neuronal networks with balanced excitatory and inhibitory activity. Science 274, 1724-1726.

Vapaatalo,H., Linden,I.B., Metsa-Ketela,T., Kangasaho,M., and Laustiola,K. (1978). Effect of carbenoxolone on phosphodiesterase and prostaglandin synthetase activities. Experientia 34, 384-385.

Varga,M.J., Weibull,C., and Everitt,E. (1991). Infectious entry pathway of adenovirus type 2. J.Virol. 65, 6061-6070.

Vergara,C., Latorre,R., Marrion,N.V., and Adelman,J.P. (1998). Calcium-activated potassium channels. Curr.Opin.Neurobiol. 8, 321-329.

Verkhratsky,A.J. and Petersen,O.H. (1998). Neuronal calcium stores. Cell Calcium 24, 333-343.

Vessey,J.P., Lalonde,M.R., Mizan,H.A., Welch,N.C., Kelly,M.E., and Barnes,S. (2004). Carbenoxolone inhibition of voltage-gated Ca channels and synaptic transmission in the retina. J.Neurophysiol. 92, 1252-1256.

Viswanathan,P.C. and Balser,J.R. (2004). Inherited sodium channelopathies: a continuum of channel dysfunction. Trends Cardiovasc.Med. 14, 28-35.

Volkov,E.M., Nurullin,L.F., Svandova,I., Nikolsky,E.E., and Vyskocil,F. (2000). Participation of electrogenic Na+-K+-ATPase in the membrane potential of earthworm body wall muscles. Physiol Res. 49, 481-484.

Wadell,G. and Norrby,E. (1969). Immunological and other biological characteristics of pentons of human adenoviruses. J.Virol. 4, 671-680.

Walmod,P.S., Kolkova,K., Berezin,V., and Bock,E. (2004). Zippers make signals: NCAM-mediated molecular interactions and signal transduction. Neurochem.Res. 29, 2015-2035.

Walters,R.W., Freimuth,P., Moninger,T.O., Ganske,I., Zabner,J., and Welsh,M.J. (2002). Adenovirus fiber disrupts CAR-mediated intercellular adhesion allowing virus escape. Cell 110, 789-799.

Wang,P.Y., Seabold,G.K., and Wenthold,R.J. (2008). Synaptic adhesion-like molecules (SALMs) promote neurite outgrowth. Mol.Cell Neurosci 39, 83-94.

Wang,X. and Bergelson,J.M. (1999). Coxsackievirus and adenovirus receptor cytoplasmic and transmembrane domains are not essential for coxsackievirus and adenovirus infection. J.Virol. 73, 2559-2562.

Waterman,S.A. (2000). Voltage-gated calcium channels in autonomic neuroeffector transmission. Prog Neurobiol. 60, 181-210.

Waters,J. and Helmchen,F. (2006). Background synaptic activity is sparse in neocortex. J.Neurosci. 26, 8267-8277.

Wei,C.J., Xu,X., and Lo,C.W. (2004). Connexins and cell signaling in development and disease. Annu.Rev.Cell Dev.Biol. 20, 811-838.

Weiger,T.M., Hermann,A., and Levitan,I.B. (2002). Modulation of calcium-activated potassium channels. J.Comp Physiol A Neuroethol.Sens.Neural Behav.Physiol 188, 79-87.

Weiss,J.L. and Burgoyne,R.D. (2002). Sense and sensibility in the regulation of voltage-gated Ca(2+) channels. Trends Neurosci 25, 489-491.

Weissman,T.A., Riquelme,P.A., Ivic,L., Flint,A.C., and Kriegstein,A.R. (2004). Calcium waves propagate through radial glial cells and modulate proliferation in the developing neocortex. Neuron 43, 647-661.

Whitham,E.M., Challiss,R.A., and Nahorski,S.R. (1991). M3 muscarinic cholinoceptors are linked to phosphoinositide metabolism in rat cerebellar granule cells. Eur.J.Pharmacol. 206, 181-189.

Wickenden,A.D., Maher,M.P., and Chaplan,S.R. (2009). HCN pacemaker channels and pain: a drug discovery perspective. Curr.Pharm.Des 15, 2149-2168.

Wickham,T.J., Mathias,P., Cheresh,D.A., and Nemerow,G.R. (1993). Integrins alpha v beta 3 and alpha v beta 5 promote adenovirus internalization but not virus attachment. Cell 73, 309-319.

Williams,E.J., Doherty,P., Turner,G., Reid,R.A., Hemperly,J.J., and Walsh,F.S. (1992). Calcium influx into neurons can solely account for cell contact-dependent neurite outgrowth stimulated by transfected L1. J.Cell Biol. 119, 883-892.

Williams,E.J., Mittal,B., Walsh,F.S., and Doherty,P. (1995). A Ca2+/calmodulin kinase inhibitor, KN-62, inhibits neurite outgrowth stimulated by CAMs and FGF. Mol.Cell Neurosci 6, 69-79.

Wladkowski,S.L., Lin,W., McPheeters,M., Kinnamon,S.C., and Mierson,S. (1998). A basolateral chloride conductance in rat lingual epithelium. J.Membr.Biol. 164, 91-101.

Wollmuth,L.P. and Hille,B. (1992). Ionic selectivity of Ih channels of rod photoreceptors in tiger salamanders. J.Gen.Physiol 100, 749-765.

Wolpert,L. (1969). Positional information and the spatial pattern of cellular differentiation. J.Theor.Biol. 25, 1-47.

Worrell,R.T., Butt,A.G., Cliff,W.H., and Frizzell,R.A. (1989). A volume-sensitive chloride conductance in human colonic cell line T84. Am.J.Physiol 256, C1111-C1119.

Wu,G. and Hamill,O.P. (1992). NPPB block of Ca(++)-activated Cl- currents in Xenopus oocytes. Pflugers Arch. 420, 227-229.

Wyse,A.T., Bavaresco,C.S., Reis,E.A., Zugno,A.I., Tagliari,B., Calcagnotto,T., and Netto,C.A. (2004). Training in inhibitory avoidance causes a reduction of Na+,K+-ATPase activity in rat hippocampus. Physiol Behav. 80, 475-479.

Xia,D., Henry,L., Gerard,R.D., and Deisenhofer,J. (1995). Structure of the receptor binding domain of adenovirus type 5 fiber protein. Curr.Top.Microbiol.Immunol. 199 (Pt 1), 39-46.

Xia,D., Henry,L.J., Gerard,R.D., and Deisenhofer,J. (1994). Crystal structure of the receptor-binding domain of adenovirus type 5 fiber protein at 1.7 A resolution. Structure. 2, 1259-1270.

Yamakage,M. and Namiki,A. (2002). Calcium channels--basic aspects of their structure, function and gene encoding; anesthetic action on the channels--a review. Can.J.Anaesth. 49, 151-164.

Yamamoto,K., Hashimoto,K., Isomura,Y., Shimohama,S., and Kato,N. (2000). An IP3-assisted form of Ca2+-induced Ca2+ release in neocortical neurons. Neuroreport 11, 535-539.

Yang,K.H., Franaszczuk,P.J., and Bergey,G.K. (2005). Inhibition modifies the effects of slow calcium-activated potassium channels on epileptiform activity in a neuronal network model. Biol.Cybern. 92, 71-81.

Yang,L. and Ling,D.S. (2007). Carbenoxolone modifies spontaneous inhibitory and excitatory synaptic transmission in rat somatosensory cortex. Neurosci.Lett. 416, 221-226.

Ye,Z.C., Wyeth,M.S., Baltan-Tekkok,S., and Ransom,B.R. (2003). Functional hemichannels in astrocytes: a novel mechanism of glutamate release. J.Neurosci. 23, 3588-3596.

Yoon,J.W., Morishima,T., McClintock,P.R., Austin,M., and Notkins,A.L. (1984). Virus-induced diabetes mellitus: mengovirus infects pancreatic beta cells in strains of mice resistant to the diabetogenic effect of encephalomyocarditis virus. J.Virol. 50, 684-690.

Ytterberg,S.R., Mahowald,M.L., and Messner,R.P. (1987). Coxsackievirus B 1-induced polymyositis. Lack of disease expression in nu/nu mice. J.Clin.Invest 80, 499-506.

Yu,H., Chang,F., and Cohen,I.S. (1995). Pacemaker current i(f) in adult canine cardiac ventricular myocytes. J.Physiol 485 (Pt 2), 469-483.

Yu,X., Duan,K.L., Shang,C.F., Yu,H.G., and Zhou,Z. (2004). Calcium influx through hyperpolarization-activated cation channels (I(h) channels) contributes to activity-evoked neuronal secretion. Proc.Natl.Acad.Sci.U.S.A 101, 1051-1056.

Yuasa,S. (1995). [Developmental mechanisms of neural network in the cerebellar system]. Nihon Shinkei Seishin Yakurigaku Zasshi 15, 177-183.

Zen,K., Liu,Y., McCall,I.C., Wu,T., Lee,W., Babbin,B.A., Nusrat,A., and Parkos,C.A. (2005). Neutrophil migration across tight junctions is mediated by adhesive interactions between epithelial coxsackie and adenovirus receptor and a junctional adhesion molecule-like protein on neutrophils. Mol.Biol.Cell 16, 2694-2703.

Zhang,J., George,A.L., Jr., Griggs,R.C., Fouad,G.T., Roberts,J., Kwiecinski,H., Connolly,A.M., and Ptacek,L.J. (1996). Mutations in the human skeletal muscle chloride channel gene (CLCN1) associated with dominant and recessive myotonia congenita. Neurology 47, 993-998.

Zholos,A., Beck,B., Sydorenko,V., Lemonnier,L., Bordat,P., Prevarskaya,N., and Skryma,R. (2005). Ca(2+)- and volume-sensitive chloride currents are differentially regulated by agonists and store-operated Ca2+ entry. J.Gen.Physiol 125, 197-211.

Zhukareva,V., Chernevskaya,N., Pimenta,A., Nowycky,M., and Levitt,P. (1997). Limbic system-associated membrane protein (LAMP) induces neurite outgrowth and intracellular Ca2+ increase in primary fetal neurons. Mol.Cell Neurosci 10, 43-55.

Zoll,J., Jongen,P., Galama,J., van Kuppeveld,F., and Melchers,W. (1993). Coxsackievirus B1-induced murine myositis: no evidence for viral persistence. J.Gen.Virol. 74 (Pt 10), 2071-2076.

Zomorrodi,R., Kroger,H., and Timofeev,I. (2008). Modeling thalamocortical cell: impact of ca channel distribution and cell geometry on firing pattern. Front Comput.Neurosci. 2, 5.

8. Abbreviation list

-/- - CAR-deficient mice (neurons)
$[Ca^{2+}]_i$ – intracellular Ca^{2+} concentration
µF – micro Farad (10^{-6} F)
µl – microliter (10^{-6} l)
µM – micomolar (10-6 M)
A - ampere
AB – antibody
Ad2 – recombinant fiber knob of Adenovirus Ad2 C428N
AP(s) – action potential(s)
C - degree Celsius
CaCCs – Ca^{2+}-activated Cl^- channels
CAM(s) – cell adhesion molecule(s)
CAR KO – mouse/neurons with CAR gene deletion
CAR-/- - CAR-deficient (neurons)
C_m – whole-cell capacitance
Cx – connexin
DIV – days *in vitro*
E.coli - Escherichia coli
EC – extracellular (solution)
ECM – extracellular matrix
E*rev* – reversal potential
F - Farad
Fig. – figure
fv – filed of view
g - conductance
G_J – junctional conductance
GST - glutathione S-transferase
h – hour(s)
I - current
IC- intracellular (solution)
$I_{Cl-(Ca)}$ – Ca^{2+}-activated Cl^- current
Ig – immunoglobulin
I_J – junctional current
IP3 - inositol 1,4,5-trisphosphate
IP3Rs - inositol 1,4,5-trisphosphate receptors
I-V – current-voltage relation
K- Kelvin
kb – kilo base
kDa kilodalton (mol. Masse)
KO – knock-out
kOhm – kilo Ohm (10^3 Ohm)
LY – lucifer yellow
m - meter
M - mol
min – minute(s)
mM – millimolar (10^{-3} M)
mm^2 – square millimeter
MOhm – mega Ohm (10^6 Ohm)
ms – millisecond(s)

mV – millivolt (10^{-3} V)
nm – nanometer (10^{-9} m)
osmo. – osmolality
P – permeability
pA – pico ampere (10^{-12} A)
PCR - polymerase chain reaction
pF – pico Farad (10^{-12} F)
PLC – phospholipase C
R_a – access resistance
R_m – membrane resistance
R_m *specific* – specific membrane resistance
RMP – resting membrane potential
rpm – revolutions per minute
R_s – series resistance
RT- room temperature, approximately 23°C
RyRs – ryanodine receptors
SDS-PAGE - sodium dodecyl sulfate polyacrylamide gel electrophoresis
sec – second(s)
TJ – tight junction(s)
U - voltage
V – volt
V_h – holding potential
V_J – junctional voltage
V_m – membrane potential
WT – wild type

9. Curriculum vitae

For reason of data protection, the curriculum vitae is not included in the online version.

Publications

Cholewa,J. and Pfluger,H.J. (2009). Descending unpaired median neurons with bilaterally symmetrical axons in the suboesophageal ganglion of *Manduca sexta* larvae. Zoology.(Jena) *112*, 251-262.

Patzke,C., Max,K., Behlke,J., **Schreiber,J**., Schmidt, H., Dorner,A., Kröger,S., Henning,M., Otto,A., Heinemann,U., and Rathjen,F.G. Functional and structural characterization of the Coxsackievirus-adenovirus receptor (CAR): complex homophilic and heterophilic interactions on neural cells. 2009 (submitted)

Schreiber, J., Jüttner, R., and Rathjen, F.G. The cell adhesion molecule coxsackie virus and adenovirus receptor (CAR) modulates intracellular Ca^{2+} and Cl^{-} conductance in cultivated cortical mouse neurons (in preparation).

Conferences and presented posters

"Functional characterization of CAR: synaptogenesis and neurite formation" **Cholewa**,J., Jüttner, R., and Rathjen, F.G. 2nd Westerburg Symposium on "Molecular Dynamic of the Chemical Synapse", August 2007, Westerburg, Germany

"Modulation of neuronal membrane properties by Coxasckievirus-Adenovirus Receptor (CAR)" **Cholewa**,J., Jüttner, R., and Rathjen, F.G. BNF Berlin Neuroscience Forum, June 2008, Liebenwalde, Germany

"Modulation of neuronal membrane properties by the Coxsackie-Adenovirus Receptor (CAR)" **Cholewa**,J., Jüttner,R., and Rathjen, F.G. Berlin Brain Days, MDC Berlin, December 2008, Berlin, Germany

10. Acknowledgments

The research presented in this PhD thesis has been carried out in the Prof. Dr. Fritz G. Rathjen laboratory at the Department of Developmental Neurobiology at the Max-Delbrück-Centrum (MDC) for Molecular Medicine in Berlin, Germany.

I wish to express my gratitude to my supervisor, Prof. Dr. Fritz G. Rathjen for giving me the opportunity to work on this project, for his encouragement and thoughtful guidance.

In particular, I am deeply indebted to Dr. René Jüttner. He introduced me to electrophysiological methods and provided me with the technical support, many helpful suggestions, important advices and discussions as well as with constant encouragement during the course of this work.

I thank all member of Prof. Rathjen's lab, especially Mechthild Henning, for technical support, discussions and a pleasant work atmosphere.

I am grateful to Prof. Dr. Rosemarie Grantyn and Prof. Dr. Thomas Jentsch for helpful suggestions and discussions.

I would like to gratefully acknowledge my husband Jörg Schreiber, for his encouragement, discussions and every-day support.

I thank the Max-Delbrück-Centrum for allowing me to enter the PhD program and for its financial support.